Mathematical models for simulation and optimization of multi-carrier energy systems

Markensteijn, A.S.

DOI
10.4233/uuid:044c083a-4eb1-4999-b789-db7150c4c7df

Publication date
2021

Document Version
Final published version

Citation (APA)
Markensteijn, A. S. (2021). *Mathematical models for simulation and optimization of multi-carrier energy systems*. [Dissertation (TU Delft), Delft University of Technology]. https://doi.org/10.4233/uuid:044c083a-4eb1-4999-b789-db7150c4c7df

Important note
To cite this publication, please use the final published version (if applicable).
Please check the document version above.

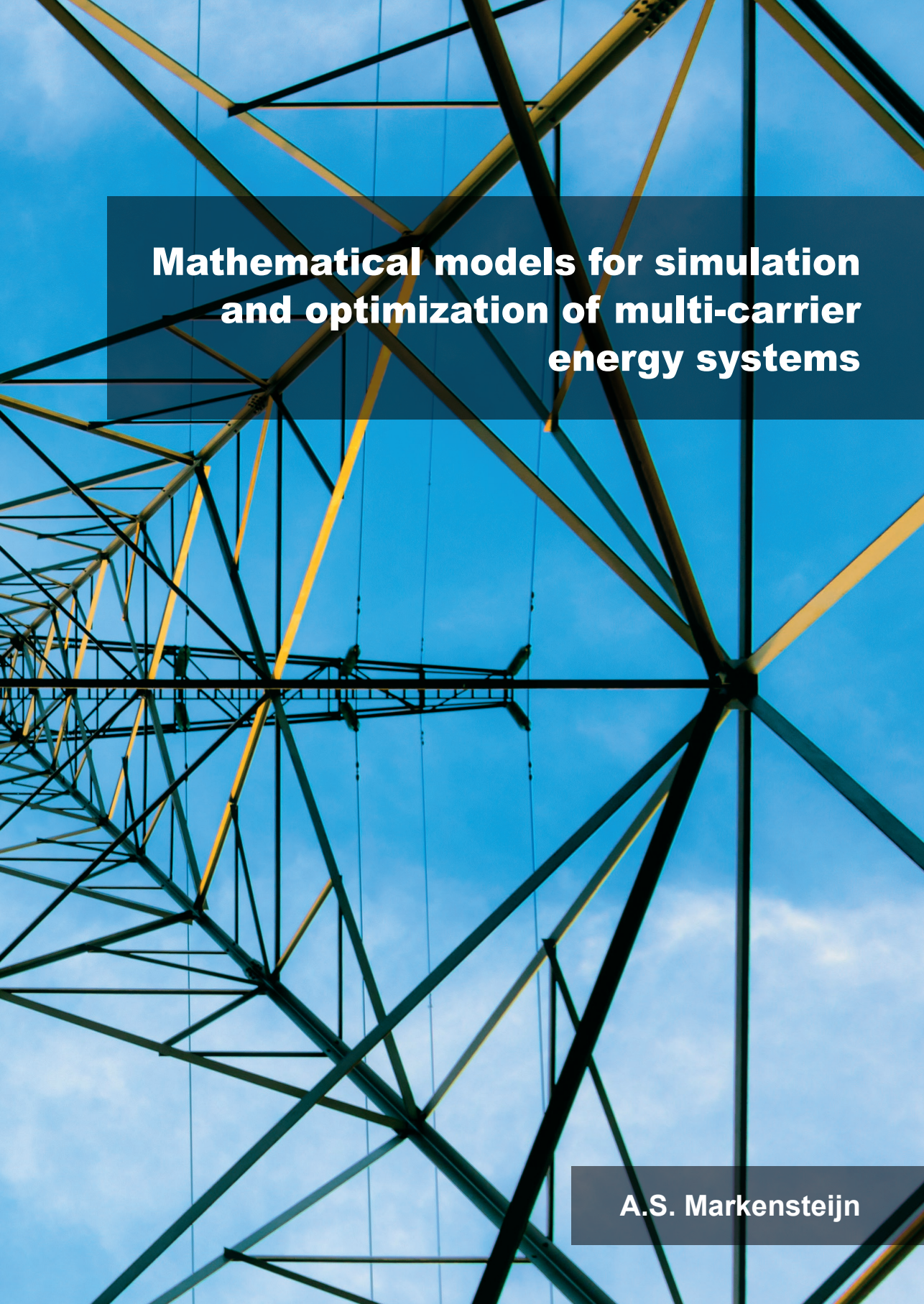

Mathematical models for simulation and optimization of multi-carrier energy systems

A.S. Markensteijn

Mathematical models for simulation and optimization of multi-carrier energy systems

PROEFSCHRIFT

ter verkrijging van de graad van doctor
aan de Technische Universiteit Delft,
op gezag van de Rector Magnificus Prof.dr.ir. T.H.J.J. van der Hagen,
voorzitter van het College voor Promoties,
in het openbaar te verdedigen op
maandag 5 juli 2021 om 10:00 uur

door

Anne Saskia MARKENSTEIJN
Wiskundig ingenieur, Technische Universiteit Delft, Nederland
geboren te Bodegraven, Nederland

Dit proefschrift is goedgekeurd door de promotor.

Samenstelling promotiecommissie:

Rector Magnificus	voorzitter
Prof.dr.ir. C. Vuik	Technische Universiteit Delft, promotor

Onafhankelijke leden:

Prof.dr. P. Mancarella	University of Melbourne en University of Manchester
Prof.dr. S. Grundel	Max Planck Institute
Prof.dr. A. van der Schaft	Rijksuniversiteit Groningen
Dr.ir. I. W. M. Pothof	Stichting Deltares en Technische Universiteit Delft
Prof.dr. P. Palensky	Technische Universiteit Delft
Prof.dr.ir. A. W. Heemink	Technische Universiteit Delft, reservelid

Overig lid:

Dr.ir. J.E. Romate	Technische Universiteit Delft

Dr.ir. J.E. Romate heeft als begeleider in belangrijke mate aan de totstandkoming van het proefschrift bijgedragen.

Mathematical models for simulation and optimization of multi-carrier energy systems
Dissertation at Delft University of Technology.

Keywords: *Adjoint approach, Decoupled load flow, Fixed-point method, Gas networks, Heat networks, Integrated energy systems, Load flow analysis, Load flow problem, Multi-carrier energy systems, Multi-carrier energy networks, Natural gas, Newton-Raphson method, Newton's method, Nonlinearly constrained optimization problem, Numerical analysis, Optimal power flow problem, Optimal flow problem, Power flow analysis, Power grids, Scaling*

ISBN: 978-94-6366-419-6

Printed by: www.proefschriftmaken.nl
An electronic version of this dissertation is available at https://repository.tudelft.nl/

Summary

Mathematical models for simulation and optimization of multi-carrier energy systems

Anne Saskia Markensteijn

Energy systems are vital in modern society, and reliable operation is crucial. Multi-carrier energy systems (MESs), which couple two or more single-carrier systems, have recently become more important, as the need for sustainable energy systems increases. Important tools for the design and operation of energy systems are steady-state simulation and optimization. Steady-state simulation, which involves solving the load flow (LF) problem, is concerned with determining the flow of energy through the system and the values of other quantities throughout the system, such as voltages and pressures, for given demands. In operational optimization, which involves solving the optimal flow (OF) problem, the distribution of generation over the various sources and the set points of controllable elements are determined such that some objective is optimized and such that the system is operated within physical limits.

LF problems and OF problems have been widely studied for single-carrier (SC) systems. However, conventional LF models for the separate single-carrier networks (SCNs) are not able to capture the full extent of the coupling. Recently, different LF models for MESs have been proposed, either using the energy hub (EH) concept, or using a case specific approach. Yet, they do not state how the graphs of the SCNs can be combined into one multi-carrier network (MCN). A good description of integrated networks of multiple energy carriers is very important. Some couplings between energy systems, while possible in practice, can lead to model problems. Although the EH concept can be applied to a general MES, it is unclear in the existing models how the EH should be represented in the graph of the MES. On the other hand, the case specific approaches are not easily applicable to general MESs. Moreover, the effect of the coupling on solvability and well-posedness of the system of nonlinear LF equations for a MES has had little attention in these models.

Operational optimization requires the detailed LF equations to be incorporated into the optimization problem. Nonlinearities of these equations cause issues with convexity and solvability of the OF problem. Hence, the formulation of the LF equations, and the way they are incorporated in the OF problem, greatly influence the solvability of the OF problem and the convergence of the optimization algorithms.

In this thesis, we address some of the existing issues and possibilities to improve on the available models. We present a graph-based framework for steady-state load flow

analysis of general MESs that consist of gas, electricity, and heat. The framework is based on connecting the SCNs to heterogeneous coupling nodes, using homogeneous dummy links, to form one connected MCN. Load flow equations are associated with each network element, including the coupling nodes, which are combined with boundary conditions to form one integrated system of nonlinear equations, that needs to be solved to find the solution to the LF problem. This is the integrated approach to formulate the LF problem of a MES.

Alternatively, the model of the connected MCN can be reformulated, such that a MES is represented by a disconnected MCN that consists of the SC networks and a coupling network. This allows for a more decoupled approach to the LF problem, in which the system of nonlinear equations, now consisting of interface conditions connecting the coupling network with the SC networks and the LF equations per SC network, can be solved making use of individual solves for each SC network.

The model framework is validated using a small example MES. Using the integrated approach, we formulate the LF problem of various example MESs, of varying size, with various coupling models and topologies, and various formulations in the single-carrier parts, and solve their LF problems using the Newton-Raphson method (NR). Using these examples, we investigate the effect of coupling on the system of LF equations and discuss the problems arising due to the coupling of SC networks on the solvability of the LF problem. Based on numerical experiments, we compare the convergence behavior of NR for the various single- and multi-carrier systems. Finally, we formulate and solve the LF problem of MESs using the integrated approach and using the decoupled approach. We compare the systems of equations, and we compare the convergence of the solution methods for the two approaches.

Furthermore, in this thesis, we consider two ways to include the LF equations in the OF problem for general MESs, called formulation I and formulation II. In formulation I, optimization is over the combined control and state variables, with the LF equations included explicitly as equality constraints. In formulation II, optimization is over the control variables only, and the LF equations are included as a subsystem, which is solved to obtain the state variables for given control variables. We compare the two formulations theoretically, and we illustrate the effect of the two formulations on the solvability of the OF problem by optimizing two MESs.

This study shows that the graph-based framework can be used to formulate and solve the steady-state LF problem for general MESs that consist of gas, electricity, and heat, both with the integrated approach and with the decoupled approach. Moreover, the framework can be used with different components and models, both in the SCNs and for the coupling units. Therefore, our framework includes and extends the currently available LF models for MESs. Furthermore, the model framework provides guidelines to obtain a solvable steady-state LF problem for MESs. We find that using the decoupled approach to perform LF analysis is slower than using the integrated approach. For the LF problem of an example MES with a tree-like structure, NR is independent of the size of the network and of the coupling, and NR requires at most as many iterations as the slowest single-carrier network.

Both formulation I and formulation II result in a solvable OF problem. For the two example MESs, the optimization algorithms require significantly fewer iterations with formulation II than with formulation I.

Samenvatting

Wiskundige modellen voor simulatie en optimalisatie van geïntegreerde energiesystemen

Anne Saskia Markensteijn

Energiesystemen zijn een essentieel onderdeel van onze samenleving, en het is cruciaal dat deze systemen betrouwbaar functioneren. Naarmate de vraag naar duurzame energiesystemen stijgt worden geïntegreerde energiesystemen, die twee of meer afzonderlijke energiesystemen aan elkaar koppelen, steeds belangrijker. Simulatie en optimalisatie zijn belangrijke middelen tijdens het ontwerpen en beheren van energiesystemen. Bij tijdonafhankelijke simulaties, waarbij het load flow (LF) probleem wordt opgelost, worden de energiestromen en andere grootheden, zoals spanning of druk, in het systeem bepaald voor een gegeven vraag naar energie. Bij optimalisatie, waarbij het optimal flow (OF) probleem wordt opgelost, wordt de totale opgewekte energie over de verschillende bronnen verdeeld, zodanig dat een bepaalde functie wordt geoptimaliseerd en er gelijktijdig aan de fysieke limieten van het energiesysteem wordt voldaan.

Er is uitgebreid onderzoek gedaan naar LF en OF problemen voor de afzonderlijke energiesystemen, maar deze conventionele LF modellen voor de afzonderlijke energienetwerken zijn niet in staat om de volledige reikwijdte van een koppeling weer te geven. Recent zijn er verschillende LF modellen ontwikkeld voor geïntegreerde energiesystemen, die gebruik maken van het energy hub (EH) concept of die uitgaan van een specifiek energiesysteem, maar deze modellen geven niet aan hoe de grafen van de afzonderlijke energiesystemen gecombineerd kunnen worden tot één geïntegreerd netwerk. Een goede beschrijving van geïntegreerde netwerken is belangrijk, want sommige koppelingen tussen de energiesystemen, die in de praktijk mogelijk zijn, kunnen leiden tot modelproblemen. Hoewel het EH concept gebruikt kan worden voor een generiek geïntegreerd energiesysteem, is het onduidelijk hoe een EH moet worden weergegeven in de graaf van het geïntegreerde energiesysteem. Aan de andere kant zijn de modellen die uitgaan van een specifiek energiesysteem lastig te gebruiken voor een generiek geïntegreerd energiesysteem. Bovendien is in deze modellen weinig aandacht besteed aan het effect van een koppeling op de oplosbaarheid en goedgestelheid van het stelsel van niet-lineaire LF vergelijkingen voor een geïntegegreerd energiesysteem.

Voor optimalisatie moeten de gedetailleerde LF vergelijkingen opgenomen worden in het optimalisatieprobleem. De niet-lineaire aard van deze vergelijkingen kan leiden

tot een verlies van convexiteit en oplosbaarheid van het OF probleem. De formulering van de LF vergelijkingen, en de manier waarop ze verwerkt worden in het OF probleem, is daarom van grote invloed op de oplosbaarheid van het OF probleem en op de convergentie van de optimalisatie-algoritmen.

In dit proefschrift bespreken we bestaande problemen van de beschikbare modellen, en bespreken we mogelijke verbeteringen. We presenteren een framework voor tijdonafhankelijke LF analyse van generieke geïntegreerde energiesystemen, bestaande uit gas, elektriciteit en warmte, gebruikmakend van de weergave van het energiesysteem als graaf. Het framework is gebaseerd op het verbinden van de afzonderlijke energienetwerken met heterogene koppelingsknopen, via dummyzijden, om één samenhangend geïntegreerd energienetwerk te vormen. LF vergelijkingen worden toegewezen aan ieder netwerkelement, inclusief de koppelingsknopen, en deze vergelijkingen worden gecombineerd met randvoorwaarden tot één geïntegreerd stelsel van niet-lineaire vergelijkingen. De oplossing van dit stelsel is de oplossing van het LF probleem. Dit is de geïntegreerde aanpak om het LF probleem van een geïntegreerd energiesysteem op te stellen.

Als alternatief kan het model van het samenhangende geïntegreerde energienetwerk aangepast worden, zodanig dat een geïntegreerd energiesysteem wordt weergegeven door een onsamenhangende graaf bestaande uit de afzonderlijke energienetwerken en een koppelingsnetwerk. Dit staat een meer losgekoppelde aanpak van het LF probleem toe waarin het stelsel van niet-lineaire vergelijkingen, dat nu bestaat uit de stelsels van LF vergelijkingen voor ieder afzonderlijk netwerk en de koppelingscondities die de verbinding vormen tussen het koppelingsnetwerk en de afzonderlijke netwerken, opgelost kan worden door het LF probleem van ieder afzonderlijk netwerk apart op te lossen.

Het framework wordt gevalideerd middels het opstellen en oplossen van het LF probleem voor een klein geïntegreerd energiesysteem. We gebruiken de geïntegreerde aanpak om het LF probleem op te stellen van verschillende energiesystemen, met een variërende grootte, verschillende koppelingsmodellen en topologieën en verschillende formuleringen van de LF vergelijkingen in de afzonderlijke netwerken, en we lossen deze LF problemen op met de methode van Newton-Raphson (NR). Met deze voorbeelden onderzoeken we het effect van een koppeling op het stelsel van LF vergelijkingen, en bespreken we de problemen met oplosbaarheid van dit stelsel veroorzaakt door het koppelen van de afzonderlijke energienetwerken. Op basis van numerieke experimenten vergelijken we het convergentiegedrag van NR voor de verschillende afzonderlijke en geïntegreerde energiesystemen. Ten slotte gebruiken we de geïntegreerde en de losgekoppelde aanpak om het LF probleem op te stellen en op te lossen. We vergelijken de stelsels van LF vergelijkingen, en we vergelijken het convergentiegedrag van de oplossingsmethoden, voor de twee aanpakken.

In dit proefschrift beschouwen we twee manieren om de LF vergelijkingen te verwerken in het OF probleem van een generiek geïntegreerd energiesysteem, die we formulering I en formulering II noemen. Bij formulering I wordt er over de controlvariabelen en toestandsvariabelen geoptimaliseerd, waarbij de LF vergelijkingen expliciet worden verwerkt als gelijkheidsvoorwaarden. Bij formulering II wordt er alleen over de controlvariabelen geoptimaliseerd, en worden de LF vergelijkingen als subsysteem verwerkt, dat opgelost wordt naar de toestandsvariabelen voor gegeven controlvariabelen. We vergelijken de formuleringen theoretisch, en we illustreren het

effect van de twee formuleringen op de oplosbaarheid van het OF probleem door twee geïntegreerde energiesystemen te optimaliseren.

Dit proefschrift laat zien dat het framework gebruikt kan worden om het tijdonafhankelijke LF probleem te formuleren en op te lossen voor generieke geïntegreerde energiesystemen die bestaan uit gas, elektriciteit en warmte, zowel met de geïntegreerde aanpak als met de losgekoppelde aanpak. Het framework kan bovendien gebruikt worden voor verschillende netwerkelementen en modellen, zowel in de afzonderlijke netwerken als voor de koppelingen. Ons framework omvat daarom de bestaande LF modellen voor geïntegreerde energiesystemen, en breidt deze modellen uit. Verder kan het framework gebruikt worden om richtlijnen af te leiden om tot een oplosbaar tijdonafhankelijk LF probleem voor geïntegreerde energiesystemen te komen. Op basis van numerieke experimenten vinden we dat het framework met de losgekoppelde aanpak leidt tot een langzamere oplossingsmethode van LF problemen dan het framework met de geïntegreerde aanpak. Voor het voorbeeld van het LF probleem van een geïntegreerd energiesysteem waarvan het netwerk een boomstructuur heeft, geldt dat NR onafhankelijk is van de grootte van het netwerk en van de koppeling, en dat NR ten hoogste zoveel iteraties nodig heeft als voor het langzaamste afzonderlijke netwerk.

Zowel formulering I als formulering II leiden tot een oplosbaar OF probleem. Voor de twee geïntegreerde energiesystemen die als voorbeeld gebruikt worden geldt dat het optimalisatie-algoritme beduidend minder iteraties nodig heeft met formulering II dan met formulering I.

Contents

Abbreviations

GHV gross heating value.

p.u. per unit.

BC boundary condition.

CHP combined heat and power plant.

EB electric boiler.

EH energy hub.

FP the fixed-point method.

GB gas boiler.

GG gas-fired generator.

IFC interface condition.

IPOPT primal-dual interior-point optimization method.

LF load flow.

MC multi-carrier.

MCN multi-carrier network.

MES multi-carrier energy system.

NR the Newton-Raphson method.

OF optimal flow.

SC single-carrier.

SCN single-carrier network.

SLSQP sequential least squares programming.

TC 'trust-constr'.

Physical network quantities

Symbol	Name	Unit	Description
δ	voltage angle	rad	Angle of the complex voltage phasor.
Δp	pressure drop	Pa	Pressure drop over a pipe.
$\Delta\varphi$	injected heat power	W	Difference in heat power between supply and return line.
ΔT	temperature difference	°C	Temperature difference, or temperature drop, over a heat exchanger or over a pipe.
E	energy of source	W	Energy flow of source or generator. One entry of $\boldsymbol{E}$.
h	head	m	Pressure head.
I	current	–	Current phasor, with angle θ and amplitude $\lvert I\rvert$.
m	mass flow	kg/s	Water mass flow rate, e.g. in a pipe.
P	active power	W	Active power, the real part of S.
p	pressure	Pa	Pressure.
φ	heat power	W	Internal energy flow of a water.
Q	reactive power	var	Reactive power, the imaginary part of S.
q	gas flow rate	kg/s	Gas mass flow rate, e.g. in a pipe or through a compressor.
S	complex power	VA	Complex power, given by $P + \mathrm{i}Q$.
T	temperature	°C	Temperature.
V	voltage	V	Voltage phasor, with angle δ and amplitude $\lvert V\rvert$.
$\lvert V\rvert$	voltage amplitude	V	Amplitude of the complex voltage phasor.

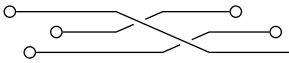

CHAPTER 1

Introduction

Energy systems are vital in modern society, and reliable operation is crucial. Multi-carrier energy systems have recently become more important, as the need for sustainable energy systems increases. Important tools for design and operation of energy system are steady-state simulation and optimization.

This chapter first explains the background and some physical aspects of energy systems. Then, the simulation and optimization of energy systems are introduced. Finally, the outline of this thesis is detailed.

1.1 Energy systems

An energy system is a physical system that generates, transports, distributes, and consumes one or more types of energy. If only one type of energy is concerned, the energy system is called a single-carrier (SC) system. Otherwise, it is called a multi-carrier (MC) system. Some examples of energy carriers are (bio)gas, electricity, heating, or cooling.

In practice, most energy systems are MC systems. Consider a power grid, which is seen as a SC system. However, certain generators convert gas to electricity, meaning that a power grid also includes the energy carrier gas. As such, it could be seen as a multi-carrier energy system (MES).

To support the realization of regional energy self-sufficiency, we look at systems from a national scale down to the distribution of energy to end-users. In this thesis, we focus on gas, electricity, and heat as energy carriers.

1.1.1 Single-carriers energy systems

This section describes the background and some practical aspects of the SC energy systems, with gas, electricity, or heat as carrier.

Icons in figures are based on designs by gstudioimagen, macrovec, and macrovector_official, from Freepik (`http://www.freepik.com`)

Gas

End-users of the gas system include industrial customers, private households, and gas-fired generators. Gas is divided into two types: high calorific gas (H-gas), and low calorific gas (L-gas). The latter is also called Groningen gas (G-gas) in the Netherlands. The end-use determines the required quality of the gas, which could be a mix of H-gas and L-gas.

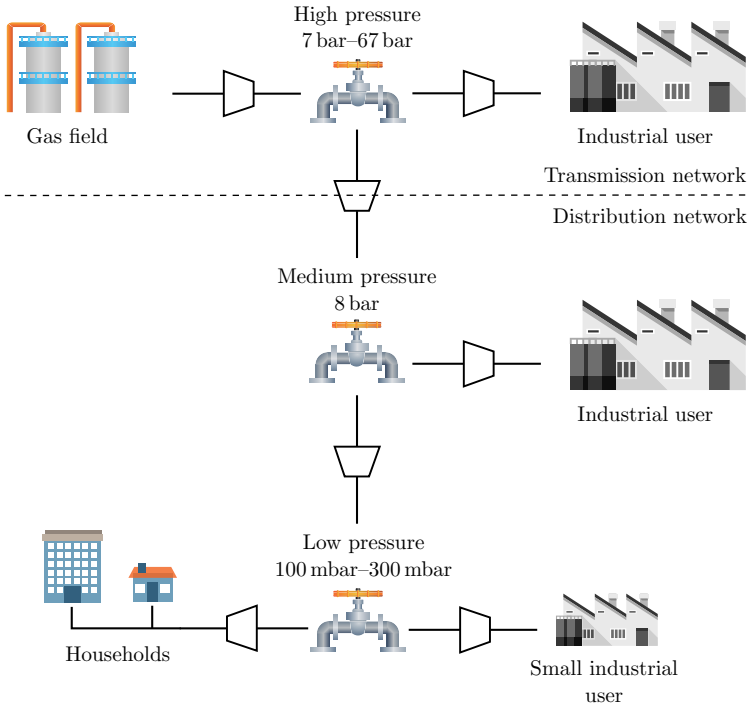

Figure 1.1: Schematic representation of a gas system.

The most basic gas transportation system is a pipeline system (e.g. [1, 2]). Sources are connected to end-users by pipelines. Gas is transported through these pipes based on pressure differences between beginning and end of a pipe.

Over large distances, the gas is transported through wide pipes at high pressures. This part of the system is called the transmission network. The gas is transferred to subsystems of smaller size, with smaller pipes and operating at lower pressures. The subsystems distribute the gas to end-users or to subsequent subsystems. This part of the system is called the distribution network.

Aside from sources, pipelines, and end-users, there are three main components in a gas system: compressors, pressure regulators, and valves. Pressure loss occurs during transportation due to friction in the pipes. Compressors are used to maintain the required pressure levels throughout the system. At the same time, various pressure levels are maintained within one system. Pressure regulators are used to change the pressure from one level to another. For instance, the pressure is lowered when gas is

transferred from the transmission network to the distribution network. Finally, valves regulate the gas flow. For instance, valves prevent flow of gas in the wrong direction, or they cut off certain regions of the system in case of a breakdown.

Figure 1.1 shows a schematic representation of a gas system, with the pressures of the Dutch system.

Electricity

End-users of the electrical system include industrial customers as well as households. Energy systems with electricity as carrier are usually called power systems. When there is no confusion between electrical power and heat power, we refer the former simply as power. The electrical system is then called a power system.

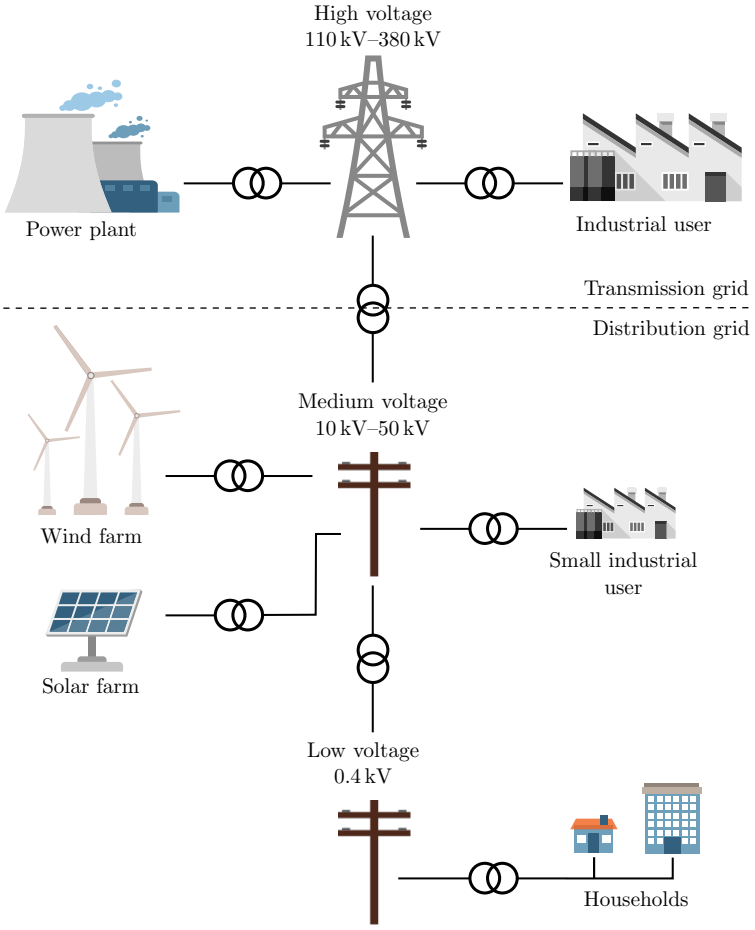

Figure 1.2: Schematic representation of an electrical system.

The total power system consists of generation, transmission, and distribution of power (e.g. [3]). Generators are connected to end-users by overhead transmission lines or underground cables.

Over large distances, the electricity is transported at high voltages. This part of the system is called the transmission grid. It connects the generators to substations near end-users. At the substations, electricity is distributed to subsystems operating at lower voltages. The subsystems distribute the electricity to end-users or to subsequent subsystems. This part of the system is called the distribution grid.

Because of historical and financial reasons, most power grids use alternating current (AC). However, if the transmission distance is long enough, direct current (DC) systems might be preferred because of the smaller incremental conductor costs. Recently, there has also been interest in DC distribution systems in the context of smart grids. In this thesis, we consider balanced three-phase AC systems. When a three-phase system is balanced, the voltages of each phase have the same magnitude, and their angles are shifted by 120°.

Figure 1.2 shows a schematic representation of a power system, with the voltages of the Dutch system.

Heat

End-users of the heat system include industrial costumers as well as (domestic) buildings (e.g. [4]). Heat demands for buildings include space heating and domestic hot water supply, which require relatively low temperature levels. The typical water temperature for hot water supply is 55 °C. Industrial uses additionally include evaporation or drying, and manufacturing of metals or other materials. Evaporation or drying requires a medium temperature, with temperatures between 100 °C–400 °C. Manufacturing of materials requires high temperature levels, with temperatures above 400 °C.

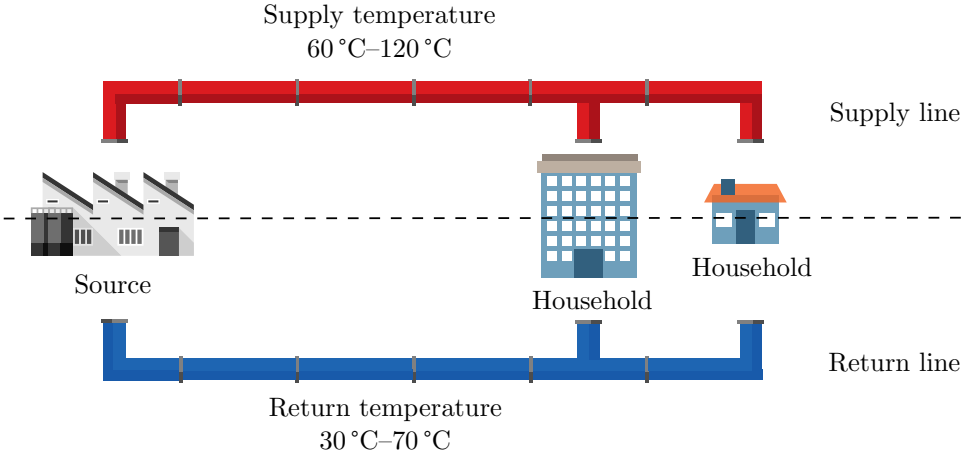

Figure 1.3: Schematic representation of a district heating system.

A general heating system consists of sources connected to end-users by double pipes (e.g. [4]). The pipes deliver the heat from source to end-user by a carrier, which is usually pressurized water. These pipes are generally short for the heating system to be financially viable. Therefore, we only consider district heating systems, where local sources supply heat to end-users within a relatively small region.

The pipes in the distribution system are double. Supply pipes transport hot water

from the sources to the end-users. After extracting heat from the water, return pipes transport the cold water from the end-users to the sources, where it is heated up again. In current systems, supply temperature varies from 60 °C to 120 °C and return temperature varies from 30 °C and 70 °C. The collection of supply pipes is called the supply line, and the collection of return pipes is called the return line.

Figure 1.3 shows a schematic representation of a district heating system.

1.1.2 Multi-carrier energy systems

Traditionally, the total energy system consists of several SC systems that are designed, operated, and controlled separately. As the need for efficient, reliable, and low carbon energy systems increases, MES have become more important [5]. In MESs, different energy carriers, such as electricity and heat, interact with each other, leading to one integrated system. Hence, MESs are sometimes called integrated energy systems. Figure 1.4 shows a schematic representation of a MES.

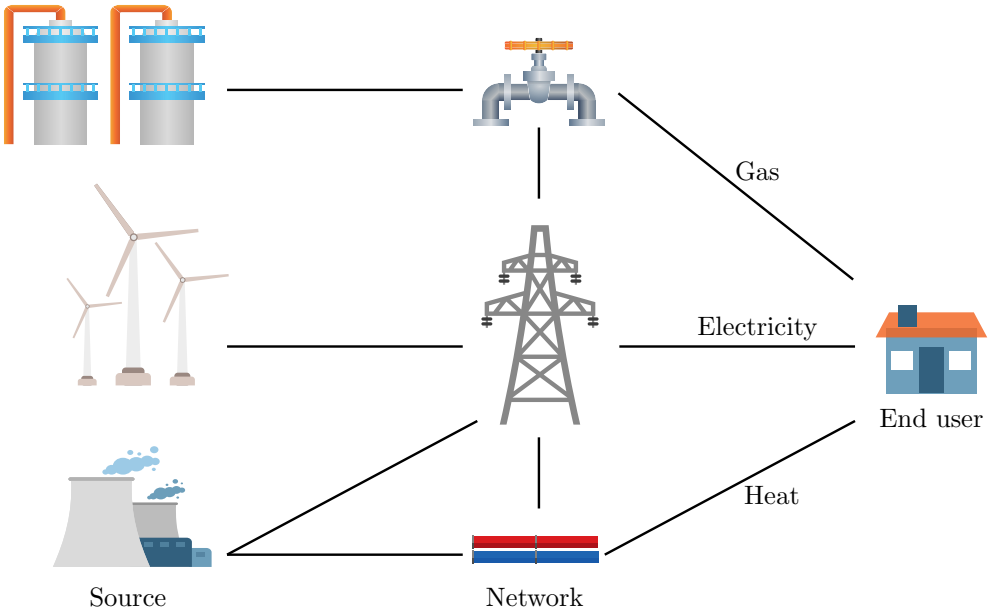

Figure 1.4: Schematic representation of a multi-carrier energy system.

The SC systems interact with each other through various system elements, which we call coupling units. The most straightforward way of interaction is through conversion units. These units convert one type of energy carrier into another. Examples include gas-fired generators, which convert gas into electricity, and combined heat and power plants (CHPs), which convert gas into electricity and heat. A CHP is also called a cogeneration plant, since it generates two energy carriers.

Another way of interaction is through active elements, for instance a compressor in a gas system. Some compressors are driven by electricity, meaning that a coupling between the power grid and the gas system exists. Elements such as compressors do

not convert one type of energy carrier into another. Instead, they serve a control purpose in one of the SC systems.

Table 1.1 gives an overview of some of the most common coupling units. Since CHP refers to any unit that converts gas to both electricity and heat, it is not included in the table separately. An example of a CHP in Table 1.1 is a gas turbine.

Table 1.1: Common coupling units for a MES.

Unit	Gas	Electricity	Heat
Turbo compressor	control	consumed	
Heat pump		consumed	produced
Gas boiler	consumed		produced
Electric boiler		consumed	produced
Circulation pump		consumed	control
Gas turbine	consumed	produced	produced
Gas-fired generator	consumed	produced	
Power-to-gas	produced	consumed	

Compared with SC energy systems, MESs are more flexible, more reliable, use more renewables and distributed generation, and have a lower carbon emission. One possible example of a MES is a regional system which is not connected to a larger grid, that is, an energy self-sufficient region.

Flexibility and reliability are increased by load shifting. For instance, an electrical demand can be supplied by the gas system through a conversion unit, effectively shifting the load from the power grid to the gas system.

The use of renewable sources and distributed generation is mainly limited by technical limits of the power grid. When different systems are integrated into a single system, any excess power generated by a renewable source can be 'stored' in the other systems through converter units. For instance, it can be stored in the gas system using power-to-gas (P2G) units. This excess power would otherwise be curtailed.

Total carbon emission is reduced due to higher efficiency of the MES compared with separate SC systems. One reason for higher efficiency is cogeneration of electrical and heat power. Additionally, a MES allows for optimal operation of the total energy system, as opposed to optimizing operations of the separate SC systems.

MESs currently also have disadvantages. First, the interaction between the various systems leads to more complex systems that are not well understood, and for which very few simulation tools are available. Furthermore, the current market is tailored to separate systems and not to one integrated system. Therefore, robust and efficient simulation and optimization tools for MES are needed.

1.2 Simulation of multi-carrier energy systems

Steady-state simulation, or steady-state analysis, is an important tool for the design and operation of energy systems. Given demands, such a simulation determines the flow of energy through the system, and the values of other quantities, such as voltages and pressures, throughout the system. In power system literature, this type of

problem is called the power flow or the load flow (LF) problem. For MES, we call this type of simulation steady-state load flow (LF) simulation or steady-state LF analysis.

Steady-state LF analysis tries to find a solution to the steady-state LF problem. For simplicity, steady-state LF analysis and the steady-state LF problem are called LF analysis and the LF problem respectively. A solution to the LF problem is mathematically feasible, but not necessarily physically feasible or optimal.

For LF analysis, energy systems are mathematically abstracted to a graph or network. Load flow problems for SCs systems have been widely studied, but load flow problems for MESs have only been proposed recently.

The currently available LF models for MESs do not state how the graphs of single-carrier networks (SCNs) can be combined into one multi-carrier network (MCN). A good description of integrated networks of multiple energy carriers is very important. Some couplings between energy systems, while possible in practice, can lead to model problems.

Furthermore, the available LF models for MES do not consider the effect of coupling on the LF problems. Usually, a coupling model introduces more unknowns than equations.

We provide a systematic analysis of the SCNs to determine how energy systems of different carriers can be combined into one MCN. Furthermore, we discuss how the models of the energy system elements should be collected to form one integrated system of LF equations, both for SCNs and for an MCN. Based on these analyses, we propose a new graph-based model framework for steady-state LF problems of general MESs.

1.3 Optimization of multi-carrier energy systems

Optimization is an important tool for the design and operation of an energy system. In operational optimization, the distribution of generation over the various sources, or the set points of controllable elements, are determined such that an objective is optimized. At the same time, the operation of the energy system must stay within physical limits. Again, these problems have been widely studied for SC systems, but optimization for MESs has only been proposed recently.

An example of operational optimization is to find a physically feasible solution to the LF problem, in which the steady-state LF analysis is extended with physical operational limits of the energy system. For gas systems, such an optimization problem is called validation of nominations [1]. Other examples are economical dispatch and optimal power flow, which are well-known operational optimization problems for power systems. Economical dispatch determines a least-cost distribution of generation, but simplifies or ignores steady-state LF equations. Optimal power flow problems find an optimal solution to some objective while satisfying both the LF equations and the physical limits of the power system.

Several objective functions are used in optimization of energy systems, such as minimizing generation costs, minimizing losses, or minimizing carbon emissions. We choose to minimize total generation costs, which is commonly used in both SC and MC systems (e.g. [6], [7], and [8]).

Currently, most optimization problems for MESs are like an economical dispatch problem, where the network transmission is simplified or ignored. In this thesis, we

consider optimization problems for MESs like optimal power flow problems, which we call optimal flow (OF) problems. This requires the detailed LF equations to be incorporated into the optimization problem. Nonlinearities of these equations cause issues with convexity and solvability of the optimization problem, as also noted in [6] and [9]. Hence, the formulation of the LF equations, and the way they are incorporated in the optimization problem, greatly influence the solvability of the optimization problem.

We analyze the effect of the LF equations on the solvability of the optimization problem for general MESs. We consider two ways to include the LF equations into the OF problem. Based on this analysis, we formulate an optimization problem for a general SC or MC energy system, providing a general optimization framework.

1.4 Outline of thesis

The rest of this thesis is structured as follows.

Chapter 2: Mathematical models of the quantities and elements in the energy systems used in steady-state simulation and optimization. This includes commonly used models in single-carrier energy systems, and various models for conversion units in multi-carrier energy systems.

Chapter 3: A systematic analysis of the SCNs to determine how energy systems of different carriers can be combined into one MCN. We introduce a coupling node to connect the SC networks into one integrated MC network. This gives a generic and uniform network representation for general MES consisting of gas, electricity, and heat.

Chapter 4: Formulation of one integrated system of LF equations, both for SCNs and for a MCN, based on the comprehensive network description of SC and MC energy systems. We discuss the effect of coupling on the LF problem, such as the need for additional boundary conditions (BCs). Together with the results from Chapter 3, Chapter 4 gives a graph-based model framework for steady-state LF problems of general MESs.

Chapter 5: Basic algorithm of the Newton-Raphson method, used for solving nonlinear system of equations. We discuss the role of scaling and permutation of the variables and equations in the Newton-Raphson method (NR). We discuss the application of NR to steady-state LF problems of MESs.

Chapter 6: Validation and illustration of the graph-based model framework for steady-state LF problems, using a MES. This MES consists of a gas network, an electricity network, and a heat network, each with three loads, which are connected through several coupling units. The coupling is modeled in three different ways, giving three MCNs for the same MES.

Chapter 7: Analysis of the effect of coupling on the solvability and well-posedness of the integrated system of nonlinear LF equations, and on the convergence of NR, based on numerical experiments.

Chapter 8: A decoupled approach to solving the LF problem of integrated MES, as an alternative to the framework presented in Chapter 4. This decoupled approach represents a MES as a disconnected MCN, by decoupling the connected MCN into SC subnetworks and a coupling subnetwork. We solve the LF problem of three example MESs, validating and demonstrating the decoupling approach.

Chapter 9: Theory regarding nonlinearly constrained optimization problems, including optimality conditions, optimization methods, and elimination of variables.

Chapter 10: Analysis of the effect of the LF equations on the solvability of the OF problem for general MESs. We consider two ways to include the LF equations in the OF problem. Based on this analysis, two formulations of the optimization problem for SC or MC energy systems are stated, providing a general optimization framework. We optimize two example MESs, demonstrating some of the theoretical advantages and disadvantaged of the formulations of the OF problem in practice.

Chapter 11: The effect of scaling on the system of equations, based dimensional analysis, in LF and OF problems is studied. We introduce a per unit scaling for MESs and compare the per unit scaling with matrix scaling. We show that these scaling methods are equivalent for NR, when using the same base values and assuming infinite precision. We show that the optimization algorithms are affected by the type of scaling.

Chapter 12: Conclusions on and some recommendations for steady-state simulation and optimization of general MESs.

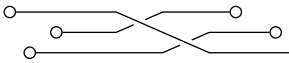

CHAPTER 2

Steady-state models of energy system elements

Steady-state simulations are an important tool for design and operation of energy systems. These simulations are based on mathematical models for each element in the system.

Steady-state simulations use time independent models. The gas, electrical, and heating SC energy systems operate at different time scales. Hydraulic changes in pressure and flow in the gas and water pipelines take seconds to reach throughout the entire system. Changes in voltages and current propagate even faster. These changes can be seen as instantaneous, and a steady-state approach can be used. Thermal changes in a heating system, however, can take hours to reach throughout the entire system. For short-term operational purposes, a steady-state approach to heat systems might be inaccurate. However, for long-term operational or design purposes, demands and generation of the system can be assumed constant in time. Therefore, a steady-state approach can be used.

This chapter gives the mathematical models of the quantities and elements in the energy systems used in steady-state simulation and optimization. First for each carrier: gas, electricity, and heat, and then for conversion units used in MESs. Unless stated otherwise, all variables and equations are in S.I. units.

2.1 Gas systems

We give the steady-state models for pipes and compressors in a gas system. For more details on models in a gas system, see for instance [1] or [2].

2.1.1 Hydraulic pipe flow

As detailed in [2], the general steady-state flow equation of gas through a pipe is derived from Bernoulli's law, assuming (i) steady-state flow, (ii) isothermal flow, (iii) negligible kinetic energy change in a pipe, (iv) constant compressibility of gas in each pipe, (v) constant friction factor coefficient along a pipe, (vi) validity of Darcy friction loss relationship across a pipe, and (vi) a horizontal pipe.

For low-pressure systems, the gauge pressures are small, and the absolute pressures are close to p_n, the pressure at standard conditions. Furthermore, the temperature

is typically close to the temperature at standard conditions, i.e. $T \simeq T_n$, and the compressibility $Z \simeq 1$. This is then used for additional simplifications of the flow equation for low-pressure systems.

Now, denote the gas mass flow in the pipe by q and the pressure drop over the pipe by Δp. The general steady-state flow equation is then given by

$$q = C^g \text{sign}\,(\Delta p)\sqrt{\frac{|\Delta p|}{\text{f}}} \tag{2.1}$$

with C^g the pipe constant for a given pipe in a gas network and f the Fanning friction factor of the pipe. The sign function is defined as

$$\text{sign}\,(x) = \begin{cases} 1, & x \geq 0 \\ -1, & x < 0 \end{cases}$$

The pressure drop and pipe constant are different for low-pressure and high-pressure systems:

$$C^g = \begin{cases} \dfrac{\pi}{8}\sqrt{\dfrac{2p_n SD^5}{T_n R_{\text{air}} L}}, & \text{for low-pressure systems} \\ \dfrac{\pi}{8}\sqrt{\dfrac{SD^5}{TR_{\text{air}} LZ}}, & \text{for high-pressure systems} \end{cases} \tag{2.2}$$

Here, S is the specific gravity of the gas, R_{air} is the gas constant of air, D is the pipe diameter, L is the pipe length, T is the temperature of the gas, and Z is the compressibility of the gas. As mentioned before, a system is a low-pressure system if the gauge pressures are small and the absolute pressures are close to p_n.

The pressure drop in (2.1) is given by

$$\Delta p = \begin{cases} p_i - p_j, & \text{for low-pressure systems; } p \text{ is gauge pressure} \\ p_i^2 - p_j^2, & \text{other; } p \text{ is absolute pressure} \end{cases} \tag{2.3}$$

with p_i and p_j the pressure at the start and end of the pipe respectively.

Various friction factor models are used, resulting in different pipe flow models. For some of those, friction factor is a function of the gas flow, such that $\text{f} = \text{f}(q)$. Commonly used friction factors are Weymouth's friction factor for high-pressure systems and turbulent flow [2]:

$$\text{f} = (20.64^2 D^{\frac{1}{3}} E^2)^{-1} \tag{2.4}$$

with E the efficiency factor of the pipe, and Pole's friction factor for systems operating between 0 mbar–75 mbar gauge [2]:

$$\text{f} = 0.0065 \tag{2.5}$$

An example of a friction factor dependent on the gas flow is the implicit Colebrook-White equation for high-pressure systems in the turbulent regime:

$$\frac{1}{2\sqrt{\text{f}}} = -2\log_{10}\left(\frac{\epsilon}{3.7D} + \frac{2.51}{\text{Re}\sqrt{\text{f}}}\right) \tag{2.6}$$

Here, ϵ is the absolute roughness of the pipe, and Re is the Reynolds number given by

$$\mathrm{Re} = \frac{4q}{\pi \mu \rho_n D}$$

with μ the kinematic viscosity of the gas, and $\rho_n = (p_n S)/(R_{\mathrm{air}} T_n)$ the density of the gas at standard conditions.

2.1.2 Compressor

Compressors in the gas network are used to compensate for pressure losses due to friction in the pipes, and allow the transport of gas over large distances. Compressors increase the pressure of the incoming gas flow, such that the outgoing gas has a higher pressure. Commonly used compressors are turbo compressors and piston compressors, and are for instance driven by gas turbines or electric motors [1].

In practice, every compressor has a feasible operating range, defined by the volume flow through the compressor, and the change in adiabatic energy of the gas. Detailed physical models of compressors exist, taking into account the operating range, drive, and adiabatic energy of the gas (e.g. [1]). In this thesis, a basic compressor model is used, which describes the increase in pressure by assuming a fixed pressure ratio r.

Denote the pressure at the inlet of the compressor by p_i, and the pressure at the outlet by p_j. The basic compressor model is then given by:

$$p_j = r p_i \tag{2.7}$$

2.2 Electrical systems

We give the models for voltage, current, and power in AC power grids, and the steady-state models for transmission lines. For more details on models in an electrical system, see for instance [3].

2.2.1 Voltage and current

In steady-state models of AC power grids, the frequency is assumed constant and uniform. The current I and voltage V are represented as complex waves, which are described by a time-independent phasor representation:

$$I = |I| \mathrm{e}^{\theta \mathrm{i}} \tag{2.8a}$$

$$V = |V| \mathrm{e}^{\delta \mathrm{i}} \tag{2.8b}$$

with $|I|$ and θ the current amplitude and current angle, $|V|$ and δ the voltage amplitude and voltage angle, and i the imaginary unit. The amplitudes $|I|$ and $|V|$ are the root-mean-square values of the time dependent sinusoidal alternating current and voltage.

2.2.2 Electrical power

The instantaneous time-dependent power over an impedance is a sinusoidal function, consisting of two parts: a unidirectional part with non-zero average, and a part with average zero that is alternately positive and negative. The average of the first part is called the active power P, and the amplitude of the second part is called the reactive power Q:

$$P = |V||I| \cos \phi \tag{2.9a}$$
$$Q = |V||I| \sin \phi \tag{2.9b}$$

Here, $\phi = \delta - \theta$ is the power factor angle, and $\cos \phi$ is the power factor. The active power P is also called the real power or the average power, and the reactive power Q is also called the imaginary power.

The corresponding phasor is the complex power:

$$S = VI^* \tag{2.10a}$$
$$= P + \mathrm{i}Q \tag{2.10b}$$

where $[\cdot]^*$ denotes the complex conjugate. Note that $P = \mathrm{Re}(S)$ and $Q = \mathrm{Im}(S)$. The amplitude of the complex power is called the apparent power.

Complex power, active power, and reactive power all have the same dimension, but for practical reasons S is generally measured in VA (volt-ampere), P in W (watt), and Q in var (volt-ampere reactive).

2.2.3 Resistance, impedance, and admittance

The basic elements of an AC electrical circuit are resistors, inductors, and capacitors. The total impedance phasor for a general element is

$$Z = \frac{\Delta V}{I} = R + \mathrm{i}X \tag{2.11}$$

with ΔV the voltage drop over the element, R the resistance, and X the reactance of the element. When $X > 0$ the element acts as an inductor, when $X < 0$ it acts as a capacitor, and when $X = 0$ it acts as a resistor.

Similarly, for a general element the admittance is given by

$$Y = \frac{I}{\Delta V} = G + \mathrm{i}B \tag{2.12}$$

with G the conductance and B the susceptance.

From (2.11) the voltage drop over an element is given by $\Delta V = ZI$, which can be seen as the extension of Ohm's law from DC to AC circuits.

2.2.4 Transmission lines

To model a transmission line, four line parameters are distinguished: the series resistance, the inductance, the capacitance, and the shunt conductance. Depending on the length L of the transmission line, a different model is used [3]. We consider

a medium-length transmission line, with $80\,\text{km} < L < 240\,\text{km}$, and a short-length transmission line, with $L < 80\,\text{km}$.

We denote the voltage at the sending end of the transmission line by V_i, and at the receiving end by V_j. I_{ij} and S_{ij} denote the current and complex power at the sending end, and I_{ji} and S_{ji} at the receiving end.

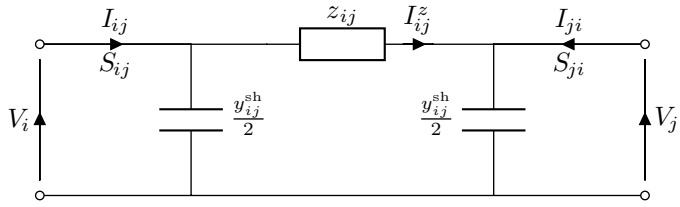

Figure 2.1: Equivalent circuit of a medium-length transmission line ($80\,\text{km} < L < 240\,\text{km}$).

The equivalent circuit of a medium-length transmission line is shown in Figure 2.1. It consists of the series impedance z_{ij} of the line, and the shunt impedance y_{ij}^{sh} of the line, which is divided equally over both ends of the line. The shunt conductance g^{sh} is generally negligibly small, such that $y^{\text{sh}} = \mathrm{i}b^{\text{sh}}$. This model for the medium-length transmission line is also called the π-line model.

Using Kirchhoff's current law, (2.11), and (2.12), the current at the sending end of the line is given by

$$I_{ij} = y_{ij}(V_i - V_j) + \mathrm{i}\frac{b_{ij}^{\text{sh}}}{2}V_i \tag{2.13}$$

The active and reactive powers at the sending end of the line are obtained by substituting the current (2.13) into the complex power equation (2.10):

$$P_{ij} = g_{ij}|V_i|^2 - |V_i||V_j|\left(g_{ij}\cos\delta_{ij} + b_{ij}\sin\delta_{ij}\right) \tag{2.14a}$$

$$Q_{ij} = -b_{ij}|V_i|^2 - |V_i||V_j|\left(g_{ij}\sin\delta_{ij} - b_{ij}\cos\delta_{ij}\right) - \mathrm{i}\frac{b_{ij}^{\text{sh}}}{2}|V_i|^2 \tag{2.14b}$$

where $\delta_{ij} := \delta_i - \delta_j$. Similar expressions hold for the active and reactive powers at the receiving end of the line:

$$P_{ji} = g_{ij}|V_j|^2 - |V_i||V_j|\left(g_{ij}\cos\delta_{ij} - b_{ij}\sin\delta_{ij}\right) \tag{2.15a}$$

$$Q_{ji} = -b_{ij}|V_j|^2 + |V_i||V_j|\left(g_{ij}\sin\delta_{ij} + b_{ij}\cos\delta_{ij}\right) - \mathrm{i}\frac{b_{ij}^{\text{sh}}}{2}|V_j|^2 \tag{2.15b}$$

The equivalent circuit of a short-length transmission line is shown in Figure 2.2. It consists of the series impedance z_{ij} of the line only.

The current at the sending end of the line is given by

$$I_{ij} = y_{ij}(V_i - V_j) \tag{2.16}$$

The active and reactive power at the sending end of the line are given by

$$P_{ij} = g_{ij}|V_i|^2 - |V_i||V_j|\left(g_{ij}\cos\delta_{ij} + b_{ij}\sin\delta_{ij}\right) \tag{2.17a}$$

$$Q_{ij} = -b_{ij}|V_i|^2 - |V_i||V_j|\left(g_{ij}\sin\delta_{ij} - b_{ij}\cos\delta_{ij}\right) \tag{2.17b}$$

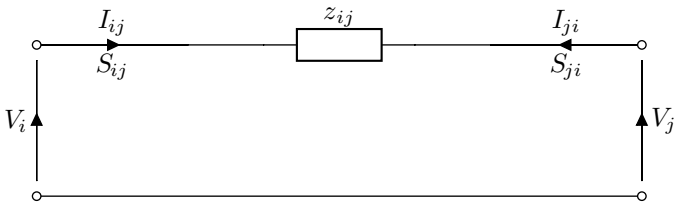

Figure 2.2: Equivalent circuit of a short-length ($L < 80\,\text{km}$) transmission line.

Similarly, at the receiving end of the line, the active and reactive power are:

$$P_{ji} = g_{ij}|V_j|^2 - |V_i||V_j|\left(g_{ij}\cos\delta_{ij} - b_{ij}\sin\delta_{ij}\right) \tag{2.18a}$$

$$Q_{ji} = -b_{ij}|V_j|^2 + |V_i||V_j|\left(g_{ij}\sin\delta_{ij} + b_{ij}\cos\delta_{ij}\right) \tag{2.18b}$$

2.3 Heating systems

Water transports heat through the pipes in a heating system. Steady-state models for a pipe consist of a hydraulic model and a thermal model. We also give a (thermal) model for heat loads. For more details on models in a heating system, see for instance [4] or [10].

In heating systems, the head h is frequently used instead of the pressure. It is related to the pressure by

$$h = \frac{p}{\rho g} \tag{2.19}$$

with g the gravitational constant and ρ the density of the water.

2.3.1 Hydraulic pipe flow

Both water and gas are fluids. As such, a similar model is used to describe flow through a pipe in a heating system as is done in a gas system.

For the water flow, we assume steady-state one-directional incompressible flow. The water flow through a pipe can then be modeled similar to the gas flow.

Denote the water mass flow in the pipe by m, and the pressure at the start and end of the pipe by p_i and p_j. The general steady-state flow equations is then given by

$$m = C^h \text{sign}\left(\Delta p\right)\sqrt{\frac{|\Delta p|}{\text{f}}} \tag{2.20}$$

For incompressible water flow, there is no difference between a high-pressure and a low-pressure system. The pressure drop is given by

$$\Delta p = p_i - p_j \tag{2.21}$$

and the pipe constant is given by

$$C^h = \frac{\pi}{8}\sqrt{\frac{2\rho D^5}{L}} \tag{2.22}$$

with ρ the density of the water.

Various friction factor models are used, resulting in different pipe flow models, as is the case for the gas network. The friction factor models are equivalent to the ones used for gas.

2.3.2 Hydraulic resistor

A hydraulic resistor gives a hydraulic model for a general element in a heating system. It can, for instance, be used as a simplified pipe-flow model.

Denote the water mass flow through the element by m, and the pressure at the start and end of the element by p_i and p_j. The general steady-state flow equations is then given by

$$m = C^h \text{sign}\,(\Delta p)\,\sqrt{|\Delta p|} \tag{2.23}$$

with C^h a constant, and Δp given by (2.21).

Comparing the general hydraulic equation of a resistor (2.23) with that of a pipe (2.20), the resistor can be seen as a pipe with constant friction factor.

2.3.3 Heat power and heat loads

The heat power φ is the internal energy flow of a fluid:

$$\varphi = C_p m T \tag{2.24}$$

with C_p the specific heat, m the mass flow, and T the temperature of the fluid.

Heat loads are elements of the heating system where heat is injected into, or taken out of, the system. Essentially, heat is exchanged between the heating system and its surroundings, such that heat loads are generally modeled as heat exchangers. A basic model for a heat exchanger expresses the total injected heat power $\Delta\varphi$ of a heat load as the change in the heat power directly before and directly after the heat exchanger. Since a heat load is a connection between the supply and the return line of the heating system, we use (2.24) for the heat power at the supply and return line sides of the heat exchanger to obtain the total injected heat power of a heat load:

$$\Delta\varphi = C_p m\,(T^s - T^r) \tag{2.25}$$

with m the water mass flow through the heat exchanger, and T^s and T^r the temperature at the supply line and return line side of the heat exchanger respectively.

If the heat load is a source, water flows from the return line to the supply line and heat power is injected into the heating system. Conversely, if a heat load is a sink, water flows from the supply line to the return line and heat power is taken from the heating system.

2.3.4 Thermal pipe flow

Heat is transported in the heating system through pipes. Convection transfers the heat through a pipe by transporting water. We assume conductive heat transfer within the fluid is negligible. There is conductive heat transfer from pipes to the surroundings, due to a temperature difference between the water in the pipes and the

surroundings. Furthermore, we assume steady-state one-directional flow, the thermal resistance of the pipe is independent of direction of flow, and we assume there is no direct thermal interaction between supply and return line (e.g. [10]).

We model the conductive heat transfer to the surroundings by Newton's law of cooling:

$$\varphi = hA\Delta T \tag{2.26}$$

with area A, heat transfer coefficient h, and temperature difference ΔT. Newton's law of cooling is analogous to Ohm's law. If the heat power φ is analogous to the current I, and the temperature difference ΔT is analogous to the voltage drop ΔV, (2.26) is analogous to (2.12), where hA can be seen as a thermal admittance.

Consider a pipe with length L, diameter D, water mass flow m, and an ambient temperature outside the pipe of T^a. The energy flows through a small volume of the pipe are shown in Figure 2.3. Conservation of energy within this volume element gives

$$C_p m \frac{\mathrm{d}T}{\mathrm{d}x} = \lambda \left(T - T^a\right) \tag{2.27}$$

where the heat transfer coefficient is defined as $\lambda := hA = h\pi D$.

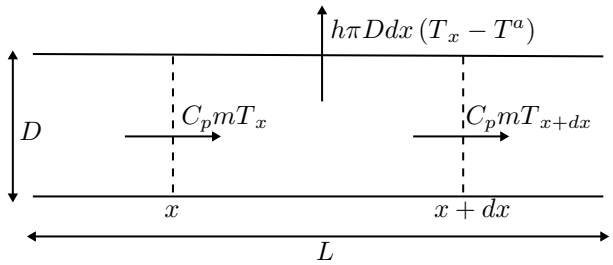

Figure 2.3: Pipe with energy flow into, and out of, a small volume of the pipe.

Denoting the temperature at the start of the pipe by T^{start}, and assuming $m > 0$, we can solve (2.27) for the temperature T^{end} at the end of the pipe:

$$T^{\text{end}} - T^a = \exp\left(\frac{-\lambda L}{C_p m}\right)\left(T^{\text{start}} - T^a\right) \tag{2.28}$$

This equation is called the temperature drop equation, and holds for both the supply and the return line. For notational simplicity, we define the temperature drop factor as

$$\psi(m) := \exp\left(\frac{-\lambda L}{C_p m}\right) \tag{2.29}$$

2.4 Conversion units

Many of the coupling units in a MES are conversion units. We give the steady-state models for several of the conversion units listed in Table 1.1.

For notational simplicity, we introduce the energy flow rate E^g of the gas flow rate q, based on the gross heating value (GHV) of the gas:

$$E^g := \text{GHV} q \tag{2.30}$$

2.4.1 Gas-fired generators

The majority of the electrical power in a power grid is generated by a synchronous machine, which converts the mechanical energy of a rotating shaft into electrical energy [3]. The shaft is rotated by the combustion of some fuel, for instance gas. The combination of a synchronous machine with the combustion of gas is called a gas-fired generator (GG).

A basic model for a GG assumes the generator operates at a fixed efficiency:

$$P = \eta E^g \tag{2.31}$$

Here, E^g is the energy of the gas flow rate into the GG, P is the electrical power produced by the GG, and $0 < \eta < 1$ is its efficiency.

A more detailed model takes the heat rate curve and the valve-point effect (VP) into account [11]:

$$E^g = aP^2 + bP + c + \left| d \sin\left(e(P^{\min} - P)\right)\right| \tag{2.32}$$

Here, a, b, c, d, and e are heat rate parameters, and $P^{\min}$ is the minimum amount of power produced by the GG.

2.4.2 Gas boilers

Generation plants in heating systems use a variety of fuels, one of which is (natural) gas (e.g. [4]). A gas boiler (GB) burns gas to create heat. A basic model for a GB assumes the boiler operates at a fixed efficiency:

$$\Delta\varphi = \eta E^g \tag{2.33}$$

Here, E^g is the energy of the gas flow rate into the GB, $\Delta\varphi$ is the heat power produced by the GB, and $0 < \eta < 1$ is its efficiency.

A more detailed model takes the part-load effect into account (e.g. [11] or [12]):

$$E^g = \frac{\Delta\varphi + r_1 E_{ss}}{r_2} \tag{2.34}$$

Here, r_1 and r_1 are parameters related to the part load effect, and E_{ss} is the steady-state input per cycle.

2.4.3 Combined heat and power plants

A combined heat and power plant (CHP) uses the excess heat from (electrical) generators to also generate heat power. In the most basic form, the heat produced during the generation of electrical power, for instance during the combustion of gas in a GG, is transferred to the heating system through a heat exchanger. CHPs are generally more thermodynamically advanced than classical boilers, such that CHPs require significantly less fuel (e.g. [4]).

Several measures are used to determine the overall efficiency of a CHP. A basic model for CHP assumes a fixed total efficiency (e.g. [4]):

$$\eta E^g = P + \Delta\varphi \tag{2.35}$$

Here, E^g is the energy of the gas flow rate into the CHP, P and $\Delta\varphi$ are the active power and the heat power produced by the CHP, and $0 < \eta < 1$ is its total efficiency.

Another basic model assumes fixed electrical and thermal efficiencies (e.g. [4]):

$$E^g = \frac{P}{\eta^{ge}} + \frac{\Delta\varphi}{\eta^{gh}} \tag{2.36}$$

Here, $0 < \eta^{ge} < 1$ is the electrical efficiency and $0 < \eta^{gh} < 1$ is the thermal efficiency.

A more detailed model, also using a total efficiency η, takes the part-load effect into account ([11] or [13]):

$$\eta E^g = P + \Delta\varphi \tag{2.37a}$$

$$P = P(\Delta\varphi, T^s) = a\Delta\varphi + bT^s + d - w(\Delta\varphi) \tag{2.37b}$$

$$w(\Delta\varphi) = \begin{cases} 0, & L_1\Delta\varphi^{\max} \le \Delta\varphi \le \Delta\varphi^{\max} \\ (L_1\Delta\varphi^{\max} - \Delta\varphi)r_1, & L_2\Delta\varphi^{\max} \le \Delta\varphi \le L_1\Delta\varphi^{\max} \\ (L_1\Delta\varphi^{\max} - \Delta\varphi)r_1 \\ +(L_2\Delta\varphi^{\max} - \Delta\varphi)r_2, & \Delta\varphi^{\min} \le \Delta\varphi \le L_2\Delta\varphi^{\max} \end{cases} \tag{2.37c}$$

Here, a, b, and d are model parameters of the CHP, $r_1, r_2 > 0$ are parameters related to the part-load effect, $0 \le L_2 < L_1 \le 1$ are limits (0 indicated no load, and 1 indicates full load), and $\Delta\varphi^{\min}$ and $\Delta\varphi^{\max}$ are the minimum and maximum heat power produced by the CHP.

2.4.4 Energy hubs

The energy hub (EH) concept was first introduced in [6], and models a coupling between different energy carriers by relating the input and output energy of the EH through a coupling matrix. An EH is not a physical conversion unit, rather, it is a model representation of one or several units. Within the EH, transmission of the energy of each carrier is not taken into account. Unidirectional flow from input to output is assumed, such that the coupling matrix is constant or a function of the input power only:

$$\boldsymbol{E}_{\text{out}} = C(\boldsymbol{E}_{\text{in}})\boldsymbol{E}_{\text{in}} \tag{2.38}$$

Assuming a MES consisting of gas, electricity, and heat, $\boldsymbol{E}_{\text{out}} = \begin{pmatrix} E^g_{\text{out}} & P_{\text{out}} & \Delta\varphi_{\text{out}} \end{pmatrix}^T$ is the vector of output energies, $\boldsymbol{E}_{\text{in}} = \begin{pmatrix} E^g_{\text{in}} & P_{\text{in}} & \Delta\varphi_{\text{in}} \end{pmatrix}^T$ is the vector of input energies, and C is the coupling matrix:

$$C = \begin{pmatrix} c^{gg} & c^{eg} & c^{hg} \\ c^{ge} & c^{ee} & c^{he} \\ c^{gh} & c^{eh} & c^{hh} \end{pmatrix} \tag{2.39}$$

Each entry $c^{\alpha\beta}$ is the coupling factor to convert energy of carrier α into energy of carrier β. This coupling factor can be a (nonlinear) function of the input power, such that $c^{\alpha\beta} = f^{\alpha}(E^{\beta})$ with $E^{\beta}_{\text{in}} \in \boldsymbol{E}_{\text{in}}$.

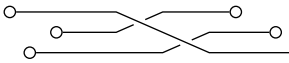

CHAPTER 3

Energy networks

Energy systems have their own terminology, which varies per carrier. Moreover, the transport of energy throughout the systems is governed by different physical laws. Mathematically, all energy systems can be represented by a graph or a network.

A network representation for SC energy system is common practice for steady-state load flow computations and for optimal flow problems. For instance, a power grid is usually represented by buses which are connected by lines.

The currently available LF models for MES do not state how the networks of SCNs can be combined into one MCN. Some couplings between energy systems, while possible in practice, can lead to model problems. To avoid such model problems, a good description of integrated networks of multiple energy carriers is very important. In this chapter, we provide a systematic analysis of the SCNs to determine how energy systems of different carriers can be combined into one MCN.

A comprehensive definition of a single-carrier energy system as a SCN, with corresponding LF models for the network elements, allows for a systematic analysis of coupling SCNs into an MCN. The existing SC network representations show a certain equivalence among the various carriers, despite the differences in the physical systems. We exploit this equivalence to define a network representation of a general energy system.

We introduce a coupling node to connect the SC networks into one integrated MC network. This coupling node can represent various coupling units. Load flow equations are associated with the network elements, including the coupling node. Therefore, we have developed a generic and uniform network representation for general MES

This chapter is based on the article:

Anne S. Markensteijn, Johan E. Romate, and Cornelis Vuik. A graph-based model framework for steady-state load flow problems of general multi-carrier energy systems. *Applied Energy*, 280:115286, December 2020. ISSN 0306-2619. doi: 10.1016/j.apenergy.2020.115286,

and additional work.

consisting of gas, electricity, and heat. This comprehensive network representation makes it possible to describe integrated energy systems in a very effective way.

This chapter first gives terms and definitions for graphs and networks. Using these definitions, the graph or network representation for the SC networks is given, including the LF variables and equations for each network element. Finally, the coupling node is introduced, and the graph or network representation of a MES is given, including the LF variables and equations.

3.1 Graph representation

3.1.1 Terms and definitions

A graph $\mathcal{G}$ is a pair $(\mathcal{V}, \mathcal{E})$, where $\mathcal{V}$ is a set of nodes or vertices v_i and $\mathcal{E}$ is a set of links or edges e_k. A link is a set of two nodes, $e_k = \{v_i, v_j\}$, or an ordered pair of nodes, $e_k = (v_i, v_j)$. A graph is directed if all links in $\mathcal{E}$ are ordered, and a graph is undirected if none of the links are ordered.

A network is a graph, directed or not, with an associated physical model. If the associated model is a representation of an energy transportation system, the network is called an energy transportation network. In such a network, the energy is transported along the links. An energy transportation network is also simply called an energy network, or a flow network.

Energy or flow enters the energy system through generation units or sources. It leaves the system at end-users. In a network, flow enters through sources and leaves through sinks, which are both called loads or terminal nodes. In the graph, these terminal nodes are a subset of $\mathcal{V}$. Inflow and outflow of a graph or network can be represented by values associated with the terminal nodes. However, flow throughout the rest of the network is associated with links or edges. For consistency, it is convenient to see inflow and outflow of a terminal node as flow through an open link connected to that node. These open links, connected to a single node only, are called terminal links. They are also called half links, as they are half of a normal link.

By definition, a terminal link can only be connected to a terminal node. Conversely, a node without a terminal link connected to it is not a terminal node. The direction of a terminal link is defined as outgoing, such that the terminal node acts as a source if the flow is opposite in direction to the terminal link, and acts as a sink if the flow is in the same direction as the terminal link. These terminal links are included explicitly in the network representation of an energy system.

Let $\mathcal{T}$ be the set of terminal links t_l. Then an energy network is represented by the collection $\mathcal{N} = \{\mathcal{V}, \mathcal{E}, \mathcal{T}\} = \{\mathcal{G}, \mathcal{T}\}$. Hence, $\mathcal{N}$ is directed if $\mathcal{G}$ is directed, and undirected if $\mathcal{G}$ is undirected.

For notational simplicity, i is used as the node index (v_i), k as the link index (e_k), and l as the terminal link index (t_l). We denote the number of nodes, links, and terminal links in the sets by $|\mathcal{V}|$, $|\mathcal{E}|$, and $|\mathcal{T}|$, respectively.

The incidence matrix describes the interconnection between nodes and links in a graph. An element of the $|\mathcal{V}| \times |\mathcal{E}|$ incidence matrix A is defined as

$$A_{ik} = \begin{cases} 1, & \text{if } e_k = \{v_i, v_j\} \\ 0, & \text{otherwise} \end{cases}$$

for every link $e_k \in \mathcal{E}$ and every node $v_i \in \mathcal{V}$ of an undirected graph $\mathcal{G} = (\mathcal{V}, \mathcal{E})$. Similarly, for a directed graph the elements of A are defined as

$$A_{ik} = \begin{cases} 1, & \text{if } e_k = (v_j, v_i) \\ -1, & \text{if } e_k = (v_i, v_j) \\ 0, & \text{otherwise} \end{cases} \tag{3.1}$$

3.1.2 Representing energy systems as energy networks

To represent an energy system as an energy network, each element of the energy system needs to be represented by a network element, and needs to have a physical model associated with it. By definition, the possible network elements are (terminal) nodes and (terminal) links. This means that any SCNs consists of these elements, even though the physical energy systems are different for each carrier. Some system elements are carrier specific, such as transformers in a power grid, but others are more general, such as an end-user. Even then, an end-user for a power grid is not the same as that of a district heating system. In an energy network, both are represented by a terminal node, with one or more terminal links connected to it. The difference between the two end-users is reflected by different physical models associated with the terminal nodes and terminal links.

Physical quantities, physical models, and model parameters of system elements are associated with network elements. Quantities associated with nodes are called nodal variables, and those associated with (terminal) links are called (terminal) link variables. Since terminal links are half of a normal link, they have the same type of quantities associated with them as links. Similarly, models associated with nodes are called nodal equations, and those associated with (terminal) links are called (terminal) link equations.

Some variables associated with terminal links are seen as nodal variables. For instance, demand of an end-user is generally seen as a nodal variable. To distinguish between (terminal) link and nodal variables, the nodal variables are called injected. If a node has more than one terminal link connected to it, the injected flow or power is the sum of all the flows or powers on the terminal links.

The physical models that are associated with network elements, are functions that depend on these variables. A nodal equation is a function of the nodal variables and of the (terminal) link variables of the links connected to that node. A link equation is a function of the link variables and of the nodal variables of two nodes which are connected by that link. A terminal link equation is a function of the terminal link variables and of the terminal node variables. There can be additional physical models, such as Kirchhoff's second law, involving several network elements.

3.2 Single-carrier energy networks

The SC gas, electricity, and heat systems all have their own terminology and different physical system. We use the general graph definition to represent each system as a SC energy network. There are two physical laws that hold for all of these SC networks, which are used in LF simulations.

Table 3.1: LF variables per network element, for each carrier.

Carrier	Node	Link	Terminal link
Gas	pressure p	flow q	flow q
Electricity	voltage angle δ	current I	current I
	voltage amplitude $\lvert V\rvert$	active power P	active power P
		reactive power Q	reactive power Q
Heat	pressure p	flow m	flow m
	temperatures T^s, T^r	temperatures T^s, T^r	temperatures T^s, T^r
		heat powers φ^s, φ^r	injected heat power $\Delta\varphi$

The first is nodal conservation of mass or energy, which is called Kirchhoff's first law or Kirchhoff's current law in power grids. This is a nodal equation, which states that the sum of the incoming and outgoing mass flow or energy is zero.

The second is Kirchhoff's second law, which states the sum of potential differences over a loop must be zero. Since this law concerns a summation over a loop, it is neither a nodal equation nor a link equations. However, it is often used in LF analysis to reduce the size of the system of nonlinear equations.

In the following sections, we give the network representation of a gas, electricity, and heating system. Furthermore, we give the variables and equations used in LF simulation, and the network elements they are associated with. The variables are summarized in Table 3.1.

3.2.1 Gas networks

A gas system is represented by a directed network $\mathcal{N}^g = \{\mathcal{V}^g, \mathcal{E}^g, \mathcal{T}^g\}$. A node can represent a sink, a source, or a junction. A junction is an intersection of pipes where the gas is redistributed. It is represented by a terminal node with zero in- or outflow. This means that all nodes in a gas network are terminal nodes. A link can represent a pipe, a compressor, a pressure regulator, or a valve.

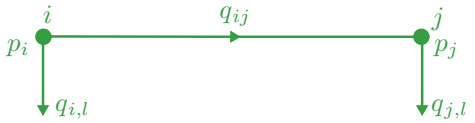

Figure 3.1: Network representation of a gas network, showing quantities of interest for LF and the network elements they are associated with. Arrows on (terminal) links show defined direction, not actual direction of flow.

The variables of interest for basic steady-state LF simulation are nodal pressure p and (terminal) link gas flow rate q. These variables, and the network elements they are associated with are shown in Table 3.1 and in Figure 3.1. This figure shows a gas network consisting of two nodes connected with one link. The arrows in this directed graph show defined direction of flow. If node i is a source, such that node j is a sink, then the flow of terminal link l of node i is opposite to the defined direction. That is, $q_{i,l} < 0$ and q_{ij}, $q_{j,l} > 0$.

Load flow equations

For steady-state LF, a basic gas network can be completely described by conservation of mass and the link equations [2]. In every node $v_i \in \mathcal{V}^g$, conservation of mass holds:

$$F_i^q := \sum_{j,\, j\neq i} q_{ji} - \sum_{j,\, j\neq i} q_{ij} - q_i = 0 \tag{3.2}$$

The first term are all link flows going into node i, the second term are all outgoing link flows, and the final term is the injected gas flow $q_i := \sum_l q_{i,l}$ of node i.

For every link $e_k \in \mathcal{E}^g$ from node $v_i \in \mathcal{V}^g$ to node $v_j \in \mathcal{V}^g$, the general link equation is given by:

$$F_k\left(q_k, p_i, p_j\right) = 0 \tag{3.3}$$

It generally holds that $q_{ij} = -q_{ji}$.

If a link represents a pipe, (2.1) is used for the link equation. The pipe flow equation (2.1) can either express the link gas flow rate as a function of pressures, or express the pressure drop as a function of link flow. We denote the link equation using the former as $F_k^{q(\Delta p)}$, and as $F_k^{\Delta p(q)}$ using the latter, such that for a pipe we have

$$F_k^{q(\Delta p)}\left(q_k, p_i, p_j\right) = q_k - C_k^g \operatorname{sign}\left(\Delta p_k\right) \mathrm{f}_k^{-\frac{1}{2}} \left|\Delta p_k\right|^{\frac{1}{2}} = 0 \tag{3.4a}$$

$$F_k^{\Delta p(q)}\left(q_k, p_i, p_j\right) = \Delta p_k - \left(C_k^g\right)^{-2} \mathrm{f}_k |q_k| q_k = 0 \tag{3.4b}$$

These equations are generally nonlinear in the pressures, unless (2.1) is used for a low-pressure system. Then, Δp_k is linear in p_i and p_j according to (2.3), such that (3.4b) is linear in the pressures.

If a link represents a compressor, the link equation (3.3) is given by (2.7):

$$F_k\left(p_i, p_j\right) = r_k p_i - p_j = 0 \tag{3.5}$$

which is independent of q_k.

3.2.2 Electrical networks

A balanced three-phase AC power grid is represented by an undirected network $\mathcal{N}^e = \{\mathcal{V}^e, \mathcal{E}^e, \mathcal{T}^e\}$. A node represents a bus, sink, or source. As in the gas network, a bus without in- or outflow is represented by a terminal node with zero in- or outflow. A link represents a transmission line or a transformer.

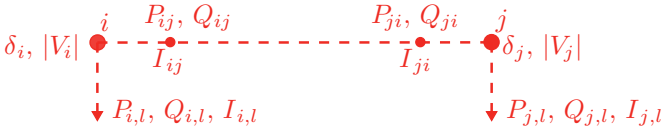

Figure 3.2: Network representation of a power grid, showing quantities of interest for LF, and the network elements they are associated with. Arrows on (terminal) links show defined direction.

The variables of interest for basic steady-state LF simulation are nodal voltage V, (terminal) link current I, and (terminal) link complex power S. These variables, and

the network elements they are associated with are shown in Table 3.1 and in Figure 3.2. This figure shows an electrical network consisting of two nodes connected with one link. The complex power S is divided into active power P and reactive power Q using (2.10b), and the voltage V is represented by its amplitude $|V|$ and angle δ using (2.8b). The arrows of the terminal link in this graph show defined direction of flow. If node i is a source, such that node j is a sink, then the flow of terminal link l of node i is opposite to the defined direction. That is, $P_{i,l} < 0$ and $P_{j,l} > 0$.

Load flow equations

Using an AC steady-state approximation, a power grid is completely described by Kirchhoff's current law, link equations, and the complex power equation [3]. In every node $v_i \in \mathcal{V}^e$, Kirchhoff's current law holds:

$$F_i^I := -\sum_{j,\, j\neq i} I_{ij} - I_i = 0 \tag{3.6}$$

with $I_i := \sum_l I_{i,l}$ the injected current of node i. Furthermore, the complex power equation (2.10a) holds in every node:

$$F_i^S := S_i - V_i (I_i)^* = 0 \tag{3.7}$$

with $S_i := \sum_l S_{i,l}$ the injected complex power.

For every link $e_k \in \mathcal{E}^e$ from node $v_i \in \mathcal{V}^e$ to node $v_j \in \mathcal{V}^e$, one or more general link equations hold:

$$F_k \left(I_{ij}, I_{ji}, S_{ij}, S_{ji}, V_i, V_j\right) = 0 \tag{3.8}$$

If a link represents a medium-length transmission line, (2.13)–(2.15) can be used for the link equations. Similarly, (2.16)–(2.18) can be used as the link equations for a link representing a short-length transmission line.

Most elements of the power grid that are represented by links, such as transmission lines, are subject to losses. In those cases, it holds that $I_{ij} \neq -I_{ji}$, $P_{ij} \neq -P_{ji}$, and $Q_{ij} \neq -Q_{ji}$. The power loss over a link is defined as the difference between the power at both ends:

$$S_k^{\text{loss}} = S_{ij} + S_{ji} \tag{3.9}$$

For electrical networks without dummy links (see Section 3.3.2), the admittance matrix is generally used (e.g. [3]). This is an $|\mathcal{V}^e| \times |\mathcal{V}^e|$ matrix Y, with off-diagonal elements equal to the negative value of the admittance between node i and node j, and diagonal elements equal to the sum of all admittances connected to node i. Consider, for example, a network where all links represent a medium-length transmission line. From (2.13) it follows that, for node i, $Y_{ij} = -y_{ij}$ and $Y_{ii} = \sum_{j,j\neq i} (y_{ij} + \mathrm{i} b_{ij}^{\text{sh}}/2)$.

3.2.3 Heat networks

The physical heating system consists of a supply line and return line, connected to each other through loads. Hence, the hydraulic part of the heat network is a closed system. The water never enters or leaves the system during operation. Heat is injected

into or extracted from the water in the network through heat exchangers at the loads. Figure 3.3 gives a model representation of a source connected to a sink by a pipe. Here, $[\cdot]^s$ and $[\cdot]^r$ indicate that a quantity is associated with the supply line or return line, respectively.

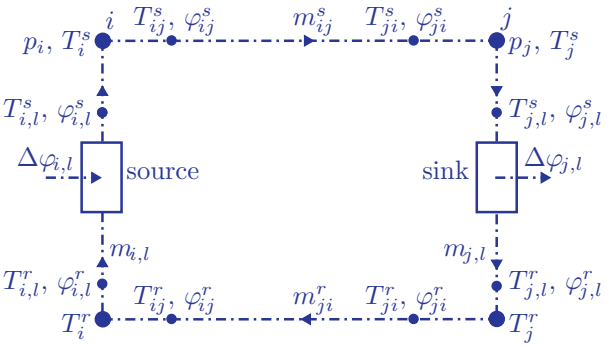

Figure 3.3: Model representation of a heating system, showing quantities of interest for LF and the elements they are associated with. Arrows show actual direction of the water flow.

We assume that the water flow in the return line is opposite in direction, but equal in size, to the water flow in the supply line [14]. The return line is not modeled explicitly, and the hydraulic part of the system is no longer closed. A heating system is then represented as a directed network $\mathcal{N}^h = \{\mathcal{V}^h, \mathcal{E}^h, \mathcal{T}^h\}$. A node represents a junction, sink, or source. A junction is an intersection of pipes where the water is redistributed. A junction has no connection between the supply and return line, so it does not have a terminal link. A pipe in the supply line is represented by a link. A terminal link represents a heat exchanger and a connection between supply and return line. We assume that a node can have only sink or only source terminal links connected to it, such that we can call the node a sink or a source respectively.

Figure 3.4 gives the network representation of a source connected to a sink by a single pipe.

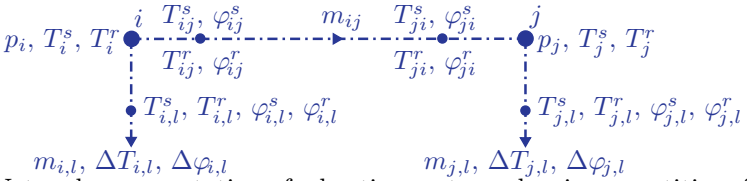

Figure 3.4: Network representation of a heating system, showing quantities of interest for LF and the network elements they are associated with. Arrows on (terminal) links show defined direction.

The variables of interest for basic steady-state LF simulations are pressure p, mass flow m, temperature T, and heat power φ. The temperatures are different in the supply and return line, so both the supply temperature T^s and the return temperature T^r are used as variables for a (terminal) link. These variables are also shown in Table 3.1 and in Figures 3.3 and 3.4, where the latter also shows the network elements that the variables are associated with.

The arrows of the (terminal) links in the directed graph in Figure 3.4 show defined direction of flow. We define $m_{ij} := m^s_{ij}$. By assumption with respect to the flow in the return line it holds that $m^r_{ij} = -m^s_{ij}$. Moreover, we assume $m_{ji} = -m_{ij}$, which holds for most physical elements represented by a link. If node i is a source, water flows from the return line to the supply line. The flow of terminal link l of node i is then opposite to the defined direction, such that $m_{i,l} < 0$. Conversely, with node j a sink, we have $m_{j,l} > 0$.

Heat enters or leaves the network only through terminal links, or as a loss over a pipe. Furthermore, we assume the conductive heat transfer within the fluid is negligible. This means that the temperature at the start of a link is equal to the nodal temperature, where the start and end of a link is defined with respect to actual direction of flow. For a link k from node i to node j, the temperatures in the supply line are given by:

$$T_k^{s,\text{start}} = \begin{cases} T^s_{ij} = T^s_i, & m_{ij} \geq 0 \\ T^s_{ji} = T^s_j, & m_{ij} < 0 \end{cases} \tag{3.10a}$$

$$T_k^{s,\text{end}} = \begin{cases} T^s_{ji}, & m_{ij} \geq 0 \\ T^s_{ij}, & m_{ij} < 0 \end{cases} \tag{3.10b}$$

Similarly, for the link temperatures in the return line we have

$$T_k^{r,\text{start}} = \begin{cases} T^r_{ji} = T^r_j, & m_{ij} \geq 0 \\ T^r_{ij} = T^r_i, & m_{ij} < 0 \end{cases} \tag{3.11a}$$

$$T_k^{r,\text{end}} = \begin{cases} T^r_{ij}, & m_{ij} \geq 0 \\ T^r_{ji}, & m_{ij} < 0 \end{cases} \tag{3.11b}$$

This also holds for terminal links. The supply temperature of a terminal link that represents a sink is equal the nodal supply temperature. Conversely, the return temperature of a terminal link that represents a source is equal to the nodal return temperature. That is, for a terminal link l connected to node i, we have

$$T^s_{i,l} = T^s_i, \quad m_{i,l} > 0 \tag{3.12a}$$

$$T^r_{i,l} = T^r_i, \quad m_{i,l} < 0 \tag{3.12b}$$

It is convenient to use the temperature difference $\Delta T_{i,l}$ over a terminal link, and injected heat power $\Delta\varphi_{i,l}$ of a terminal link:

$$\Delta T_{i,l} = T^s_{i,l} - T^r_{i,l} \tag{3.13a}$$

$$\Delta\varphi_{i,l} = \varphi^s_{i,l} + \varphi^r_{i,l} \tag{3.13b}$$

If the terminal link represents a source, then $m_{i,l}$, $\Delta\varphi_{i,l} < 0$. Conversely, $m_{i,l}$, $\Delta\varphi_{i,l} > 0$ if the terminal link represents a sink.

Load flow equations

The load flow model for a heat network consists of a hydraulic and a thermal part. Using a steady-state approximation, the hydraulic part is similar to the model for

a gas network, such that conservation of mass holds in every node $v_i \in \mathcal{V}^h$, and a hydraulic link equation holds for every link $e_k \in \mathcal{E}^h$ from node $v_i \in \mathcal{V}^h$ to node $v_j \in \mathcal{V}^h$. The thermal part is completely described by conservation of energy, thermal link equations, and the heat power equation.

In every node $v_i \in \mathcal{V}^h$, conservation of mass holds:

$$F_i^m := \sum_{j,\, j\neq i} m_{ji} - \sum_{j,\, j\neq i} m_{ij} - m_i = 0 \tag{3.14}$$

The first term are all link flows going into node i, the second term are all outgoing link flows, and the final term is the injected mass flow $m_i := \sum_l m_{i,l}$ of node i.

For every link $e_k \in \mathcal{E}^h$ from node $v_i \in \mathcal{V}^h$ to node $v_j \in \mathcal{V}^h$, the general hydraulic link equation is given by:

$$F_k\left(m_k, p_i, p_j\right) = 0 \tag{3.15}$$

If a link represents a pipe, (2.20) is used for the link equation. For heat networks, the pipe flow is generally expressed as a function of the pressures:

$$F_k\left(m_k, p_i, p_j\right) = \Delta p_k - (C_k^h)^{-2} \mathrm{f}_k |m_k| m_k = 0 \tag{3.16}$$

This link equation is nonlinear in the mass flow, and linear in the pressures, since (2.21) is used for Δp_k. Furthermore, it holds that $m_{ij} = -m_{ji}$.

For the thermal part, conservation of energy holds in every node $v_i \in \mathcal{V}^h$, both in the supply line and in the return line:

$$F_i^{s,\varphi} = \sum_{j,\, j\neq i} \varphi_{ij}^s + \sum_{j,\, j\neq i} \varphi_{ji}^s + \sum_l \varphi_{i,l}^s \tag{3.17a}$$

$$F_i^{r,\varphi} = \sum_{j,\, j\neq i} \varphi_{ij}^r + \sum_{j,\, j\neq i} \varphi_{ji}^r + \sum_l \varphi_{i,l}^r \tag{3.17b}$$

Using the heat power equation (2.24) and using that $m_{ij} = -m_{ji}$, we determine the heat powers in de directed network, taking into account the defined direction of flow. The link heat powers are:

$$\begin{aligned} \varphi_{ij}^s &= C_p m_{ij} T_{ij}^s, \qquad \varphi_{ij}^r = -C_p m_{ij} T_{ij}^r \\ \varphi_{ji}^s &= -C_p m_{ij} T_{ji}^s, \quad \varphi_{ji}^r = C_p m_{ij} T_{ji}^r \end{aligned} \tag{3.18}$$

Similarly, the heat powers on a terminal link are:

$$\varphi_{i,l}^s = C_p m_{i,l} T_{i,l}^s \tag{3.19a}$$

$$\varphi_{i\,l}^r = -C_p m_{i,l} T_{i,l}^r \tag{3.19b}$$

Assuming a constant specific heat C_p of the water, and using (3.18) and (3.19) for the heat powers φ, conservation of energy (3.17) reduces to a mixing rule:

$$F_i^{T^s} = \sum_{e_k \in \mathcal{E}_{\mathrm{out}}^h} m_{ij}^s T_{ij}^s - \sum_{e_k \in \mathcal{E}_{\mathrm{in}}^h} m_{ij}^s T_{ji}^s + \sum_l m_{i,l} T_{i,l}^s \tag{3.20a}$$

$$F_i^{T^r} = -\sum_{e_k \in \mathcal{E}_{\mathrm{out}}^h} m_{ij}^s T_{ij}^r + \sum_{e_k \in \mathcal{E}_{\mathrm{in}}^h} m_{ij}^s T_{ji}^r - \sum_l m_{i,l} T_{i,l}^r \tag{3.20b}$$

Here, $\mathcal{E}^h_{\text{out}}$ are all the outgoing links of node i with respect to defined direction of flow. That is, $\mathcal{E}^h_{\text{out}} := \{e_k \in \mathcal{E} | e_k = (v_i, v_j)\}$. Similarly, $\mathcal{E}^h_{\text{in}} := \{e_k \in \mathcal{E} | e_k = (v_j, v_i)\}$ are all the incoming links of node i.

The general thermal link equations for the supply and return line are given by:

$$F_k^{s,\psi}\left(T_k^{s,\text{start}}, T_k^{s,\text{end}}, m_k\right) = 0 \tag{3.21a}$$

$$F_k^{r,\psi}\left(T_k^{r,\text{end}}, T_k^{r,\text{end}}, m_k\right) = 0 \tag{3.21b}$$

The temperatures $T_k^{s,\text{start}}$ and $T_k^{s,\text{end}}$ are given by (3.10), and $T_k^{r,\text{start}}$ and $T_k^{r,\text{end}}$ are given by (3.11). If a link represents a pipe, (2.28) is used for the thermal link equations.

Pipes in a heating network are subject to thermal losses. For the links representing such pipes, it holds that $\varphi_{ij}^s \neq -\varphi_{ji}^s$, and $\varphi_{ij}^r \neq -\varphi_{ji}^r$. The heat power loss over a link is defined as the difference between the heat power at both ends of the link. Since the link is a representation of a pipe in the supply line and a pipe in return line, the total heat power loss over the link is $\varphi_k^{\text{loss}} = \varphi_k^{s,\text{loss}} + \varphi_k^{r,\text{loss}}$, where

$$\varphi_k^{s,\text{loss}} = \varphi_{ij}^s + \varphi_{ji}^s \tag{3.22a}$$

$$\varphi_k^{r,\text{loss}} = \varphi_{ij}^r + \varphi_{ji}^r \tag{3.22b}$$

A terminal link $t_l \in \mathcal{T}^h$ connected to node $v_i \in \mathcal{V}^h$, has a thermal terminal link equation. If the terminal link represents a heat source or sink, (2.25) is used for the terminal link equation:

$$F_{i,l}^{\varphi}\left(m_{i,l}, T_{i,l}^s, T_{i,l}^r, \Delta\varphi_{i,l}\right) = -\Delta\varphi_{i,l} + C_p m_{i,l} \Delta T_{i,l} = 0 \tag{3.23}$$

where $\Delta T_{i,l}$ is given by (3.13a), and $\Delta\varphi_{i,l}$ is given by (3.13b).

3.3 Multi-carrier energy networks

A MES is represented as a multi-carrier network (MCN) by coupling the nodes of SCNs to form one integrated network. Two nodes can be connected in three ways: connect the two nodes by a link, merge the two nodes into one node, or introduce an additional node and connect the nodes to it.

A link is a network component with two flow connections, making it difficult to use as a representation of a coupling involving more than two carriers, such as a CHP. That is, it cannot be used to connect more than two nodes. Moreover, a physical interpretation of a coupling link is not straightforward.

Coupling by merging two nodes is complicated by the nodal variables. Suppose we want to merge two electrical nodes, each with a voltage magnitude $|V|$ and voltage angle δ, into one new electrical node. Some combined $|V|$ and δ must then be defined for this new node, or a node with multiple voltages must be allowed. Coupling two nodes of a different carrier by merging introduces similar difficulties.

Therefore, we couple networks by introducing an additional node, called a coupling node.

3.3.1 Coupling node

No variables are associated with the coupling node, meaning that it does not belong to any of the SCNs. If the coupling node is used to couple networks with the same carrier, the coupling node is called homogeneous. Similarly, it is called heterogeneous when used to couple networks with different carriers. Nodes and links of an SCN are called homogeneous. A network is then called heterogeneous if it has one or more heterogeneous nodes, and homogeneous if it consists of only homogeneous nodes and links.

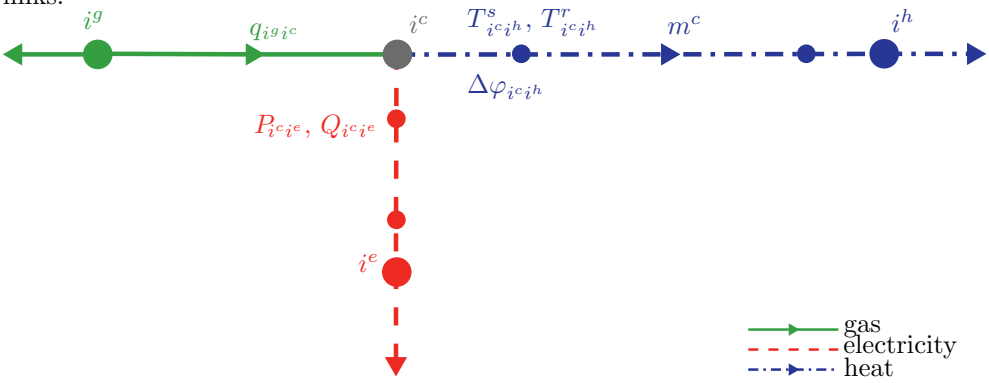

Figure 3.5: Network representation of a coupling node, showing quantities of interest for LF and the network elements they are associated with.

A heterogeneous coupling node can be connected to a (terminal) link of any carrier. However, no variables are associated with the coupling node, so that links representing certain physical components cannot be connected. For instance, a link representing a gas pipe cannot be connected, since the flow model (3.4) associated with the link requires both start and end node to have a nodal pressure p. We introduce a dummy link to couple a (heterogeneous) coupling node to any other node.

Figure 3.5 shows the network representation of a heterogeneous coupling node connecting a gas network, an electrical network, and a heat network. The arrows on the (terminal) links show defined directions, not the actual directions of flow. Hence, the coupling node concept allows for bidirectional flow.

A MES is then represented by a network $\mathcal{N} = \{\mathcal{V}, \mathcal{E}, \mathcal{T}\}$. The vertex set is the collection of all homogeneous SC nodes and all coupling nodes, such that $\mathcal{V} = \mathcal{V}^g \cup \mathcal{V}^e \cup \mathcal{V}^h \cup \mathcal{V}^c$. Similarly, the edges and terminal edges are the collections of all homogeneous SC edges and terminal edges, such that $\mathcal{E} = \mathcal{E}^g \cup \mathcal{E}^e \cup \mathcal{E}^h$ and $\mathcal{T} = \mathcal{T}^g \cup \mathcal{T}^e \cup \mathcal{T}^h$. Hence, the vertex, edge, and terminal edge sets of any two SCN are disjoint.

3.3.2 Dummy links

Dummy links do not represent any physical component, they merely show a connection between nodes. If a dummy link connects a coupling node and a SC node, the dummy link is considered homogeneous and of the same carrier as the SC node. As such, it has the same variables associated with it as any other link of that carrier. These variables are shown in Figure 3.5, at the side of the coupling node only. Similar to

(3.13b), the heat power produced or consumed by the coupling unit is given by

$$\Delta\varphi_{i^c i^h} = \varphi^s_{i^c i^h} + \varphi^r_{i^c i^h} \tag{3.24}$$

Even though dummy links do not represent a physical component, they can be seen as lossless pipes or lines.

A lossless transmission line conserves electrical energy across the line. Therefore, it holds that $I_{i^c i^e} = -I_{i^e i^c}$, $P_{i^c i^e} = -P_{i^e i^c}$, and $Q_{i^c i^e} = -Q_{i^e i^c}$. Indeed, (3.9) then gives $S^{\text{loss}}_k = 0$. A dummy link does not have additional link equations, such that P and Q are independent of V_{i^e} and I.

Similarly, a lossless heat pipe does not lose heat to its surroundings. Therefore, it holds that $\varphi^s_{i^c i^h} = -\varphi^s_{i^h i^c}$, and $\varphi^r_{i^c i^h} = -\varphi^r_{i^h i^c}$. Indeed, (3.22) then gives $\varphi^{s,\text{loss}}_k = \varphi^{r,\text{loss}}_k = 0$. Moreover, it holds that $T^s_{i^c i^h} = T^s_{i^h i^c}$, and $T^r_{i^c i^h} = T^r_{i^h i^c}$. A heat dummy link can be seen as a perfectly insulated pipe. Using (3.10a) and (3.11a) for a heat dummy link, we find

$$\begin{aligned} T^s_{i^c i^h} &= T^s_{i^h i^c} = T^s_{i^h}, \quad m_{i^c i^h} < 0 \\ T^r_{i^c i^h} &= T^r_{i^h i^c} = T^r_{i^h}, \quad m_{i^c i^h} \geq 0 \end{aligned} \tag{3.25}$$

3.3.3 Load flow equations

In every heterogeneous coupling node $v_i \in \mathcal{V}^c$, one or more coupling equations hold. For a coupling node i connected with dummy links to a homogeneous node j of each carrier, we assume the coupling equations to be of the general form:

$$F^{c,E}_i\left(q_{ij},\, P_{ij},\, Q_{ij},\, m_{ij},\, T^s_{ij},\, T^r_{ij},\, \Delta\varphi_{ij}\right) = 0 \tag{3.26}$$

This general form can be easily adjusted if a coupling node has multiple links, or no links, of a carrier connected to it.

Any physical coupling unit for which the model equation(s) are of the form (3.26), can be represented by a (heterogeneous) coupling node. Most conversion units, such as GGs, CHPs, electric boilers (EBs), or P2G units are modeled in such a way. Moreover, the coupling node concept allows for both linear and nonlinear models. For instance, a linear model (2.31) or a nonlinear model (2.32) can be used for the coupling equation (3.26) of a GG.

If a coupling unit produces or consumes heat, one of the coupling equations (3.26) is a heat power equation similar to (3.23). Substituting (3.18) in (3.24) gives the nodal heat power equation for a coupling node:

$$F^{c,\varphi}_i\left(m_{i^c i^h},\, T^s_{i^c i^h},\, T^r_{i^c i^h},\, \Delta\varphi_{i^c i^h}\right) = -\Delta\varphi_{i^c i^h} + C_p m_{i^c i^h}(T^s_{i^c i^h} - T^r_{i^c i^h}) = 0 \tag{3.27}$$

Here, $T^s_{i^c i^h}$ and $T^r_{i^c i^h}$ are given by (3.25). Note that $\Delta\varphi_{i^c i^h} > 0$ if the coupling produces energy, and $\Delta\varphi_{i^c i^h} < 0$ if the coupling consumes energy.

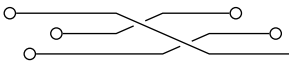

CHAPTER 4

Steady-state load flow problems

As stated in Section 1.2, steady-state load flow (LF) analysis tries to find a solution to the steady-state LF problem. That is, given demands, LF analysis determines the flow of energy carriers through the system, and the values of other quantities, such as voltages and pressures, throughout the system. Load flow problems for SCs systems have been widely studied, but load flow problems for MESs have only been proposed recently.

Two types of models for MESs can be distinguished. The first uses the energy hub (EH) concept for the coupling between SCNs, the other a case specific approach.

The EH concept was first introduced in [6], and later extended or adopted in [15, 16, 17]. The graph representation of the EH is unclear or the connection of the EH to the rest of the network is not described, such that load flow analysis for the entire network is not possible.

The second type of LF models for MESs combines the existing equations for the SCNs and models for the coupling units into one system of equations. This allows for load flow analysis of the full MES, and for a more detailed model of the coupling units. This approach is used in [18, 19, 20, 8, 11, 21, 22]. However, it is not specified how to integrate the single-carrier models using a general coupling component, making it difficult to use this approach for a general MES.

The available load flow models for MESs do not consider the effect of coupling on

---

This chapter is based on the articles:

Anne S. Markensteijn, Johan E. Romate, and Cornelis Vuik. A graph-based model framework for steady-state load flow problems of general multi-carrier energy systems. *Applied Energy*, 280:115286, December 2020. ISSN 0306-2619. doi: 10.1016/j.apenergy.2020.115286,

Anne S. Markensteijn, Johan E. Romate, and Cornelis Vuik. A graph-based framework for steady-state load flow analysis of multi-carrier energy networks. Technical Report 19-01, Delft University of Technology, Delft Institute of Applied Mathematics, 2019,

and additional work.

the system of LF equations. Usually, a coupling model introduces more unknowns than equations. Additional equations or boundary conditions (BCs) are needed for the total system to be solvable. In the models encountered so far, some or all of the energy flows to or from the couplings are assumed known as additional BCs. However, this effectively decouples the integrated system of LF equations of the MES into the separate single-carrier parts, such that the flexibility provided by coupling the energy systems into one MES is not fully used. To obtain a truly integrated model description of a MES, the additional BCs must be imposed elsewhere in the MCN. Not all combinations of load flow equations and BCs for such integrated energy systems (consisting of gas, electricity, and heat) lead to well-posed problems. For good solvability of the integrated load flow problem, the BCs used are of primary importance.

Combining the generic network description of MESs with a thorough analysis of the BCs, we propose a graph-based model framework for steady-state load flow problems of general MESs. LF equations are associated with the various network elements, including the coupling node, see Chapter 3. Collecting all the equations gives the integrated system of equations for steady-state load flow analysis of a MES. This framework makes it possible to describe integrated energy systems in a very efficient way.

In this chapter, we first discuss the need for additional BCs. Then, we describe how to collect the LF equations of the network elements into one integrated system of equations. Various formulations of this system of equations are discussed. Together with the comprehensive graph representation of a MES as detailed in Chapter 3, this gives the graph-based model framework for steady-state load flow problems of general MESs. Finally, we introduce derived variables and the extended LF problem.

4.1 Node types and boundary conditions

Typically, the SCNs have more variables than equations. Therefore, some variables are assumed known, which we call the boundary conditions (BCs) of the network. Even in the SCNs, the choice of BCs is important to formulate a well-posed problem (e.g. [1] for gas and [23] for heat). A BC can be placed on a node, a link, or a terminal link. Usually, they are placed on a (terminal) node or on its terminal link. A node type is assigned to every node based on the known variables.

The standard node types for SCNs are shown in Table 4.1 (e.g. [2] for gas and [3] for electricity). Some of the specified or unknown variables are injected variables, which are actually associated with a terminal link l connected to node i. If there is no ambiguity, nodal and terminal link indices are omitted. Heat nodes that are not a sink or a source are junctions, which are nodes that have no inflow or outflow in the network. In the physical heating system, these corresponds to junctions in the pipelines, without a connection between the supply and the return line.

For the temperatures on the heat nodes and terminal links, assumptions are made based on conservation of energy. For a load node modeling a sink, we use (3.12a) to eliminate $T^s_{i,l}$ as variable. Similarly, we use (3.12b) to eliminate $T^r_{i,l}$ for a source.

For an MCN, the dummy and terminal links of a coupling generally introduce more variables than the coupling node introduces equations. A coupling node i connected to one homogeneous node j of each carrier introduces 6 variables: q_{ij}, P_{ij}, Q_{ij}, m_{ij},

Table 4.1: Standard node types for single-carrier networks.

Network	Node type	Specified	Unknown
Gas	reference	p	q
	load	q	p
Electricity	slack	$\|V\|$, δ	P, Q
	generator (PV)	P, $\|V\|$	Q, δ
	load (PQ)	P, Q	$\|V\|$, δ
Heat	source reference slack	T_i^s, p	T_i^r, $T_{i,l}^s$, $\Delta\varphi$, m
	load (source)	$T_{i,l}^s$ and $\Delta\varphi < 0$	T_i^s, T_i^r, p, m
	load (sink)	$T_{i,l}^r$ and $\Delta\varphi > 0$	T_i^s, T_i^r, p, m
	junction	$m = 0$	T_i^s, T_i^r, p

$\Delta\varphi_{ij}$, and T_{ij}^s or T_{ij}^r. On the other hand, it generally introduces 2 equations: (3.26) and (3.27).

These extra degrees of freedom could be used for optimization purposes. However, for steady-state LF, (additional) BCs are needed in an MCN to make the system well posed. One commonly used option is to prescribe one or more of the coupling energies (e.g. [6, 11, 22, 17]), but this effectively decouples the integrated network. If one or more of the coupling energies are known, the coupling equations of most coupling units can be used to directly determine (some of) the other energies. These energies, combined with the already prescribes ones, can then be used as BCs for the SCNs. In that case, there is no need to model the LF problem as one integrated system of equations, and the advantages provided by a coupling are not fully captured. Therefore, we will assume all coupling (energy) flows unknown. That is, we assume q, P, Q, m, $\Delta\varphi$ on the dummy links connected to the coupling node unknown. If a coupling unit produces or consumes heat, T^s, T^r, or ΔT of the heat dummy link can be assumed known as a BC without decoupling the system of equations. The additionally required BCs are imposed elsewhere in the MCN, that is, they are imposed in the single-carrier parts.

Imposing the additionally required BCs on the homogeneous nodes may lead to new node types, as also observed in [19] for a power grid. Consider, for instance, a gas network connected to a power grid through a GG. Suppose the electrical node to which we couple is a slack node before coupling, such that P and Q are unknown, and $|V|$ and δ are known. We could then replace these unknown input powers with the unknown coupling powers, such that the coupling, or the gas network, could be considered as the slack for the power grid. However, the coupling powers flow into the power grid through a dummy link. Since we want to replace the slack powers with the coupling powers, the total injected power of the electrical node should be zero after coupling. Hence, the electrical node turns into a new node with P, Q, $|V|$, and δ known, called a PQVδ-node.

Table 4.2 gives some, but not all, possible new node types. The names of the node types indicate which variables are assumed known. Not all of these are realistic from a physical perspective. For instance, a heat sink slack node would physically be a

Table 4.2: Some possible new node types for multi-carrier networks.

Carrier	Node type	Specified	Unknown
Gas	slack	-	p, q
	reference load	p, q	-
Electricity	PVδ	P, $\|V\|$, δ	Q
	QVδ	Q, $\|V\|$, δ	P
	PQVδ	P, Q, $\|V\|$, δ	-
Heat	source reference	$T^s_{i,l}$, p, and $\Delta\varphi < 0$	T^s_i, T^r_i, m
	sink reference	$T^r_{i,l}$, p, and $\Delta\varphi > 0$	T^s_i, T^r_i, m
	source temperature	T^s_i, $T^s_{i,l}$, and $\Delta\varphi < 0$	T^r_i, p, m
	reference	p, $m = 0$	T^r_i, T^s_i
	temperature	T^s_i, $m = 0$	T^r_i, p
	reference temperature	T^s_i, p, $m = 0$	T^r_i
	sink slack	T^r_i, p	T^s_i, $T^r_{i,l}$, $\Delta\varphi$, m
Coupling	standard	-	T^s or T^r
	temperature	T^s or T^r	-

node where the pump to regularize pressure is located at a sink instead of at a source. However, they might be needed to solve the integrated system of equations.

In addition to these standard and new node types, it is possible to assume ΔT known as a BC for elements that produce or consume heat. For heat terminal links or heat dummy links, this means ΔT is assumed known instead of T^s if the element acts as a heat source, and ΔT is assumed known instead of T^r if the element acts as a heat sink. This holds both for the heat nodes in Tables 4.1–4.2, and for the coupling nodes in Table 4.2. For heat terminal links, ΔT is given by (3.13), for heat dummy links from a coupling node i^c to i^h, ΔT is given by $\Delta T_{i^c i^h} = T^s_{i^c i^h} - T^r_{i^c i^h}$.

4.2 Formulations of the load flow problem

The steady-state load flow problem is formulated by collecting the load flow equations into one system of equations. The size of this system for the SCNs is reduced by substituting the BCs and by substituting some equations into others. For each carrier, several formulations for the system of equations are used (see e.g. [2] for gas, [3, 24, 25] for electricity, and [26, 8] for heat).

4.2.1 Gas networks

The nodal, loop, or nodal-loop formulations are commonly used formulations for the SC gas network [2]. Another option is the full formulation. In this thesis, the nodal formulation and the full formulation are used for the SC gas network.

Usually, one of the sources is taken as the reference node, and all other nodes are load nodes.

Full formulation

The full formulation collects the nodal conservation of mass (3.2) for each node with known injected flow, and the link equations (3.3) into one system of equations:

$$\boldsymbol{F}^g(\boldsymbol{x}^g) = \begin{pmatrix} \boldsymbol{F}^q \\ \boldsymbol{F}^L \end{pmatrix} = \boldsymbol{0}, \quad \boldsymbol{x}^g = \begin{pmatrix} \boldsymbol{q} \\ \boldsymbol{p}^g \end{pmatrix} \tag{4.1}$$

with $\boldsymbol{p}^g$ the vector of unknown nodal pressures, $\boldsymbol{q}$ the vector of unknown link flows, $\boldsymbol{F}^q$ the vector of conservation of mass, and $\boldsymbol{F}^L$ the vector of link equations.

In the full formulation, (3.4a) or (3.4b) can be used in $\boldsymbol{F}^L$ for a link representing a pipe. The conservation of mass $\boldsymbol{F}^q$ is linear in $\boldsymbol{q}$ and independent of $\boldsymbol{p}$.

Conservation mass can be written as a linear system of equations using the incidence matrix (3.1) of the network:

$$\boldsymbol{F}^q = A^{g\prime}\boldsymbol{q} - \boldsymbol{q}^{\text{inj}} = \boldsymbol{0} \tag{4.2}$$

with $\boldsymbol{q}^{\text{inj}}$ the vector of known nodal injected flows q_i, and $A^{g\prime}$ the reduced incidence matrix of the gas network, which only takes into account the nodes with known injected flow.

Nodal formulation

The nodal formulation collects the nodal conservation of mass (3.2) for each node with known injected flow. The link equations (3.3) are substituted into conservation of mass to eliminate link flow as a variable. The system of equations is given by

$$\boldsymbol{F}^g(\boldsymbol{x}^g) = \boldsymbol{F}^q = \boldsymbol{0}, \quad \boldsymbol{x}^g = \boldsymbol{p}^g \tag{4.3}$$

with $\boldsymbol{p}^g$ the vector of unknown nodal pressures and $\boldsymbol{F}^q$ the vector of conservation of mass. In this case, (4.2) becomes

$$\boldsymbol{F}^q = A^{g\prime}\boldsymbol{q}(\boldsymbol{p}) - \boldsymbol{q}^{\text{inj}} = \boldsymbol{0}$$

The link equations (3.3) can only be substituted into the nodal equations (3.2) if the link equations can be rewritten such that the link flow q is expressed as a function of nodal pressures p. This means that (3.4a) must be used as the link equation for pipes. Moreover, the nodal formulation cannot be used for a network with compressors, as (3.5) is independent of q.

The size of the system is reduced compared to (4.1). On the other hand, conservation of mass $\boldsymbol{F}^q$ can be nonlinear, depending on the specific link equations used.

4.2.2 Electrical networks

In this thesis, the complex power formulation in polar coordinates is used for the SC electrical network [3]. For every node i, the link equations (3.8) are substituted in Kirchhoff's current law (3.6), which is subsequently substituted in the complex power equation (3.7). This nodal equation, which gives conservation of energy, is then split in the active power part F^P and reactive power part F^Q, where $F^S = F^P + \mathrm{i}F^Q$.

With P_{ij} and Q_{ij} the powers obtained from (3.8), and P_i and Q_i the known injected powers, the nodal equations are

$$F_i^P = P_i + \sum_{j,j\neq i} P_{ij}(\delta_i, \delta_j, |V_i|, |V_j|) \tag{4.4a}$$

$$F_i^Q = Q_i + \sum_{j,j\neq i} Q_{ij}(\delta_i, \delta_j, |V_i|, |V_j|) \tag{4.4b}$$

For each node i with known injected P, (4.4a) is taken into the system of equations, and (4.4b) is taken for each node with known injected Q. Usually, one of the generators is taken is the slack node, the other generators are taken as generator nodes, and the demands are taken as load nodes. The system of (nonlinear) equations is given by:

$$\boldsymbol{F}^e(\boldsymbol{x}^e) = \begin{pmatrix} \boldsymbol{F}^P \\ \boldsymbol{F}^Q \end{pmatrix} = \boldsymbol{0}, \quad \boldsymbol{x}^e = \begin{pmatrix} \boldsymbol{\delta} \\ |\boldsymbol{V}| \end{pmatrix} \tag{4.5}$$

Here, $\boldsymbol{F}^P$ and $\boldsymbol{F}^Q$ are the vectors of conservation of energy for every node with known injected active power or known injected reactive power, and $\boldsymbol{\delta}$ and $|\boldsymbol{V}|$ are the vectors of unknown nodal voltage angle and voltage amplitude.

For non-dummy links, the second term in (4.4) can be expressed using the admittance matrix Y. Denoting the set of all non-dummy links by $\mathcal{E}^e_{\mathrm{nd}}$, and the set of all dummy links by $\mathcal{E}^e_{\mathrm{d}}$, (4.4) becomes

$$F_i^S = S_i + V_i \sum_{j,ij\in\mathcal{E}^e_{\mathrm{nd}}} Y_{ij}^* V_i^* + \sum_{j,ij\in\mathcal{E}^e_{\mathrm{d}}} S_{ij} \tag{4.6}$$

4.2.3 Heat networks

The heat network consist of a hydraulic model and a thermal model, which we combine into one integrated hydraulic-thermal model. Generally, a loop formulation is used in the hydraulic part. In this thesis, however, we use a formulation similar to the full formulation of the gas network.

The terminal link mass flows and temperatures are generally substituted to reduce the system size. We call this formulation the standard formulation. Another option is to keep the terminal link flows and temperatures as variables, which we call the terminal link formulation.

For both formulations, some of the (terminal) link temperatures are substituted by the nodal temperatures based on the actual direction of flow, according to (3.10) and (3.11) for links, and (3.12) for terminal links.

The thermal link equations (3.21) can usually be rewritten such that T_k^{end} is a function of m_k and T_k^{start}. This temperature is subsequently substituted in the mixing-rule (3.20).

In addition to the terminal link formulation and standard formulation, there are two options for the BCs for the terminal links of loads, as described in Section 4.1.

We assume that a slack node has only one terminal link connected to it. The mass flow is determined using conservation of mass (3.14), such that

$$m_{i,l} = \sum_{j,\, j\neq i} m_{ji} - \sum_{j,\, j\neq i} m_{ij}$$

Then, (3.23) gives the injected heat power $\Delta\varphi_{i,l}$ of the slack node.

Usually, one of the sources is taken as source reference slack node, and the other nodes are taken as junction or as load nodes.

Terminal link formulation

For the hydraulic part, the nodal conservation of mass (3.14) for each node with known injected heat power and known terminal link supply or return temperature, and the hydraulic link equations (3.15) are collected. For the thermal part, the supply line mixing-rule (3.20a) for every node with T_i^s unknown and every source node with $T_{i,l}^s$ unknown, the return line mixing-rule (3.20b) for every node with T_i^r unknown and every sink node with $T_{i,l}^r$ unknown, and the heat power equation (3.23) for all terminal links with known injected heat power and known supply or return temperature are collected.

If $T_{i,l}^s$ or $T_{i,l}^r$ is known for loads, it is substituted in (3.20) and in (3.23). If instead $\Delta T_{i,l}$ is known, $T_{i,l}^s$ or $T_{i,l}^r$ is added as a variable, and (3.13a) is added to the system of equations as

$$F_{i,l}^{\Delta T} = T_{i,l}^s - T_{i,l}^r - \Delta T_{i,l}$$

The system of nonlinear equations for the terminal link formulation is then given by:

$$\boldsymbol{F}^h = \begin{pmatrix} \boldsymbol{F}^m \\ \boldsymbol{F}^L \\ \boldsymbol{F}^{T^s} \\ \boldsymbol{F}^{T^r} \\ \boldsymbol{F}^{\varphi} \\ \boldsymbol{F}^{\Delta T} \end{pmatrix} = \boldsymbol{0}, \quad \boldsymbol{x}^h = \begin{pmatrix} \boldsymbol{m}^L \\ \boldsymbol{m}^{TL} \\ \boldsymbol{p}^h \\ \boldsymbol{T}^s \\ \boldsymbol{T}^r \\ \boldsymbol{T}^{TL,s} \\ \boldsymbol{T}^{TL,r} \end{pmatrix} \tag{4.7}$$

with $\boldsymbol{m}^L$ the vector of link mass flows, $\boldsymbol{m}^{TL}$ the vector of unknown terminal link mass flows of loads, $\boldsymbol{p}^h$ the vector of unknown nodal pressures, $\boldsymbol{T}^s$ and $\boldsymbol{T}^r$ the vectors of unknown nodal supply and return temperatures, $\boldsymbol{T}^{TL,s}$ and $\boldsymbol{T}^{TL,r}$ the vectors of unknown terminal link supply and return temperatures, $\boldsymbol{F}^m$ the vector of conservation of mass for every non slack node, $\boldsymbol{F}^L$ the vector of link equations, $\boldsymbol{F}^{T^s}$ the vector of supply line mixing-rules, $\boldsymbol{F}^{T^r}$ the vector of return line mixing-rules, $\boldsymbol{F}^{\varphi}$ the vector of heat power equations for each terminal link with known $\Delta\varphi$, and $\boldsymbol{F}^{\Delta T}$ the vector of temperature difference equations for each terminal link with known ΔT.

The conservation of mass $\boldsymbol{F}^m$ is linear in the mass flows $\boldsymbol{m}^L$ and $\boldsymbol{m}^{TL}$, and independent of $\boldsymbol{p}^h$. It can be written as a linear system of equations using the incidence matrix (3.1) of the network:

$$\boldsymbol{F}^m = A^{h\prime}\boldsymbol{m}^L - \boldsymbol{m}^{\text{inj}} = \boldsymbol{0} \tag{4.8}$$

with $\boldsymbol{m}^{\text{inj}}$ the vector of nodal injected flows m_i of the non slack nodes, which is a sum of part of the terminal link flows in $\boldsymbol{m}^{TL}$, and $A^{h\prime}$ the reduced incidence matrix of the heat network, which only takes into account the non slack nodes.

The supply line mixing-rule $\boldsymbol{F}^{T^s}$ is independent of the return temperatures $\boldsymbol{T}^r$ and $\boldsymbol{T}^{TL,r}$, and the return line mixing-rule $\boldsymbol{F}^{T^r}$ is independent of the supply line temperatures $\boldsymbol{T}^s$ and $\boldsymbol{T}^{TL,s}$.

If $T^s_{i,l}$ or $T^r_{i,l}$ is known for all loads, $\boldsymbol{F}^{\Delta T}$, $\boldsymbol{T}^{TL,s}$ and $\boldsymbol{T}^{TL,r}$ are not part of the system of LF equations.

Standard formulation

In the standard formulation, the flow $m_{i,l}$ of each terminal link is written as a function of $T^s_{i,l}$, $T^r_{i,l}$ and $\Delta\varphi_{i,l}$, using (3.23), and substituted into the other equations. If ΔT is known for loads, then $T^s_{i,l}$ or $T^r_{i,l}$ is expressed as a function of $\Delta T_{i,l}$ and T^r_i or T^s_i, using (3.13a), and substituted into the other equations. The system of nonlinear equations is then given by:

$$\boldsymbol{F}^h = \begin{pmatrix} \boldsymbol{F}^m \\ \boldsymbol{F}^L \\ \boldsymbol{F}^{T^s} \\ \boldsymbol{F}^{T^r} \end{pmatrix} = \boldsymbol{0}, \quad \boldsymbol{x}^h = \begin{pmatrix} \boldsymbol{m}^L \\ \boldsymbol{p}^h \\ \boldsymbol{T}^s \\ \boldsymbol{T}^r \end{pmatrix} \tag{4.9}$$

This system of equations is smaller than (4.7). However, conservation of mass (4.8) now becomes

$$\boldsymbol{F}^m = A^{h\prime}\boldsymbol{m}^L - \boldsymbol{m}^{\text{inj}}(\boldsymbol{T}^s, \boldsymbol{T}^r) = \boldsymbol{0}$$

which is nonlinear and depends on the supply and return temperatures. Furthermore, the supply line mixing-rule $\boldsymbol{F}^{T^s}$ depends on $\boldsymbol{T}^r$, and the return line mixing-rule $\boldsymbol{F}^{T^r}$ depends on $\boldsymbol{T}^s$.

4.2.4 Coupling nodes

In every coupling node, one or more coupling equations (3.26) hold. If a coupling node represents a coupling unit that produces or consumes heat, the heat power equation (3.27) holds for each heat dummy link connected to the coupling node. Similar to the SC heat network, if, for such a dummy link, $T^s_{i^c i^h}$ or $T^r_{i^c i^h}$ is known, it is substituted in (3.27), and in the mixing-rule $\boldsymbol{F}^{T^s}$ or $\boldsymbol{F}^{T^r}$ in (4.7) or (4.9) of the heat part. Otherwise, if $\Delta T_{i^c i^h}$ is known, $T^s_{i^c i^h}$ or $T^r_{i^c i^h}$ is added as a variable, and a temperature difference equation is added to system for each dummy heat link:

$$F^{c,\Delta T}_{i^c i^h} = T^s_{i^c i^h} - T^r_{i^c i^h} - \Delta T_{i^c i^h}$$

If more than one heat dummy link is connected to a coupling node, an additional equation based on conservation of mass or energy, like a mixing-rule, might be needed to accurately determine the temperatures on the dummy links.

The system of equations for the coupling part of an MCN is then given by:

$$\boldsymbol{F}^c = \begin{pmatrix} \boldsymbol{F}^{c,E} \\ \boldsymbol{F}^{c,\varphi} \\ \boldsymbol{F}^{c,\Delta T} \end{pmatrix} = \boldsymbol{0}, \quad \boldsymbol{x}^c = \begin{pmatrix} \boldsymbol{q} \\ \boldsymbol{P} \\ \boldsymbol{Q} \\ \boldsymbol{m} \\ \boldsymbol{\Delta\varphi} \\ \boldsymbol{T}^s \\ \boldsymbol{T}^r \end{pmatrix} \tag{4.10}$$

Here, $\boldsymbol{F}^{c,E}$ is the vector of nodal coupling equations, $\boldsymbol{F}^{c,\varphi}$ is the vector of heat power equations, $\boldsymbol{F}^{c,\Delta T}$ the vector of temperature difference equations, $\boldsymbol{T}^s$ and $\boldsymbol{T}^r$ are the vectors of unknown supply and return dummy link temperatures, and $\boldsymbol{q}$, $\boldsymbol{P}$, $\boldsymbol{Q}$, $\boldsymbol{m}$, and $\boldsymbol{\Delta\varphi}$ are the vectors of the coupling gas flow, active power, reactive power, water link mass flow, and injected heat power.

4.2.5 Multi-carrier energy networks

The load flow equations of the SC parts and the coupling part are combined to form the integrated system of nonlinear equations describing the steady-state LF problem for a MES.

Since a (heterogeneous) coupling node is connected by homogeneous (dummy) links to the homogeneous SC nodes, the coupling flows q^c, P^c, Q^c, and m^c are included in the nodal conservation laws of the SCNs. Furthermore, m^c, and the temperatures $T^{s,c}$, and $T^{r,c}$ on the heat dummy link are included in (3.20) of the heat network, and $T^r_{i^h}$ is included in the heat power equation for the coupling node, if the coupling unit produces heat.

Combining the SC systems (4.1) or (4.3), (4.5), and (4.7) or (4.9) with the coupling part (4.10), gives the integrated system of equations for a MES:

$$\boldsymbol{F}(\boldsymbol{x}) = \begin{pmatrix} \boldsymbol{F}^g(\boldsymbol{x}^g,\, \boldsymbol{x}^c) \\ \boldsymbol{F}^e(\boldsymbol{x}^e,\, \boldsymbol{x}^c) \\ \boldsymbol{F}^h(\boldsymbol{x}^h,\, \boldsymbol{x}^c) \\ \boldsymbol{F}^c(\boldsymbol{x}^c,\, \boldsymbol{x}^h) \end{pmatrix} = \boldsymbol{0}, \quad \boldsymbol{x} = \begin{pmatrix} \boldsymbol{x}^g \\ \boldsymbol{x}^e \\ \boldsymbol{x}^h \\ \boldsymbol{x}^c \end{pmatrix} \tag{4.11}$$

Using dummy links to connect the SC into one MCN shows the connection between the SC parts explicitly. This connection is more difficult to see when the coupling flows are incorporated into injected nodal flows, as is commonly done. Furthermore, using dummy links, the LF models of the SC parts are only slightly altered, and the effect of coupling is included through the coupling part of the system of equations. However, since the additionally required BCs are imposed in the SC parts, an SC part might be overdetermined while another might be underdetermined. This is discussed in more detail in Section 5.3.

4.3 Model framework

The proposed graph-based model framework for steady-state load flow problems of MES is summarized as follows, which is also shown in Figure 4.1.

First, the SC gas, electricity, and heat systems to be combined into a MES are represented by a network as described in Section 3.2. Then, the desired coupling units are represented by a coupling node, and connected to SC networks using dummy links, as described in Section 3.3. The resulting graph is the MCN corresponding to the MES. Third, LF equations are chosen for each network element, see Chapter 2, and node types, or BCs, are chosen. Then, the load flow equations are collected into one integrated system of equations (4.11), giving the LF problem for the MES. Finally, this system of nonlinear equations is solved using NR, which is explained in Chapter 5.

The node types, and the location of the coupling nodes in the graph, must be carefully chosen. Certain combinations of node types, or graph topologies, can result

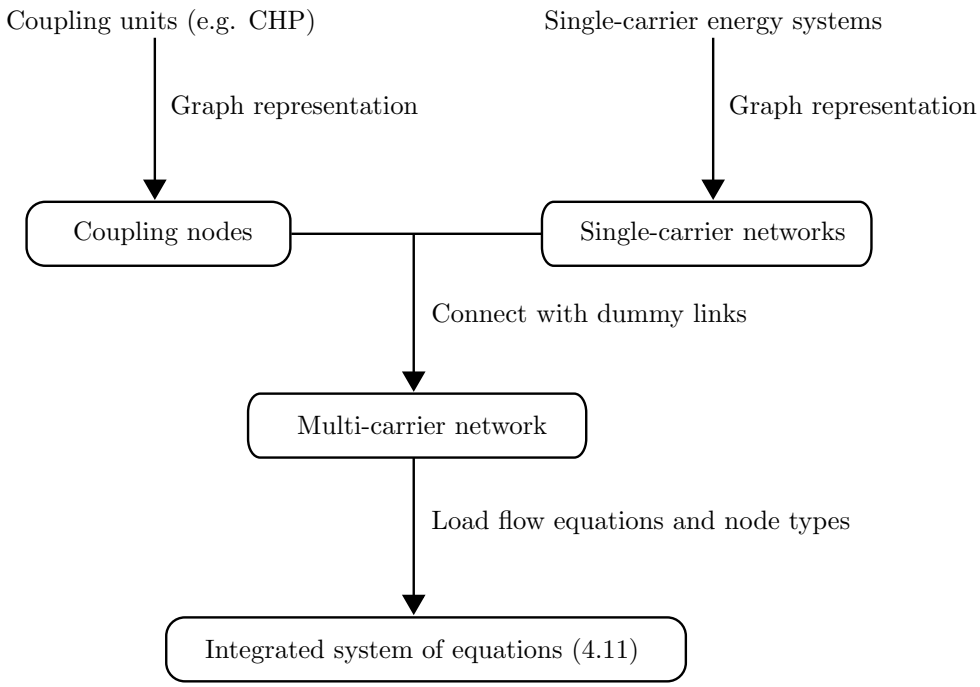

Figure 4.1: Flowchart of the graph-based model framework for steady-state load flow problems of MESs.

in systems of equations that are not (uniquely) solvable. A necessary condition for the LF problem to be uniquely solvable is that the number of equations $\boldsymbol{F}$ is equal to the number of variables $\boldsymbol{x}$. We will call such a system, with equal number for variables and (non)linear equations, a square system. However, even with a square system, the LF problem might still be ill-posed, such that are no or multiple solutions. The effect of node types and coupling models on solvability and well-posedness of the steady-state LF problem is discussed in Section 7.1.

The LF models and network elements can represent a variety of physical components of an energy system, such that the model framework is applicable to general MESs. Moreover, using different coupling components, models, or node types, results in different MCNs for the same MES. The model framework is illustrated and validated in Chapter 6.

An alternative solution method for steady-state LF analysis of general integrated MESs is discussed in Chapter 8.

4.4 Derived variables

The LF problem is concerned with solving a system of nonlinear equations (4.11) for the state variables $\boldsymbol{x}$, given BCs. With these state variables, all other quantities of interest in the network can be determined. Those quantities are derived variables based on the state variables. For instance, in a power grid the state variables usually

are the nodal voltage amplitudes and nodal voltage angles, and the derived variables include complex power through a line and injected reactive power at a generator.

The division of network variables into state variables and derived variables is not unique, since there are various ways to formulate the LF problem. In the nodal formulation (4.3) for a gas network, the state variables are the nodal pressures, while the gas flows on the links are derived variables. In the loop formulation it is the other way around, such that the state variables are the gas link flows and the nodal pressures are the derived variables.

We combine the state variables $\boldsymbol{x}^F \in \mathbb{R}^{N_F}$ and derived variables $\boldsymbol{x}^G \in \mathbb{R}^{N_G}$ into the extended state variables:

$$\boldsymbol{x} := \begin{pmatrix} x_1^G & \dots & x_{N_G}^G & x_1^F & \dots & x_{N_F}^F \end{pmatrix}^T \tag{4.12}$$

We extend the standard LF equations and state variables with the derived variables and with the (non)linear equations needed to derive them, leading to the extended LF problem:

$$\boldsymbol{F}\left(\boldsymbol{x}^F\right) = \boldsymbol{0} \tag{4.13a}$$

$$\boldsymbol{G}\left(\boldsymbol{x}^G, \boldsymbol{x}^F\right) = \boldsymbol{0} \tag{4.13b}$$

Here, (4.13a) is the system of (non)linear steady-state LF equations (4.11) and $\boldsymbol{G} : \mathbb{R}^{N_F+N_G} \to \mathbb{R}^{N_G}$ are additional load flow equations. To solve the extended LF problem (4.13), the standard LF problem (4.13a) is solved for the state variables $\boldsymbol{x}^F$. Then, using this $\boldsymbol{x}^F$, the additional equations (4.13b) determine the derived variables $\boldsymbol{x}^G$.

Generally, the entries of $\boldsymbol{x}^G$ are independent of each other, and (4.13b) can easily be rewritten to give an analytic expression for each $x^G \in \boldsymbol{x}^G$ dependent only on $\boldsymbol{x}^F$. Hence, obtaining $\boldsymbol{x}^G$ from (4.13b) generally does not require solving a system of nonlinear equation.

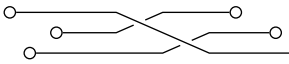

CHAPTER 5

The Newton-Raphson method

Steady-state LF analysis of energy networks requires solving the system of nonlinear LF equations (4.11). We consider a general systems of nonlinear equations:

$$\boldsymbol{F}(\boldsymbol{x}) = \mathbf{0} \tag{5.1}$$

It is generally not possible to find an analytical solution to a system of nonlinear equations. Iterative methods are used to find an approximation of the solution. Various methods exist, for instance fixed-point methods, but we will use the Newton-Raphson method (NR).

First, we give the basic iterative scheme and algorithm for NR. Then, we provide the iterative scheme of NR when the variables or equations are scaled or permuted. We show that scaling and permutation does not affect the iterates of NR. Finally, we discuss the application of NR to steady-state LF problems of MESs.

5.1 Basic iterative scheme

Consider the square nonlinear system of N equations (5.1), with $\boldsymbol{F} : \mathbb{R}^N \to \mathbb{R}^N$ continuously differentiable. This system is solved iteratively, using a linearization of $\boldsymbol{F}$ at each iteration. The Jacobian matrix J is given by

$$J = \nabla \boldsymbol{F} := \begin{pmatrix} \frac{\partial F_1}{\partial x_1} & \cdots & \frac{\partial F_1}{\partial x_N} \\ \vdots & & \vdots \\ \frac{\partial F_N}{\partial x_1} & \cdots & \frac{\partial F_N}{\partial x_N} \end{pmatrix} \tag{5.2}$$

Given an initial guess $\boldsymbol{x}^0$, in every iteration k, the linear system

$$J\left(\boldsymbol{x}^k\right)\boldsymbol{s}^k = -\boldsymbol{F}\left(\boldsymbol{x}^k\right) \tag{5.3}$$

is solved to determine the update $\boldsymbol{s}$ to the current iterate. Any linear solver can be used. The iteration scheme of NR is given in Algorithm 5.1.

Some error measure is needed to determine if the current iterate is close to the solution. Based on (5.1), the vector $\boldsymbol{F}(\boldsymbol{x}^k)$ can be seen as the residual vector at iteration k. A commonly used error measure e^k is the residual norm $\|\boldsymbol{F}(\boldsymbol{x}^k)\|$ or the

Algorithm 5.1 The Newton-Raphson method in multiple dimensions.

Set $k := 0$.
Choose initial guess $\boldsymbol{x}^0$, maximum number of iterations $k^{\max}$, and tolerance τ.
Calculate e^0 using (5.4).
while $e^k > \tau$ and $k < k^{\max}$ **do**:
    Solve $\boldsymbol{s}^k$ from $J(\boldsymbol{x}^k)\boldsymbol{s}^k = -\boldsymbol{F}(\boldsymbol{x}^k)$
    Set $\boldsymbol{x}^{k+1} := \boldsymbol{x}^k + \boldsymbol{s}^k$
    Set $k := k + 1$
    Calculate e^k using (5.4)
end while

relative residual norm $\|\boldsymbol{F}(\boldsymbol{x}^k)\| / \|\boldsymbol{F}(\boldsymbol{x}^0)\|$. We use the residual norm for the error measure:

$$e^k = \|\boldsymbol{F}(\boldsymbol{x}^k)\|_2 \tag{5.4}$$

NR is said to be converged when the error measure of the final iteration is smaller than a chosen tolerance τ. The algorithm is terminated when convergence is reached, or when the maximum number of iterations $k^{\max}$ is exceeded.

One of the advantages of NR is the local quadratic convergence. That is, if some iterate $\boldsymbol{x}^K$ is close to the solution $\boldsymbol{x}^*$, then there exists a constant $c \geq 0$ such that $\|\boldsymbol{x}^{k+1} - \boldsymbol{x}^*\| \leq c\|\boldsymbol{x}^k - \boldsymbol{x}^*\|^2$ for all iterations $k \geq K$.

One of the disadvantages of basic NR is that global convergence is not guaranteed: If the initial guess is too far from the (global) solution, NR can have problems converging, or it might diverge. Furthermore, the system (5.3) needs to be solved at every iteration, which causes problems if the system is ill-conditioned, or if $J\left(\boldsymbol{x}^k\right)$ is singular.

The Jacobian $J\left(\boldsymbol{x}^k\right)$ needs to be determined every iteration. If an analytical expression is not available, or if the computation is too expensive, the Jacobian can be approximated numerically. The most straightforward and widely used approximation is a finite difference approximation:

$$J_{nm} = \frac{\partial F_n}{\partial x_m} \approx \frac{F_n(\boldsymbol{x} + \Delta x \boldsymbol{e}_m) - F_n(\boldsymbol{x})}{\Delta x}, \quad n, m = 1, \ldots, N \tag{5.5}$$

with Δx the step size and $\boldsymbol{e}_m$ a vector with element m equal to 1 and all other elements equal to 0.

5.2 Scaling and permutation

In many mathematical models of practical problems, the dependent and independent variables, and the value of the equations, in (5.1) can be several orders of magnitude apart. This can cause issues in Algorithm 5.1, as the smaller variables or equations might be ignored [27]. To avoid such convergence issues, we scale $\boldsymbol{x}$ and $\boldsymbol{F}$ to be of (roughly) the same order of magnitude.

Let $T_x, T_F \in \mathbb{R}^{N \times N}$ be nonsingular matrices, called transformation matrices. We define the transformed variables as $\hat{\boldsymbol{x}} := T_x \boldsymbol{x}$ and the transformed equations as $\hat{\boldsymbol{F}} := T_F \boldsymbol{F}(\boldsymbol{x})$.

The linear system (5.3) is adjusted to $\hat{J}(\boldsymbol{x}^k)\hat{\boldsymbol{s}}^k = -\hat{\boldsymbol{F}}(\boldsymbol{x}^k)$ and the new scaled iterate is determined by $\hat{\boldsymbol{x}}^{k+1} = \hat{\boldsymbol{x}}^k + \hat{\boldsymbol{s}}^k$. The iteration scheme of transformed NR in multiple dimensions is given in Algorithm 5.2.

Algorithm 5.2 Transformed NR in multiple dimensions.

Set $k := 0$.
Choose initial guess $\boldsymbol{x}^0$, maximum number of iterations $k^{\max}$, and tolerance τ.
Calculate $\hat{\boldsymbol{x}}^0 = T_x\boldsymbol{x}^0$.
Calculate $\hat{e}^0$ using (5.6).
while $\hat{e}^k > \tau$ and $k < k^{\max}$ **do**:
  Calculate $\hat{\boldsymbol{F}}^k = T_F\boldsymbol{F}(T_x^{-1}\hat{\boldsymbol{x}}^k)$ and $\hat{J}^k = T_F J(T_x^{-1}\hat{\boldsymbol{x}}^k)T_x^{-1}$
  Solve $\hat{\boldsymbol{s}}^k$ from $\hat{J}^k\hat{\boldsymbol{s}}^k = -\hat{\boldsymbol{F}}^k$
  Set $\hat{\boldsymbol{x}}^{k+1} := \hat{\boldsymbol{x}}^k + \hat{\boldsymbol{s}}^k$
  Set $k := k + 1$
  Calculate $\hat{e}^k$ using (5.6)
end while

As stopping criterion of transformed NR, we take $\hat{e}^k \leq \tau$, with the transformed error given by

$$\hat{e}^k = \|\hat{\boldsymbol{F}}^k\|_2 = \|T_F\boldsymbol{F}\left(T_x^{-1}\hat{\boldsymbol{x}}^k\right)\|_2 \tag{5.6}$$

For the transformed step, it holds that $\hat{\boldsymbol{s}}^k = -T_x J\left(\boldsymbol{x}\right)^{-1}\boldsymbol{F}\left(\boldsymbol{x}^k\right) = T_x\boldsymbol{s}^k$, meaning that scaling and permutation do not affect the NR iterations. More details and the proof are given in Appendix A.

Even though the NR iterates are not affected by transformation, the stopping criterion of the algorithm might be. For instance, if the same tolerance τ is used in the stopping criterion of the original Algorithm 5.1 as in the stopping criterion of the transformed Algorithm 5.2, the algorithms will terminate at a different iteration number, since typically $e^k \neq \hat{e}^k$.

If T_x and T_F are diagonal matrices, $\boldsymbol{x}$ and $\boldsymbol{F}$ are only scaled and not permuted. Specifically, T_x is a diagonal matrix with $(T_x)_{nn} = (x_b)_n$, where $(x_b)_n$ is the base value of $x_n \in \boldsymbol{x}$. Similarly, T_F is a diagonal matrix with $(T_F)_{nn} = (F_b)_n$, where $(F_b)_n$ is the base value of $F_n \in \boldsymbol{F}$. We refer to $\hat{\boldsymbol{x}}$ and $\hat{\boldsymbol{F}}$ as the scaled variables and equations, respectively.

5.3 Application to steady-state load flow problems of multi-carrier energy systems

To solve the steady-state LF problem for general MESs, we use NR to solve the nonlinear system (4.11). Some remarks regarding the Jacobian and the initial guess can be made based on the structure of the system and the individual LF equations.

5.3.1 Jacobian

Due to the choice for a (heterogeneous) coupling node connected to the SCNs by (homogeneous dummy) links, the Jacobian matrix for the system of equation (4.11)

is given by:

$$J = \begin{pmatrix} J^{gg} & J^{ge} & J^{gh} & J^{gc} \\ J^{eg} & J^{ee} & J^{eh} & J^{ec} \\ J^{hg} & J^{he} & J^{hh} & J^{hc} \\ J^{cg} & J^{ce} & J^{ch} & J^{cc} \end{pmatrix} = \begin{pmatrix} J^{gg} & 0 & 0 & J^{gc} \\ 0 & J^{ee} & 0 & J^{ec} \\ 0 & 0 & J^{hh} & J^{hc} \\ 0 & 0 & J^{ch} & J^{cc} \end{pmatrix} \tag{5.7}$$

where the submatrices are defined as

$$J^{\alpha\beta} = \frac{\partial \boldsymbol{F}^{\alpha}}{\partial \boldsymbol{x}^{\beta}}, \quad \alpha, \beta \in \{g, e, h, c\}$$

This distinct structure holds for any MCN for which the individual LF equations satisfy the general forms as described in Chapter 3. Since the BCs additionally required by the coupling are imposed in the SC parts, these submatrices will generally not be square. In other words, an SC part might be overdetermined while another might be underdetermined. Therefore, the system (5.3) can generally not be solved blockwise, without reordering first.

Using dummy links to connect the SC into one MCN shows the connection between the SC parts explicitly, as already mentioned in Section 4.2.5. This is reflected by the distinct structure of the Jacobian matrix (5.7). This structure also shows that the effect of coupling is included through the coupling part of the system of equations. That is, due to the use of dummy links for the connections, we have $J^{\alpha\beta} = 0$ for all $\alpha \neq \beta$ with $\alpha, \beta \in \{g, e, h\}$. Appendix B.1 gives details on the submatrices.

5.3.2 Initial guess

In general, it is difficult to derive conditions to guarantee convergence, both for fixed-point methods and for NR. If the problem is ill-posed, such that the Jacobian matrix is singular, NR will not find a solution.

Even if the problem is well-posed, care has to be taken when initializing the solution vector. A badly chosen initial guess $\boldsymbol{x}^0$ can cause convergence problems for the solver. Moreover, it can lead to singular Jacobians, depending on the models used.

A well-known problem in SC gas (and heat) networks is a flat initial guess for the pressures, resulting in undefined first derivatives. A similar problem occurs with the thermal models in the heat network if a zero mass flow rate is used as initial guess. See Appendix B for more details.

5.3.3 Singular Jacobians in a heat network

Even if a proper initial guess is chosen, the mixing-rule in a heat network can cause the LF problem to become ill-posed, resulting in a singular Jacobian.

For any $\boldsymbol{x}^h$ that satisfies the system of LF equations (4.7) or (4.9), each node i has both inflow and outflow of water. However, during NR, there might be an iterate such that node i has only inflow or only outflow. This results in convergence issues, caused by the mixing-rule (3.20). To avoid these problems, we adjust the mixing-rule.

If a junction node or a source node has only inflow from the pipes in the supply line, the supply line mixing-rule (3.20a) is independent of T_i^s. Hence, the Jacobian

J^{hh} is singular, causing issues with the solvability of the linear system (5.3). Similarly, the return line mixing-rule (3.20b) is independent of T_i^r if node i is a junction or a sink with only outflow into the pipes of the supply line.

To avoid a singular Jacobian in these cases, we adjust the mixing-rule by using conservation of mass. We assume conservation of mass (3.14) holds (even though this is not true, in these cases), and add it to the mixing-rule. That is, in case of a junction or source with only inflow, we define the outflow into the pipes in the supply line (which is zero) to be equal to the inflow from the pipes (which is nonzero), and vice versa for a junction or sink with only outflow. These newly defined nonzero mass flows are then added to the mixing-rule.

For any junction or source i with only inflow from the pipes in the supply line, the supply line mixing-rule (3.20a) is adjusted to

$$F_i^{T^s} = \sum_{e_k \in \mathcal{E}^h_{\text{out}}} m_{ij}^s T_{ij}^s - \sum_{e_k \in \mathcal{E}^h_{\text{in}}} m_{ij}^s T_{ji}^s + \sum_l m_{i,l} T_{i,l}^s \boxed{+\big(-\sum_{e_k \in \mathcal{E}^h_{\text{out}}} m_{ij}^s + \sum_{e_k \in \mathcal{E}^h_{\text{in}}} m_{ij}^s - \sum_l m_{i,l}\big) T_i^s}$$

where the adjustment is shown in box.

Similarly, for any junction or sink i with only outflow from the pipes in the supply line, the return line mixing-rule (3.20b) is adjusted to

$$F_i^{T^r} = -\sum_{e_k \in \mathcal{E}^h_{\text{out}}} m_{ij}^s T_{ij}^r + \sum_{e_k \in \mathcal{E}^h_{\text{in}}} m_{ij}^s T_{ji}^r - \sum_l m_{i,l} T_{i,l}^r \boxed{+\big(\sum_{e_k \in \mathcal{E}^h_{\text{out}}} m_{ij}^s - \sum_{e_k \in \mathcal{E}^h_{\text{in}}} m_{ij}^s + \sum_l m_{i,l}\big) T_i^r}$$

Since conservation of mass is not satisfied in these cases, the added term is nonzero, and $F_i^{T^s}$ now depends on T_i^s and $F_i^{T^r}$ depends on T_i^r.

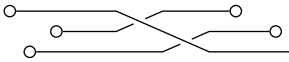

CHAPTER 6

Validation of load flow model framework

To illustrate and validate the model framework proposed in Section 4.3, we consider a small MES, which is based on a case study introduced in [11], and later adapted in [17] using an extended EH approach. For comparison, and to show that our framework is applicable to general MES, we consider three different ways of coupling the single-carrier networks of this MES, two similar to the couplings used in [11] and one similar to [17]. That is, the coupling is modeled in three different ways, resulting in three MCNs for the same MES.

6.1 Networks and models

Figure 6.1 shows the networks for the three ways of coupling. In network 1, we use a GG at node 0^c, a GB at node 1^c, and a CHP at node 2^c for the coupling. In network 2, we use two EHs. In network 3, we use a GG at node 0^c, a GB at node 1^c and at node 3^c, and a CHP at node 2^c for the coupling. For all three networks, the same models are used in the SC part. The parameter values used in the equations for all three networks are summarized in Tables C.14–C.16 in Appendix C.3.

In the gas network, the links from 0^g to 1^g, from 0^g to 2^g, and from 3^g to 2^g, represent pipes, and the link from 1^g to 2^g represents a compressor. The pipes are modeled using the steady-state flow equation (2.1), with the pipe constant (2.2) and

This chapter is based on the articles:

Anne S. Markensteijn, Johan E. Romate, and Cornelis Vuik. A graph-based model framework for steady-state load flow problems of general multi-carrier energy systems. *Applied Energy*, 280:115286, December 2020. ISSN 0306-2619. doi: 10.1016/j.apenergy.2020.115286,

Anne S. Markensteijn, Johan E. Romate, and Cornelis Vuik. A graph-based framework for steady-state load flow analysis of multi-carrier energy networks. Technical Report 19-01, Delft University of Technology, Delft Institute of Applied Mathematics, 2019,

and additional work.

pressure drop (2.3) for high-pressure networks. For the friction factor, we use the implicit Colebrook-White equation (2.6). Since the network contains a compressor, we use the full formulation (4.1). We use (3.4b) for the link equation of the pipes, and (3.5) for the link equation of the compressor.

In the electrical network, all links represent transmission lines, which we model as short lines. We use (2.17) and (2.18) for the active and reactive powers in (4.4).

In the heat network, all links represent pipes. For the hydraulic model, we use the steady-state flow equation (2.20), with the pipe constant (2.22), pressure drop (2.21), and friction factor (2.6). For the thermal pipe model, we use (2.28). We use the terminal link formulation (4.7), with (3.16) for the hydraulic link equations.

Note that the parameter values used in the heat network, as proposed by [11], and used by [17] (see Table C.14), are not typical. For instance, the roughness is bigger and the diameter is smaller than those of typical pipes (e.g. [4] for typical pipe dimension). With the mass flows through the pipes reported in [17], this leads to pressure drops up to 17 bar/km, while 1 bar/km–3 bar/km is typical in heat networks. However, for validation purposes of our model, we will use the same parameters for pipes in the heat network as proposed by [11].

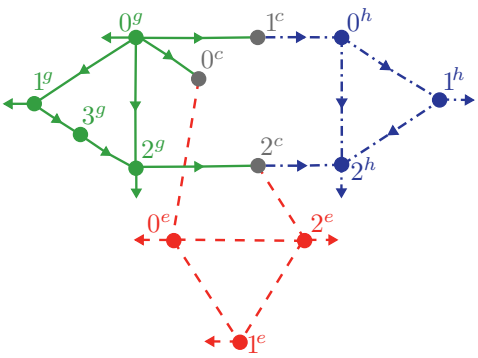

(a) Network 1: GG, GB, and CHP.

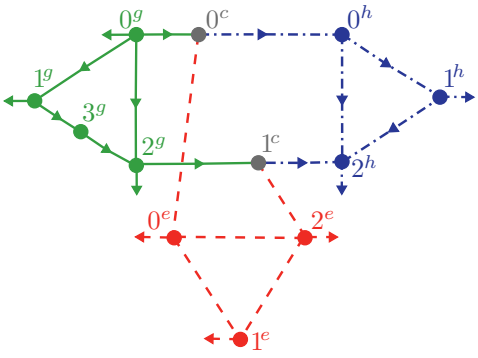

(b) Network 2: EHs.

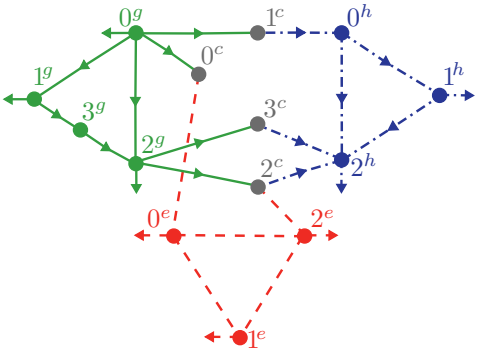

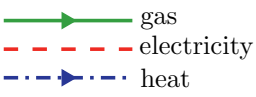

(c) Network 3: GG, two GBs, and CHP.

Figure 6.1: MES network topologies. Network 1 (a) and 3 (c) are based on [11], network 2 (b) is based on [17]. Arrows on links and terminal links show defined direction of flow.

In network 1, node 0^c represents a GG, node 1^c a GB, and node 2^c a CHP. We use linear models (2.33) and (2.36) for the GB and CHP, and use the nonlinear model (2.32) for the GG, such that the nodal coupling equations (3.26) are

$$F_{0^c}^{c,E} = \mathrm{GHV} q_{0^g 0^c} - a P_{0^c 0^e}^2 - b P_{0^c 0^e} - c - \left| d \sin\left(e(P^{\min} - P_{0^c 0^e})\right) \right| \tag{6.1a}$$

$$F_{1^c}^{c,E} = \Delta\varphi_{1^c 0^h} - \eta_{\mathrm{GB}} \mathrm{GHV} q_{0^g 1^c} \tag{6.1b}$$

$$F_{2^c}^{c,E} = \mathrm{GHV} q_{2^g 2^c} - \frac{P_{2^c 2^e}}{\eta_{\mathrm{CHP}}} - \frac{\Delta\varphi_{2^c 2^h}}{\eta_{\mathrm{CHP}}} \tag{6.1c}$$

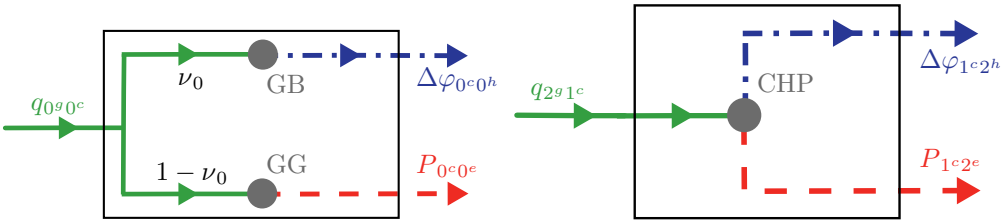

(a) EH at 0^c. **(b)** EH at 1^c.

Figure 6.2: Representation of the EHs in network 2, related to network 1. Arrows show actual direction of flow.

In network 2, both nodes represent an EH. Figure 6.2 shows a representation of the EHs, illustrating the relation to the coupling units in network 1. The coupling matrices are chosen such that the EHs model the same conversion of energy as the coupling components in network 1. Using (2.38), the nodal coupling equations (3.26) are

$$F_{0^c}^{c,E} = \begin{pmatrix} P_{0^c 0^e} \\ \Delta\varphi_{0^c 0^h} \end{pmatrix} - \begin{pmatrix} \nu_0 \eta_{\mathrm{GG}} \\ (1-\nu_0)\eta_{\mathrm{GB}} \end{pmatrix} \left(\mathrm{GHV} q_{0^g 0^c}\right) \tag{6.2a}$$

$$F_{1^c}^{c,E} = \begin{pmatrix} P_{1^c 2^e} \\ \Delta\varphi_{1^c 2^h} \end{pmatrix} - \begin{pmatrix} \nu_1 \eta_{\mathrm{CHP}} \\ (1-\nu_1)\eta_{\mathrm{CHP}} \end{pmatrix} \left(\mathrm{GHV} q_{2^g 1^c}\right) \tag{6.2b}$$

with ν_0 and ν_1 dispatch factors, and η_{GG} the efficiency of the (linearized) GG. To ensure consistency with network 1, we take

$$\eta_{\mathrm{GG}} = \frac{\widetilde{P}_{0^c 0^e}}{\mathrm{GHV}\widetilde{q}_{0^g 0^c}} \approx 0.45$$

$$\nu_0 = \frac{\widetilde{q}_{0^g 0^c}}{\widetilde{q}_{0^g 0^c} + \widetilde{q}_{0^g 1^c}} \approx 0.77$$

$$\nu_1 = \frac{\widetilde{P}_{2^c 2^e}}{\widetilde{P}_{2^c 2^e} + \Delta\widetilde{\varphi}_{2^c 2^h}} \approx 0.27$$

with $\widetilde{q}$, $\widetilde{P}$, and $\Delta\widetilde{\varphi}$ the coupling flows of network 1.

In network 3, node 0^c represents a GG, node 1^c and 3^c a GB, and node 2^c a CHP. We use the models (2.34) and (2.37) for the GBs and CHP, as proposed in [11], which

are linear but more detailed than (6.1b) and (6.1c). For the GG, we use (6.1a). The nodal coupling equations (3.26) for the GBs and CHP are

$$F^{c,E}_{0^c} = \mathrm{GHV} q_{0^g 0^c} - aP^2_{0^c 0^e} - bP_{0^c 0^e} - c - \left| d \sin\left(e(P^{\min} - P_{0^c 0^e})\right)\right| \tag{6.3a}$$

$$F^{c,E}_{1^c} = \mathrm{GHV} q_{0^g 1^c} - \frac{\Delta\varphi_{1^c 0^h} + r_1 E_{ss}}{r_2} \tag{6.3b}$$

$$F^{c,E}_{2^c} = \mathrm{GHV} q_{2^g 2^c} - \frac{P_{2^c 2^e}}{\eta_{\mathrm{CHP}}} - \frac{\Delta\varphi_{2^c 2^h}}{\eta_{\mathrm{CHP}}} \tag{6.3c}$$

$$F^{c,P}_{2^c} = P_{2^c 2^e} - a\Delta\varphi_{2^c 2^h} - bT^s_{2^c 2^h} - d + w(\Delta\varphi_{2^c 2^h}) \tag{6.3d}$$

$$F^{c,E}_{3^c} = \mathrm{GHV} q_{2^g 3^c} - \frac{\Delta\varphi_{3^c 2^h} + r_1 E_{ss}}{r_2} \tag{6.3e}$$

where $w(\Delta\varphi_{2^c 2^h})$ is given by (2.37c). The parameter values, see Table C.16, are chosen to match the solution given [11].

6.2 Node types

We assume T^s known for all heat-producing coupling components. As BCs for the heat terminal links, we specify $T^s_{i,l}$ for sources, and $T^r_{i,l}$ for sinks.

For network 1 and network 2, we assume all coupling energies unknown. For comparison and validation, we assume $\Delta\varphi$ known, for the GB represented by node 3^c and for the CHP, in network 3.

The coupling models (6.1) and (6.3) for network 1 and network 3 require two additional BCs more than the coupling models (6.2) for network 2, if T^s is known for all coupling nodes. Tables 6.1–6.3 give the nodes types used for the two networks. Due to the amount of additional BCs required in network 1, node 2^h is a non-physical

Table 6.1: Node type set for network 1, coupled with a GG, a GB, and a CHP.

Node	Node type	Specified	Unknown
0^g	ref.	p^g	q
1^g	load	q	p^g
2^g	ref. load	p^g, q	-
3^g	load	$q = 0$	p^g
0^e	PQVδ	P, Q, $\lvert V\rvert$, δ	-
1^e	load	P, Q	$\lvert V\rvert$, δ
2^e	PQV	P, Q, $\lvert V\rvert$	δ
0^h	ref.	p^h, $m = 0$	T^s, T^r
1^h	load (sink)	$T^r_{1,0}$, and $\Delta\varphi_{1,0} > 0$	T^s, T^r, p^h, $m_{1,0}$
2^h	load (sink) ref.	$T^r_{2,0}$, $\Delta\varphi_{2,0} > 0$, p^h	T^s, T^r, $m_{2,0}$
0^c	standard	-	-
1^c	temp.	$T^s_{1^c 0^h}$	-
2^c	temp.	$T^s_{2^c 2^h}$	-

Table 6.2: Node type set for network 2, coupled with EHs.

Node	Node type	Specified	Unknown
0^g	ref.	p^g	q
1^g	load	q	p^g
2^g	load	q	p^g
3^g	load	$q = 0$	p^g
0^e	PQVδ	P, Q, $\lvert V\rvert$, δ	-
1^e	load	P, Q	$\lvert V\rvert$, δ
2^e	PQV	P, Q, $\lvert V\rvert$	δ
0^h	ref.	p^h, $m = 0$	T^s, T^r
1^h	load (sink)	$T^r_{1,0}$, and $\Delta\varphi_{1,0} > 0$	T^s, T^r, p^h, $m_{1,0}$
2^h	load (sink)	$T^r_{2,0}$, and $\Delta\varphi_{2,0} > 0$	T^s, T^r, p^h, $m_{2,0}$
0^c	temp.	$T^s_{0^c0^h}$	-
1^c	temp.	$T^s_{1^c2^h}$	-

Table 6.3: Node type set for network 3, coupled with a GG, two GBs, and a CHP.

Node	Node type	Specified	Unknown
0^g	ref.	p^g	q
1^g	load	q	p^g
2^g	load	q	p^g
3^g	load	$q = 0$	p^g
0^e	PQVδ	P, Q, $\lvert V\rvert$, δ	-
1^e	load	P, Q	$\lvert V\rvert$, δ
2^e	PQV	P, Q, $\lvert V\rvert$	δ
0^h	ref.	p^h, $m = 0$	T^s, T^r
1^h	load (sink)	$T^r_{1,0}$, and $\Delta\varphi_{1,0} > 0$	T^s, T^r, p^h, $m_{1,0}$
2^h	load (sink)	$T^r_{2,0}$, and $\Delta\varphi_{2,0} > 0$	T^s, T^r, p^h, $m_{2,0}$
0^c	standard	-	-
1^c	temp.	$T^s_{1^c0^h}$	-
2^c	temp. heat	$T^s_{2^c2^h}$, $\Delta\varphi_{2^c2^h}$	-
3^c	temp. heat	$T^s_{3^c2^h}$, $\Delta\varphi_{3^c2^h}$	-

sink reference node. This shows that the coupling units determine the additional BCs required. Conversely, requiring realistic or physical BCs for all nodes limits the coupling units that can be used to couple SCNs.

The chosen node sets are not unique. For instance, instead of the node set given for network 2, node 2^h can be taken as sink reference node and T^s for node 1^c can be kept as unknown. The corresponding system of LF equations would then also be solvable for a suitable initial guess.

With the node sets in Tables 6.1–6.3, the system of LF equations for the MES (4.11) consists of 32 equations and variables for network 1, 33 equations and variables for network 2, and 35 equations and variables for network 3. The values used for the BCs are given in Tables C.23–C.31 in the appendix.

6.3 Solution to load flow problem

To solve the system of equations (4.11) for each network, we use scaled NR, see Algorithm 5.2, with a tolerance $\tau = 10^{-6}$. For the scaling, we use the base values given in Table C.17, and for the initial guess to the solution vector, we use the values given in Tables C.20–C.22.

Table 6.4: Relative error of results for the gas network, for network 1 (a), 2 (b), and 3 (c).

	p			q^{inj}				q		
Node	(a)	(b)	(c)	(a)	(b)	(c)	**Link**	(a)	(b)	(c)
0	0	0	0	$8.341{\cdot}10^{-3}$	$8.343{\cdot}10^{-3}$	$4.674{\cdot}10^{-6}$	0-1	0.38880	0.38880	0.38880
1	0.28699	0.28699	0.28699	0.08649	0.08649	0.08649	0-2	2.4112	2.4112	2.4111
2	0.31549	0.31549	0.31548	0	0	0	3-2	0.61152	0.61152	0.61153
3	0.28700	0.28700	0.28699	-	-	-	1-3	0.61152	0.61152	0.61153

Table 6.5: Relative error of results for the electrical network, for network 1 (a), 2 (b), and 3 (c).

	$\lvert V\rvert$			δ			S^{inj}		
Node	(a)	(b)	(c)	(a)	(b)	(c)	(a)	(b)	(c)
0	0	0	0	0	0	0	$6.897{\cdot}10^{-4}$	$6.897{\cdot}10^{-4}$	$6.897{\cdot}10^{-4}$
1	$8.163{\cdot}10^{-5}$	$8.166{\cdot}10^{-5}$	$4.695{\cdot}10^{-5}$	$4.721{\cdot}10^{-3}$	$4.726{\cdot}10^{-3}$	$2.018{\cdot}10^{-5}$	0	0	0
2	0	0	0	0.01111	0.01112	$8.354{\cdot}10^{-5}$	0	0	0
	S_{ij}			S_{ji}			S_{ij}^{loss}		
Link	(a)	(b)	(c)	(a)	(b)	(c)	(a)	(b)	(c)
0-1	$3.833{\cdot}10^{-3}$	$3.837{\cdot}10^{-3}$	$2.161{\cdot}10^{-5}$	$4.057{\cdot}10^{-3}$	-	$1.250{\cdot}10^{-5}$	$6.924{\cdot}10^{-3}$	$6.930{\cdot}10^{-3}$	$7.349{\cdot}10^{-5}$
0-2	$9.436{\cdot}10^{-3}$	$9.407{\cdot}10^{-3}$	$3.404{\cdot}10^{-5}$	$9.975{\cdot}10^{-3}$	-	$2.186{\cdot}10^{-5}$	0.01691	0.01693	$7.036{\cdot}10^{-5}$
1-2	0.02371	0.02373	$7.308{\cdot}10^{-5}$	0.02336	-	$1.181{\cdot}10^{-4}$	0.03057	0.03060	$3.783{\cdot}10^{-3}$

Table 6.6: Relative error of results for the hydraulic part of the heat network, for network 1 (a), 2 (b), and 3 (c).

	Δp			m		
Link	(a)	(b)	(c)	(a)	(b)	(c)
0-1	0.03894	0.03894	0.03857	$1.131 \cdot 10^{-4}$	0.01933	$8.069 \cdot 10^{-5}$
0-2	0.10209	0.10215	0.10491	$1.423 \cdot 10^{-3}$	0.05072	$1.464 \cdot 10^{-4}$
1-2	0.07549	0.07550	0.07575	$6.521 \cdot 10^{-5}$	0.03813	$7.600 \cdot 10^{-5}$

Table 6.7: Relative error of results for the thermal part of the heat network, for network 1 (a), 2 (b), and 3 (c).

	T^s			T^r		
Node	(a)	(b)	(c)	(a)	(b)	(c)
0	$4.737{\cdot}10^{-16}$	0	$1.184{\cdot}10^{-16}$	$1.987{\cdot}10^{-5}$	$2.968{\cdot}10^{-3}$	$9.459{\cdot}10^{-6}$
1	$2.103{\cdot}10^{-5}$	0.01665	$7.522{\cdot}10^{-7}$	$1.421{\cdot}10^{-16}$	0	0
2	$4.418{\cdot}10^{-5}$	$4.380{\cdot}10^{-5}$	$1.540{\cdot}10^{-6}$	$3.113{\cdot}10^{-6}$	0.01017	$3.353{\cdot}10^{-6}$
	$\Delta\varphi^{\text{loss}}$					
Link	(a)	(b)	(c)			
0-1	$1.040{\cdot}10^{-4}$	$1.041{\cdot}10^{-4}$	$1.062{\cdot}10^{-4}$			
0-2	$2.232{\cdot}10^{-5}$	$4.605{\cdot}10^{-3}$	$5.117{\cdot}10^{-5}$			
1-2	$3.435{\cdot}10^{-4}$	0.02906	$3.795{\cdot}10^{-4}$			

Table 6.8: Relative error of results for coupling part of the network, for network 1 (a), 2 (b), and 3 (c).

	q			P		
Node	(a)	(b)	(c)	(a)	(b)	(c)
0	0.01182	0.03156	$6.111{\cdot}10^{-6}$	$7.224{\cdot}10^{-3}$	0.03540	$3.883{\cdot}10^{-6}$
1	0.09336	$1.057{\cdot}10^{-4}$	$1.567{\cdot}10^{-4}$	-	0.03540	-
2	$1.064{\cdot}10^{-4}$	-	$1.961{\cdot}10^{-5}$	0.03537	-	$3.932{\cdot}10^{-5}$
3	-	-	$1.142{\cdot}10^{-3}$	-	-	-
	Q			$\Delta\varphi$		
Node	(a)	(b)	(c)	(a)	(b)	(c)
0	$4.195{\cdot}10^{-4}$	$6.587{\cdot}10^{-3}$	$4.188{\cdot}10^{-7}$	-	$5.092{\cdot}10^{-4}$	-
1	-	$6.587{\cdot}10^{-3}$	-	1.9995	$5.246{\cdot}10^{-4}$	$7.184{\cdot}10^{-6}$
2	$6.581{\cdot}10^{-3}$	-	$3.566{\cdot}10^{-6}$	$5.349{\cdot}10^{-4}$	-	0
3	-	-	-	-	-	0

To validate our model framework, we compare the solution of network 1, 2, or 3, with the solution given in [11] or [17], based on the relative error:

$$e = \max(|\boldsymbol{x}^* - \boldsymbol{x}|/|\boldsymbol{x}^*|)$$

where $\boldsymbol{x}^*$ is the solution given [11] or [17] and $\boldsymbol{x}$ the solution of network 1, 2, or 3. Since we use slightly different models from the ones used in [11] and [17], we expect our solution to be close, but not equal, to the solutions given in [11] and [17].

Tables 6.4–6.8 give the relative error between the solution of network 1, 2, or 3, and the solution given in [11] or [17]. The gas data in Table 6.4–6.8 is compared with the data from [11], as the solution in the gas part is not given in [17]. Similarly, the pressure drops in Table 6.6 are compared with the data from [17], as the solution for the pressure in the heat network is not given in [11]. For all other quantities, the solution of network 1 and 3 is compared with [11], while the solution in network 2 is compared with [17]. The full solution to the LF problem is given in Tables C.23–C.31.

Our results for network 1 match the ones found in [11], except for the gas network. However, plugging in their pressures values in the flow equation (2.1) does not give their gas pipe flows. The ratio between their presented gas flows and the flows obtained from the flow equations seems to be a factor $\ln 10$.

Our results for network 2 match the ones found in [17], except for small differences in the heat network. The model used in [17] for sinks and sources is different from the one used here. That is, in [17] $\Delta T_{i,l} = T_i^s - T_i^r$ is used for both sinks and sources, whereas we use the temperature difference in (3.13a). Second, they use a different thermal model for the pipe lines. Finally, they use Buzzelli's friction factor, whereas we use Colebrook-White (2.6) in the hydraulic model for the pipe lines. With our pipe flow model, their reported mass flow m_{01} results in a nodal head $h_1 = 225.05\,\mathrm{m}$, instead of $h_1 = 10.666\,\mathrm{m}$ as given in [17].

The other small differences are due to differences in BCs, and different formulations of the system of load flow equations. In [11] and [17], the heat powers of the coupling components are assumed known, while, for our BCs in network 1 and 2, the heat network determines the required heat power. Through the coupling equations, the coupling gas flows and active power can be determined, which are then effectively a specified value from the perspective of the single-carrier gas and electrical networks. Due to small differences in the coupling heat powers between our result and the one presented in [11] and [17], the result in the gas and electrical part is also slightly different.

To avoid the errors in the rest of the network caused by these small differences in the coupling heat power, we take $\Delta\varphi$ known for the GB represented by node 3^c and for the CHP in the BCs of network 3. Comparing the results of network 3 with the results of network 1 and with the results of [11], we indeed find that the results of network 3 match those of [11] more closely. See for instance the voltage angle in Table 6.5 and the active and reactive coupling powers in Tables 6.8. With this we can explain the small differences between the models in the literature and our own models.

This example illustrates that our proposed model framework can indeed be used to model steady-state load flow for general MESs. Moreover, our framework can be used with different components and models, both in the SCNs and for the coupling units. Therefore, our framework includes and extends the currently available load flow models for MESs.

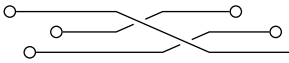

CHAPTER 7

Numerical results for steady-state load flow problems

As mentioned in Section 4.3, the choice of the additional BCs is important for the solvability and well-posedness of the integrated system of nonlinear LF equations. Furthermore, the specific formulation of the system of LF equations in the SC networks and the formulation of the integrated system of equations influence the solvability of the LF problem and the convergence behavior of NR. Using the graph-based modelframework to formulate the steady-state LF problem, we analyze the effect of coupling on the solvability and well-posedness of the system of equations, and on the convergence of NR.

First, we investigate the effect of coupling on the solvability and well-posedness, using a small MES with sets of BCs. Then, we investigate the convergence of NR by considering the LF problem for example MESs of varying size, with various coupling models and topologies, and various formulations in the single-carrier parts.

7.1 Solvability and well-posedness

For an MCN, additional BCs are required for the nonlinear system of LF equations to be solvable. The choice of these BCs influences the solvability and well-posedness of the LF problem. The node types, and the location of the coupling nodes in the graph, must be carefully chosen. Certain combinations of node types, or graph topologies, can result in systems of equations that are not (uniquely) solvable.

This chapter is based on the articles:

Anne S. Markensteijn, Johan E. Romate, and Cornelis Vuik. On the Solvability of Steady-State Load Flow Problems for Multi-Carrier Energy Systems. In *IEEE Milan PowerTech 2019*, 2019,

Anne S. Markensteijn and Cornelis Vuik. Convergence of Newton's Method for Steady-State Load Flow Problems in Multi-Carrier Energy Systems. In *IEEE PES Innovative Smart Grid Technologies (ISGT Europe 2020)*, 2020.

To investigate the effect of the node types, we consider a small MES. Two different types of coupling are considered, leading to two MCNs representing the same MES. For both of these MCNs, we formulate the LF problem using two different sets of node types. We solve the resulting systems of LF equations using NR.

7.1.1 Networks and models

Figure 7.1 shows the network topologies of the MES. The network in Figure 7.1a is coupled with a GB and a CHP, while the network in Figure 7.1b is coupled with a single EH. Using the EH as shown in Figure 7.2 means that both networks model the same MES.

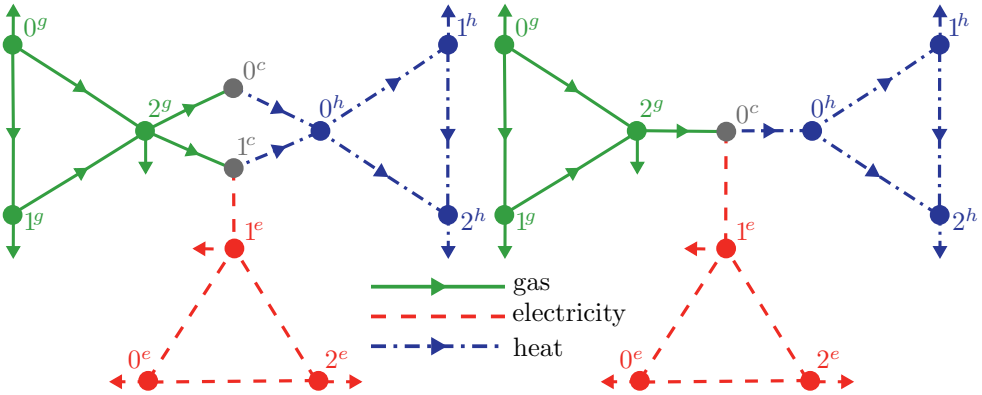

(a) Coupled with a GB (0^c) and a CHP (1^c). **(b)** Coupled with an EH.

Figure 7.1: Network topologies of one MES. Arrows on links and terminal links show defined direction of flow.

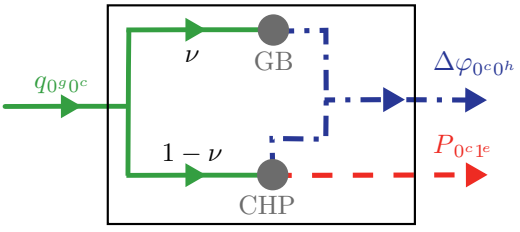

Figure 7.2: Model representation of the EH in Figure 7.1b.

Each SC network consists of three nodes, all connected to each other. The gas network and power grid have an external source, connected at node 0^g and 0^e respectively. The heat network has no external source; all heat is provided by the gas network. The networks are coupled at node 2^g of the gas network, node 1^e of the power grid, and node 0^h of the heat network. For both networks, the same models are used in the SC part. The parameter values used in the equations for both networks are summarized in Tables C.32–C.34 in Appendix C.4.

In the gas network, all links represent pipes, which are modeled using the steady-state flow equation (2.1), with the pipe constant (2.2) and pressure drop (2.3) for low-pressure networks, and with Pole's friction factor (2.5). We use (3.4b) for the link equation of the pipes.

In the electrical network, all links represent transmission lines, which we model as short lines. We use (2.17) and (2.18) for the active and reactive powers in (4.4).

In the heat network, all links represent pipes. For the hydraulic model, we use the steady-state flow equation for resistors (2.23), with constant $C^h = 1/\rho g$. For the thermal pipe model, we use (2.28). We use the terminal link formulation (4.7), with (3.16) for the hydraulic link equations.

In the first network, node 0^c represents a GB and node 1^c a CHP, which we model using (2.33) and (2.35), such that the nodal coupling equations (3.26) are

$$F^{c,E}_{0^c} = \Delta\varphi_{0^c0^h} - \eta_{\mathrm{GB}}\mathrm{GHV}q_{2^g0^c} \tag{7.1a}$$

$$F^{c,E}_{1^c} = \mathrm{GHV}q_{2^g1^c} - \frac{P_{1^c1^e}}{\eta_{\mathrm{CHP}}} - \frac{\Delta\varphi_{1^c0^h}}{\eta_{\mathrm{CHP}}} \tag{7.1b}$$

In the second network, the GB and CHP are represented by one EH, as shown in Figure 7.2. The coupling matrix is chosen such that the EH models the same conversion of energy as the GB and CHP. Using (2.38), the nodal coupling equations (3.26) are

$$F^{c,E}_{0^c} = \begin{pmatrix} P_{0^c1^e} \\ \Delta\varphi_{0^c0^h} \end{pmatrix} - \begin{pmatrix} \mu(1-\nu)\eta_{\mathrm{CHP}} \\ \nu\eta_{\mathrm{GB}} + (1-\mu)(1-\nu)\eta_{\mathrm{CHP}} \end{pmatrix} \left(\mathrm{GHV}q_{2^g0^c}\right) \tag{7.2}$$

with ν the factor of gas dispatched to the GB, and μ the factor of gas converted to active power by the CHP. This model is consistent with (7.1) for appropriate values of ν and μ.

7.1.2 Node types

The loop created between nodes 2^g and 0^h in the first network (Figure 7.1a) restricts the possible node types, regarding solvability. If only the total amount of gas consumed and total amount of heat provided by the coupling components is known, it leaves infinitely many options to distribute those energy flows over the GB and the CHP. For the first network, the node types must be chosen such that either both gas flows, or both heat flows, can be determined uniquely. Since none of the coupling flows are specified, this is impossible in the gas network. In the heat network, it is possible if both outflow temperatures are specified such that $T^s_{0^c0^h} \neq T^s_{1^c0^h}$, and if the supply temperature in node 0^h is specified. If instead of (3.27), a heat power equation with $\Delta T = T^s_{i^h} - T^s_{i^h}$ is used (e.g. [17]), this would not be possible.

This problem does not arise for the network with the EH (Figure 7.1b), because the EH concept specifies both ratios ν and μ in (7.2), and because there is no loop between nodes 2^g and 0^h. However, if for this network one of the coupling flow $q_{2^g0^c}$, $P_{0^c1^e}$, or $\Delta\varphi_{0^c0^h}$ is determined by one of the SCNs, the other two energies are known through the coupling equations (7.2). This effectively fixes those two energies as BCs in the other two SC networks, limiting the allowable node types in those two SC networks.

Due to the differences in network topology between Figure 7.1a and Figure 7.1b, and in coupling equations (7.1) and (7.2), different node types are needed for the total system (4.11) to be solvable. Table 7.1 gives two sets for both networks for which the system is well posed. For both networks, the first set has no additional BCs in gas, while the second set has.

Table 7.1: Node type sets with BCs for the networks shown in Figure 7.1.

	set 1		**set 2**		**set 1 EH**		**set 2 EH**	
Node	**Type**	**Specified**	**Type**	**Specified**	**Type**	**Specified**	**Type**	**Specified**
0^g	ref.	p^g	ref.	p^g	ref.	p^g	ref.	p^g
1^g	load	q	load	q	load	q	load	q
2^g	load	q	ref. load	p^g, q	load	q	ref. load	p^g, q
0^e	slack	$\|V\|$, δ	slack	$\|V\|$, δ	slack	$\|V\|$, δ	slack	$\|V\|$, δ
1^e	PQVδ	P, Q, $\|V\|$, δ	PQV	P, Q, $\|V\|$	PQV	P, Q, $\|V\|$	PQV	P, Q, $\|V\|$
2^e	load	P, Q	load	P, Q	load	P, Q	load	P, Q
0^h	ref. temp.	T^s, p^h, $m{=}0$	ref. temp.	T^s, p^h, $m{=}0$	ref.	p^h, $m{=}0$	junction	$m{=}0$
1^h	load (sink)	$T^r_{1,0}$, $\Delta\varphi_{1,0}$	load (sink)	$T^r_{1,0}$, $\Delta\varphi_{1,0}$	load (sink)	$T^r_{1,0}$, $\Delta\varphi_{1,0}$	load ref. slack	T^r_1, p^h
2^h	load (sink)	$T^r_{2,0}$, $\Delta\varphi_{2,0}$	load (sink)	$T^r_{2,0}$, $\Delta\varphi_{2,0}$	load (sink)	$T^r_{2,0}$, $\Delta\varphi_{2,0}$	load (sink)	$T^r_{2,0}$, $\Delta\varphi_{2,0}$
0^c	temp.	$T^s_{0^c0^h}$	temp.	$T^s_{0^c0^h}$	temp.	$T^s_{0^c0^h}$	temp.	$T^s_{0^c0^h}$
1^c	temp.	$T^s_{1^c0^h}$	temp.	$T^s_{1^c0^h}$	-	-	-	-

In the first example, with the network shown in Figure 7.1a, node types are chosen such that the heat network can determine the coupling heat power flows. For the first node set, the nodes are chosen such that the power grid determines the active power required from the CHP. The coupling equations then determine the coupling gas flows. For the second node set, the nodes are chosen such that, given the heat flow produced by the GB (node 0^c), the gas network can determined the gas flow supplied to the CHP. The coupling equations then determine the active power produced by the CHP.

For the example with the EH, shown in Figure 7.1b, the first node set is chosen such that the heat network determines the coupling heat power. The coupling equations then determine the coupling gas flow and active power.

The second node set, for the example with the EH, is chosen such that the gas network determines the coupling gas flow. The coupling equations then determine the coupling heat power and active power. Taking nodes 1^h and 2^h as sink nodes, and assuming there is no external heat source, leaves the heat network without a slack for the heat power, which could lead to an ill-posed problem. If $\Delta\varphi_{0^c0^h} \gg |\Delta\varphi_{1,0}| + |\Delta\varphi_{2,0}|$, the water mass flow in the pipes will become very small, that is $m_{ij} \approx 0$. If 1^h and 2^h are load nodes, $T^r_{1,0}$, $T^r_{2,0}$, and the heat powers would be known. Since $T^s_{0^c0^h}$ is also known, it follows from the heat power equations (3.23) and (3.27) that $T^r_0 \ll T^s_{0^c0^h}$, $T^s_1 \gg T^r_{1,0}$, and $T^s_{2^h} \gg T^r_{2,0}$. In this example, this leads to a numerically singular Jacobian matrix (i.e. $|J(\boldsymbol{x}^k)| \approx 0$, such that the linear solver in NR is unable to find a solution at iteration k). To avoid this, a slack for the heat power must be introduced. One option is to make node 0^h a slack node. However, this would model a situation with an external heat source connected to node 0^h. Another option is to take one of the sink nodes 1^h or 2^h as slack nodes. Although this is not physically realistic, we choose the second option to show the effect of node types on convergence behavior.

The chosen coupling unit and model determines the topology of the MCN and the

used coupling equations. This influences the possibilities for imposing the additionally required BCs in the SC networks, and subsequently influences the integrated system of LF equations. Choosing the wrong node types leads to an ill-posed or unsolvable LF problem.

7.1.3 Solving the load flow problem

To solve the system of equations (4.11) for both networks, we use scaled NR, see Algorithm 5.2, with a tolerance $\tau = 10^{-6}$, and the base values for scaling given in Table C.35. We use the full formulation (4.1) in the gas part, and the standard formulation (4.9) in the heat part.

Figure 7.3 shows the convergence behavior of NR for all four examples, that is, for the two node sets in Table 7.1 for both networks in Figure 7.1. We can see that

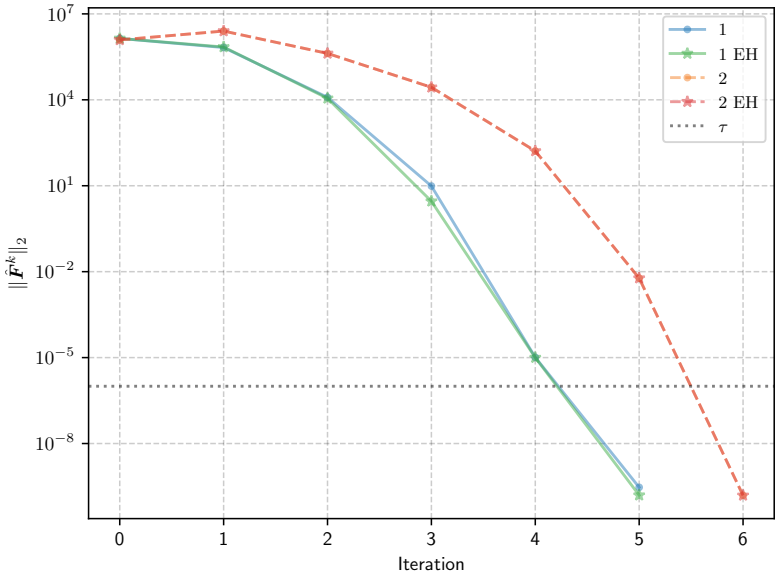

Figure 7.3: Error $\|\hat{\boldsymbol{F}}^k\|_2$ of NR, for the networks in Figure 7.1 with the node sets in Table 7.1. The curves for node set 2 are indistinguishable at this scale.

NR converges for all four examples. For each node set, the convergence behavior of the two networks is similar, showing that the coupling model does not influence convergence behavior for this MES. Node set 2 takes more iterations to convergence than node set 1, for both networks. This difference is due to the additional BC in gas for the second node set.

Even though this MES is too small to draw general quantitative conclusions regarding the convergence of NR, the number of iterations needed by NR are different for the two node sets. Therefore, these examples show that the choice of node types influences the convergence behavior of NR, even if the BCs are chosen such that the LF problem is uniquely solvable.

7.2 Convergence of the Newton-Raphson method

Various formulations of the LF problem are used in each of the SC networks. Moreover, different coupling models lead to different integrated systems of equations for the LF problem of MESs. To investigate the effect of coupling, and the effect of the formulation of the LF problem in the SC parts, on the convergence of NR for the LF problem of MESs, we consider a MES of varying size, with various coupling models and topologies, and various formulations in the single-carrier parts. We compare the convergence behavior of NR for the various SCNs and MCNs.

7.2.1 Networks and models

The MES consists of a base network, coupling 3-node SC gas, electricity, and heat networks. For each carrier, node 1 is a source, and node 3 is a sink. For the electrical network and the heat network, node 2 is an additional source.

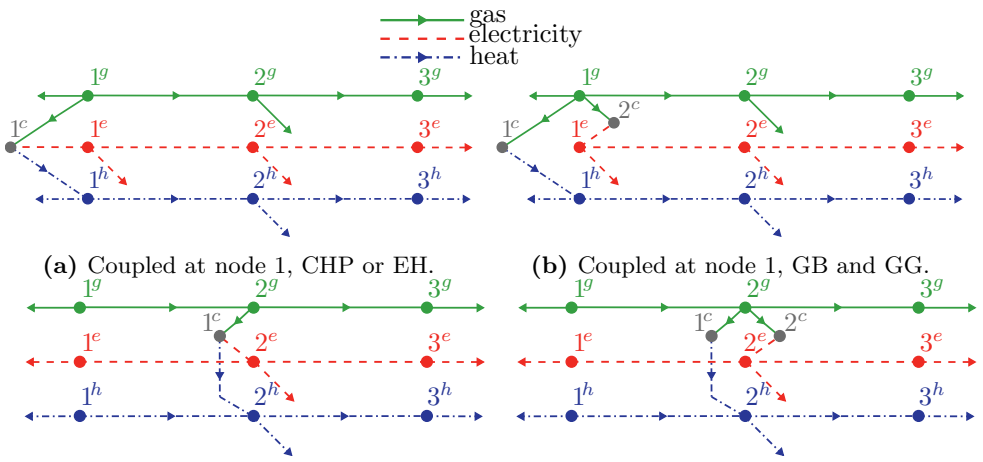

(a) Coupled at node 1, CHP or EH.

(b) Coupled at node 1, GB and GG.

(c) Coupled at node 2, CHP or EH.

(d) Coupled at node 2, GB and GG.

Figure 7.4: MES network topologies, using various couplings. Arrows on links and terminal links show defined direction of flow.

We consider coupling components that convert gas to electricity, heat, or both, to connect the SC networks. One electrical and one heat source are replaced with a coupling, such that the SCNs are coupled at node 1 or at node 2. The networks are coupled by a single node representing a CHP or an EH, or by two nodes representing a GB and a GG. Figure 7.4 shows the possible topologies for the base case MES.

This base case can be extended by replacing the sink at node 3 of each SC network by a tree-like structure which we call 'streets'. There are s streets, $S_1 - S_s$, which are all connected to node 3 of the base SC network through a junction node. Each street consists of n loads, $L_1 - L_n$, connected to the main street links by junctions, m of which, $J_1 - J_m$, are connected to two loads. Figure 7.5 shows the topology of such an extended SC network, which consists of $3+s(2n-m+1)$ nodes and $2+s(2n-m+1)$ links. The extended MES is created by coupling the SCNs in the same way as for the

base network.

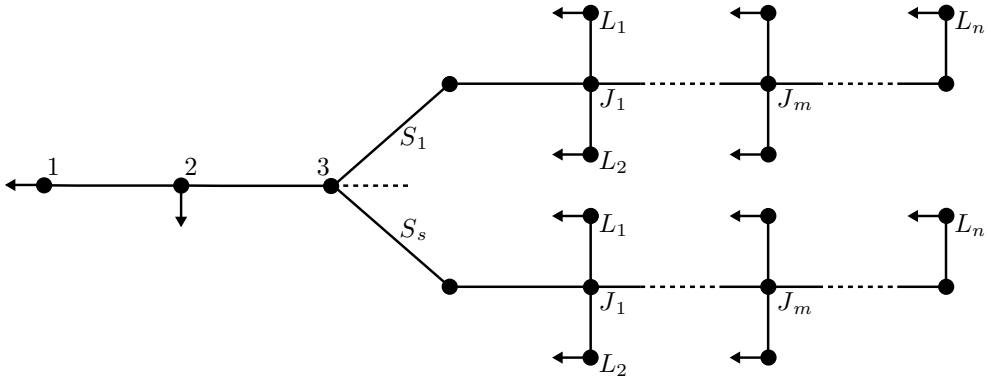

Figure 7.5: Extension of SC networks, with s streets consisting of n loads. Arrows on links and terminal links show defined direction of flow.

For all four types of coupling, and for both the base case and the extended case, the same models are used in the SC parts. The parameter values used in the equations are given in Tables C.42–C.52 in Appendix C.5.

In the gas network, all links represent pipes, which are modeled using the steady-state flow equation (2.1), with the pipe constant (2.2) and pressure drop (2.3) for high-pressure networks, and with Weymouth's friction factor (2.4). We consider both (3.4a) and (3.4b) for the link equation of the pipes.

In the electrical network, all links represent transmission lines, which we model as medium-length lines. We use (2.14) and (2.15) for the active and reactive powers in (4.4).

In the heat network, all links represent pipes. For the hydraulic model, we use the steady-state flow equation (2.20), with pipe constant (2.22) and pressure drop (2.21), and with Pole's friction factor (2.5). For the thermal pipe model, we use (2.28). We use the terminal link formulation (4.7), with (3.16) for the hydraulic link equations.

For the coupling components, we use linear models (2.33) and (2.36) for the GB and CHP, we use linear model (2.31) or nonlinear model (2.32) for the GG, and we use (2.38) for the EH, with $\boldsymbol{E}_{\text{out}} = \begin{pmatrix} P_{\text{out}} & \Delta\varphi_{\text{out}} \end{pmatrix}^T$, $\boldsymbol{E}_{\text{in}} = \begin{pmatrix} E^g_{\text{in}} \end{pmatrix}$, $c^{ge} = 1/2\eta_{\text{GG}}$, and $c^{gh} = 1/2\eta_{\text{GB}}$.

7.2.2 Node types

We consider both types of BC for the heat load nodes, as described in Section 4.1. That is, for each terminal link l connected to node i, we either assume $\Delta T_{i,l}$ known, or we assume $T^r_{i,l}$ known for sinks and $T^s_{i,l}$ known for sources.

Table 7.2 gives the node types used for the LF problem in the SCNs, based on which variables are specified. Note that the electrical and heat network do not necessarily have a physical solution. For instance, if $|\Delta\varphi_{2,0}| > |\Delta\varphi_{3,0}| > 0$, the source slack node 1^h would have to behave as a sink, which is unphysical.

Node 1 is the slack node in all three SCNs, such that LF analysis determines the amount of injected flow or energy entering node 1. Replacing the slacks of the

Table 7.2: Node type set with BCs for the SC base networks.

	Gas		Electricity		Heat	
Node	**Type**	**Spec.**	**Type**	**Spec.**	**Type**	**Specified**
1	ref.	p^g	slack	$\|V\|$, δ	source ref. slack	T^s, p^h
2	load	q	gen.	P, $\|V\|$	load (source)	$T^s_{2,0}$ or ΔT, $\Delta\varphi$
3	load	q	load	P, Q	load (sink)	$T^r_{3,0}$ or ΔT, $\Delta\varphi$

electrical and heat network with a coupling is then straightforward. The electrical and heat SC parts of the MES will determine the coupling powers $\Delta\varphi^c$ and P^c, after which the coupling equations for a CHP, or for a GB and a GG, uniquely determine coupling gas flow q^c. For the EH, the coupling equation needs only P^c or $\Delta\varphi^c$ to uniquely determine q^c and $\Delta\varphi^c$ or P^c. Hence, either the electrical or the heat network will need an additional slack.

Conversely, node 2 was a generator or a source node in the SC electrical and heat network, such that P and $\Delta\varphi$ were given. Replacing those sources with the coupling, after which P^c and $\Delta\varphi^c$ are unknown, means BCs must be chosen such that the SC parts can determine q^c, P^c, or $\Delta\varphi^c$ for the coupling equation(s) to be able to determine the others.

Table 7.3: Node type sets with BCs for the networks, coupled at node 1, shown in Figures 7.4a and 7.4b.

	CHP or GB+GG		EH	
Node	**set 1**	**set 2**	**set 1**	**set 2**
1^g	p^g	p^g	p^g	p^g
2^g	q	q	q	q
3^g	q	q	q	q
1^e	P, Q, $\|V\|$, δ	P, Q, $\|V\|$, δ	Q, $\|V\|$, δ	P, Q, $\|V\|$, δ
2^e	P, $\|V\|$	P, $\|V\|$	P, $\|V\|$	P, $\|V\|$
3^e	P, Q	P, Q	P, Q	P, Q
1^h	T^s, p^h, $m=0$	p^h, $m=0$	T^s, p^h, $m=0$	T^s, p^h
2^h	$T^s_{2,0}$ or ΔT, $\Delta\varphi$	$T^s_{2,0}$ or ΔT, $\Delta\varphi$	$T^s_{2,0}$ or ΔT, $\Delta\varphi$	$T^s_{2,0}$ or ΔT, $\Delta\varphi$
3^h	$T^r_{3,0}$ or ΔT, $\Delta\varphi$	$T^r_{3,0}$ or ΔT, $\Delta\varphi$	$T^r_{3,0}$ or ΔT, $\Delta\varphi$	$T^r_{3,0}$ or ΔT, $\Delta\varphi$
1^c	-	T^s	-	T^s
2^c	-	-	-	-

Tables 7.3 and 7.4 give the various node sets of BCs, only showing the specified values, used in the MCNs for the base case. We consider two different node sets if the SCNs are coupled at node 1, and we consider three different node sets if the SCNs are coupled at node 2.

The BCs for nodes 1 and 2 of the extended case are the same as in Table 7.2 for the SC networks and the same as in Table 7.3 and Table 7.4 for the MCNs, node 3 is

a junction, and the additional nodes are junction or load (sink) nodes.

Table 7.4: Node type sets with BCs for the networks, coupled at node 2, shown in Figures 7.4c and 7.4d.

	CHP or GB+GG			EH		
Node	**set 1**	**set 2**	**set 3**	**set 1**	**set 2**	**set 3**
1^g	p^g, q	p^g, q	p^g	p^g, q	p^g	p^g
2^g	q	q	q	q	q	q
3^g	q	q	q	q	q	q
1^e	P, $\lvert V\rvert$	$\lvert V\rvert$, δ	P, $\lvert V\rvert$	$\lvert V\rvert$, δ	P, $\lvert V\rvert$	$\lvert V\rvert$, δ
2^e	P, Q, $\lvert V\rvert$, δ	P, Q, $\lvert V\rvert$	P, Q, $\lvert V\rvert$, δ	P, Q, $\lvert V\rvert$	P, Q, $\lvert V\rvert$, δ	P, Q, $\lvert V\rvert$
3^e	P, Q	P, Q	P, Q	P, Q	P, Q	P, Q
1^h	T^s, p^h	p^h, $T^s_{1,0}$ or ΔT, $\Delta\varphi$	p^h, $T^s_{1,0}$ or ΔT, $\Delta\varphi$	T^s, p^h	T^s, p^h	p^h, $T^s_{1,0}$ or ΔT, $\Delta\varphi$
2^h	$m{=}0$	$m{=}0$	$m{=}0$	$m{=}0$	$m{=}0$	$m{=}0$
3^h	$T^r_{3,0}$ or ΔT, $\Delta\varphi$	$T^r_{3,0}$ or ΔT, $\Delta\varphi$	$T^r_{3,0}$ or ΔT, $\Delta\varphi$	$T^r_{3,0}$ or ΔT, $\Delta\varphi$	$T^r_{3,0}$ or ΔT, $\Delta\varphi$	$T^r_{3,0}$ or ΔT, $\Delta\varphi$
1^c	T^s	T^s	T^s	T^s	T^s	T^s
2^c	-	-	-	-	-	-

7.2.3 Solving the load flow problem

For the SC gas network, and for the gas part in the MC network, we consider the nodal system (4.3) with (3.4a) for the link equations, and the full system (4.1) with (3.4a) or (3.4b) for the link equations, giving three different formulations of the SC gas LF problem.

For the SC heat network, and for the heat part in the MC network, we consider the terminal link formulation (4.7) and the standard formulation (4.9), both with either $T_{i,l}$ or ΔT known for the heat load nodes, giving four different formulations of the SC heat LF problem.

For the MESs, we consider the base case MCNs with the topologies as shown in Figures 7.4a–7.4b and the node sets given in Table 7.3 when coupled at node 1, and the topologies shown in Figures 7.4c–7.4d and the nodes sets given in Table 7.4 when coupled at node 2. The extended cases use the same node sets, and we take 30 nodes per SCN ($n = 5, m = 2, s = 3$) for a medium network, or 323 nodes per SCN ($n = 10, m = 5, s = 20$) for a large network.

To solve the system of equations for each SCN, and the system of equations (4.11) for the MCNs, we use scaled NR, see Algorithm 5.2, with a tolerance $\tau = 10^{-6}$. As base values for scaling, we take the values given in Table C.45 for the base case. We take the same base values for the extended cases, except for p^g for which we take $p^g_b = 50 \cdot 10^5$ Pa, see Table C.53.

We use a flat initial guess of NR, except for a linear profile for $\boldsymbol{p}^g$, $\boldsymbol{p}^h$, and $\boldsymbol{T}^s$, where the nodes furthest from the source have the lowest value. See Appendix C.5.2 for more details.

Figure 7.6 shows the convergence behavior of NR for the three SCNs, using the largest network, as an example. Table 7.5 summarizes the iterations needed by NR to converge. The convergence of NR for the SCNs shows very similar behavior for all network sizes. However, the convergence is different for the various formulations in the gas network and in the heat network.

For the gas network, using link equation $F^{\Delta p(q)}$ (3.4b) results in slightly faster convergence than $F^{q(\Delta p)}$ (3.4a). With the latter, the nodal and full formulation give

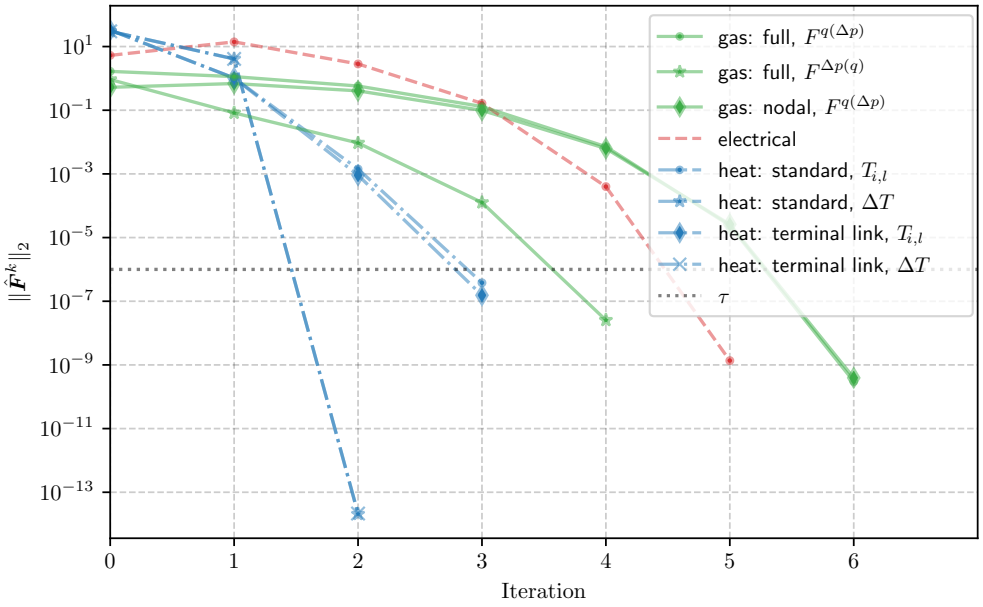

Figure 7.6: Convergence of NR for the extended SCNs, with $n = 10$, $m = 5$, and $s = 20$, using various formulations in gas and in heat.

Table 7.5: NR iterations for different formulations of the LF problem of SCNs.

		Case (number of nodes per SCN)		
Carrier	**Formulation**	**Base**	**Ext. medium (30)**	**Ext. large (323)**
Gas	nodal, $F^{q(\Delta p)}$	4	6	6
	full, $F^{q(\Delta p)}$	4	6	6
	full, $F^{\Delta p(q)}$	3	5	4
Electricity		2	3	5
Heat	standard, $T_{i,l}$	3	3	3
	standard, ΔT	2	2	2
	terminal link, $T_{i,l}$	3	3	3
	terminal link, ΔT	2	2	2

the same results. For the heat network, convergence shows no difference between the terminal link or the standard formulation. Assuming $\Delta T_{i,l}$ known for a heat load, instead of assuming $T^r_{i,l}$ known for sinks and $T^s_{i,l}$ for sources, gives better convergence. Hereafter, we only show the results of the LF problem for the MESs with the full formulation in gas and the terminal link formulation, with ΔT known, in heat. Using the nodal formulation in gas, and standard formulation or terminal link formulation with $T_{i,l}$ known in heat, give similar results.

Figure 7.7 shows the convergence of NR for the base case MES coupled at node 2, using different topologies, coupling components, and all node sets. In total, this

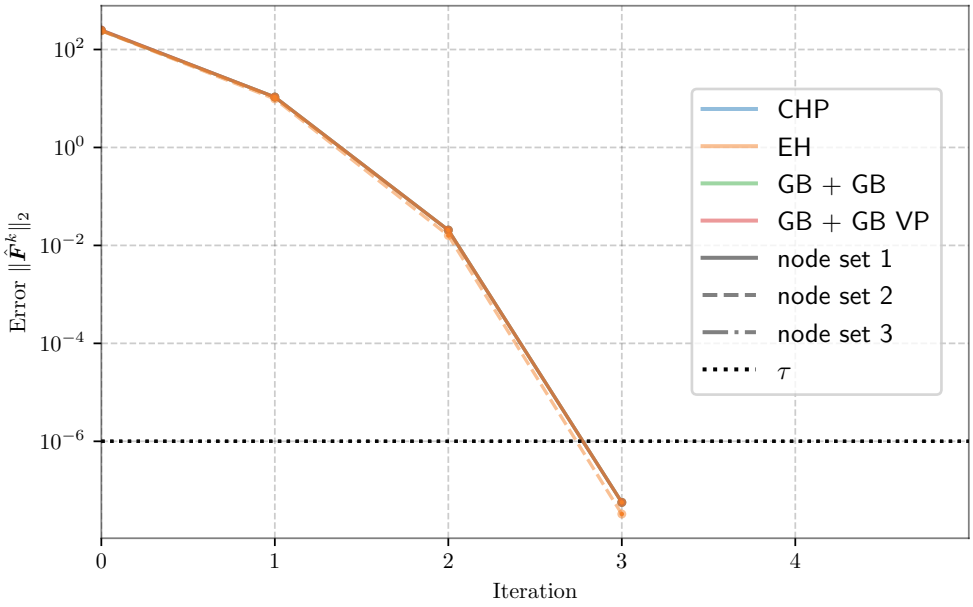

Figure 7.7: Convergence of NR for the base case MES, coupled at node 2, using full formulation with $F^{\Delta p(q)}$ in gas, and terminal link formulation with $\Delta T_{i,l}$ known in heat. Most of the curves are indistinguishable at this scale.

figure shows the convergence of twelve cases, namely four different types of coupling with three different node sets each. The convergence in Figure 7.7 is typical for this MES. Numerical experiments show similar convergence for the extended case coupled at node 2, and for the base and extended case coupled at node 1, for all considered topologies, coupling components, and node sets.

For comparison of the various couplings and the various sizes, we give the results for the node sets in which the coupling component functions as a slack for the heat network. That is, we use node set 1 when coupling at node 1, and node set 3 when coupling at node 2. Table 7.6 shows the number of iterations needed by NR to converge for the base and extended case MESs, for these two node sets. Numerical experiments show similar results for the other node sets, and other formulations. Given a formulation of the SC parts, the NR iterations for the MCNs follow a similar pattern for both points of coupling, all four coupling components and models, and all node sets. Hence, for this example, the convergence behavior of the MES is determined by the SCNs, and not by the coupling. Moreover, we find that for the extended case, the number of iterations barely increases if the size of the network increases, both for the SCNs and for the MCNs.

The independence of the convergence of NR on the type of coupling, seen in this example, could be due to the topology and the choice of BCs. All node sets are chosen such that the steady-state LF problem can be solved uniquely for one or two SCNs, with the coupling energy as unknown. The coupling equations can then be used to compute the other coupling energies or energy, which serve as a BC for the other

Table 7.6: NR iterations for LF problem of the MCNs of various sizes.

Size	Form. gas	Coupled at	CHP	GB+GG	GB+GG VP	EH	Max. SC
base	full, $F^{q(\Delta p)}$	node 1	4	4	4	4	4
		node 2	4	4	4	4	4
	full, $F^{\Delta p(q)}$	node 1	3	3	3	3	3
		node 2	3	3	3	3	3
medium $n = 5$ $m = 2$ $s = 3$	full, $F^{q(\Delta p)}$	node 1	6	6	6	6	6
		node 2	6	6	6	6	6
	full, $F^{\Delta p(q)}$	node 1	5	5	5	5	5
		node 2	5	5	5	5	5
large $n = 10$ $m = 5$ $s = 20$	full, $F^{q(\Delta p)}$	node 1	6	6	6	6	6
		node 2	6	6	6	6	6
	full, $F^{\Delta p(q)}$	node 1	4	4	4	4	5
		node 2	4	4	4	4	5

SCNs. Hence, the LF problem for the example MESs could be solved by sequentially solving the SC LF problems, instead of solving one integrated system of equations. In other words, the Jacobian matrix (5.7) used in NR could easily be reordered into block upper triangular form, where the coupling part is included with the SC parts. This may induce the solution paths of the subsystems to be very similar to those of the individual subsystems when solved separately, so that the number of iterations of the integrated systems is automatically near the maximum of the iteration numbers of the individual subsystems. Similar convergence behavior could be expected for other MESs where the integrated LF problem can easily be decomposed into solvable SC subsystems.

For these example MCNs, NR for the LF problems of the MES requires at most as many iterations as the slowest SCN. Moreover, the number of NR iterations are independent of the coupling and almost independent of the size of the network.

7.3 Final remarks

The node types determine in which SC part of the MCN most of the solver work is done. For the example in Section 7.1, the focus is on the electrical part for the first node set and on the gas part for the second node set. It might be possible to choose BCs such that the work is done in the SC network that is easiest to solve, but further research is required. Moreover, if the difference in convergence behavior of the SC parts is larger than in this example, we expect to see a bigger influence of the node type sets on the convergence of NR for the MCN.

For the example in Section 7.2, the size-independency of NR might be due to the tree-structure of the considered networks. Further research is required to determine the influence of the size of the network on the convergence of NR for a network that contains (more) loops.

The independence of the convergence of NR on the type of coupling could be due to the topology and the choice of BCs. The SCNs of the considered MES do not depend on each other, rather, one SC part depends on the other two. When solving

the integrated system of LF equations, the SC parts are essentially solved in parallel, so that the number of iterations of the integrated system is automatically near the maximum number of iterations of the SCNs. We expect similar convergence behavior for other MESs where the integrated LF problem can easily be decomposed into solvable SC subsystems. Such a decomposition is not as straightforward for the first example MES, for which the convergence of NR is indeed influenced by the coupling and the node type sets.

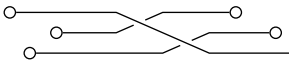

CHAPTER 8

A decoupled approach to solving the load flow problem

The framework to perform steady-state LF analysis of MESs, as given in Section 4.3, represents a MES as one connected MCN, after which the single system of equations (4.11) is solved using NR. However, SC energy systems have been widely studied, such that dedicated models and solvers exist. Using these SC models and solvers within this framework is not straightforward, due to the single connected MCN. Furthermore, the SC energy systems of the various carriers are usually maintained and controlled by different systems operators. Issues with sharing detailed network data amongst the various operators might prohibit a MES to be modeled as a single MCN. One option to model a MES as an integrated system, while keeping the SC energy systems (relatively) separate, is to adopt a decoupling approach, similar to domain decomposition (DD). This approach allows the use of dedicated SC solvers, and does not require all data to be shared amongst the various subsystems.

The decoupling approach disconnects the SC systems from the coupling part, and models each SC system, the coupling, and the interaction between the systems separately. A similar approach is used in [8], for a case study of a combined electricity and heat system, but has not yet been used for MESs consisting of gas, electricity, and heat. We provide a decoupling approach to general MESs, based on a disconnected or decoupled network representation. This approach provides an alternative to the framework in Figure 4.1, to perform steady-state LF analysis of integrated MESs.

The definition of the links and terminal links, and the choice for a coupling node, allows for the decoupling of the single connected MCN into SCNs and a (heterogeneous) coupling network. This provides a framework to represent general MESs as a disconnected MCN, consisting of several SCNs and one or more coupling networks.

For each of these subnetworks, the extended LF problem (4.13) can be solved. In addition to these subproblems, the connection between the SC and coupling subnetworks needs to be taken into account, which we call the interface conditions (IFCs). Combining the LF problems of the subnetworks with the IFCs gives a system of (non)linear equations, that models the LF problem for the integrated MES, and which is an alternative to the system (4.11). We consider three ways to solve this alternative system: the fixed-point method (FP), NR, and accelerated FP.

First, we discuss how to decouple a connected MCN into SCNs and a (heterogeneous) coupling network. We introduce the IFCs, which model the connections between the subnetworks. Then, we describe how to formulate the LF problem of the

MES, based on the LF problems of the subsystems and on the IFCs. We discuss the three ways to solve the resulting nonlinear system of equations, and we compare the decoupled approach to solving the LF problem (4.11). Finally, we use the decoupled approach to solve the LF problem of some small example MESs.

8.1 Decoupling a multi-carrier network

Decoupling an MCN is relatively straightforward, and is the opposite of coupling the SCNs as described in Section 3.3. We decouple the MCN by cutting all dummy links that connect a homogeneous node to a (heterogenous) coupling node.

By definition, a terminal link is half of a link, such that cutting a link results in two (homogeneous) terminal links. The link quantities that are associated with one side of the link will be a terminal link quantity of only one of the created terminal links. Link quantities that are associated with the entire link will be a terminal link quantity of both terminal links. This process is shown in Figure 8.1, for a coupling that produces heat.

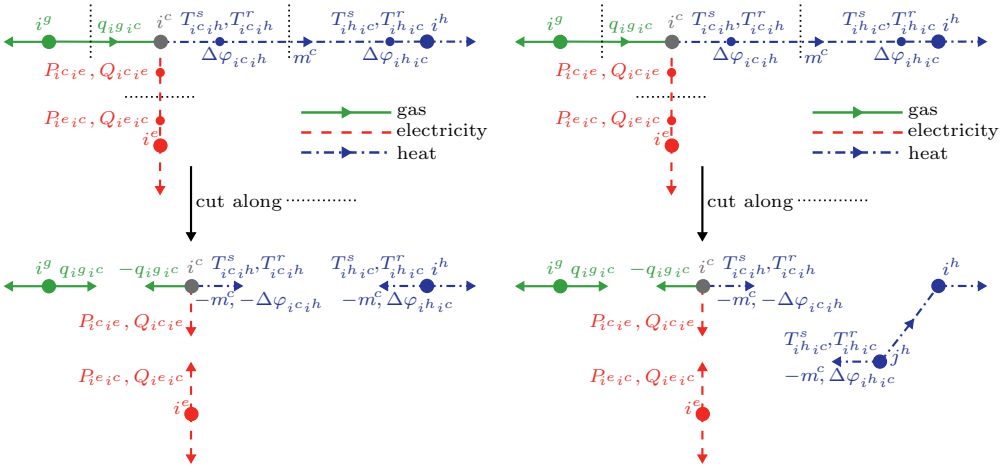

(a) Node i^h is a source. **(b)** Node i^h is a sink.

Figure 8.1: Decoupling an MCN, assuming the coupling produces heat, by cutting the (dummy) links, with node i^h a source (a) or a sink (b). Arrows on links and terminal links show defined direction of flow.

Since dummy links only show a connection between two nodes, but do not represent any physical component, cutting a dummy link simply results in two terminal links. Cutting a non-dummy link might be possible, but requires a strategy to 'cut' the model of the physical element represented by the link. In this thesis, we only consider cutting dummy links.

We assume heat nodes can only have one type of terminal link, either sink or source, connected to them, see Section 3.2.3. Cutting a (dummy) link connected to a heat node leaves a terminal link connected to that node. If this node already has a terminal link connected to it, we might end up with both sink and source terminal

links connected to one heat node. If this would be the case, an additional node is added to the SC heat network instead, to which the newly created terminal link is connected. This additional node is connected with a dummy link to the original heat node. Both the original and the additional heat node now have terminal links of only one type connected to them. This is shown in Figure 8.1b, where node j^h is the additional node.

In practice, this issue might not occur, as, usually, to create a connected MCN, some heat source nodes of the SC heat network are connected to a coupling unit that produces heat. Hence, a coupling unit that produces heat will not be connected to a heat sink node in the MCN. If such an MCN is decoupled by cutting the dummy links, this will result in new source terminal links that have to be connected to the heat source nodes. This does not require extra steps, and is shown in Figure 8.1a.

The nodal coupling equation (3.26) remains on the coupling node, but is now a function of terminal link quantities instead of link quantities. For coupling units that produce or consume heat, the heat power equation (3.27) is replaced by (3.23) on each terminal link created by cutting the dummy link.

If a MES has multiple coupling components, the corresponding MCN can have multiple coupling nodes. Decoupling the connected MCN by cutting all dummy links gives a disconnected MCN with multiple coupling nodes, which are also disconnected from each other. The collection of these coupling nodes can be seen as one (disconnected) heterogeneous network, or each coupling node can be seen as a separate (connected) heterogeneous network. In this thesis, we view the coupling nodes as one disconnected heterogeneous network.

By cutting all the dummy links between a homogeneous node and a heterogeneous node, a connected MCN is decoupled, or decomposed, into its SC parts and its coupling part. For each of these subnetworks, the extended LF problem (4.13) can be solved. Denoting the BCs of a (sub)network by $\boldsymbol{b}$, we can write the extended LF problem, for each $\alpha \in \{g, e, h, c\}$, as

$$\boldsymbol{h}^\alpha(\boldsymbol{x}^\alpha; \boldsymbol{b}^\alpha) := \begin{pmatrix} \boldsymbol{F}^\alpha(\boldsymbol{x}^\alpha; \boldsymbol{b}^\alpha) \\ \boldsymbol{G}^\alpha(\boldsymbol{x}^\alpha; \boldsymbol{b}^\alpha) \end{pmatrix} = \boldsymbol{0} \tag{8.1}$$

Given appropriate BCs $\boldsymbol{b}^\alpha$, this system can be solved for the (extended) state variables $\boldsymbol{x}^\alpha$. We use (4.1) or (4.3) for the gas LF equations $\boldsymbol{F}^g$, (4.5) for the electrical LF equations $\boldsymbol{F}^e$, (4.7) or (4.9) for the heat LF equations $\boldsymbol{F}^h$, and (4.10) for the LF equations $\boldsymbol{F}^c$ of the coupling network.

8.1.1 Interface conditions

In order to formulate the LF problem of the integrated MES, the interaction between the SC subnetworks and the coupling subnetwork should also be taken into account, in addition to the subproblems (8.1). We model this interaction through interface conditions (IFCs). The subnetworks are created by cutting the dummy links of the MCN. Since the dummy links represented the connection between the SC networks and the coupling nodes, the subnetworks interact through the terminal links obtained after cutting the dummy links.

The IFCs relate the quantities on the terminal links of the various subnetworks to each other. For instance, if a gas dummy link from gas node i^g to coupling node i^c is

cut into terminal links l, as shown in Figure 8.1, the IFC for this connection is given by

$$q_{i^g,l} = -q_{i^c,l} \tag{8.2}$$

Figure 8.1 also shows that these terminal links flows are related to the dummy link flow of the connected MCN as $q_{i^g,l} = -q_{i^c,l} = q_{i^g i^c}$.

Similarly, the IFCs for an electrical dummy link between node i^e and i^c, cut into terminal links l, are given by

$$P_{i^e,l} = -P_{i^c,l} \tag{8.3a}$$
$$Q_{i^e,l} = -Q_{i^c,l} \tag{8.3b}$$

The terminal link powers are related to the dummy link powers of the connected MCN as $P_{i^e,l} = P_{i^e i^c}$, $P_{i^c,l} = P_{i^c i^e}$, $Q_{i^e,l} = Q_{i^e i^c}$, and $Q_{i^c,l} = Q_{i^c i^e}$.

If a coupling node produces heat, a heat dummy link from i^c to i^e is cut into two source terminal links l. The IFCs are then given by

$$m_{i^h,l} = m_{i^c,l} \tag{8.4a}$$
$$\Delta\varphi_{i^h,l} = \Delta\varphi_{i^c,l} \tag{8.4b}$$
$$T^s_{i^h,l} = T^s_{i^c,l} \tag{8.4c}$$
$$T^r_{i^h,l} = T^r_{i^c,l} \tag{8.4d}$$

The terminal link quantities are related to the dummy link quantities of the connected MCN as $m_{i^h,l} = m_{i^c,l} = -m_{i^c i^h}$, $\Delta\varphi_{i^h,l} = \Delta\varphi_{i^c,l} = -\Delta\varphi_{i^c i^h}$, $T^s_{i^h,l} = T^s_{i^c,l} = T^s_{i^c i^h}$, and $T^r_{i^h,l} = T^r_{i^c,l} = T^r_{i^h i^c}$.

The subnetworks require BCs for their LF problems (8.1) to be solvable. Generally, this requires the assumption that some of the quantities on the terminal links, obtained after cutting the dummy links, are known. In other words, some of these terminal link quantities are part of the BCs $\boldsymbol{b}^\alpha$ and the rest are part of the (extended) state variables $\boldsymbol{x}^\alpha$.

8.2 Formulation of the load flow problem

Even though the MES is represented by a decoupled MCN, we still want to perform steady-state LF analysis for the integrated MES. To do this, the output of one subnetwork is taken as BC for another subnetwork, through the IFCs. The steady-state LF problem of the integrated MES, represented by a decoupled MCN, is then obtained by combining the LF equations of the SC subnetworks and of the coupling subnetwork with the IFCs.

Since the output of one subnetwork is taken as BC for another subnetwork, one of the quantities in an IFC is a variable in the extended LF problem of one subnetwork, and the other quantity is a BC for another subnetwork. Therefore, each IFC in (8.2)–(8.4) is of the form $b^\alpha = \pm x^\beta$, with $x^\beta \in \boldsymbol{x}^\beta$ and $b^\alpha \in \boldsymbol{b}^\alpha$, for $\alpha, \beta \in \{g, e, h, c\}$, and $\alpha \neq \beta$.

Only a part of the (extended) state variables $\boldsymbol{x}^\alpha$ and of the BCs $\boldsymbol{b}^\alpha$ of each subsystem are used in the IFCs, namely only those quantities associated with the terminal

links obtained after cutting the dummy links. Denoting those parts by $\boldsymbol{v} \subseteq \boldsymbol{x}$ and $\boldsymbol{u} \subseteq \boldsymbol{b}$ respectively, the IFCs (8.2)–(8.4) can be written as

$$\boldsymbol{u}^g = A^{cg}\boldsymbol{v}^c \tag{8.5a}$$
$$\boldsymbol{u}^e = A^{ce}\boldsymbol{v}^c \tag{8.5b}$$
$$\boldsymbol{u}^h = A^{ch}\boldsymbol{v}^c \tag{8.5c}$$
$$\boldsymbol{u}^c = \begin{pmatrix} A^{gc} & 0 & 0 \\ 0 & A^{ec} & 0 \\ 0 & 0 & A^{hc} \end{pmatrix} \begin{pmatrix} \boldsymbol{v}^g \\ \boldsymbol{v}^e \\ \boldsymbol{v}^h \end{pmatrix} \tag{8.5d}$$

The matrices $A^{\alpha\beta}$ are sparse matrices with non-zero elements equal to ± 1. For the coupling subnetwork, $\boldsymbol{v}^c$ and $\boldsymbol{u}^c$ are assumed to be ordered like $\boldsymbol{x}^c$ in (4.10), with terminal link quantities instead of dummy link quantities. For notational simplicity, we denote each of the IFCs (8.5a)–(8.5d) as:

$$\boldsymbol{u}^\alpha = \boldsymbol{g}^{\mathrm{I},\alpha}(\boldsymbol{v}) \tag{8.6}$$

Given these $\boldsymbol{u}^\alpha$ (and the rest of $\boldsymbol{b}^\alpha$), the extended LF problem (8.1) of each subnetwork can be solved for $\boldsymbol{v}^\alpha$ (and the rest of $\boldsymbol{x}^\alpha$). That is, we can determine $\boldsymbol{v}^\alpha$ for a given $\boldsymbol{u}^\alpha$, for each $\alpha \in \{g, e, h, c\}$, assuming (8.1) is well-posed. We denote these subproblems as

$$\boldsymbol{v}^\alpha = \boldsymbol{g}^\alpha(\boldsymbol{u}^\alpha) \tag{8.7}$$

Since these subproblems correspond to solving the extended LF problem (8.1), it is, in general, not possible to derive an explicit algebraic expression for $\boldsymbol{g}^\alpha$.

The subnetworks of the decoupled MCN only interact with each other through the IFCs. Hence, the values of the terminal link variables $\boldsymbol{v}$ (and BCs $\boldsymbol{u}$) are the only data that needs to be communicated between the various subsystems. This limits the data that has to be shared among the operators of the subsystems, and does not require the operators to share detailed network data or models. For instance, an operator of a gas network does not need to share pressure values, but only the gas flows going to or coming from a coupling unit.

We combine the IFCs (8.6) with the implicit relations (8.7), for each $\alpha \in \{g, e, h, c\}$, to formulate the steady-state LF problem of the integrated MES, represented by a decoupled MCN:

$$\boldsymbol{y} = \boldsymbol{g}(\boldsymbol{y}) \tag{8.8}$$

In this thesis, we consider two ways to form (8.8) by collecting (8.6) and (8.7). For the first option, we collect the equations and variables per carrier, such that

$$\boldsymbol{g}(\boldsymbol{y}) = \begin{pmatrix} \boldsymbol{g}^g(\boldsymbol{u}^g) \\ \boldsymbol{g}^{\mathrm{I},g}(\boldsymbol{v}^c) \\ \boldsymbol{g}^e(\boldsymbol{u}^e) \\ \boldsymbol{g}^{\mathrm{I},e}(\boldsymbol{v}^c) \\ \boldsymbol{g}^h(\boldsymbol{u}^h) \\ \boldsymbol{g}^{\mathrm{I},h}(\boldsymbol{v}^c) \\ \boldsymbol{g}^c(\boldsymbol{u}^c) \\ \hdashline \boldsymbol{g}^{\mathrm{I},c}(\boldsymbol{v}^g, \boldsymbol{v}^e, \boldsymbol{v}^h) \end{pmatrix} := \begin{pmatrix} \boldsymbol{g}_1(\boldsymbol{y}_1, \boldsymbol{y}_2) \\ \hdashline \boldsymbol{g}_2(\boldsymbol{y}_1) \end{pmatrix}, \quad \boldsymbol{y} = \begin{pmatrix} \boldsymbol{v}^g \\ \boldsymbol{u}^g \\ \boldsymbol{v}^e \\ \boldsymbol{u}^e \\ \boldsymbol{v}^h \\ \boldsymbol{u}^h \\ \boldsymbol{v}^c \\ \hdashline \boldsymbol{u}^c \end{pmatrix} := \begin{pmatrix} \boldsymbol{y}_1 \\ \hdashline \boldsymbol{y}_2 \end{pmatrix} \tag{8.9}$$

For the second option, we exploit the structure of the decoupled MCN. Since the SC subnetworks only interact with the coupling subnetwork, and vice versa, and only through the IFCs, we take

$$\boldsymbol{g}(\boldsymbol{y}) = \begin{pmatrix} \boldsymbol{g}^g(\boldsymbol{u}^g) \\ \boldsymbol{g}^e(\boldsymbol{u}^e) \\ \boldsymbol{g}^h(\boldsymbol{u}^h) \\ \hdashline \boldsymbol{g}^{\mathrm{I},c}(\boldsymbol{v}^g, \boldsymbol{v}^e, \boldsymbol{v}^h) \\ \hdashline \boldsymbol{g}^c(\boldsymbol{u}^c) \\ \hdashline \boldsymbol{g}^{\mathrm{I},g}(\boldsymbol{v}^c) \\ \boldsymbol{g}^{\mathrm{I},e}(\boldsymbol{v}^c) \\ \boldsymbol{g}^{\mathrm{I},h}(\boldsymbol{v}^c) \end{pmatrix} := \begin{pmatrix} \boldsymbol{g}_1(\boldsymbol{y}_4) \\ \boldsymbol{g}_2(\boldsymbol{y}_1) \\ \boldsymbol{g}_3(\boldsymbol{y}_2) \\ \boldsymbol{g}_4(\boldsymbol{y}_3) \end{pmatrix}, \quad \boldsymbol{y} = \begin{pmatrix} \boldsymbol{v}^g \\ \boldsymbol{v}^e \\ \boldsymbol{v}^h \\ \hdashline \boldsymbol{u}^c \\ \hdashline \boldsymbol{v}^c \\ \hdashline \boldsymbol{u}^g \\ \boldsymbol{u}^e \\ \boldsymbol{u}^h \end{pmatrix} := \begin{pmatrix} \boldsymbol{y}_1 \\ \boldsymbol{y}_2 \\ \boldsymbol{y}_3 \\ \boldsymbol{y}_4 \end{pmatrix} \tag{8.10}$$

The division of $\boldsymbol{g}$ and $\boldsymbol{y}$ into two subsystems in (8.9) and four subsystems in (8.10) is used in Section 8.3.3.

Note that each of $\boldsymbol{g}^g$, $\boldsymbol{g}^e$, $\boldsymbol{g}^h$, and $\boldsymbol{g}^c$, given by (8.7), corresponds to solving the extended LF problem (8.1). These LF subproblems contain all the detailed network models and all the state variables, which are not explicitly part of (8.8). Moreover, dedicated SC solvers can be used for these subproblems.

8.3 Solving the load flow problem

To perform steady-state LF analysis of an integrated MES, using a decoupled MCN, the system of nonlinear equations (8.8) has to be solved (instead of (4.11), which is solved if a MES is represented by one connected MCN). We consider three ways to solve this system: FP to solve (8.8) as a single system, NR to solve $\boldsymbol{y} - \boldsymbol{g}(\boldsymbol{y}) = \boldsymbol{0}$ instead, and an accelerated version of FP.

All of these methods to solve (8.8) require $\boldsymbol{g}$ to be computed. To compute $\boldsymbol{g}^g$, $\boldsymbol{g}^e$, $\boldsymbol{g}^h$, and $\boldsymbol{g}^c$ in (8.7), the extended LF problem (8.1) needs to be solved, for a given $\boldsymbol{u}^\alpha$. We use NR as described in Chapter 5 to solve each of these subsystems.

8.3.1 Basic FP

Consider the nonlinear system $\boldsymbol{y} = \boldsymbol{g}(\boldsymbol{y})$, with $\boldsymbol{g} : D \to D$, $\boldsymbol{y} \in D$, and a domain $D \subseteq \mathbb{R}^N$. This system is solved iteratively using FP by setting

$$\boldsymbol{y}^{k+1} = \boldsymbol{g}(\boldsymbol{y}^k) \tag{8.11}$$

at each iteration k. Starting at some initial guess $\boldsymbol{y}^0$, this gives a sequence $\{\boldsymbol{y}^k\}_{k=0}^{\infty}$.

Global convergence can be guaranteed for FP under certain conditions. If there exists a constant $\rho < 1$, such that $\|J(\boldsymbol{y})\| \leq \rho$, with $\|\cdot\|$ some matrix norm and $J = \nabla \boldsymbol{g}$ the Jacobian matrix, then the FP iteration scheme (8.11) is guaranteed to converge to the unique fixed point $\boldsymbol{y}^*$ of $\boldsymbol{g}$ for any initial guess $\boldsymbol{y}^0 \in D$. However, FP has linear convergence, as opposed to the (local) quadratic convergence of NR.

To solve the LF problem (8.8) with the basic FP scheme (8.11), we use Algorithm 8.1. The subsystems (8.1) in step 7 are solved using NR (see Algorithm 5.1 or Algorithm 5.2). To reduce total computation time, we only solve the extended LF problem (8.1) if the change in $\boldsymbol{u}$ between two FP iterations is 'large'. Otherwise, the

Algorithm 8.1 Basic FP applied to the integrated LF problem (8.8).

1: Set $k := 0$.
2: Choose initial guess $\boldsymbol{y}^0$, maximum number of iterations $k^{\max}$, overall tolerance τ, and LF tolerance τ_F.
3: Compute or set error e^0.
4: **while** $e^k > \tau$ and $k < k^{\max}$ **do**:
5: **for** $\alpha \in \{g, e, h, c\}$ **do**:
6: **if** $k = 0$ **or** $\|(\boldsymbol{u}^\alpha)^k - (\boldsymbol{u}^\alpha)^{k-1})\| > \tau_F$ **then**:
7: Compute $\boldsymbol{g}^\alpha((\boldsymbol{u}^\alpha)^k)$ by solving (8.1) to a tolerance τ_F.
8: **else**:
9: Set $\boldsymbol{g}^\alpha((\boldsymbol{u}^\alpha)^k) := (\boldsymbol{v}^\alpha)^k$.
10: **end if**
11: **end for**
12: **for** $\alpha \in \{g, e, h\}$ **do**:
13: Compute $\boldsymbol{g}^{\mathrm{I},\alpha}((\boldsymbol{v}^c)^k)$.
14: **end for**
15: Compute $\boldsymbol{g}^{\mathrm{I},c}((\boldsymbol{v}^g)^k, (\boldsymbol{v}^e)^k, (\boldsymbol{v}^h)^k)$.
16: Set $\boldsymbol{y}^{k+1} := \boldsymbol{g}(\boldsymbol{y}^k)$.
17: Set $k := k + 1$.
18: Compute error e^k using (8.12) or (8.13).
19: **end while**

previous solution is used, such that $\boldsymbol{v}^{k+1} = \boldsymbol{v}^k$. Furthermore, these subsystems are independent of each other, such that steps 5–11 could be done in parallel, as could steps 12–14.

Algorithm 8.1 is terminated at iteration k if $e^k \leq \tau$. We consider two error measures for this stopping criterion. The first is commonly used for FP methods:

$$e^k = \|\boldsymbol{y}^k - \boldsymbol{y}^{k-1}\|_2 \tag{8.12}$$

The second is based on the accuracy of the LF solutions of the subnetworks, to resemble the error (5.4) used when solving (4.11), the LF problem of the connected MCN. Since the LF subsystems in step 7 are solved using NR, $\boldsymbol{F}^\alpha((\boldsymbol{x}^\alpha)^{K_k})$ is computed at each FP iteration k, for $\alpha \in \{g, e, h, c\}$ and with K_k the final iteration number of NR. The error of the FP iteration is then determined as

$$e^k = \|\boldsymbol{F}^k\|_2, \quad \boldsymbol{F}^k = \begin{pmatrix} \boldsymbol{F}^{g,k} \\ \boldsymbol{F}^{e,k} \\ \boldsymbol{F}^{h,k} \\ \boldsymbol{F}^{c,k} \end{pmatrix} \tag{8.13}$$

where $\boldsymbol{F}^{\alpha,k} := \boldsymbol{F}^\alpha((\boldsymbol{x}^\alpha)^{K_k})$, for $\alpha \in \{g, e, h, c\}$.

8.3.2 The Newton-Raphson method

To solve the LF problem (8.8) using NR, we apply Algorithm 5.1 (or Algorithm 5.2) to the system $\boldsymbol{F}(\boldsymbol{y}) := \boldsymbol{y} - \boldsymbol{g}(\boldsymbol{y}) = \boldsymbol{0}$, which has Jacobian matrix $J_F(\boldsymbol{y}^k) = I - J(\boldsymbol{y}^k)$

with I the identity matrix. At every outer NR iteration k, $\boldsymbol{g}(\boldsymbol{y}^k)$ is computed by following steps 5–15 in Algorithm 8.1.

If all LF models and network data would be available, the Jacobian $J(\boldsymbol{y}^k)$ can be determined analytically, see Appendix B.2. However, we solve the system (8.8), instead of (4.11) for the connected MCN, to allow limited data transfer between the operators of the SC networks, such that the detailed LF models and data of the subnetworks are not available. In that case, the Jacobian $J(\boldsymbol{y}^k)$ can be approximated by (5.5), using a finite difference approach. This requires the computation of $\boldsymbol{g}(\boldsymbol{y} + \Delta y \boldsymbol{e}_m)$ for $m = 1, \ldots, N$, in addition to $\boldsymbol{g}(\boldsymbol{y})$, which drastically increases the number of solves of LF subsystems in each outer iteration k.

8.3.3 Accelerated FP

The basic iteration scheme (8.11) of FP has linear convergence, which can be accelerated by an approach similar to the adjustment of the Jacobi method to the Gauss-Seidel method for solving linear systems. Instead of using iteration scheme (8.11), part of the variables are updated during a single iteration step. Assuming all components of $\boldsymbol{y}$ are computed in order, the iteration scheme is adjusted to

$$\boldsymbol{y}_n^{k+1} = \boldsymbol{g}(\boldsymbol{y}_1^{k+1}, \ldots, \boldsymbol{y}_{n-1}^{k+1}, \boldsymbol{y}_n^k, \ldots, \boldsymbol{y}_N^k) \tag{8.14}$$

for all $n = 1, \ldots, N$. Although this adjustment can accelerate convergence, it generally does not change the order of convergence, such that iteration scheme (8.14) still has linear convergence.

Cutting the dummy links of the connected MCN decomposes it into the SC networks and a coupling network. The resulting system of LF equations (8.8) is then naturally divided into four system of LF problems for the subnetworks and four systems of IFCs. We combine these eight systems as (8.9) or as (8.10) to form the system of LF equations (8.8). Based on this structure, we use the accelerated FP scheme (8.14) to solve the LF problem (8.8). The effect of the ordering on the convergence of accelerated FP is investigated in Section 8.5

If the system of equations (8.8) is ordered as (8.9), $\boldsymbol{g}$ and $\boldsymbol{y}$ can be divided into two subsystems, $\boldsymbol{g}_1$ and $\boldsymbol{g}_2$, and $\boldsymbol{y}_1$ and $\boldsymbol{y}_2$, respectively, such that the accelerated FP scheme (8.14) becomes

$$\begin{aligned} \boldsymbol{y}_1^{k+1} &= \boldsymbol{g}_1(\boldsymbol{y}_1^k, \boldsymbol{y}_2^k) \\ \boldsymbol{y}_2^{k+1} &= \boldsymbol{g}_2(\boldsymbol{y}_1^{k+1}) \end{aligned}$$

To solve (8.8) ordered as (8.9) using the accelerated FP scheme, we use Algorithm 8.2.

If the system of equations (8.8) is ordered as (8.10), $\boldsymbol{g}$ and $\boldsymbol{y}$ can each be divided into four subsystems, $\boldsymbol{g}_1$, $\boldsymbol{g}_2$, $\boldsymbol{g}_3$ and $\boldsymbol{g}_4$, and $\boldsymbol{y}_1$, $\boldsymbol{y}_2$, $\boldsymbol{y}_3$ and $\boldsymbol{y}_4$, respectively, such that the accelerated FP scheme (8.14) becomes

$$\begin{aligned} \boldsymbol{y}_1^{k+1} &= \boldsymbol{g}_1(\boldsymbol{y}_4^k) \\ \boldsymbol{y}_2^{k+1} &= \boldsymbol{g}_2(\boldsymbol{y}_1^{k+1}) \\ \boldsymbol{y}_3^{k+1} &= \boldsymbol{g}_2(\boldsymbol{y}_2^{k+1}) \\ \boldsymbol{y}_4^{k+1} &= \boldsymbol{g}_2(\boldsymbol{y}_3^{k+1}) \end{aligned}$$

Algorithm 8.2 Accelerated FP applied to the LF problem (8.8) with (8.9).

1: Set $k := 0$.
2: Choose initial guess $\boldsymbol{y}^0$, maximum number of iterations $k^{\max}$, overall tolerance τ, and LF tolerance τ_F.
3: Compute or set error e^0.
4: **while** $e^k > \tau$ and $k < k^{\max}$ **do**:
5: Steps 5–14 from Algorithm 8.1.
6: Set $\boldsymbol{y}_1^{k+1} := \boldsymbol{g}_1(\boldsymbol{y}_1^k, \boldsymbol{y}_2^k)$.
7: Compute $\boldsymbol{g}^{\mathrm{I},c}((\boldsymbol{v}^g)^{k+1}, (\boldsymbol{v}^e)^{k+1}, (\boldsymbol{v}^h)^{k+1})$.
8: Set $\boldsymbol{y}_2^{k+1} := \boldsymbol{g}_2(\boldsymbol{y}_1^{k+1})$.
9: Set $k := k + 1$.
10: Compute error e^k using (8.12) or (8.13).
11: **end while**

To solve (8.8) ordered as (8.10) using the accelerated FP scheme, we use Algorithm 8.3. We call this method for solving the LF problem of an integrated MES, decoupled load flow. It can be seen as a DD approach to the nonlinear system of LF equations (4.11).

Algorithm 8.3 Accelerated FP applied to the LF problem (8.8) with (8.10).

1: Set $k := 0$.
2: Choose initial guess $\boldsymbol{y}^0$, maximum number of iterations $k^{\max}$, overall tolerance τ, and LF tolerance τ_F.
3: Compute or set error e^0.
4: **while** $e^k > \tau$ and $k < k^{\max}$ **do**:
5: **for** $\alpha \in \{g, e, h\}$ **do**:
6: Steps 6–10 from Algorithm 8.1.
7: **end for**
8: Set $\boldsymbol{y}_1^{k+1} := \boldsymbol{g}_1(\boldsymbol{y}_4^k)$.
9: Compute $\boldsymbol{g}^{\mathrm{I},c}((\boldsymbol{v}^g)^{k+1}, (\boldsymbol{v}^e)^{k+1}, (\boldsymbol{v}^h)^{k+1})$.
10: Set $\boldsymbol{y}_2^{k+1} := \boldsymbol{g}_2(\boldsymbol{y}_1^{k+1})$.
11: Steps 6–10 from Algorithm 8.1 with $\alpha = c$.
12: Set $\boldsymbol{y}_3^{k+1} := \boldsymbol{g}_3(\boldsymbol{y}_2^{k+1})$.
13: Steps 12–14 from Algorithm 8.1.
14: Set $\boldsymbol{y}_4^{k+1} := \boldsymbol{g}_4(\boldsymbol{y}_3^{k+1})$.
15: Set $k := k + 1$.
16: Compute error e^k using (8.12) or (8.13).
17: **end while**

Algorithm 8.2 and Algorithm 8.3 iterate between the LF problems of the subnetworks and the IFCs. Some MCNs are coupled in such a way that one subnetwork determines the BCs for the others. For instance, if node 1^c in the network in Figure 7.4 represents an EH, BCs can be chosen such that the heat part determines the heat power produced by the EH. The nodal coupling equations of the EH then give the active power produced, and gas flow consumed, by the EH. If we decouple this MCN, and formulate the LF problem (8.8), Algorithm 8.2 would need only 2 iterations, and

Algorithm 8.3 only 1, to find the solution. In other words, if the subnetworks of the decoupled MCN do not depend on each other, no iterations between the subsystems is required to solve the LF problem of the MES. We say that a MES that is represented by such an MCN is not fully integrated.

8.4 Relation to permutation of the load flow problem for a connected multi-carrier network

There are some similarities between the decoupled approach and permuting the system of LF equations (4.11) for a connected MCN. These similarities become clear when looking at the Jacobian of the permuted system.

With LF using a connected MCN, the SC parts and the coupling part of the LF system (4.11) generally are not square systems, as discussed in Section 4.2.5 and Section 5.3.1.

With decoupled LF, the subsystems (8.1) of the SCNs and of the coupling network of the decoupled MCN are square systems. Part of the BCs of the subnetworks in the decoupled MCN are obtained from the state variables of the other subnetworks, through the IFCs. This means that information obtained from the coupling is combined with the SC subnetworks, and vice versa.

We can adopt a similar approach to the system of LF equations (4.11), which is based on a connected MCN, by permuting the equations and variables such that the SC parts and the coupling part become square systems. This permutation is not unique, just like the sets of node types for the subnetworks in the decoupled MCN are not unique.

For the decoupled MCN, the coupling equations are part of the LF subproblem of the coupling subnetwork. Therefore, we choose to not combine coupling equations in (4.11) with the LF equations of the SC parts, instead we keep them separate as a subsystem when permuting. We move some of the coupling variables from $\boldsymbol{x}^c$ to the corresponding SC variables, but not the other way around. For instance, a coupling gas flow q^c can be included with $\boldsymbol{x}^g$ instead of $\boldsymbol{x}^c$. The permutation of (4.11) is chosen to match the structure of the LF problem (8.8) using a decoupled MCN. See for instance Appendix C.1, where (C.2) is such an permutation of the original LF system (C.1) for the gas-electricity MES used in Section 8.5.1.

Permutation changes the structure of the Jacobian matrix of the system of LF equations (4.11), which is originally structured as (5.7). Since we keep the coupling equations as a subsystem, the SC parts of the connected MCN do not interact with each other directly, but only through the coupling equations. However, we permute the variables such that some of the coupling variables are included with the SC variables. Denoting the permuted variables by $\hat{\boldsymbol{x}}$, and the permuted equations by $\hat{\boldsymbol{F}}$, the permuted Jacobian matrix of the LF using a connected MCN is then given by

$$\hat{J} = \begin{pmatrix} \hat{J}^{gg} & 0 & 0 & \hat{J}^{gc} \\ 0 & \hat{J}^{ee} & 0 & \hat{J}^{ec} \\ 0 & 0 & \hat{J}^{hh} & \hat{J}^{hc} \\ \hat{J}^{cg} & \hat{J}^{ce} & \hat{J}^{ch} & \hat{J}^{cc} \end{pmatrix} \tag{8.15}$$

If an appropriate permutation is chosen, the submatrices $\hat{J}^{gg}$, $\hat{J}^{ee}$, $\hat{J}^{hh}$, and $\hat{J}^{cc}$ are

square. Each diagonal submatrix $\hat{J}^{\alpha\alpha}$ corresponds to the LF problem (8.1) of a subnetwork in the decoupled MCN, while the off-diagonal submatrices $\hat{J}^{\alpha\beta}$ correspond to the IFCs (8.5) of the decoupled MCN. Hence, the equations and variables of the LF problem of the connected MES can be reordered to match the structure of the LF problem of the disconnected MCN.

Note that a permutation of (4.11) does not affect the iterates of NR, as discussed in Section 5.2. However, if the system (4.11) is permuted such that the submatrices $\hat{J}^{\alpha\alpha}$ are square, DD or block iterative methods can be used to solve the linear system $\hat{J}^k \hat{\boldsymbol{s}}^k = -\hat{\boldsymbol{F}}^k$ in Algorithm 5.2. Unlike the decoupled LF approach, such a DD approach still requires the detailed models and data of the SC networks to be available, and does not use dedicated LF solvers for SC parts. In this thesis, we do not consider DD in the linear system of NR.

If a permutation exists such that the Jacobian (8.15) is a block upper triangular matrix, with square submatrices on the diagonal, the SC parts of the MES are not interdependent on each other. As stated in Section 8.3.3, using the decoupled LF method to solve the LF of such a MES means that Algorithm 8.3 would only need 1 iteration to find a solution. Since NR is not affected by permutation, solving permuted (4.11) with NR would still require several iterations.

8.5 Numerical results

To illustrate the decoupled approach, we perform steady-state LF analysis for three small MESs. We use the three methods described in Section 8.3 to solve the LF problem (8.8). For comparison, we also solve the LF problem (4.11), both with and without permutation, using NR. We compare the convergence of these various methods, and compare the final solution.

The first and second MES consist of only two carriers, and the third MES consist of gas, electricity, and heat. Each of these MESs have two coupling units to create a MES in which the SC systems depend on each other, such that the MES is truly integrated, as described in Section 8.3.3.

8.5.1 Gas-electricity multi-carrier energy system

The first MES consist of a two-node gas network and a two-node electrical network, connected to each other with two coupling nodes. Figure 8.2 shows the connected and decoupled network representations of this MES.

Models and node types

In the gas network, node 0^g is a source, node 1^g is a sink, and the link from 0^g to 1^g represents a pipe. In the electrical network, both nodes are sinks, and the link from 0^e to 1^e represents a short transmission line. See Appendix C.1 for details on the models.

Both coupling nodes represent a GG, for which we use the linear model (2.31). The nodal coupling equations (3.26) for the connected MCN, shown in Figure 8.2a,

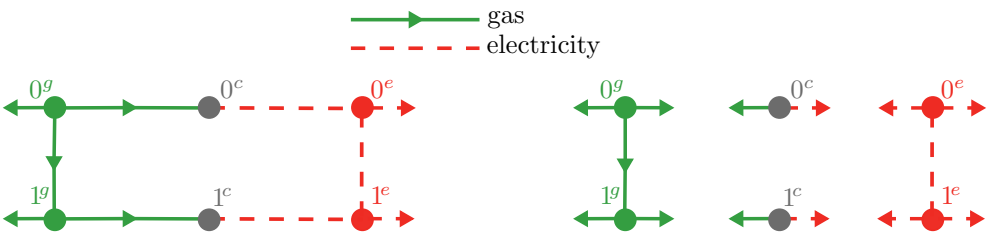

(a) Connected MCN. **(b)** Decoupled MCN.

Figure 8.2: Connected and decoupled network representation of a gas-electricity MES. Arrows on links and terminal links show defined direction of flow.

are then

$$F_{0^c}^{c,E} = P_{0^c 0^e} - \eta_{0^c}\text{GHV}q_{0^g 0^c}$$
$$F_{1^c}^{c,E} = P_{1^c 1^e} - \eta_{1^c}\text{GHV}q_{1^g 1^c}$$

and the nodal coupling equations (3.26) for the disconnected MCN, shown in Figure 8.2b, are

$$F_{0^c}^{c,E} = P_{0^c} - \eta_{0^c}\text{GHV}(-q_{0^c})$$
$$F_{1^c}^{c,E} = P_{1^c} - \eta_{1^c}\text{GHV}(-q_{1^c})$$

The parameter values used in the equations are summarized in Tables C.1–C.2 in Appendix C.1.

Table 8.1 gives the node type sets we use as BCs, for the connected and disconnected MCN. Note that these node sets lead to a LF problem that might not have a physically realistic solution, depending on the values of the BCs. Specifically, energy only enters the network in node 0^g, and we assume this inflow q_0 known. If this inflow is taken too small or too large, a (physically realistic) solution to the LF problem (4.11) or (8.8) does not exist. The values used for the BCs are given in Tables C.4–C.6 in Appendix C.1.

Table 8.1: Node type sets for the gas-electricity network.

	Connected		**Decoupled**	
Node	**Type**	**Specified**	**Type**	**Specified**
0^g	ref. load	p, q_0	ref.	p, q_0
1^g	load	q_1	load	q_1, $q_{1,1}$
0^e	PQV	P_0, Q_0, $\lvert V\rvert$	gen.	P_0, $P_{0,1}$, Q_0, $\lvert V\rvert$
1^e	PQVδ	P_1, Q_1, $\lvert V\rvert$, δ	slack	P_1, $P_{1,1}$, Q_1, $\lvert V\rvert$, δ
0^c	standard	-	qQ	q_{0^c}, Q_{0^c}
1^c	standard	-	PQ	P_{1^c}, Q_{1^c}

With the node sets in Table 8.1, the system of LF equations for the connected MCN (4.11) consists of 9 equations and variables, while the system of LF equations

for the decoupled MCN (8.8) consists of 12 equations and variables. For the decoupled LF problem, we take

$$\begin{aligned} \boldsymbol{v}^g &= \begin{pmatrix} q_{0,1} \end{pmatrix}, \quad \boldsymbol{v}^e = \begin{pmatrix} P_{1,1} & Q_{0,1} & Q_{1,1} \end{pmatrix}^T, \quad \boldsymbol{v}^c = \begin{pmatrix} -q_{1^c} & P_{0^c} \end{pmatrix}^T, \\ \boldsymbol{u}^g &= \begin{pmatrix} q_{1,1} \end{pmatrix}, \quad \boldsymbol{u}^e = \begin{pmatrix} P_{0,1} \end{pmatrix}, \qquad\qquad \boldsymbol{u}^c = \begin{pmatrix} q_{0^c} & P_{1^c} & Q_{0^c} & Q_{1^c} \end{pmatrix}^T \end{aligned} \tag{8.16}$$

See Appendix C.1 for details on the IFCs and the systems of LF equations.

Solving the load flow problem

To solve the system of equations (4.11) for the connected MCN, we use scaled NR with and without permutation. To solve the system of equations (8.8) for the decoupled MCN, we use the methods described in Section 8.3. In NR, we take a tolerance $\tau = 10^{-7}$, and in Algorithms 8.1, 8.2, and 8.3 we take tolerances $\tau = 10^{-5}$ and $\tau_F = 10^{-7}$. We use scaling for all methods, with the base values as given in Table C.3.

For NR, the Jacobian J can be determined analytically or it can be approximated by (5.5). For FP, both the basic version and the accelerated version, we can use (8.12) or (8.13) as error e in the stopping criterion. We consider the original and the permuted system (4.11), and we use (8.9) or (8.10) to order the equations and variables in (8.8). This gives a total of 14 ways to solve the LF problem.

Table 8.2: Solver information of the LF problem of the gas-electricity MES.

				# **solves** (8.1)		
Method	**System**	J **or** e	**# iters**	**gas**	**elec.**	**coup.**
NR on (4.11)	orig.	an.	4			
	perm.	an.	4			
NR	(8.9)	an.	4	4	4	4
		appr.	5	*	*	*
	(8.10)	an.	4	4	4	4
		appr.	4	*	*	*
FP	(8.9)	(8.12)	729	723	725	729
		(8.13)	744	731	735	743
	(8.10)	(8.12)	729	723	725	729
		(8.13)	744	731	735	743
Acc. FP	(8.9)	(8.12)	535	342	343	352
		(8.13)	473	314	314	315
	(8.10)	(8.12)	193	193	193	193
		(8.13)	182	181	181	181

Table 8.2 gives the results for the three methods described in Section 8.3 to solve (8.8) and for NR applied to (4.11). The second columns indicates how the equations and variables are ordered in the system of LF equations. The third column states if the exact or approximated J is used in NR, or which error e is used in FP. The column '#

iters' gives the total number of (outer) iterations required by the method to converge. The final three columns give the total number of times that the LF problem (8.1) is solved, for each subsystem, in NR on (8.8) with analytical J, and in Algorithms 8.1, 8.2, and 8.3. For NR on (8.8) with approximated J, the LF subproblem (8.1) needs to be solved several times to compute (5.5), in addition to the solves required to compute $\boldsymbol{F}(\boldsymbol{y})$, which is indicated by '$*$' in Table 8.2.

All methods converge to a solution; to validate this LF solution, we determine the variables $\boldsymbol{x}$ corresponding to the LF problem of the connected MCN, and compare those variables with the solution $\boldsymbol{x}^*$ of LF problem (4.11) solved without permutation. For all methods, the found solution is close to the reference solution $\boldsymbol{x}^*$, that is, $\max(|\boldsymbol{x}^* - \boldsymbol{x}|/|\boldsymbol{x}^*|) \sim \tau$ or smaller. Therefore, the decoupled approach can be used, with any of the three methods described in Section 8.3, to solve the LF problem of this gas-electricity MES.

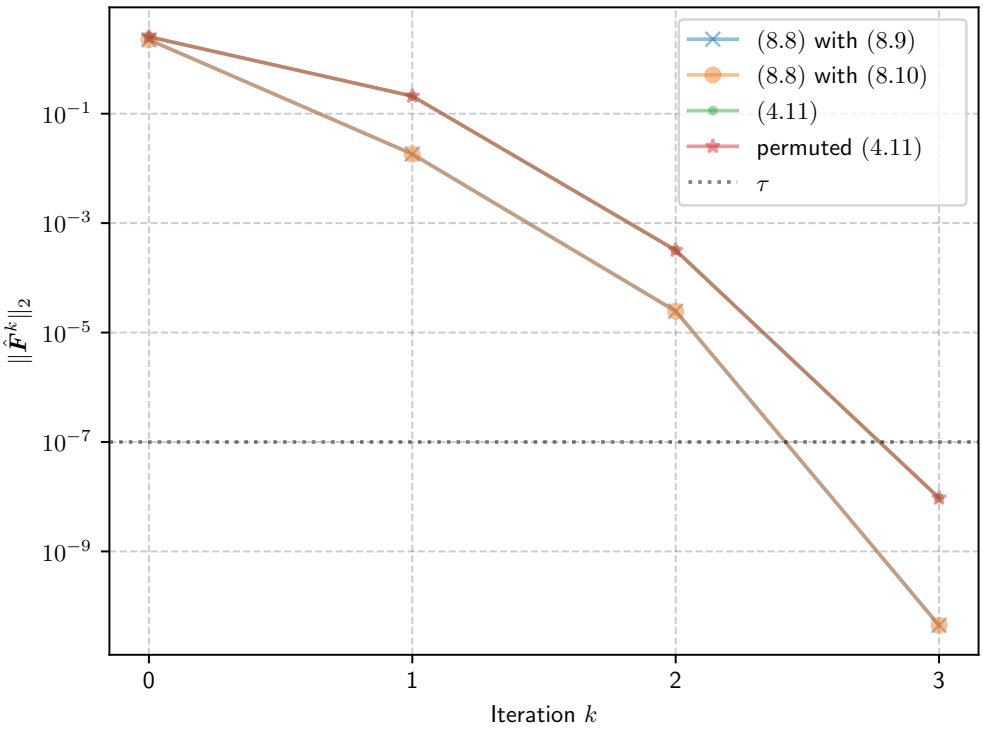

Figure 8.3: Convergence of NR to solve (4.11) or (8.8) for the gas-electricity MES. The lines '(8.8) with (8.9)' and '(8.8) with (8.10)' are indistinguishable, as are the lines '(4.11)' and 'permuted (4.11)'.

Table 8.2 shows that the order of the variables and equations does not affect NR, neither when applied to (4.11), nor when applied to (8.8). This is illustrated in Figure 8.3, which shows the convergence of NR, where J is determined analytically. This figures also shows that NR has quadratic convergence for these LF problems.

Figure 8.4 shows the convergence of basic and accelerated FP, with (8.13) for the

error measure. We can see, both in Table 8.2 and in Figure 8.4, that the order of the variables and equations does not affect basic FP but does affect accelerated FP. For the latter, using (8.10) for the ordering results in faster convergence than using (8.9), as expected, since the ordering of (8.10) is chosen to exploit the structure of the interdependencies amongst the subsystems. Furthermore, accelerated FP indeed converges faster than basic FP. Even though accelerated FP convergences faster, both basic FP and accelerated FP show linear convergence.

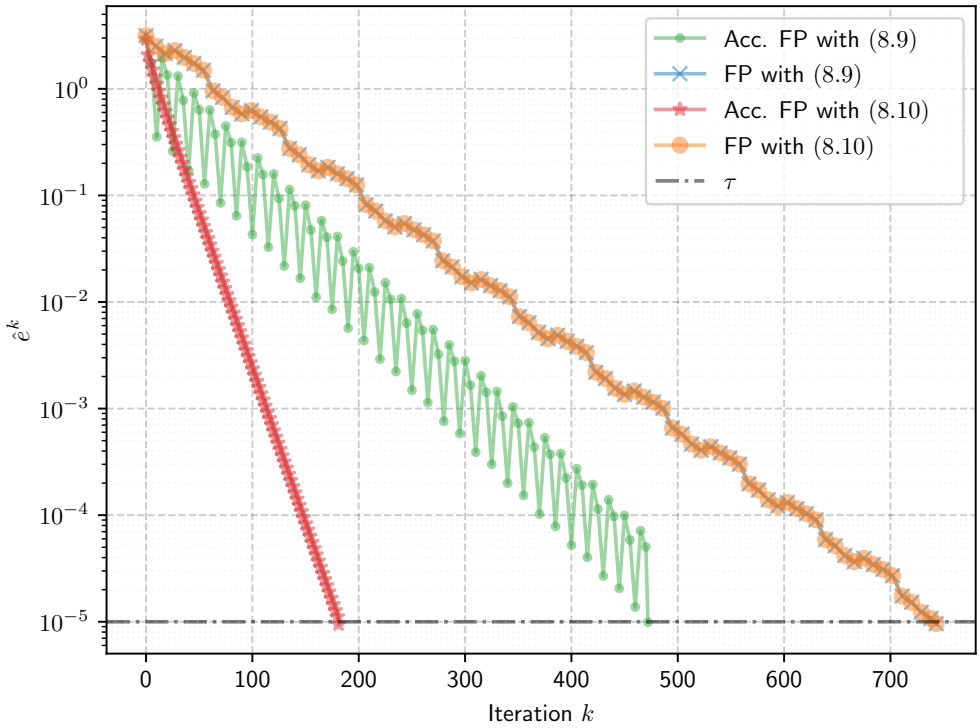

Figure 8.4: Convergence of FP (Alg. 8.1) and accelerated FP (Alg. 8.2 or Alg. 8.3), for the gas-electricity MES, using error (8.13). The lines 'FP with (8.9)' and 'FP with (8.10)' are indistinguishable.

Finally, comparing the fourth column with the final three columns in Table 8.2, we see that the subsystem (8.1) does not need to be solved at every outer iteration of Algorithms 8.1, 8.2, and 8.3 for FP to find a solution to the LF problem, since the number of times that (8.1) is solved is smaller than or equal to the total number of outer iterations for these methods. Hence, using an if-statement as in step 6 of Algorithm 8.1 reduces the total CPU time.

8.5.2 Electricity-heat multi-carrier energy system

The second MES consists of a two-node electrical network and a two-node heat network, connected to each other with two coupling nodes. Figure 8.5 shows the con-

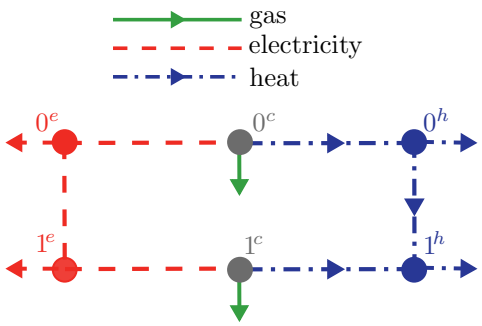

(a) Connected multi-carrier network.

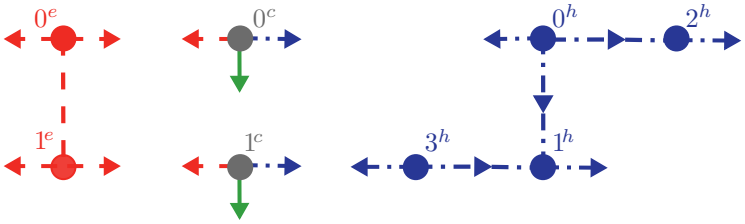

(b) Decoupled multi-carrier network.

Figure 8.5: Connected and decoupled network representation of an electricity-heat MES. Arrows on links and terminal links show defined direction of flow.

nected and the decoupled network representation of this MES. Both electrical nodes and both heat nodes in the connected MCN are sinks, such that energy enters the network as gas through the couplings, which produce electricity and heat.

Models and node types

In the electrical part of the connected network, both nodes are sinks, and the link from 0^e to 1^e represents a short transmission line. In the heat part of the connected network, both nodes are sinks, and the link from 0^h to 1^h represents a pipe. See Appendix C.2 for details on the models.

Both coupling nodes represent an EH, for which we use the linear model (2.38). The nodal coupling equations (3.26) for the connected MCN, shown in Figure 8.5a, are then

$$F^{c,E}_{0^c} = \begin{pmatrix} P_{0^c 0^e} \\ \Delta\varphi_{0^c 0^h} \end{pmatrix} - \begin{pmatrix} c_0^{ge} \\ c_0^{gh} \end{pmatrix} \mathrm{GHV}(-q_{0^c})$$

$$F^{c,E}_{1^c} = \begin{pmatrix} P_{1^c 1^e} \\ \Delta\varphi_{1^c 1^h} \end{pmatrix} - \begin{pmatrix} c_1^{ge} \\ c_1^{gh} \end{pmatrix} \mathrm{GHV}(-q_{1^c})$$

and the nodal coupling equations (3.26) for the disconnected MCN, shown in Fig-

ure 8.5b, are

$$F_{0^c}^{c,E} = \begin{pmatrix} P_{0^c} \\ -\Delta\varphi_{0^c} \end{pmatrix} - \begin{pmatrix} c_0^{ge} \\ c_0^{gh} \end{pmatrix} \mathrm{GHV}(-q_{0^c})$$
$$F_{1^c}^{c,E} = \begin{pmatrix} P_{1^c} \\ -\Delta\varphi_{1^c} \end{pmatrix} - \begin{pmatrix} c_1^{ge} \\ c_1^{gh} \end{pmatrix} \mathrm{GHV}(-q_{1^c})$$

The parameter values used in the equations are summarized in Tables C.7–C.8 in Appendix C.2.

Table 8.3 gives the the node type sets we use as BCs, for the connected and disconnected MCN. In the connected MCN, nodes 0^h and 1^h are sinks, in the disconnected MCN, nodes 1^h and 2^h are sinks and nodes 0^h and 3^h are sources. The values used for the BCs are given in Tables C.10–C.13 in Appendix C.2.

Table 8.3: Node type sets for the electricity-heat network.

	Connected		**Decoupled**	
Node	**Type**	**Specified**	**Type**	**Specified**
0^e	PQV	P_0, Q_0, $\lvert V\rvert$	gen.	P_0, $P_{0,1}$, Q_0, $\lvert V\rvert$
1^e	PQVδ	P_1, Q_1, $\lvert V\rvert$, δ	slack	P_1, $P_{1,1}$, Q_1, $\lvert V\rvert$
0^h	ref. load	p, $T^r_{0,0}$, $\Delta\varphi_0$	slack	p, T^s_0
1^h	load	$T^r_{1,0}$, $\Delta\varphi_1$	load	$T^r_{1,0}$, $\Delta\varphi_1$
2^h			ref. load	p, $T^r_{2,0}$, $\Delta\varphi_2$
3^h			ref. load	p, $T^s_{3,0}$, $\Delta\varphi_3$
0^c	temp.	$T^s_{0^c0^h}$	QTφ	Q_{0^c}, $T^s_{0^c}$, $\Delta\varphi_{0^c}$, $T^r_{0^c}$, m_{0^c}
1^c	temp.	$T^s_{1^c1^h}$	PQT	P_{1^c}, Q_{1^c}, $T^s_{1^c}$, $T^r_{1^c}$, m_{1^c}

With the node sets in Table 8.3, the system of LF equations for the connected MCN (4.11) consists of 19 equations and variables, while the system of LF equations for the decoupled MCN (8.8) consists of 24 equations and variables. For the decoupled LF problem, we take

$$\boldsymbol{v}^e = \begin{pmatrix} P_{1,1} & Q_{0,1} & Q_{1,1} \end{pmatrix}^T, \qquad \boldsymbol{v}^h = \begin{pmatrix} m_0 & m_3 & \Delta\varphi_0 \end{pmatrix}^T,$$
$$\boldsymbol{u}^e = \begin{pmatrix} P_{0,1} \end{pmatrix}, \qquad \boldsymbol{u}^h = \begin{pmatrix} \Delta\varphi_3 \end{pmatrix},$$
$$\boldsymbol{v}^c = \begin{pmatrix} -q_{0^c} & -q_{1^c} & P_{0^c} & -\Delta\varphi_{1^c} \end{pmatrix}^T,$$
$$\boldsymbol{u}^c = \begin{pmatrix} P_{1^c} & Q_{0^c} & Q_{1^c} & m_{0^c} & m_{1^c} & \Delta\varphi_{0^c} \end{pmatrix}^T$$

See Appendix C.2 for details on the IFCs.

Solving the load flow problem

We use the same methods as for the gas-electricity MES to solve the LF problems (4.11) and (8.8), see Section 8.5.1, such that we again consider 14 ways to solve the LF problem. In NR, we take a tolerance $\tau = 10^{-7}$, and in Algorithms 8.1, 8.2, and

Table 8.4: Solver information of the LF problem of the electricity-heat MES.

				# **solves** (8.1)		
Method	**System**	J **or** e	**# iters**	**elec.**	**heat**	**coup.**
NR on (4.11)	orig.	an.	6			
	perm.	an.	6			
NR	(8.9)	an.	4	4	4	4
		appr.	5	$*$	$*$	$*$
	(8.10)	an.	4	4	4	4
		appr.	5	$*$	$*$	$*$
FP	(8.9)	(8.12)	69	69	69	69
		(8.13)	66	65	65	65
	(8.10)	(8.12)	69	69	69	69
		(8.13)	66	65	65	65
Acc. FP	(8.9)	(8.12)	50	33	33	34
		(8.13)	50	33	33	33
	(8.10)	(8.12)	21	21	21	21
		(8.13)	19	18	18	18

8.3 we take tolerances $\tau = 10^{-6}$ and $\tau_F = 10^{-7}$. We use scaling for all methods, with the base values as given in Table C.9.

Table 8.4 gives the results for the three methods described in Section 8.3 and for NR applied to (4.11). Again, the second column indicates how the equations and variables are ordered in the system of LF equations, the third column states if the exact or approximated J is used in NR, or which error e is used in FP, the fourth column gives the total number of (outer) iterations required by the method to converge, and the final three columns give the total number of times that the LF problem (8.1) is solved, for each subsystem. For NR on (8.8) with approximated J, the LF subproblem (8.1) needs to be solved several times to compute (5.5), in addition to the solves required to compute $\boldsymbol{F}(\boldsymbol{y})$, which is indicated by '$*$' in Table 8.4.

All methods converge to a solution, which is close to the reference solution $\boldsymbol{x}^*$ of the LF problem (4.11) solved without permutation, that is, $\max(|\boldsymbol{x}^* - \boldsymbol{x}|/|\boldsymbol{x}^*|) \sim \tau$ or smaller. Therefore, the decoupled approach can be used, with any of the three methods described in Section 8.3, to solve the LF problem of this electricity-heat MES.

The results are similar to the gas-electricity MES. Table 8.4 shows that NR and basic FP are not affected by the order of the variables and equations, whereas accelerated FP is. For accelerated FP, using (8.10) for the ordering results in faster convergence than using (8.9). Furthermore, accelerated FP indeed converges faster than basic FP, though both show linear convergence. This is illustrated in Figure 8.6, which shows the convergence of basic and accelerated FP, with (8.13) for the error measure. Finally, Table 8.4 shows that the subsystem (8.1) does not need to be solved at every outer iteration of Algorithms 8.1, 8.2, and 8.3 for FP to find a solution to

the LF problem.

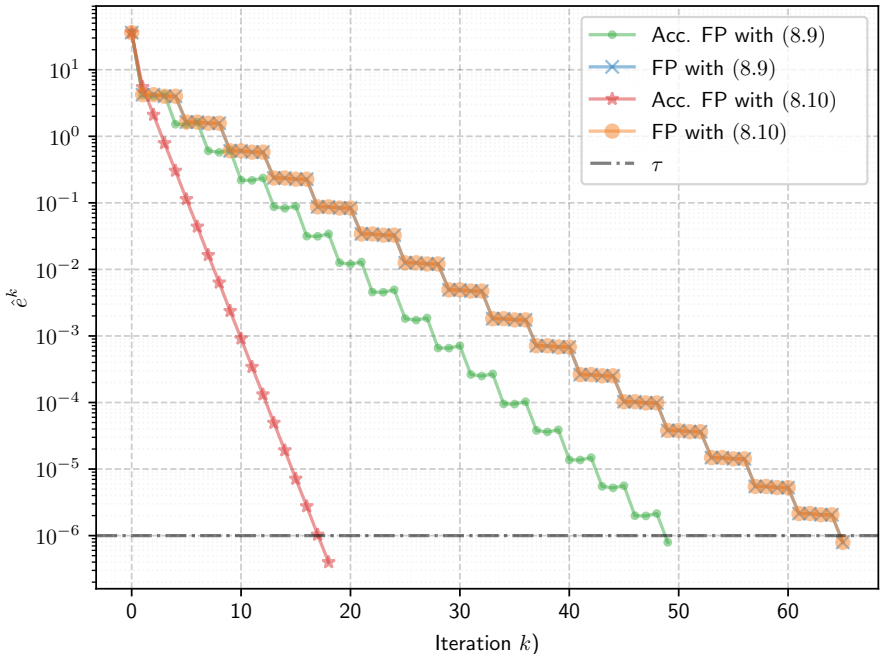

Figure 8.6: Convergence of FP (Alg. 8.1) and accelerated FP (Alg. 8.2 or Alg. 8.3), for the electricity-heat MES, using error (8.13). The lines 'FP with (8.9)' and 'FP with (8.10)' are indistinguishable.

8.5.3 Multi-carrier energy system with three carriers

The third MES consist of gas, electricity, and heat SC networks, and is the same MES as used in Chapter 6, coupled with EHs. Figure 8.7 shows the connected and the decoupled network representation of this MES.

Models and node types

We use the same LF equations as in Chapter 6, which are also detailed in Appendix C.3, with the parameter values as given Tables C.14–C.16.

Both coupling nodes represent an EH, for which we use the linear model (2.38). The nodal coupling equations (3.26) in the connected MCN, shown in Figure 8.7a, are given by (6.2), and the nodal coupling equations (3.26) in the disconnected MCN, shown in Figure 8.7b, are

$$F_{0^c}^{c,E} = \begin{pmatrix} P_{0^c} \\ -\Delta\varphi_{0^c} \end{pmatrix} - \begin{pmatrix} \nu_0\eta_{\mathrm{GG}} \\ (1-\nu_0)\eta_{\mathrm{GB}} \end{pmatrix} \mathrm{GHV}(-q_{0^c}) \tag{8.17a}$$

$$F_{1^c}^{c,E} = \begin{pmatrix} P_{1^c} \\ -\Delta\varphi_{1^c} \end{pmatrix} - \begin{pmatrix} \nu_1\eta_{\mathrm{CHP}} \\ (1-\nu_1)\eta_{\mathrm{CHP}} \end{pmatrix} \mathrm{GHV}(-q_{1^c}) \tag{8.17b}$$

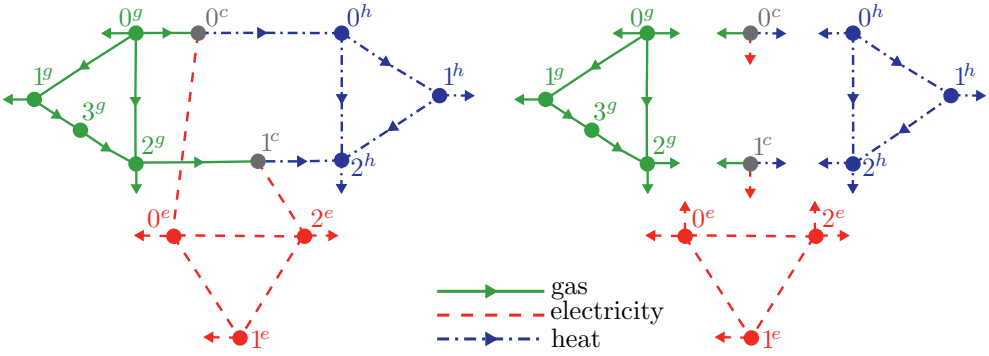

(a) Connected MCN. **(b)** Decoupled MCN.

Figure 8.7: Connected and decoupled network representation of a MES, based on [17], with EHs as coupling units. Arrows on links and terminal links show defined direction of flow.

For the decoupled approach, we use different BCs in the electrical network than in Chapter 6. Instead of the node type sets in Table 6.2, we use the node types in Table 8.5, for the connected and disconnected MCN. The values used for the BCs are given in Tables C.23–C.31.

Table 8.5: Node type sets for the gas-electricity-heat MES.

	Connected		**Decoupled**	
Node	**Type**	**Specified**	**Type**	**Specified**
0^g	ref.	p^g	ref.	p^g, $q_{0,1}$
1^g	load	q_1	load	q_1
2^g	load	q_2, $q_{2,1}$	load	q_2, $q_{2,1}$
3^g	load	$q_3 = 0$	load	$q_3 = 0$
0^e	PQV	P_0, Q_0, $\lvert V\rvert$	gen.	P_0, $P_{0,1}$, Q_0, $\lvert V\rvert$
1^e	load	P_1, Q_1	load	P_1, Q_1
2^e	PQVδ	P_2, Q_2, $\lvert V\rvert$, δ	slack	P_2, $P_{2,1}$, Q_2, $\lvert V\rvert$
0^h	ref.	p^h, $m = 0$	slack	p^h, T^s_0
1^h	load	$T^r_{1,0}$, $\Delta\varphi_1$	load	$T^r_{1,0}$, $\Delta\varphi_1$
2^h	load	$T^r_{2,0}$, $\Delta\varphi_2$	load	$T^r_{2,0}$, $\Delta\varphi_2$
3^h			ref. load	p^h, $T^s_{3,0}$, $\Delta\varphi_3$
0^c	temp.	$T^s_{0^c0^h}$	QTφ	Q_{0^c}, $T^s_{0^c}$, $\Delta\varphi_{0^c}$, $T^r_{0^c}$, m_{0^c}
1^c	temp.	$T^s_{1^c1^h}$	PQT	P_{1^c}, Q_{1^c}, $T^s_{1^c}$, $T^r_{1^c}$, m_{1^c}

With the node sets in Table 8.5, using the full formulation in the gas network and terminal link formulation in the heat network, the system of LF equations for the

connected MCN (4.11) consists of 33 equations and variables, while the system of LF equations for the decoupled MCN (8.8) consists of 36 equations and variables. The node types in the decoupled MCN are such that the BCs of the gas network depend on the state variables of the electrical and heat networks through the coupling network, but not the other way around. The state variables of the gas network are then not part of the IFCs, and for the decoupled LF problem we take

$$\begin{aligned}
\boldsymbol{v}^g &= \emptyset, & \boldsymbol{v}^e &= \begin{pmatrix} P_{2,1} & Q_{0,1} & Q_{2,1} \end{pmatrix}^T, \\
\boldsymbol{u}^g &= \begin{pmatrix} q_{0,1} & q_{2,1} \end{pmatrix}^T, & \boldsymbol{u}^e &= \begin{pmatrix} P_{0,1} \end{pmatrix}, \\
\boldsymbol{v}^h &= \begin{pmatrix} m_0 & m_3 & \Delta\varphi_0 \end{pmatrix}^T, & \boldsymbol{v}^c &= \begin{pmatrix} -q_{0^c} & -q_{1^c} & P_{0^c} & -\Delta\varphi_{1^c} \end{pmatrix}^T, \\
\boldsymbol{u}^h &= \begin{pmatrix} \Delta\varphi_3 \end{pmatrix}, & \boldsymbol{u}^c &= \begin{pmatrix} P_{1^c} & Q_{0^c} & Q_{1^c} & m_{0^c} & m_{1^c} & \Delta\varphi_{0^c} \end{pmatrix}^T
\end{aligned}$$

See Appendix C.3 for details on the IFCs.

Solving the load flow problem

We consider the same 14 ways to solve the LF problems (4.11) and (8.8) as in the previous two examples. In NR, we take a tolerance $\tau = 10^{-7}$, and in Algorithms 8.1, 8.2, and 8.3 we take tolerances $\tau = 10^{-6}$ and $\tau_F = 10^{-7}$. We use scaling for all methods, with the base values as given in Table C.18. For the initial guess, we use the same values as in Table C.21, except for the voltage angles, for which we take $\delta_0 = 0\,\text{rad}$ as initial guess, and δ_2 is given as part of the BCs.

This example is essentially an extension of the electricity-heat MES, for which all 14 ways could be used to solve the LF problem. However, for this MES, both basic and accelerated FP, using (8.9) or (8.10), are unable to find a solution to (8.8). The FP iterates of the active power and heat power produced by the EHs diverge, until $\Delta\varphi_3 > 0$, such that node 3^h would act as a sink instead of a source. Since node 3^h is assumed to be a source, the LF model of the heat network is undefined for $\Delta\varphi_3 > 0$, and the FP algorithm is terminated.

With the parameters in Table C.16 for the EH models (8.17), some eigenvalues λ_k of the Jacobian of (8.8) are outside of the unit circle, such that $\|J(\boldsymbol{y})\| := \max_k(\lambda_k) > 1$. This means that FP is not guaranteed to converge to a solution of the LF problem (8.8). The coupling matrices of the EHs can be chosen such that the spectrum of $J(\boldsymbol{y})$ falls within the unit circle, such that $\|J(\boldsymbol{y})\| \leq 1$, but this means we would solve the LF problem of a different MES. In conclusion, this MES cannot be solved with FP for this way of decoupling.

Table 8.6 gives the results for NR applied to (4.11) and applied to (8.8). These methods converge to a solution, which is close to the reference solution $\boldsymbol{x}^*$ of LF problem (4.11) solved without permutation, that is, $\max(|\boldsymbol{x}^* - \boldsymbol{x}|/|\boldsymbol{x}^*|) \sim \tau$ or smaller. Again, we see that NR is not affected by the order of the variables and equations.

For this MES, FP cannot be used to solve the decoupled LF problem, but NR can be used. Since NR applied to (8.8) with an approximated J does not require the detailed network models and data to be shared amongst the subsystems, see Section 8.3.2, the decoupled approach can still be used to solve the LF problem of this MES.

Table 8.6: Solver information of the LF problem of the gas-electricity-heat MES.

				# **solves** (8.1)			
Method	**System**	J **or** e	**# iters**	**gas**	**elec.**	**heat**	**coup.**
NR on (4.11)	orig.	an.	6				
	perm.	an.	6				
NR	(8.9)	an.	3	1	3	3	3
		appr.	8	*	*	*	*
	(8.10)	an.	3	1	3	3	3
		appr.	8	*	*	*	*

8.6 Final remarks

A decoupling approach is developed to solve the LF problem of an integrated MES with dedicated SC solvers, and with limited communication between the various subsystems. In the decoupling approach, a connected MCN is decoupled into its SC parts and its coupling part by cutting the dummy links into two terminal links, such that a general MES can be represented as a disconnected MCN. Then, the interaction between the SC networks and the coupling network is modeled using interface conditions (IFCs), and the (extended) LF problem for each subnetwork, including the coupling network, is formulated. Combining the IFCs with these LF subproblems gives a system of (non)linear equations that models the LF problem for the integrated MES, and which is an alternative to the system of LF equations using the connected MCN.

The LF subproblems and IFCs can be combined in any order to form the system of LF equations, and we consider two different orderings. We use three ways to solve the system of LF equations for the disconnected MCN: the fixed-point method (FP), NR, and accelerated FP. The LF problem of the subnetworks needs to be solved for several (outer) iterations of each of these three methods.

The decoupled approach is used to formulate and solve the LF problem of a gas-electricity MES, an electricity-heat MES, and a gas-electricity-heat MES. For the first two examples, FP, NR, and accelerated FP find the solution to the LF problem. For the third example, FP and accelerated FP diverge, but NR finds the solution to the LF problem. For all examples, the order of the variables and equations in the system of LF equations does not affect NR or basic FP. Accelerated FP is affected by the ordering, and exploiting the structure of subnetworks results in faster convergence. Both basic and accelerated FP show linear convergence, whereas NR shows quadratic convergence.

The examples show that the decoupled approach can be used to solve the LF problem of integrated MESs. However, FP does not always find a solution, and when it does, it has linear convergence. Moreover, the LF problem of each subnetwork needs to be solved multiple times during the FP or NR iterations. Therefore, the decoupled approach is slower than solving the LF problem of the connected MCN. On the other hand, the decoupled approach allows the use of dedicated solvers for the LF problem of the SC subnetworks, and the decoupled approach does not require sharing of detailed

model and network data amongst the various subsystems. Therefore, the decoupled approach might be preferred to the connected approach in certain situations.

Further research is required to accelerate FP and NR used in the decoupled approach, and to investigate the possible convergence issues of FP.

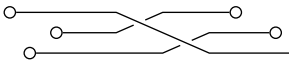

CHAPTER 9

Optimization

Optimization problems are concerned with finding a solution that minimizes or maximizes some objective function, while satisfying a set of constraints. We consider a minimization problem with (non)linear equality and inequality constraints:

$$\min_{\boldsymbol{y}} \quad f(\boldsymbol{y}) \tag{9.1a}$$

$$\text{s.t} \quad \boldsymbol{h}(\boldsymbol{y}) = \boldsymbol{0} \tag{9.1b}$$

$$\boldsymbol{g}(\boldsymbol{y}) \geq \boldsymbol{0} \tag{9.1c}$$

Here, $f : \mathbb{R}^N \to \mathbb{R}$ is the objective function, $\boldsymbol{y} \in \mathbb{R}^N$ is the vector of optimization variables, $\boldsymbol{h} : \mathbb{R}^N \to \mathbb{R}^{M_h}$ are the equality constraints, and $\boldsymbol{g} : \mathbb{R}^N \to \mathbb{R}^{M_g}$ the inequality constraints. The (in)equality constraints are element wise, that is, (9.1c) denotes $\boldsymbol{g}_n(\boldsymbol{y}) \geq 0$ for all $n \in \{1, \ldots, M_g\}$.

An optimization problem with nonlinear equality or inequality constraints is called a nonlinearly constrained optimization problem. A vector $\boldsymbol{y}$ that satisfies all constraints is called feasible, and the set of all feasible vectors is called the feasible region. The optimization problem is called infeasible if there is no feasible $\boldsymbol{y}$.

The goal of the optimization problem is to find a vector $\boldsymbol{y}^*$ that is feasible and minimizes the objective function $f(\boldsymbol{y})$. Such a global minimum $\boldsymbol{y}^*$ does not always exist, and when it does, it is not always possible to find $\boldsymbol{y}^*$ analytically [28]. For practical problems, numerical techniques are used to find an acceptable, feasible, approximate solution.

Optimality conditions are used to determine if a vector $\boldsymbol{y}$ is a solution to an optimization problem, and these conditions form the basis for many numerical solvers.

In this chapter, we first give the first-order and second-order optimality conditions. Then, we discuss some commonly used optimization methods for unconstrained and constrained optimization problems. Finally, we introduce elimination of variables, and discuss the effect on the optimization problem and on the optimization methods.

9.1 Optimality conditions

To state the optimality conditions, we assume that the objective function f and constraint functions $\boldsymbol{h}$ and $\boldsymbol{g}$ are twice-continuously differentiable. Furthermore, we

define the Lagrangian function for the constrained optimization problem (9.1) as

$$\mathcal{L}(\boldsymbol{y}, \boldsymbol{\lambda}, \boldsymbol{\mu}) := f(\boldsymbol{y}) - \boldsymbol{\lambda}^T \boldsymbol{h}(\boldsymbol{y}) - \boldsymbol{\mu}^T \boldsymbol{g}(\boldsymbol{y}) \tag{9.2}$$

with $\boldsymbol{\lambda} \in \mathbb{R}^{M_h}$ and $\boldsymbol{\mu} \in \mathbb{R}^{M_g}$ Lagrange multipliers. Its gradient is given by

$$\nabla_{\boldsymbol{y}} \mathcal{L}(\boldsymbol{y}, \boldsymbol{\lambda}, \boldsymbol{\mu}) = \nabla f(\boldsymbol{y}) - \boldsymbol{\lambda}^T \nabla \boldsymbol{h}(\boldsymbol{y}) - \boldsymbol{\mu}^T \nabla \boldsymbol{g}(\boldsymbol{y}) \tag{9.3}$$

Here, $\nabla_{\boldsymbol{x}} f(\boldsymbol{x}) := \begin{pmatrix} \frac{\partial f}{\partial x_1} & \dots & \frac{\partial f}{\partial x_N} \end{pmatrix}$ denotes the gradient of f to $\boldsymbol{x}$ and

$$\nabla_{\boldsymbol{x}} \boldsymbol{f}(\boldsymbol{x}) := \begin{pmatrix} \frac{\partial f_1}{\partial x_1} & \dots & \frac{\partial f_1}{\partial x_N} \\ \vdots & & \vdots \\ \frac{\partial f_M}{\partial x_1} & \dots & \frac{\partial f_M}{\partial x_N} \end{pmatrix}$$

denotes the Jacobian of $\boldsymbol{f}$ with respect to $\boldsymbol{x}$.

Furthermore, we assume that the linear independence constraint qualifications hold. That is, we assume that the gradients at $\boldsymbol{y}^*$ of the equality constraints $\boldsymbol{h}$, and the gradients at $\boldsymbol{y}^*$ of the subset of the inequality constraints $\boldsymbol{g}$ that are active, are linearly independent [28, 29].

9.1.1 First-order conditions

Suppose $\boldsymbol{y}^*$ is a local solution of the optimization problem (9.1), and assume that the linear independence constraint qualifications hold. The first-order necessary optimality conditions are then [29]:

$$\nabla_{\boldsymbol{y}} \mathcal{L}(\boldsymbol{y}^*, \boldsymbol{\lambda}^*, \boldsymbol{\mu}^*) = 0, \tag{9.4a}$$
$$h_m(\boldsymbol{y}^*) = 0, \quad \text{for } m = 1, \dots, M_h, \tag{9.4b}$$
$$g_m(\boldsymbol{y}^*) \geq 0, \quad \text{for } m = 1, \dots, M_g, \tag{9.4c}$$
$$\boldsymbol{\mu}_m^* \geq 0, \quad \text{for } m = 1, \dots, M_g, \tag{9.4d}$$
$$\boldsymbol{\mu}_m^* g_m(\boldsymbol{y}^*) = 0, \quad \text{for } m = 1, \dots, M_g \tag{9.4e}$$

The first condition (9.4a) states that $\boldsymbol{y}^*$ is a stationary point of the Lagrangian (9.2) for $\boldsymbol{\lambda}^*$ and $\boldsymbol{\mu}^*$. Conditions (9.4b) and (9.4c) ensure feasibility of the solution. The final conditions (9.4e) are the complementarity conditions. The first-order conditions (9.4) are known as the Karush-Kuhn-Tucker (KKT) conditions, and any local solution $\boldsymbol{y}^*$ of the optimization problem (9.1) satisfies these KKT conditions.

9.1.2 Second-order conditions

The first-order conditions are not always enough to determine if a move along a tangent to a feasible arc decreases or increases the objective function f. Hence, a second-order necessary condition is used, which is related to the curvature of the objective function [28].

The tangent $\boldsymbol{p}$ to the feasible arc of $\boldsymbol{y}^*$ satisfies

$$\frac{\partial \boldsymbol{h}}{\partial \boldsymbol{y}}(\boldsymbol{y}^*)\boldsymbol{p} = \boldsymbol{0} \tag{9.5}$$

Assuming that the constraint qualifications hold, (9.5) completely characterizes the tangent $\boldsymbol{p}$ to a feasible arc.

The Hessian matrix of a scalar function f to $\boldsymbol{x}$ is defined as:

$$\nabla_{\boldsymbol{xx}} f(\boldsymbol{x}) := \begin{pmatrix} \frac{\partial^2 f}{\partial x_1 \partial x_1} & \cdots & \frac{\partial^2 f}{\partial x_N \partial x_1} \\ \vdots & & \vdots \\ \frac{\partial^2 f}{\partial x_1 \partial x_N} & \cdots & \frac{\partial^2 f}{\partial x_N \partial x_N} \end{pmatrix}$$

A second-order necessary optimality condition is then; for all $\boldsymbol{p}$ satisfying (9.5), it must hold that

$$\boldsymbol{p}^T \nabla_{\boldsymbol{yy}} \mathcal{L}(\boldsymbol{y}^*, \boldsymbol{\lambda}^*, \boldsymbol{\mu}^*) \boldsymbol{p} \geq 0 \tag{9.6}$$

In other words, (9.6) states that the projected Hessian of the Lagrangian function must be positive definite.

9.2 Optimization methods

Optimization methods are iterative methods. They start with an initial guess $\boldsymbol{y}^0$ and produce a sequence of iterates $\boldsymbol{y}^k$ until a solution is found within a required accuracy or the algorithm is terminated.

Almost all methods are descent methods, which require the objective function f to decrease for each new iterate.

Many optimization methods are based on the KKT and second-order optimality conditions. Methods for constrained problems often involve solving unconstrained subproblems. We will briefly discuss methods for unconstrained optimization problems, before discussing methods for constrained problems. See for instance [28] or [29] for more details.

9.2.1 Methods for unconstrained problems

Two types of optimization methods for nonlinear unconstrained problems can be distinguished: line-search methods and trust-region methods. Both types of method determine the new iterate by taking a step of length α in direction $\boldsymbol{d}$ from the current iterate:

$$\boldsymbol{y}^{k+1} = \boldsymbol{y}^k + \alpha^k \boldsymbol{d}^k$$

A line-search method first determines a search direction $\boldsymbol{d}^k$ for the next step, for instance using a first-order approximation to f. Then, the step length α^k is chosen such that f is decreased satisfactorily.

A trust-region method first chooses a maximum step length α^k, called the trust-region radius. Then, the method tries to find a search direction $\boldsymbol{d}^k$ that decreases f satisfactorily. If such a search direction cannot be found, the trust-region radius is reduced, and the method looks for a new search direction. Several trial search directions might be computed before a suitable one is found.

9.2.2 Methods for constrained problems

Various methods exist for nonlinearly constrained optimization problems, and there is no standard categorization of these methods. We consider projected Lagrangian methods, sequential quadratic programming (SQP) methods, and interior-point (IP) methods. Many algorithms are a combination of two or more methods.

Projected Lagrangian methods

The (sufficient) optimality conditions imply that the solution $\boldsymbol{y}^*$ of a nonlinearly constrained problem (9.1) can be defined as the solution of a linearly constrained subproblem with an objective function related to the Lagrangian function, and with appropriate linear constraints [28]. Since the objective function of this subproblem is based on the Lagrangian, the Lagrange multipliers $\boldsymbol{\lambda}$ and $\boldsymbol{\mu}$ need to be estimated.

The algorithms of projected Lagrangian methods generally involve a sequence of these subproblems. Various choices for objective functions of the subproblem are used. Examples are quadratic functions, for instance in SQP methods, or least-squares functions.

SQP

Sequential quadratic programming methods aim to find an approximate solution to the original problem (9.1), by solving a sequence of quadratic programming subproblems. The solution of the subproblem is used to determine the new iterate to the original problem.

SQP methods can be viewed as an application of NR to the KKT conditions. Consider an optimization problem with nonlinear equality constraints and without inequality constraints, that is, consider (9.1a)–(9.1b). For this problem, the KKT conditions (9.4) can be written as a system of nonlinear equations:

$$\boldsymbol{F}(\boldsymbol{y}, \boldsymbol{\lambda}) = \begin{pmatrix} \nabla f(\boldsymbol{y}) - \boldsymbol{\lambda}^T \nabla \boldsymbol{h}(\boldsymbol{y}) \\ \boldsymbol{h}(\boldsymbol{y}) \end{pmatrix} = \boldsymbol{0}$$

Applying (5.3), NR updates $\boldsymbol{p}_y^k$ and $\boldsymbol{p}_h^k$ are determined by solving

$$\begin{pmatrix} \nabla^2_{\boldsymbol{yy}} \mathcal{L}(\boldsymbol{y}, \boldsymbol{\lambda}) & -\nabla \boldsymbol{h}(\boldsymbol{y}) \\ \nabla \boldsymbol{h}(\boldsymbol{y}) & 0 \end{pmatrix} \begin{pmatrix} \boldsymbol{p}_y^k \\ \boldsymbol{p}_h^k \end{pmatrix} = \begin{pmatrix} -\nabla f(\boldsymbol{y}) + \boldsymbol{\lambda}^T \nabla \boldsymbol{h}(\boldsymbol{y}) \\ -\boldsymbol{h}(\boldsymbol{y}) \end{pmatrix} = -\boldsymbol{F}(\boldsymbol{y}, \boldsymbol{\lambda})$$

Then, $\boldsymbol{y}^k$ and $\boldsymbol{\lambda}^k$ are updated as

$$\begin{pmatrix} \boldsymbol{y}^{k+1} \\ \boldsymbol{\lambda}^{k+1} \end{pmatrix} = \begin{pmatrix} \boldsymbol{y}^k \\ \boldsymbol{\lambda}^k \end{pmatrix} + \begin{pmatrix} \boldsymbol{p}_y^k \\ \boldsymbol{p}_h^k \end{pmatrix}$$

SQP methods can also be seen as a projected Lagrangian methods. The quadratic subproblem at iteration k is obtained by linearizing the equality and inequality constraints (9.1b) and (9.1c):

$$\min_{\boldsymbol{p}^k} \quad f^k + \nabla f^k \boldsymbol{p}^k + \frac{1}{2} (\boldsymbol{p}^k)^T \nabla^2_{\boldsymbol{yy}} \mathcal{L}^k \boldsymbol{p}^k \tag{9.7a}$$

$$\text{s.t} \quad \nabla \boldsymbol{h}(\boldsymbol{y}^k) \boldsymbol{p}^k + \boldsymbol{h}(\boldsymbol{y}^k) = \boldsymbol{0} \tag{9.7b}$$

$$\nabla \boldsymbol{g}(\boldsymbol{y}^k) \boldsymbol{p}^k + \boldsymbol{g}(\boldsymbol{y}^k) \geq \boldsymbol{0} \tag{9.7c}$$

where $f^k = f(\boldsymbol{y}^k)$ and $\mathcal{L}^k = \mathcal{L}(\boldsymbol{y}^k, \boldsymbol{\lambda}^k, \boldsymbol{\mu}^k)$ are the objective (9.1a) and Lagrangian (9.2) of the original problem at iteration k.

The subproblem (9.7) is solved for $\boldsymbol{p}^k$, with corresponding Lagrange multipliers $\boldsymbol{\lambda}^{k+1}$ and $\boldsymbol{\mu}^{k+1}$. The new iterate for $\boldsymbol{y}$ is determined as $\boldsymbol{y}^{k+1} = \boldsymbol{y}^k + \boldsymbol{p}^k$.

Interior-point methods

Interior-point (IP) methods, also called barrier methods, are mainly used for inequality constrained problems. Slack variables $\boldsymbol{s}$ are added to the inequality constraints $\boldsymbol{g}$ to turn them into equality constraints. A barrier function is added to f using a barrier parameter $\mu > 0$. This gives a barrier subproblem for the original problem (9.1), for a given μ:

$$\min_{\boldsymbol{y},\,\boldsymbol{s}} \quad f(\boldsymbol{y}) - \mu \sum_{m=1}^{M_g} \ln(s_m) \tag{9.8a}$$

$$\text{s.t} \quad \boldsymbol{h}(\boldsymbol{y}) = \boldsymbol{0} \tag{9.8b}$$

$$\boldsymbol{g}(\boldsymbol{y}) - \boldsymbol{s} = \boldsymbol{0} \tag{9.8c}$$

$$\boldsymbol{s} \geq \boldsymbol{0} \tag{9.8d}$$

A barrier method finds an approximate solution to the original problem (9.1) by solving the barrier subproblem (9.8) for a sequence of barrier parameters μ converging to zero.

In early barrier methods, a slightly different barrier function was used, which prevented iterates from leaving the feasible region. This required a feasible initial guess $\boldsymbol{y}^0$, after which all iterates $\boldsymbol{y}^k$ remained within the feasible region. Hence the name interior-point methods. Newer IP methods do not require a feasible initial guess and do not retain strict feasibility.

9.3 Elimination of variables

The size of the optimization space, and the number of equality constraints, can be reduced by elimination of variables (e.g. [28], [29]).

We divide the N optimization variables $\boldsymbol{y}$ into control variables $\boldsymbol{u} \in \mathbb{R}^{N_u}$ and state variables $\boldsymbol{x} \in \mathbb{R}^{N_x}$, such that $N_x + N_u = N$:

$$\boldsymbol{y} := \begin{pmatrix} u_1 & \dots & u_{N_u} & x_1 & \dots & x_{N_x} \end{pmatrix}^T \tag{9.9}$$

This distinction turns the general optimization problem (9.1) into

$$\min_{\boldsymbol{x},\,\boldsymbol{u}} \quad f(\boldsymbol{x}, \boldsymbol{u}) \tag{9.10a}$$

$$\text{s.t} \quad \boldsymbol{h}(\boldsymbol{x}; \boldsymbol{u}) = \boldsymbol{0} \tag{9.10b}$$

$$\boldsymbol{\gamma}(\boldsymbol{x}, \boldsymbol{u}) \geq \boldsymbol{0} \tag{9.10c}$$

$$\boldsymbol{u}^{lb} \leq \boldsymbol{u} \leq \boldsymbol{u}^{ub} \tag{9.10d}$$

$$\boldsymbol{x}^{lb} \leq \boldsymbol{x} \leq \boldsymbol{x}^{ub} \tag{9.10e}$$

with $\boldsymbol{u}^{lb}$ and $\boldsymbol{u}^{ub}$ the lower and upper bounds for the control variables, and $\boldsymbol{x}^{lb}$ and $\boldsymbol{x}^{ub}$ the lower and upper bounds for the state variables. The inequality constraints (9.1) of the general optimization problem are divided into (non)linear inequality constraints $\boldsymbol{\gamma} : \mathbb{R}^N \to \mathbb{R}^{M_\gamma}$ and linear bounds (9.10d) and (9.10e) on $\boldsymbol{u}$ and $\boldsymbol{x}$ respectively.

We eliminate the state variables and the equality constraints, giving a second formulation of the optimization problem:

$$\min_{\boldsymbol{u}} \quad f\left(\boldsymbol{x}(\boldsymbol{u}),\, \boldsymbol{u}\right) \tag{9.11a}$$

$$\text{s.t} \quad \boldsymbol{g}\left(\boldsymbol{x}(\boldsymbol{u}),\, \boldsymbol{u}\right) \geq \boldsymbol{0} \tag{9.11b}$$

$$\boldsymbol{u}^{lb} \leq \boldsymbol{u} \leq \boldsymbol{u}^{ub} \tag{9.11c}$$

$$\text{with} \quad \boldsymbol{g}\left(\boldsymbol{x}(\boldsymbol{u}),\, \boldsymbol{u}\right) = \begin{pmatrix} \boldsymbol{\gamma}\left(\boldsymbol{x}(\boldsymbol{u}),\, \boldsymbol{u}\right) \\ \boldsymbol{x}(\boldsymbol{u}) - \boldsymbol{x}^{lb} \\ \boldsymbol{x}^{ub} - \boldsymbol{x}(\boldsymbol{u}) \end{pmatrix} \tag{9.11d}$$

The relation $\boldsymbol{x}(\boldsymbol{u})$ is given implicitly by the equality constraints (9.10b). This elimination requires the system of equality constraints to be solvable.

Problem formulations (9.10) and (9.11) each have several advantages and disadvantages. Problem (9.11) has a smaller optimization space, due to the elimination of $\boldsymbol{x}$. However, this also increases the nonlinearity of the inequality constraints and objective function, and the linear bounds (9.10e) are turned into (non)linear inequality constraints (9.11b). Moreover, elimination of variables using nonlinear equations may result in errors ([29] pp. 426–428).

An advantage of (9.11) is that the system of equations (9.10b) is solved separately, allowing the use of dedicated solvers for this subproblem. These dedicated solvers might be more efficient at solving system of equality constraints than the optimization algorithm. However, this system of equations needs to be solved several times during the optimization algorithm, which might increase the total computation time of the optimization algorithm for (9.11) compared with formulation (9.10), depending on the efficiency of the dedicated subsolver.

Another effect of eliminating the equality constraints is that they are satisfied at each iteration of the optimizer when solving problem (9.11). Depending on the optimization algorithm, equality constraints are not satisfied at every iteration, such that (9.10b) is not always satisfied when using optimization problem (9.10). Therefore, problem (9.11) can be preferred to (9.10) if feasibility has to be ensured.

9.4 Direct and adjoint approach

Eliminating the state variables $\boldsymbol{x}$ and the equality constraints $\boldsymbol{h}$ implies that solving problem (9.11) requires additional steps in the optimization algorithm. Most optimizers use the gradient of the objective function and the Jacobian of the (in)equality constraints. For problem (9.11), these derivatives can be determined by a direct or an adjoint approach (e.g. [30] and [31]). The direct approach is also called the forward approach, and the adjoint approach is also called the backward approach. The gradient of the objective (9.11a) and the Jacobian of the inequality constraints (9.11b)

to the control variables are given by

$$\frac{\mathrm{d}f}{\mathbf{d}\boldsymbol{u}} = \frac{\partial f}{\partial \boldsymbol{x}}\frac{\mathbf{d}\boldsymbol{x}}{\mathbf{d}\boldsymbol{u}} + \frac{\partial f}{\partial \boldsymbol{u}} \tag{9.12a}$$

$$\frac{\mathbf{d}\boldsymbol{g}}{\mathbf{d}\boldsymbol{u}} = \frac{\partial \boldsymbol{g}}{\partial \boldsymbol{x}}\frac{\mathbf{d}\boldsymbol{x}}{\mathbf{d}\boldsymbol{u}} + \frac{\partial \boldsymbol{g}}{\partial \boldsymbol{u}} \tag{9.12b}$$

For simplicity, we denote partial derivatives by a subscript, e.g. $\boldsymbol{g}_{\boldsymbol{u}} := \frac{\partial \boldsymbol{g}}{\partial \boldsymbol{u}}$. Furthermore, we define $v := \frac{\mathbf{d}\boldsymbol{x}}{\mathbf{d}\boldsymbol{u}}$, such that $v \in \mathbb{R}^{N_x} \times \mathbb{R}^{N_u}$. For the system of equality constraints (9.10b) it holds that:

$$\mathbf{d}\boldsymbol{h} = \frac{\partial \boldsymbol{h}}{\partial \boldsymbol{x}}\mathbf{d}\boldsymbol{x} + \frac{\partial \boldsymbol{h}}{\partial \boldsymbol{u}}\mathbf{d}\boldsymbol{u}$$

Since $\boldsymbol{h}(\boldsymbol{x};\boldsymbol{u}) = \mathbf{0}$, we can choose $\mathbf{d}\boldsymbol{x}$ and $\mathbf{d}\boldsymbol{u}$ such that $\mathbf{d}\boldsymbol{h} = \mathbf{0}$, giving

$$\boldsymbol{h}_{\boldsymbol{x}} v = -\boldsymbol{h}_{\boldsymbol{u}} \tag{9.13}$$

9.4.1 Direct approach

In the direct or forward approach, (9.12) is determined using (9.13) directly. That is, the gradient and the Jacobian are given by

$$\frac{\mathrm{d}f}{\mathbf{d}\boldsymbol{u}} = f_{\boldsymbol{x}} v + f_{\boldsymbol{u}} \tag{9.14a}$$

$$\frac{\mathbf{d}\boldsymbol{g}}{\mathbf{d}\boldsymbol{u}} = \boldsymbol{g}_{\boldsymbol{x}} v + \boldsymbol{g}_{\boldsymbol{u}} \tag{9.14b}$$

$$\text{where } \boldsymbol{h}_{\boldsymbol{x}} v = -\boldsymbol{h}_{\boldsymbol{u}} \tag{9.14c}$$

Here, v is determined by solving (9.14c). Hence, the direct approach requires solving N_u linear systems of size $N_x \times N_x$ any time $\frac{\mathrm{d}f}{\mathbf{d}\boldsymbol{u}}$ or $\frac{\mathbf{d}\boldsymbol{g}}{\mathbf{d}\boldsymbol{u}}$ is calculated.

9.4.2 Adjoint approach

In the adjoint or backward approach, we introduce $\boldsymbol{\lambda}^T := f_{\boldsymbol{x}}\boldsymbol{h}_{\boldsymbol{x}}^{-1}$ and $\mu^T := \boldsymbol{g}_{\boldsymbol{x}}\boldsymbol{h}_{\boldsymbol{x}}^{-1}$ to determine (9.12). With these definitions of $\boldsymbol{\lambda} \in \mathbb{R}^{N_x}$ and $\mu \in \mathbb{R}^{N_x} \times \mathbb{R}^{M_\gamma + 2N_x}$, we have $f_{\boldsymbol{x}} v = -\boldsymbol{\lambda}^T \boldsymbol{h}_{\boldsymbol{u}}$ and $\boldsymbol{g}_{\boldsymbol{x}} v = -\mu^T \boldsymbol{h}_{\boldsymbol{u}}$. The gradient and the Jacobian are then given by

$$\frac{\mathrm{d}f}{\mathbf{d}\boldsymbol{u}} = -\boldsymbol{\lambda}^T \boldsymbol{h}_{\boldsymbol{u}} + f_{\boldsymbol{u}} \tag{9.15a}$$

$$\frac{\mathbf{d}\boldsymbol{g}}{\mathbf{d}\boldsymbol{u}} = -\mu^T \boldsymbol{h}_{\boldsymbol{u}} + \boldsymbol{g}_{\boldsymbol{u}} \tag{9.15b}$$

$$\text{where } \boldsymbol{h}_{\boldsymbol{x}}^T \boldsymbol{\lambda} = f_{\boldsymbol{x}}^T \tag{9.15c}$$

$$\boldsymbol{h}_{\boldsymbol{x}}^T \mu = \boldsymbol{g}_{\boldsymbol{x}}^T \tag{9.15d}$$

Here, $\boldsymbol{\lambda}$ and μ are determined by solving (9.15c) and (9.15d) respectively. Hence, the adjoint approach requires solving $1 + M_\gamma + 2N_x$ linear systems of size $N_x \times N_x$ any time $\frac{\mathrm{d}f}{\mathbf{d}\boldsymbol{u}}$ or $\frac{\mathbf{d}\boldsymbol{g}}{\mathbf{d}\boldsymbol{u}}$ is calculated.

9.4.3 Comparison

The direct approach requires solving (9.14c), which are N_u linear systems of size $N_x \times N_x$. The adjoint approach requires solving (9.15c) and (9.15d), which are $1+M_\gamma+2N_x$ linear systems of size $N_x \times N_x$. Since the linear systems in both approaches have the same size, the adjoint approach might be more efficient than the direct approach if $N_u > 1 + M_\gamma + 2N_x$. In other words, the adjoint approach might be faster if the number of control variables is large compared to the number of (nonlinear) inequality constraints. For optimization problems of energy systems, this is generally not the case.

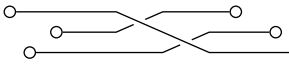

CHAPTER 10

Optimal flow problems

In an optimal flow (OF) problem, one tries to minimize or maximize an objective function, while satisfying operational constraints or physical limits of the energy system, as mentioned in Section 1.3. To ensure that the optimal solution satisfies operational constraints, the LF equations are used in OF. The way the LF equations are included in the optimization problem influences the solvability of the optimization problem. Most optimization problems for MES simplify these equations, or do not consider network transmission at all (e.g. [18, 6, 7, 32, 9, 33, 34]).

Various formulations of the LF equations exist for modeling energy systems, both in the SC and in the MC case, see Section 4.2. Moreover, there are multiple ways to incorporate the LF equations in the optimization problem. Usually, the LF equations are directly included in the OF problem as equality constraints. Nonlinearities in these constraints cause issues with convexity and solvability of the optimization problem, as also noted in [6] and [9]. Hence, the formulation of the LF equations, and the way they are incorporated in the OF problem, greatly influence the solvability of the OF problem.

In this chapter, we provide an analysis of the effect of the LF equations on the solvability of the OF problem for general MESs. We formulate an OF problem for a general single- or multi-carrier energy system, providing a general optimization framework.

First, we give the objective function to be minimized. Then, the effect of which network quantities are chosen as variables and which are considered known is dis-

This chapter is based on the articles:

Anne S. Markensteijn, Johan E. Romate, and Cornelis Vuik. Optimal flow for general multi-carrier energy systems, including load flow equations. *Results in Control and Optimization*, January 2021 [Under review],

Anne S. Markensteijn, Johan E. Romate, and Cornelis Vuik. Optimal flow for general multi-carrier energy systems, including load flow equations. Technical Report 20-06, Delft University of Technology, Delft Institute of Applied Mathematics, December 2020.

cussed. Third, we describe the two ways of including the LF equations, that is, as equality constraints or as subsystem, in an OF framework. Based on this, two formulations of the general optimization problem for MESs are stated. Advantages and disadvantages of both formulations are discussed. Then, we give the methods used for solving the OF problem, and discuss the use of the direct and adjoint approach. Finally, the two formulations of the OF problem are used to optimize example MESs, demonstrating some of the theoretical advantages and disadvantages of the formulations of the OF problem in practice.

10.1 Objective function

As the objective, we minimize total generation costs. We model the costs of each source as a quadratic function of its energy flow. The objective function is the sum of the costs of the sources:

$$f(\boldsymbol{E}) = \sum_{E \in \boldsymbol{E}} a_E + b_E E + c_E E^2 \tag{10.1}$$

Here, $\boldsymbol{E}$ is the vector of energy flows of the sources. For instance, for a gas source with mass flow q we have $\mathrm{GHV}q \in \boldsymbol{E}$, and for a gas-fired generator that produces active power P we have $P \in \boldsymbol{E}$. The parameters a_E, b_E, and c_E specify the cost of the energy source related to energy flow E.

The sum of quadratic functions is twice-continuously differentiable. Moreover, the objective function f is convex in $\boldsymbol{E}$ for suitable parameters a_E, b_E, and c_E. Both the differentiability and convexity have several mathematical advantages (e.g. [28], [29]).

10.2 Variables and bounds

To apply the elimination of variables as described in Section 9.3, the network quantities of interest are divided into control and (extended) state variables. This division also has a practical interpretation for energy systems. The choice of variables determines if linear bounds or (non)linear inequality constraints are needed to model operational limits.

In optimization problems, the derived variables are also used, either in the objective function or with respect to physical limits of the energy system. Therefore, we use the extended state variables (4.12), divided into state variables $\boldsymbol{x}^F$ and derived variables $\boldsymbol{x}^G$, in the OF framework.

10.2.1 Control variables

The optimization variables $\boldsymbol{y}$ are divided into control variables $\boldsymbol{u}$ and extended state variables $\boldsymbol{x}$ as (9.9). By definition, the state variables cannot be control variables. When a design optimization problem is considered, the control variables can include design variables such as the diameter of a gas pipe. We consider an OF problem, which is an operational optimization problem. The control variables are quantities in the energy system that are controllable in practice. They can include set points, which are (a subset of) the BCs of the LF problem, or model parameters such as

transformer tap-ratios or dispatch factors of EHs. Including model parameters as variables would require derivatives of the objective and constraint functions to these parameters. Since the model parameters would be part of the control variables $\boldsymbol{u}$, which are given for the LF equations, including the model parameters as variables does not change the nature of the optimization problem and the proposed framework. Therefore, we assume the model parameters are given, leaving only the BCs of the LF problem as possible control variables.

Solving the LF problem determines the state variables in the network, for given BCs. That is, for any $\boldsymbol{u}$, the nonlinear system (4.13) can be solved for $\boldsymbol{x}^F$ and $\boldsymbol{x}^G$, assuming the LF problem is well-posed. For notational simplicity, we denote the extended LF problem (4.13) by

$$\boldsymbol{h}\left(\boldsymbol{x};\, \boldsymbol{u}\right) := \begin{pmatrix} \boldsymbol{G}\left(\boldsymbol{x};\, \boldsymbol{u}\right) \\ \boldsymbol{F}\left(\boldsymbol{x};\, \boldsymbol{u}\right) \end{pmatrix} = \boldsymbol{0} \tag{10.2}$$

However, not every $\boldsymbol{u}$ results in a physically feasible extended state $\boldsymbol{x}$.

10.2.2 Bounds

To ensure physical feasibility of the set points $\boldsymbol{u}$, bounds are imposed on network quantities. Bounds imposed on variables $\boldsymbol{y}$ are simple linear inequality constraints (e.g. (9.10d) and (9.10e)) in the optimization problem. Bounds imposed on network quantities not in $\boldsymbol{y}$ have to be included as (non)linear inequality constraints (9.10c) that are a function of $\boldsymbol{y}$. These inequality constraints can be highly nonlinear.

When the energy flows of sources are part of the optimization variables, i.e. when $\boldsymbol{E} \subseteq \boldsymbol{y}$, the objective function (10.1) is convex in $\boldsymbol{y}$. However, when some of the energy flows in $\boldsymbol{E}$ are derived quantities that are not included in the extended state $\boldsymbol{x}$, the nonlinearity of the objective function increases, and it may no longer be convex in $\boldsymbol{y}$.

To avoid (highly) nonlinear inequality constraints, and to reduce the nonlinearity of the objective function, derived variables can be included in the extended state. On the other hand, including the derived variables in $\boldsymbol{x}$ increases the optimization space and the number of LF equations in the (extended) LF problem. Depending on the optimization algorithm, using extended state variables instead of only the regular state variables can be beneficial.

10.3 Two problem formulations

The optimization problem determines a solution that minimizes the objective function, while satisfying the LF problem and while staying within the operational limits of the network. We consider two ways to formulate the OF problem, which we call formulation I and formulation II. Formulation I includes the LF equations as equality constraints, while formulation II includes them as subsystem. Formulation I gives an optimization problem like (9.10), while formulation II applies nonlinear elimination of variables, resulting in an optimization problem like (9.11). We repeat them here for convenience.

10.3.1 Formulation I: load flow as equality constraints

The most straightforward way to satisfy the LF equations during optimization, is to include them as equality constraints directly and optimize over the combined control and (extended) state variables (as is done in e.g. [6], [7], and [8]). This gives an optimization problem like (9.10), such that formulation I for the OF problem is

$$\min_{\boldsymbol{x},\,\boldsymbol{u}} \quad f\left(\boldsymbol{x},\,\boldsymbol{u}\right) \tag{10.3a}$$

$$\text{s.t} \quad \boldsymbol{h}\left(\boldsymbol{x};\,\boldsymbol{u}\right) = \boldsymbol{0} \tag{10.3b}$$

$$\boldsymbol{\gamma}\left(\boldsymbol{x},\,\boldsymbol{u}\right) \geq \boldsymbol{0} \tag{10.3c}$$

$$\boldsymbol{u}^{lb} \leq \boldsymbol{u} \leq \boldsymbol{u}^{ub} \tag{10.3d}$$

$$\boldsymbol{x}^{lb} \leq \boldsymbol{x} \leq \boldsymbol{x}^{ub} \tag{10.3e}$$

The objective function (10.3a) is given by (10.1), the equality constraints (10.3b) are given by the extended system of LF equations (10.2), and the inequality constraints (10.3c) represent the bounds for any network quantities not included in $\boldsymbol{y}$.

10.3.2 Formulation II: load flow as subsystem

Another way to formulate the optimization problem is to apply (nonlinear) elimination of variables and constraints. We eliminate the extended state variables $\boldsymbol{x}$, using the extended LF equations (10.2), to get an optimization over the control variables $\boldsymbol{u}$ only. This gives an optimization problem like (9.11), such that formulation II for the OF problem is

$$\min_{\boldsymbol{u}} \quad f\left(\boldsymbol{x}(\boldsymbol{u}),\,\boldsymbol{u}\right) \tag{10.4a}$$

$$\text{s.t} \quad \boldsymbol{u}^{lb} \leq \boldsymbol{u} \leq \boldsymbol{u}^{ub} \tag{10.4b}$$

$$\boldsymbol{g}\left(\boldsymbol{x}(\boldsymbol{u}),\,\boldsymbol{u}\right) \geq \boldsymbol{0} \tag{10.4c}$$

$$\text{with} \quad \boldsymbol{g}\left(\boldsymbol{x}(\boldsymbol{u}),\,\boldsymbol{u}\right) = \begin{pmatrix} \boldsymbol{\gamma}\left(\boldsymbol{x}(\boldsymbol{u}),\,\boldsymbol{u}\right) \\ \boldsymbol{x}(\boldsymbol{u}) - \boldsymbol{x}^{lb} \\ \boldsymbol{x}^{ub} - \boldsymbol{x}(\boldsymbol{u}) \end{pmatrix} \tag{10.4d}$$

The relation $\boldsymbol{x}(\boldsymbol{u})$ is implicitly given by the extended LF problem (10.2). That is, for any given $\boldsymbol{u}$, the (extended) state $\boldsymbol{x}$ satisfies the LF equations, and is obtained by solving $\boldsymbol{x}$ from (10.2).

10.3.3 Comparison

If bounds are only imposed on network quantities that are included in $\boldsymbol{y}$, then (10.3c) is not included in optimization problem (10.3), and $\boldsymbol{\gamma}$ is not included in (10.4). Similarly, bounds do not have to be imposed on all variables in $\boldsymbol{y}$. Using nonlinear inequality constraints $\boldsymbol{\gamma}$ in (10.3c) or in (10.4c) instead of including derived variables in the extended state variables is an example of (nonlinear) elimination of variables as well. This type of elimination is commonly used in optimal power flow problems.

Formulations I and II have several advantages and disadvantages, in addition to the ones mentioned in Section 9.3. The use of a dedicated solver for (10.2) in formulation

II is especially interesting when optimizing MESs. A user solving the optimization problem does not need to have access to the LF model; they only need access to the output and be able to set the input. For MESs, the operator of each carrier might have their own LF solver. Moreover, ensuring (physical) feasibility at each iteration by elimination of variables might avoid solvability issues of the optimization algorithm. As such, formulation II might be preferred over formulation I.

The same quadratic objective function is used in both problems. If the objective function depends on $\boldsymbol{x}$, then it might have some nonlinear dependency on $\boldsymbol{u}$, other than quadratic, in problem (10.4). The (in)equality constraints (10.3b) and (10.3c) are generally nonlinear in $\boldsymbol{y}$, while (10.3d) and (10.3e) are linear inequality constraints. If bounds are imposed on variables in $\boldsymbol{y}$ only, such that (10.3c) is not included, problem (10.3) is an optimization problem with nonlinear equality constraints and linear inequality constraints. If (10.3c) is included, problem (10.3) is an optimization problem with nonlinear equality and nonlinear inequality constraints. The inequality constraints (10.4c) are generally nonlinear in $\boldsymbol{u}$, regardless of whether $\boldsymbol{\gamma}$ is included or not. Problem (10.4) is an optimization problem with nonlinear inequality constraints, but has no equality constraints. Both problems (10.3) and (10.4) are nonlinearly constrained optimization problems.

Since the two formulations have advantages and disadvantages, we compare the two formulations using some example MCNs.

10.4 Solving the optimal flow problem

OF problems (10.3) and (10.4) are nonlinear, (in)equality constrained, multivariable optimization problems. It is generally not possible to analytically determine if the KKT and second-order optimality conditions are met. Moreover, when the objective function is concave, or when the (in)equality constraints are nonlinear, which is the case for most load flow equations, the solution space might be non-convex. Hence, we use numerical solvers to approximate an optimal solution, see also Section 9.2.

Badly scaled optimization problems cause convergence issues for the optimizer [27]. We use matrix scaling to scale the variables and equations, and scale the objective function as well. See Section 11.5 for the effect of scaling on the optimizers, and a comparison with per unit scaling.

10.4.1 Optimizers

To solve problems (10.3) and (10.4) we consider three solvers used for nonlinearly constrained optimization problems: The 'trust-constr' (TC) and SLSQP methods from SciPy [35], and IPOPT [36].

The TC method is a trust-region IP method for large-scale nonlinear optimization problems, based on the algorithm developed in [37]. Inequality constraints are handled by introducing a barrier function. The resulting barrier subproblems are solved using an adapted version of the Byrd-Omojokun Trust-Region SQP Method ([29] p. 549). The TC method is a projected Lagrangian method.

The sequential least squares programming (SLSQP) method is based on the algorithm developed in [38]. It is a projected Lagrangian method, where a sequence of linearly constrained quadratic programming subproblems is created. The Hessian of

the Lagrangian is factorized, turning the quadratic subproblem into a least-squares problem. Hence, a sequence of least-squares subproblems is solved. Unlike the TC method, the SLSQP method does not require the Hessian of the Lagrangian.

IPOPT is a primal-dual interior-point optimization method for large-scale nonlinear optimization problems, using the algorithm developed in [36]. Like the TC method, inequality constraints are handled by introducing a barrier function. These barrier subproblems are solved by applying NR to the system of primal-dual equations. The search directions for the next iterate are determined by linearizing these primal-dual equations. The step sizes are determined by a backtracking line-search procedure, which is a variant of a filter method, to ensure global convergence.

10.4.2 Derivatives

All three optimizers use the gradient of the objective function and the Jacobian of the (in)equality constraints. For formulation II, we can use the direct and adjoint approach to determine these derivatives, see Section 9.4. We use formulation II.A and II.B to refer to formulation II with the direct or adjoint approach respectively.

The TC method uses the Hessian of the objective function. For the general objective function (10.1) the Hessian is a constant diagonal matrix. This is also true for problem (10.3) in formulation I, where $E \in \boldsymbol{y}$ for all $E \in \boldsymbol{E}$, such that

$$H_{nm} := \frac{\partial^2 f}{\partial y_n \partial y_m} = \begin{cases} 2c_E, & y_n = y_m := E \in \boldsymbol{E} \\ 0, & \text{otherwise} \end{cases}$$

In formulation II, where $\boldsymbol{x}$ depends (implicitly) on $\boldsymbol{u}$, the Hessian is no longer constant if any of the energy flows E in the objective is part of $\boldsymbol{x}$ instead of $\boldsymbol{u}$. Therefore, we let TC determine the Hessian numerically for formulation II.

10.4.3 Additional steps for formulation II

Formulation II of the LF problem includes the state variables $\boldsymbol{x}$ and associated LF equations as subsystem, which requires additional steps in the optimization algorithm. Whenever one of the extended state variables $\boldsymbol{x}(\boldsymbol{u})$ is needed while solving problem (10.4), the extended LF problem (10.2) would need to be solved. Since $\boldsymbol{x}(\boldsymbol{u})$ might be used several times per iteration of the optimizer, the system (10.2) might be solved multiple times per optimizer iteration. To increase efficiency, we store the values $\boldsymbol{x}(\boldsymbol{u})$ of the previous iteration. Furthermore, the extended LF problem (10.2) is only solved to determine a new $\boldsymbol{x}(\boldsymbol{u})$ if $\boldsymbol{u}$ has changed significantly since the last solve, or if the LF equations with the current $\boldsymbol{x}$ are not satisfied within a desired tolerance. Suppose $\boldsymbol{x}^k$ and $\boldsymbol{u}^i$ are the previous values of the extended state and control variables, and $\boldsymbol{u}^{i+1}$ are the current control variables. The extended LF problem (10.2) is only solved if

$$||\boldsymbol{u}^{i+1} - \boldsymbol{u}^i||_2 > \tau_u \tag{10.5a}$$

$$\text{or } ||\boldsymbol{h}\left(\boldsymbol{x}^k, \boldsymbol{u}^i\right)||_2 > \tau_h \tag{10.5b}$$

with τ_u and τ_h tolerances. We store $||\boldsymbol{h}\left(\boldsymbol{x}, \boldsymbol{u}\right)||_2$ any time (10.2) is solved to evaluate (10.5b) without having to recalculate the LF equations.

10.5 Comparison of formulations and solvers

Combining all possible ways described in Section 10.3 and Section 10.4 to formulate and solve the OF problem leads to multiple cases. To compare these various formulations and aspects of the optimization problem, we optimize two different MESs. We mainly compare the various formulations and aspects based on the efficiency of the optimizer. That is, first we determine if an optimal solution is found. Then, the number of iterations and number of function calls to the objective functions required by the optimizer are used as a measure for efficiency.

We compare formulation I and formulation II, that is, the way that LF is incorporated into OF, for both MESs. Additionally, for each MES we focus on some of the formulations and aspects of solving the OF problem. Since scaling greatly improves the convergence of the optimizers for the OF problem, we only consider the scaled OF problem.

The first MES is the same system as used in Chapter 6. The coupling of this MES is modeled in two different ways, giving two MCN representations for the same MES. For both versions, we use a single formulation of the LF equations. Bounds are imposed on all variables $\boldsymbol{y}$ or on the control variables $\boldsymbol{u}$ only. Within the optimizers, the inequality constraints are taken as hard constraints or as soft constraints. With hard constraints, each iteration of the optimizer must satisfy all inequality constraints. With soft constraints, iterates are allowed to violate the inequality constraints, but the final solution must satisfy all constraints. We consider both, since hard constraints might help keep the iterates feasible. Hence, we use this MES to focus on the inequality constraints.

The second MES is the same system as used in Section 7.2. It is represented by one MCN, but we use multiple formulations of the LF equations. We consider two options in the gas part and two in the heat part. Bounds are imposed on (most of) the variables $\boldsymbol{y}$. We look at the effect of imposing bounds on some derived variables, which might not be included in $\boldsymbol{y}$, depending on the formulation of the system of LF equations. Finally, we vary the size of the MCN, as detailed in Section 7.2. Hence, this MES focuses on the effect of the LF formulation on OF.

10.5.1 Costs of energy sources

The cost parameters a_E, b_E, and c_E in the objective function (10.1) are chosen to represent the variable operation and maintenance costs of the energy sources. The focus of this research is on the mathematical formulation of the optimization problem, and the inclusion of the LF equations within an optimization framework. As such, the values of the cost parameters a_E, b_E, and c_E are chosen to be realistic, but are not meant to be accurate values of any specific energy source.

For non-coupling sources or (external) grid connections, we take $a_E = c_E = 0$ for all carriers. The operational costs of the coupling components are based on the produced energy. A CHP produces both electricity P and heat $\Delta\varphi$, but the heat is 'waste' from the production of electricity, such that it is considered free. Table 10.1 gives the cost parameters, per energy source and per carrier.

Table 10.1: Cost parameters in the objective function (10.1), per energy source.

Source	Energy E	a_E [€/h]	b_E [€/(MW h)]	c_E [€/(MW^2 h)]
ext. grid	gas E^g	0	15	0
	elec. P	0	40	0
	heat $\Delta\varphi$	0	16	0
CHP	elec. P	0	5	0.05
	heat $\Delta\varphi$	0	16	0
GG	elec. P	0	2	0.02
GB	heat $\Delta\varphi$	0	1	0.01

10.5.2 MES 1: Effect of inequality constraints

The first MES is the same system as used in Chapter 6. We model the energy system by two different networks, the first using a GG, GB, and a CHP for the coupling, as shown in Figure 6.1a, and the second using EHs, as shown in Figure 6.1b. See also Appendix C.3 for more details.

Problem formulations

Both networks have only one external source, connected to node 0^g. The electrical and heat powers are produced by the couplings. The energy vector $\boldsymbol{E}$ of the objective function (10.1) is

$$\boldsymbol{E} = \begin{pmatrix} -\mathrm{GHV} q_{0,0} & P_{0^c0^e} & P_{2^c2^e} & \Delta\varphi_{1^c0^h} \end{pmatrix}^T, \quad \text{for network 1}$$
$$\boldsymbol{E} = \begin{pmatrix} -\mathrm{GHV} q_{0,0} & P_{0^c0^e} & P_{1^c2^e} & \Delta\varphi_{0^c0^h} \end{pmatrix}^T, \quad \text{for network 2}$$

Table 6.1 and Table 6.2 give the BCs for network 1 and network 2 respectively. We take some of these known variables as control variables in the OF problem:

$$\boldsymbol{u} = \begin{pmatrix} p_2^g & |V_2| & p_2^h & T^s_{2^c2^h} \end{pmatrix}^T, \quad \text{for network 1}$$
$$\boldsymbol{u} = \begin{pmatrix} |V_2| & T^s_{1^c2^h} \end{pmatrix}^T, \quad \text{for network 2}$$

The choice for control variables is different for the two networks, since the BCs used in LF are different.

For the LF problem, we use the full formulation (4.1) in the gas network, and the terminal link formulation (4.7) in the heat network. The extended state variables for

network 1 are then:

$$\begin{aligned}
\boldsymbol{x}^G &= \begin{pmatrix} q_{0,0} \end{pmatrix} \\
\boldsymbol{x}^{F,g} &= \begin{pmatrix} q_{01} & q_{02} & q_{32} & q_{13} & p_1^g & p_3^g \end{pmatrix}^T \\
\boldsymbol{x}^{F,e} &= \begin{pmatrix} \delta_1 & \delta_2 & |V_1| \end{pmatrix}^T \\
\boldsymbol{x}^{F,h} &= \begin{pmatrix} m_{01} & m_{02} & m_{12} & m_{1,0} & m_{2,0} & p_1^h \\
& & & T_0^s & T_1^s & T_2^s & T_0^r & T_1^r & T_2^r \end{pmatrix}^T \\
\boldsymbol{x}^{F,c} &= \begin{pmatrix} q_{0^g0^c} & q_{0^g1^c} & q_{2^g2^c} & P_{0^c0^e} & P_{2^c2^e} & Q_{0^c0^e} \\
& & & Q_{2^c2^e} & m_{1^c0^h} & m_{2^c2^h} & \Delta\varphi_{1^c0^h} & \Delta\varphi_{2^c2^h} \end{pmatrix}^T
\end{aligned}$$

and the extended state variables for network 2 are:

$$\begin{aligned}
\boldsymbol{x}^G &= \begin{pmatrix} q_{0,0} \end{pmatrix} \\
\boldsymbol{x}^{F,g} &= \begin{pmatrix} q_{01} & q_{02} & q_{32} & q_{13} & p_1^g & p_2^g & p_3^g \end{pmatrix}^T \\
\boldsymbol{x}^{F,e} &= \begin{pmatrix} \delta_1 & \delta_2 & |V_1| \end{pmatrix}^T \\
\boldsymbol{x}^{F,h} &= \begin{pmatrix} m_{01} & m_{02} & m_{12} & m_{1,0} & m_{2,0} & p_1^h \\
& & & p_2^h & T_0^s & T_1^s & T_2^s & T_0^r & T_1^r & T_2^r \end{pmatrix}^T \\
\boldsymbol{x}^{F,c} &= \begin{pmatrix} q_{0^g0^c} & q_{2^g1^c} & P_{0^c0^e} & P_{1^c2^e} & Q_{0^c0^e} \\
& & & Q_{1^c2^e} & m_{0^c0^h} & m_{1^c2^h} & \Delta\varphi_{0^c0^h} & \Delta\varphi_{1^c2^h} \end{pmatrix}^T
\end{aligned}$$

Hence, there are 37 variables for network 1, consisting of 32 state variables $\boldsymbol{x}^F$, 1 derived variable $\boldsymbol{x}^G$, and 4 control variables $\boldsymbol{u}$, and 36 variables for network 2, consisting of 33 state variables $\boldsymbol{x}^F$, 1 derived variable $\boldsymbol{x}^G$, and 2 control variables $\boldsymbol{u}$.

The extended LF problem (10.2) is not solvable (for a physically feasible solution) for all values of $\boldsymbol{u}$. The bounds imposed on $\boldsymbol{u}$ are chosen such that the LF problem is solvable. This requires relatively tight bounds, especially for p_2^g and p_2^h.

We can impose bounds on $\boldsymbol{u}$ only, or on the extended state variables $\boldsymbol{x}$ as well. We solve the OF problem in both cases, with bounds on $\boldsymbol{u}$ only, and with bounds on $\boldsymbol{y}$. Moreover, we consider hard and soft inequality constraints within the optimizer.

This gives a total of 12 different formulations and solution methods of the OF problem for both network representations of this MES. That is, we use formulation I (10.3) for the OF problem, including the LF equations as equality constraints, or we use formulation II (10.4), eliminating the LF equations. For the latter, we can use the direct approach II.A or the adjoint approach II.B when solving the optimization problem. For each of these, we impose bounds on $\boldsymbol{u}$ or on $\boldsymbol{y}$, and we use soft or hard bounds within the optimizers. In addition to these 12 options, we use TC, SLSQP, or IPOPT as optimizer, see Section 10.4.1.

Table 10.2 gives the number and size of the linear systems (9.14c) and (9.15c)–(9.15d) for formulation II.A and II.B, respectively. Using soft or hard constraints does not change the system size. For both formulation II.A and II.B, the size of the linear systems is equal, since $\boldsymbol{h}_{\boldsymbol{x}}$ is square. If bounds are imposed on $\boldsymbol{u}$ only, there are no (nonlinear) inequality constraints on $\boldsymbol{x}(\boldsymbol{u})$, such that the OF problem is given by (10.4a)–(10.4b). In that case, only (9.12a) is needed, such that only (9.15c) needs to

be solved for formulation II.B. Hence, formulation II.B requires solving fewer linear systems than formulation II.A when bounds are imposed on $\boldsymbol{u}$ only, while formulation II.B requires solving significantly more linear systems than formulation II.A when bounds are imposed on $\boldsymbol{y}$ (i.e. on both $\boldsymbol{u}$ and $\boldsymbol{x}$).

Table 10.2: Number and size of the linear systems (9.14c) and (9.15c)–(9.15d) for formulation II.A and II.B respectively, for both networks.

		Network 1		Network 2	
bounds on	**OF form.**	**# lin. sys.**	**size lin. sys.**	**# lin.**	**size lin.**
$\boldsymbol{u}$	II.A	4	33×33	2	34×34
	II.B	1	33×33	1	34×34
$\boldsymbol{y}$	II.A	4	33×33	2	34×34
	II.B	67	33×33	69	34×34

Results

We set the tolerance for the OF problem, the tolerance τ_h for the extended LF problem, and the tolerance τ_u to 10^{-6}, and use matrix scaling to scale the problem. The maximum number of iterations for the optimizers is 40, and the maximum number of iterations for NR to solve the extended LF problem (10.2) within formulation II is 10. The optimizers were unlikely to find a solution if it did not find one within these 40 iterations. For the scaling, we take the base values as given in Table C.19 and we take $f_b = 10^{10}$ for the objective function.

Table 10.3 and Table 10.4 give the results for network 1 and 2 respectively. The first columns gives the case number, for ease of reference. A dash ('-') indicates the optimizer is unable to find a solution for that particular case. The columns '# iters' and '# f' give the number of iterations and number of calls to the objective function of the optimizer respectively. The last column gives the error of the LF equations $\|\hat{\boldsymbol{F}}\|_2$ for the found optimal solution.

First, we compare the optimizers. For network 1, TC and IPOPT are not able to find a solution for any of the cases. In Table 10.3, we see that SLSQP finds a solution for all cases for network 1. For network 2, see Table 10.4, IPOPT finds a solution for all cases, and TC and SLSQP for all cases that use formulation II.

Since hard constraints might avoid convergence issues due to infeasible iterates, we consider both soft and hard constraints. Comparing cases 1–3 with 4–6 and cases 7–9 with 10–12 in Table 10.3 and in Table 10.4, we can see that there are no cases for which any of the optimizers find a solution with hard constraints but not with soft constraints. Furthermore, we have seen, in various examples, that using appropriate values for the bounds, and using a reasonable initial guess, are more effective to ensure feasible iterates than imposing hard constraints. Therefore, we see no advantage to using hard constraints compared with soft constraints.

Now, we consider imposing bounds on $\boldsymbol{u}$ or $\boldsymbol{y}$, that is, we compare cases 1–6 with 7–12. For network 1 and formulation I, there is no difference between bounds on $\boldsymbol{u}$ or $\boldsymbol{y}$ (cf. 1 and 4 with 7 and 10 in Table 10.3). For network 1 and formulation II,

Table 10.3: Optimizer information of the OF problem for network 1.

				# iters	# f	$\|\hat{\boldsymbol{F}}\|_2$
case	**bounds**	**constr.**	**OF form.**	**SLSQP**	**SLSQP**	**SLSQP**
1	$\boldsymbol{u}$	soft	I	21	32	$4.782 \cdot 10^{-7}$
2			II.A	15	38	$2.674 \cdot 10^{-10}$
3			II.B	15	38	$2.674 \cdot 10^{-10}$
4		hard	I	21	32	$4.782 \cdot 10^{-7}$
5			II.A	15	38	$2.674 \cdot 10^{-10}$
6			II.B	15	38	$2.674 \cdot 10^{-10}$
7	$\boldsymbol{y}$	soft	I	21	32	$4.782 \cdot 10^{-7}$
8			II.A	9	42	$6.606 \cdot 10^{-7}$
9			II.B	8	42	$1.312 \cdot 10^{-7}$
10		hard	I	21	32	$4.782 \cdot 10^{-7}$
11			II.A	9	42	$6.606 \cdot 10^{-7}$
12			II.B	8	42	$1.312 \cdot 10^{-7}$

Table 10.4: Optimizer information of the OF problem for network 2.

				# iters			# f			$\|\hat{\boldsymbol{F}}\|_2$		
case	**bounds**	**constr.**	**OF form.**	**TC**	**SLSQP**	**IPOPT**	**TC**	**SLSQP**	**IPOPT**	**TC**	**SLSQP**	**IPOPT**
1	$\boldsymbol{u}$	soft	I	-	-	15	-	-	16	-	-	$3.744 \cdot 10^{-9}$
2			II.A	20	6	10	14	7	11	$2.696 \cdot 10^{-7}$	$8.532 \cdot 10^{-7}$	$5.605 \cdot 10^{-7}$
3			II.B	20	6	10	14	7	11	$2.696 \cdot 10^{-7}$	$8.532 \cdot 10^{-7}$	$5.605 \cdot 10^{-7}$
4		hard	I	-	-	15	-	-	16	-	-	$4.232 \cdot 10^{-9}$
5			II.A	16	6	10	10	7	11	$2.723 \cdot 10^{-7}$	$8.532 \cdot 10^{-7}$	$5.605 \cdot 10^{-7}$
6			II.B	16	6	10	10	7	11	$2.723 \cdot 10^{-7}$	$8.532 \cdot 10^{-7}$	$5.605 \cdot 10^{-7}$
7	$\boldsymbol{y}$	soft	I	30	-	14	30	-	15	$1.944 \cdot 10^{-8}$	-	$3.817 \cdot 10^{-8}$
8			II.A	24	9	9	27	22	10	$7.465 \cdot 10^{-7}$	$4.268 \cdot 10^{-8}$	$4.163 \cdot 10^{-8}$
9			II.B	24	9	9	27	22	10	$7.465 \cdot 10^{-7}$	$4.257 \cdot 10^{-8}$	$4.163 \cdot 10^{-8}$
10		hard	I	26	-	14	26	-	15	$1.124 \cdot 10^{-6}$	-	$3.817 \cdot 10^{-8}$
11			II.A	15	9	9	9	22	10	$1.455 \cdot 10^{-7}$	$4.268 \cdot 10^{-8}$	$4.163 \cdot 10^{-8}$
12			II.B	15	9	9	9	22	10	$1.455 \cdot 10^{-7}$	$4.257 \cdot 10^{-8}$	$4.163 \cdot 10^{-8}$

imposing bounds on $\boldsymbol{y}$ reduces the number of iterations (cf. 2, 3, 5, and 6 with 8, 9, 11, and 12 in Table 10.3). For network 2 and formulation I, TC is only able to find a solution when bounds are imposed on $\boldsymbol{y}$ (cf. 1 and 4 with 7 and 10 in Table 10.4). For network 2 and formulation II, SLSQP requires fewer iterations with bounds imposed on $\boldsymbol{u}$ than with bounds imposed on $\boldsymbol{y}$ (cf. 2, 3, 5, and 6 with 8, 9, 11, and 12 in Table 10.4). The other optimizers seem to be less affected by this in this case. Hence, if one can choose between imposing bounds on $\boldsymbol{u}$ only or on $\boldsymbol{y}$, it depends on the network and the optimizer which is best.

Finally, we consider the inclusion of the LF equations in the OF problem, that is, we compare formulation I (cases 1, 4, 7, and 10) with formulation II. Figure 10.1 gives the error of the LF equations at every iteration of the optimizer, for the OF problem of network 1 with soft bounds on $\boldsymbol{y}$ (cases 7–9) using SLSQP, and illustrates the difference between the two formulations. Figure 10.1 shows that the LF equations are satisfied at every iteration of the optimizer when using formulation II, while this is not the case for formulation I, as already mentioned in Section 9.3.

Table 10.4 shows that there are cases where a solution cannot be found using

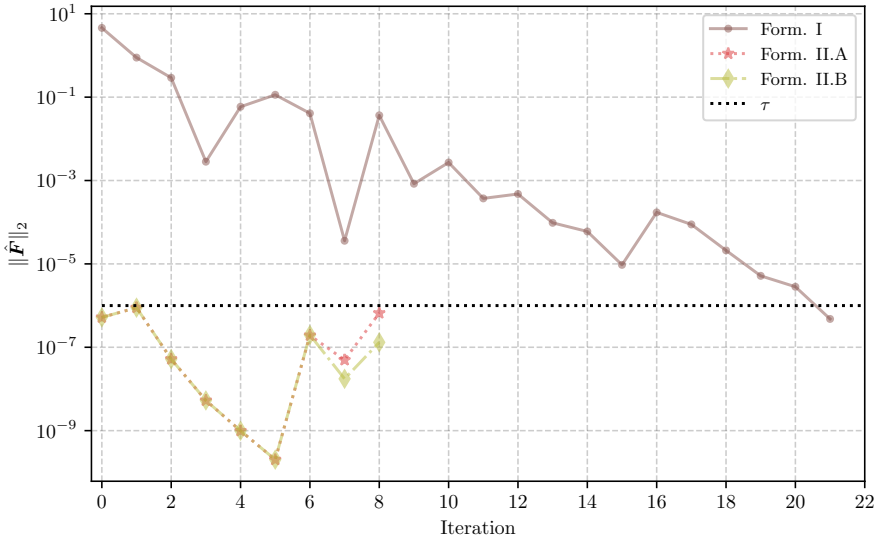

Figure 10.1: Error of scaled LF equations $\|\hat{\boldsymbol{F}}\|_2$ at every iteration of the optimizer for network 1 (Figure 6.1a), for the OF problem with soft bounds on $\boldsymbol{y}$, using SLSQP.

formulation I while it is found using formulation II. However, there are also cases where both formulation I and II result in a solution. Table 10.3 and Table 10.4 both show that formulation II requires fewer iterations than formulation I, for all considered cases. Formulations II.A and II.B show very similar performance. Therefore, formulation II is more efficient than formulation I.

Comparing the final error of the LF equations for formulation I and II for each case, given in the final column of both tables, we see that the errors of the LF equation of the final solution are slightly different. This means that formulation I and formulation II result in different iterates for the same optimization algorithm. This can also be seen in Figure 10.1, since the error of the LF equations for formulation I is different from that of formulation II at each iteration.

Based on this MES, we find that there is no substantial difference between soft and hard constraints. TC performs worse than SLSQP and IPOPT. If one can choose between imposing bounds on $\boldsymbol{u}$ only or on $\boldsymbol{y}$, it depends on the network and the optimizer which is best. Finally, both formulation I and II can be used for the OF problem, and formulation II is more efficient than formulation I, in terms of number of iterations required by the optimizer.

10.5.3 MES 2: Effect of LF formulations

The second MES is the same system as used in Section 7.2, which consists of a base network, coupling 3-node single-carrier gas, electricity, and heat networks. An extended network is created by replacing the sink at node 3 of each SCN by streets, shown in Figure 7.5, giving networks of varying size. See also Appendix C.5 for more details.

We consider the base network coupled at node 1 with a single EH, which is the

network shown in Figure 7.4a, and an extended network with 163 nodes per SCN ($n = 10, m = 5, s = 10$).

Problem formulations

Nodes 1^g, 1^e, 2^e, and 2^h are external single-carrier sources. The EH produces electrical power and heat power, such that it is a source to the electrical and heat networks. The energy vector $\boldsymbol{E}$ in the objective function (10.1) is then

$$\boldsymbol{E} = \begin{pmatrix} -\text{GHV}q_{1,0} & -P_{1,0} & -P_{2,0} & P_{1^c1^e} & -\Delta\varphi_{2,0} & \Delta\varphi_{1^c1^h} \end{pmatrix}^T$$

where $q_{1,0}$, $P_{1,0}$, $P_{2,0}$, $\Delta\varphi_{2,0} < 0$ and $P_{1^c1^e}$, $\Delta\varphi_{1^c1^h} > 0$.

We use set 1 of the EH in Table 7.3, with $q = 0$ for node 2^g and $T^s_{2,0}$ and $T^r_{3,0}$ known for the heat load nodes, as BCs of the LF problem for the base network. For the extended networks, the additional nodes are load or junction nodes, where we assume $T^r_{i,l}$ known for the heat load (sink) nodes. We take some of these known variables as control variables in OF:

$$\boldsymbol{u} = \begin{pmatrix} |V_2| & P_2 & T^s_{2,0} & \Delta\varphi_{2,0} \end{pmatrix}^T$$

We use two formulations of the LF equations in the gas part, and two in the heat part. In a gas network, we use the nodal formulation (4.3) and the full formulation (4.1) with (3.4b) for the link equations. In the nodal formulation, the link flows q_k are derived variables, while they are part of the state variables $\boldsymbol{x}^F$ in the full formulation. In the heat network, we use the terminal link formulation (4.7) and the standard formulation (4.9). In the standard formulation, the terminal link flows $m_{i,l}$ are derived variables, while they are part of the state variables $\boldsymbol{x}^F$ in the terminal link formulation.

If the link gas flows q_k or terminal link mass flows $m_{i,l}$ are derived variables, we do not include them in $\boldsymbol{x}^G$. The extended state variables are then:

$$\begin{aligned}
\boldsymbol{x}^{G,g} &= \begin{pmatrix} q_{1,0} \end{pmatrix} \\
\boldsymbol{x}^{G,e} &= \begin{pmatrix} P_{1,0} & Q_{2,0} \end{pmatrix}^T \\
\boldsymbol{x}^{F,g}_n &= \begin{pmatrix} p^g_2 & p^g_3 \end{pmatrix}^T \\
\boldsymbol{x}^{F,g}_f &= \begin{pmatrix} q_{12} & q_{32} & p^g_2 & p^g_3 \end{pmatrix}^T \\
\boldsymbol{x}^{F,e} &= \begin{pmatrix} \delta_2 & \delta_3 & |V_3| \end{pmatrix}^T \\
\boldsymbol{x}^{F,h}_s &= \begin{pmatrix} m_{12} & m_{23} & p^h_2 & p^h_3 & T^s_2 & T^s_3 & T^r_1 & T^r_2 & T^r_3 \end{pmatrix}^T \\
\boldsymbol{x}^{F,h}_t &= \begin{pmatrix} m_{12} & m_{23} & m_{2,0} & m_{3,0} & p^h_2 \\
&\qquad\qquad p^h_3 & T^s_2 & T^s_3 & T^r_1 & T^r_2 & T^r_3 \end{pmatrix}^T \\
\boldsymbol{x}^{F,c} &= \begin{pmatrix} q_{1^g1^c} & P_{1^c1^e} & Q_{1^c1^e} & m_{1^c1^h} & \Delta\varphi_{1^c1^h} & T^s_{1^c1^h} \end{pmatrix}^T
\end{aligned}$$

with $\boldsymbol{x}^{F,g}_n$ and $\boldsymbol{x}^{F,g}_f$ the gas state variables using the nodal or the full formulation, and $\boldsymbol{x}^{F,h}_s$ and $\boldsymbol{x}^{F,h}_t$ the heat state variables using the standard or terminal link formulation.

Again, the extended LF problem (10.2) is not solvable (for a physically feasible solution) for all values of $\boldsymbol{u}$. The bounds imposed on $\boldsymbol{u}$ are chosen such that the LF

problem is solvable. We also impose bounds on the (extended) state variables $\boldsymbol{x}^{G,g}$, $\boldsymbol{x}^{G,e}$, $\boldsymbol{x}^{F,g}$, $\boldsymbol{x}^{F,e}$, $\boldsymbol{x}^{F,h}$, and $\boldsymbol{x}^{F,c}$. In addition, we consider imposing bounds on the gas link mass flows q_k, electrical link complex power $|S_k|^2 = P_k^2 + Q_k^2$, and heat terminal link mass flows $m_{i,l}$. For the nodal and standard formulation, q_k and $m_{i,l}$ are derived variables, as is $|S_k|^2$. Bounds are imposed through (nonlinear) inequality constraints (10.3c) or (10.4c). For each gas and electrical link k and each heat terminal link l, the inequality constraints are:

$$\boldsymbol{\gamma}_k^g = \begin{pmatrix} q_k(p_i, p_j) - q_k^{lb} \\ q_k^{ub} - q_k(p_i, p_j) \end{pmatrix} \geq \mathbf{0} \tag{10.6a}$$

$$\gamma_k^e = (|S_k|^2)^{ub} - P_k^2 - Q_k^2 \geq 0 \tag{10.6b}$$

$$\boldsymbol{\gamma}_{i,l}^h = \begin{pmatrix} m_{i,l}(\Delta\varphi_{i,l}, T_{i,l}^s, T_{i,l}^r) - m_{i,l}^{lb} \\ m_{i,l}^{ub} - m_{i,l}(\Delta\varphi_{i,l}, T_{i,l}^s, T_{i,l}^r) \end{pmatrix} \geq \mathbf{0} \tag{10.6c}$$

Here, the heat terminal link mass flow $m_{i,l}$ is a function of terminal link heat powers $\Delta\varphi_{i,l}$, terminal link supply temperature $T_{i,l}^s$, and terminal link return temperature $T_{i,l}^r$ using the heat power equation (3.23).

If the full formulation is used in gas, and the terminal link formulation is used in heat, q_k and $m_{i,l}$ are part of $\boldsymbol{x}^F$. If bounds are then imposed on these variables, they are included as bounds (10.3e) or (10.4d) instead of using (10.6a) and (10.6c).

We have seen in Section 10.5.2 that there is no difference between using soft and hard constraints in the optimizers, so we only consider soft constraints for this network. Furthermore, we do not consider the TC optimizer, since it performs worse than SLSQP and IPOPT.

This gives a total of 24 formulations and solution methods of the OF problem. That is, we use formulation I (10.3) for the OF problem, including the LF equations as equality constraints, or we use formulation II (10.4), eliminating the LF equations. For the latter, we can use the direct approach II.A or the adjoint approach II.B when solving the optimization problem. For each of these, we use one of the four possible formulations of the LF problems, based on the nodal formulation with pipe flow equations (3.4a) or the full formulation with pipe flow equations (3.4b) in the gas part, and the standard formulation or the terminal link formulation in the heat part. Moreover, we impose bounds on the (derived) variables q_k, $|S_k|^2$, and $m_{i,l}$, or we do not impose these bounds. In addition to these 24 options, we use SLSQP and IPOPT as optimizers, see Section 10.4.1. Finally, we consider various sizes of the network.

Table 10.5 gives the system size of the OF problem for these 24 formulations, for the base network. The number of bounds on $x \in \boldsymbol{x}$ should be counted double, as they are lower and upper bounds. The system sizes are different for the various formulations. However, using the adjoint approach, or formulation II.B, always requires more linear systems to be solved than using the direct approach, or formulation II.A. For both approaches, the size of the linear systems is equal, since $\boldsymbol{h}_{\boldsymbol{x}}$ is square.

Results

We set the tolerance for the OF problem, the tolerance τ_h for the extended LF problem, and the tolerance τ_u to 10^{-6}, and use matrix scaling to scale the problem. The maximum number of iterations for the optimizers is 50, and the maximum number

Table 10.5: Size of $\boldsymbol{u}$, $\boldsymbol{x}^G$, $\boldsymbol{x}^F$, $\boldsymbol{\gamma}$, and the number of $x \in \boldsymbol{x}$ on which bounds are imposed, for the various formulations of the OF problem for the base network. The last two columns give the number and size of the linear systems (9.14c) and (9.15c)–(9.15d) for formulation II.A and II.B, respectively.

case	bounds on q_k, $\lvert S_k\rvert^2$, $m_{i,l}$	form. gas	form. heat	$\boldsymbol{x}^G$	$\boldsymbol{x}^F$	$\boldsymbol{u}$	$\boldsymbol{\gamma}$	# x with bounds	OF form.	# lin. sys.	size lin. sys.
2	no	full	term. link	3	24	4	0	23	II.A	4	27×27
3									II.B	47	27×27
5			standard	3	22	4	0	23	II.A	4	25×25
6									II.B	47	25×25
8		nodal	term. link	3	22	4	0	23	II.A	4	25×25
9									II.B	47	25×25
11			standard	3	20	4	0	23	II.A	4	23×23
12									II.B	47	23×23
14	yes	full	term. link	3	24	4	2	27	II.A	4	27×27
15									II.B	57	27×27
17			standard	3	22	4	6	25	II.A	4	25×25
18									II.B	57	25×25
20		nodal	term. link	3	22	4	6	25	II.A	4	25×25
21									II.B	57	25×25
23			standard	3	20	4	10	23	II.A	4	23×23
24									II.B	57	23×23

of iterations for NR to solve the extended LF problem (10.2) within formulation II is 20. The optimizers were unlikely to find a solution if it did not find one within these 50 iterations. For the scaling, for both the base network and the extended network, we take the base values as given in Table C.46 and we take $f_b = 1$ for the objective function, which means we do not scale the objective function.

Figure 10.2 and Figure 10.3 show the difference in the energy flows of the sources between a reference LF solution and the optimal solutions. The reference LF solution is given in Tables C.47–C.51 in Appendix C.5. For the gas input, only the part of the total gas input into node 1 that is used by the coupling is shown, that is, only $-q_{1,0} - q_{3,0}$ is shown. We can see that energy flows of the optimal solution are distributed differently over the sources compared with the LF solution. Most significantly, $P_{1,0} \approx 0$ for the optimal solutions. However, Figure 10.2b shows that the total active power and heat power of the sources are roughly equal. Since $P_{1,0} \approx 0$, the total gas input $-q_{1,0}$ is larger for the optimal solutions, as we can see in Figure 10.2a. Figure 10.3 shows that the total generation costs of the optimal solutions are lower than those of the reference LF solution, as expected.

Table 10.6 gives the results for the base network. Again, he first column gives the case number for ease of reference, and a dash ('-') indicates the optimizer did not find a solution for that particular case.

For the base-case network, SLSQP is able to find a solution for slightly more cases of the OF problem than IPOPT. When both find a solution, SLSQP converges in significantly fewer iterations than IPOPT.

Then, we consider the effect of imposing bounds on q_k, $m_{i,l}$, and $|S_k|^2$, that is, we compare cases 1–12 with cases 13–24. If bounds are imposed (cases 1–12), Table 10.6 shows that an optimal solution is found for more options of the OF problem. The number of iterations required to find a solution is roughly equal with or without these

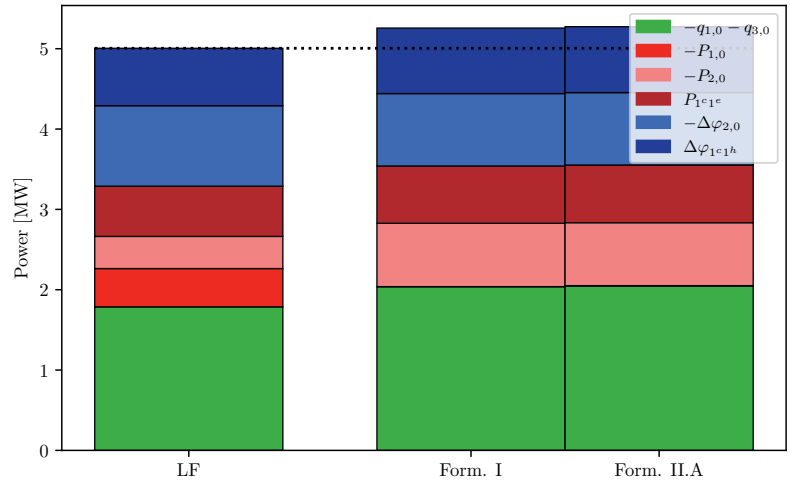

(a) With gas input; the part that goes towards the coupling.

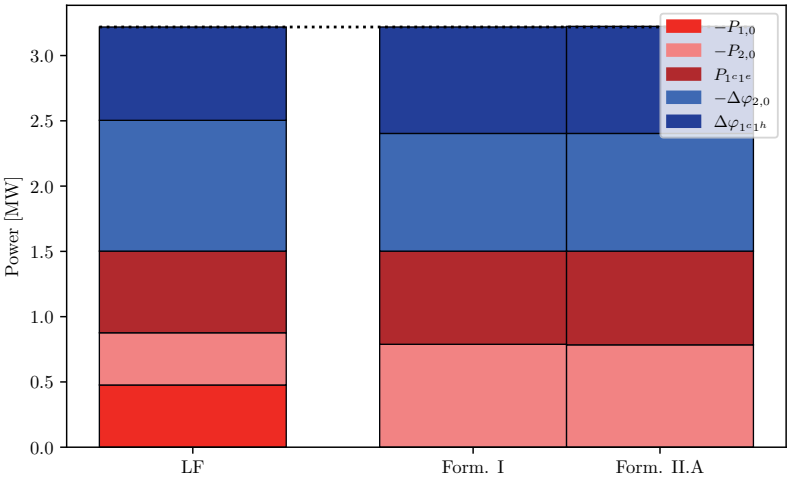

(b) Without gas input

Figure 10.2: Energy of sources $\boldsymbol{E}$ for the base network. The first bar shows a reference LF solution, the others show OF solutions, without bounds on q_k, $m_{i,l}$, and $|S_k|^2$, full formulation in gas, terminal link flow formulation in heat, using SLSQP and matrix scaling.

bounds, except for one formulation of the OF problem. With nodal formulation in gas and standard formulation in heat, IPOPT requires significantly more iterations if bounds are imposed than if they are not imposed (cf. cases 10–12 with 22–24), for all three formulations I, II.A, and II.B.

Comparing the various formulations of the LF equations in Table 10.6, that is, nodal or full formulation in gas and standard or terminal link formulation in heat, we can see that the number of iterations required to find a solution is different for the

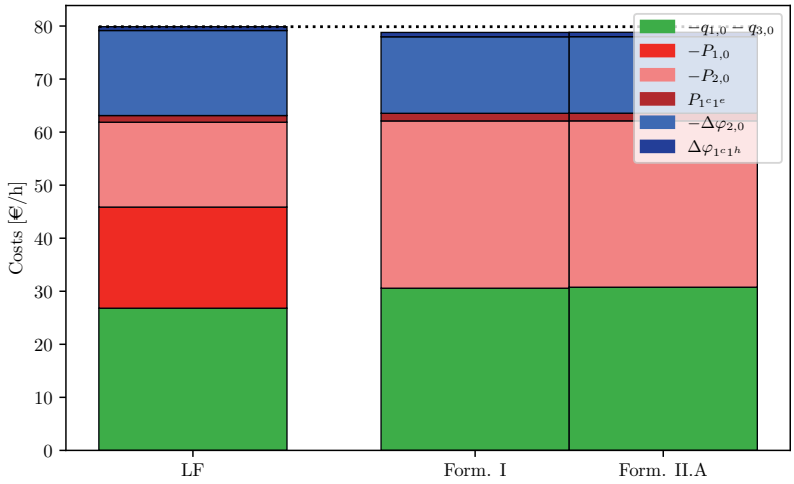

Figure 10.3: Generation costs for the base network. The gas input is only the part that goes towards coupling. The first bar shows a reference LF solution, the others show OF solutions, without bounds on q_k, $m_{i,l}$, and $|S_k|^2$, full formulation in gas, terminal link flow formulation in heat, using SLSQP and matrix scaling.

Table 10.6: Optimizer information of the OF problem for the base network.

					# iters		# f	
case	**bounds on q_k, $\lvert S_k\rvert^2$, $m_{i,l}$**	**form. gas**	**form. heat**	**OF form.**	**SLSQP**	**IPOPT**	**SLSQP**	**IPOPT**
1	no	full	term. link	I	14	41	24	59
2				II.A	15	-	46	-
3				II.B	15	-	46	-
4			standard	I	17	13	25	14
5				II.A	6	-	16	-
6				II.B	6	-	16	-
7		nodal	term. link	I	13	16	23	18
8				II.A	-	-	-	-
9				II.B	49	-	50	-
10			standard	I	14	19	17	20
11				II.A	7	10	7	11
12				II.B	7	10	7	11
13	yes	full	term. link	I	12	27	22	33
14				II.A	7	21	7	29
15				II.B	7	21	7	29
16			standard	I	16	36	32	42
17				II.A	7	48	7	117
18				II.B	7	-	7	-
19		nodal	term. link	I	11	29	12	35
20				II.A	7	21	7	29
21				II.B	7	21	7	29
22			standard	I	14	40	17	97
23				II.A	7	18	7	26
24				II.B	7	18	7	26

various formulations. These differences are minor, expect for one formulation. For the OF problem without bounds on q_k, $m_{i,l}$, and $|S_k|^2$, nodal formulation in gas, and terminal link formulation in heat (cases 7–9), a solution is not found with formulation II. This shows that the formulation of the system of LF equations influences the solvability of the OF problem and influences the convergence of the optimizers.

Finally, we consider the inclusion of the LF equations in the OF problem, that is, we compare formulation I (cases 1, 4, 7, 10, 13, 16, 19, and 22) with formulation II. For this network, there are some formulations of the OF problem where a solution is found using formulation I but not when using formulation II.A or II.B. However, if all three formulations I, II.A, and II.B find a solution, formulation II requires significantly fewer iterations than formulation I.

Table 10.7 gives the results for the network with 163 nodes per SCN. For this extended network, SLSQP and IPOPT find a solution in the same cases, although IPOPT requires more iterations than SLSQP.

Table 10.7: Optimizer information of the OF problem for the extended network (163 nodes per carrier, $n = 10, m = 5, s = 10$).

					# iters		# f	
case	**bounds on q_k, $\lvert S_k\rvert^2$, $m_{i,l}$**	**form. gas**	**form. heat**	**OF form.**	**SLSQP**	**IPOPT**	**SLSQP**	**IPOPT**
1	no	full	term. link	I	-	-	-	-
2				II.A	5	24	5	40
3				II.B	5	24	5	40
4			standard	I	-	-	-	-
5				II.A	3	24	3	40
6				II.B	3	24	3	40
7		nodal	term. link	I	-	-	-	-
8				II.A	5	15	5	40
9				II.B	5	15	5	40
10			standard	I	-	-	-	-
11				II.A	15	14	15	22
12				II.B	3	14	3	22
13	yes	full	term. link	I	-	-	-	-
14				II.A	5	31	5	32
15				II.B	5	32	5	33
16			standard	I	-	-	-	-
17				II.A	-	-	-	-
18				II.B	-	-	-	-
19		nodal	term. link	I	-	-	-	-
20				II.A	5	30	5	31
21				II.B	5	28	5	29
22			standard	I	-	-	-	-
23				II.A	12	28	14	30
24				II.B	12	28	13	30

As for the base network, we can see in Table 10.7 that the formulation of the LF problem influences the solvability of the OF problem and influences the convergence of the optimizers. Most notably, no solution is found for the OF problem with bounds on q_k, $m_{i,l}$, and $|S_k|^2$, full formulation in gas, and standard formulation in heat (cases 16–18). SLSQP requires more iterations for the OF problem with bounds on q_k, $m_{i,l}$, and $|S_k|^2$, nodal formulation in gas, and standard formulation in heat (cases 22-24),

than for the other cases (except case 11, which also uses the nodal formulation in gas and standard formulation in heat). IPOPT requires fewer iterations for the OF problem without bounds on q_k, $m_{i,l}$, and $|S_k|^2$ and nodal formulation in gas (cases 7–12), than for the other OF formulations.

Finally, we compare formulations I, II.A, and II.B. No solution is found using formulation I, for any of the formulations of LF. Furthermore, there are some differences between formulation II.A and II.B, both for SLSQP and IPOPT. The difference is most noticeable for the OF problem without bounds on q_k, $m_{i,l}$, and $|S_k|^2$, nodal formulation in gas, and standard formulation in heat (cases 11 and 12), using SLSQP. This is illustrated in Figure 10.4, which shows the error of the scaled LF equations $\|\hat{\boldsymbol{F}}\|_2$ at each iteration of the optimizer for these cases. We can see that formulations II.A and II.B result in different iterates, and a different number of iterates. For the other cases, these differences are minor. Since formulations II.A and II.B are simply different methods to calculate the required gradients, see Section 9.4, these differences are caused by numerical errors. As such, formulations II.A and II.B are not equivalent.

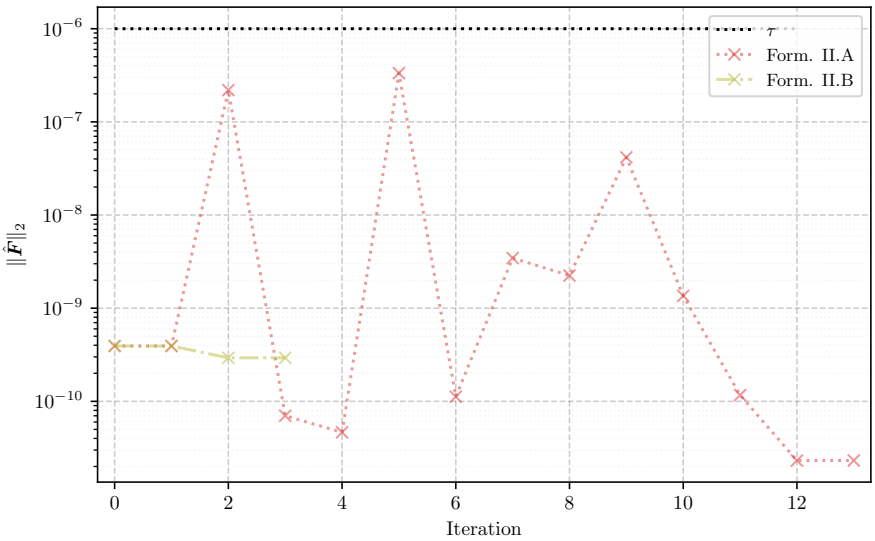

Figure 10.4: Error of scaled LF equations $\|\hat{\boldsymbol{F}}\|_2$ at every iteration of the optimizer for the extended network (163 nodes per carrier, $n = 10, m = 5, s = 10$), bounds on q_k, $m_{i,l}$, and $|S_k|^2$, nodal formulation in gas, and standard formulation in heat (cases 11 and 12), using SLSQP. Comparison of formulation II.A. and formulation II.B.

Based on this MES, we find that formulations II.A and II.B are not equivalent when solving the OF problem. The formulation of the LF equations influences the solvability of the OF problem, and the convergence of the optimizers. If a solution is found for all three formulations I, II.A, and II.B, formulation II requires significantly fewer iterations than formulation I.

10.6 Final remarks

The formulation of the LF equations, both the individual equations and the system of equations, influences the solvability and convergence of the OF problem. The formulation of the system of LF equations determines which variables are state variables and which are derived variables, which subsequently determines the nonlinearity of the (in)equality constraints and objective function. Moreover, the formulation of the system of LF equations is related to the choice of BCs for the LF problem, which determines the choice of control variables in the OF problem. The best formulation of the LF equations, and the best choice for the control variables, depends on the specific problem and network.

Bounds on the control variables are used to keep the iterates (physically) feasible, by ensuring the extended LF problem is solvable. Hence, choosing appropriate bounds for the control variables is crucial in formulating a solvable OF problem. Additional bounds on (extended) state variables and derived variables increase the complexity of the optimization problem and (can) increase the nonlinearity. Hence, they influence the solvability of the OF problem and the convergence of the optimizers. Whether bounds should be imposed depends on the specific problem and energy system.

Including the LF equations as equality constraints or as subsystem both result in a solvable OF problem. That is, both formulation I and formulation II can be used to optimize a MES. Formulation II reduces the size of the optimization space compared with formulation I, but increases the nonlinearity of the objective function and constraints. In formulation II, the LF equations are solved separately for multiple iterations of the optimizer. This allows the use of a dedicated separate solver for the LF problem. Furthermore, it ensures the LF equations are satisfied at each iteration of the optimizer. However, it might increase CPU time.

For the two example MESs, formulation II requires significantly fewer iterations than formulation I, if an optimal solution is found for both formulations. Furthermore, formulations II.A and II.B are not equivalent due to numerical errors. For some OF problems, II.A and II.B result in different iterates of the optimizers.

The OF problem for a MES can be formulated in various ways, with respect to choice of state variables, control variables, and BCs, with respect to the formulation of the LF equations, with respect to including the LF equations in the OF problem, and with respect to bounds and inequality constraints. Which way is best depends on the specific network and problem considered.

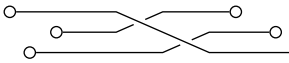

CHAPTER 11

Scaling

The parameters and the dependent and independent variables in the LF equations can be several orders of magnitude apart, even within one single-carrier network (SCN). For instance, $q \sim 1\,\mathrm{kg/s}$ whereas $p \sim 10^5\,\mathrm{Pa}$. These different scales might result in problems with solving the system of nonlinear LF equations, see Section 5.2. In MESs, the SCN variables, which have various scales, are combined. This requires a consistent way to scale the LF equations for MESs.

In SC electricity networks, per unit (p.u.) scaling is generally used (e.g. [3]). In the per unit system, every variable and parameter is scaled to obtain dimensionless quantities and equations. In gas and heat networks, a more ad hoc approach to scaling is used. In [17], the p.u. system is extended to the heat network, for consistency throughout an example MES. There is no equivalent of the p.u. system for a gas network.

Another option to scale the system of nonlinear LF equations is by scaling the equations and variables using scaling matrices, without scaling the equation parameters. Even though this method is a well known scaling method, see Section 5.2, it is not generally used for LF equations in any of the SCNs or in MCNs.

To investigate the effect of scaling on the system of LF equations, we consider dimensional analysis. We introduce a p.u. scaling for MESs, by extending the p.u. scaling of an electricity network to gas and heat. We compare per unit scaling with matrix scaling, and show that they are equivalent for NR, when using the same base

This chapter is based on the articles:

Anne S. Markensteijn, Johan E. Romate, and Cornelis Vuik. Scaling of the steady-state load flow equations for multi-carrier energy systems. In *Numerical Mathematics and Advanced Applications ENUMATH 2019*, volume 139 of *Lecture Notes in Computational Science and Engineering*. Springer, May 2021. ISBN 978-3-030-55874-1,

Anne S. Markensteijn, Johan E. Romate, and Cornelis Vuik. Optimal flow for general multi-carrier energy systems, including load flow equations. Technical Report 20-06, Delft University of Technology, Delft Institute of Applied Mathematics, December 2020.

values and assuming infinite precision. The advantages and disadvantages of both methods are discussed.

Using two example MESs, we investigate the effect of the two scaling methods on the convergence of NR for LF problem and on the convergence of optimization algorithms for OF problems. Despite numerical (round-off) errors, both scaling methods show the same convergence behavior for NR. The optimization algorithms are affected by the type of scaling.

11.1 Dimensional analysis

The LF equations are a mathematical representation of a physical phenomenon. Physical quantities are not just numerical values, they also have a dimension and a unit measure associated with them. For instance, the diameter D of a gas pipe has dimension 'length', and could have a unit measure of 1 cm and a value of 15. Denoting the length unit measure by l and the value of D by k, we can write $D = kl$. We can scale D by changing the unit measure with a scaling factor $k_l \in \mathbb{R}$, and generally $k_l > 0$, such that $l \to k_l l$. Using this new unit measure for D will change the unit measure and the value (to k/k_l), but not the dimension.

Based on the logic as laid out for dimensional analysis in for instance [39] or [40], quantities can only be combined in limited ways. Quantities can be multiplied, which multiplies the dimension in the same way. To add two quantities, they must have the same dimension and the same unit measure. Other functional relations are only possible if all arguments are dimensionless. For instance, if $f(x) = \sin(x)$, then both $f(x)$ and x must be dimensionless. Using these concepts recursively, a function of multiple arguments can be constructed. An equation that satisfies these properties is called complete [39]. A consequence is that the algebraic form of the equation is unit independent. That is, if the unit measure of any dimension is changed, the algebraic form of the equation remains the same. However, the value of the function might be changed, just like the value of some of the quantities is changed. This can be seen as follows.

Since two (or more) terms can only be added if the terms have the same dimension and unit measure, we can limit ourselves to functions consisting of only one term. Furthermore, for dimensionless quantities, or for a dimensionless group consisting of the power product of some quantities, the changes in unit measures cancel out. Hence, we only need to consider the change in value of functions that are a power product of the variables:

$$f(x_1, \ldots, x_N) = x_1^{a_1} \cdots x_N^{a_N}$$

We can assume that all $x_n \in \{x_1, \ldots, x_N\}$ have a single (primary) dimension. Scaling each x_n by changing the unit measures of the primary dimensions by a factor k_n gives

$$\begin{aligned} f(x_1, \ldots, x_N) \to f(k_1 x_1, \ldots, k_N x_N) &= (k_1^{a_1} \cdots k_N^{a_N})(x_1^{a_1} \cdots x_N^{a_N}) \\ &= (k_1^{a_1} \cdots k_N^{a_N}) f(x_1, \ldots, x_N) \end{aligned} \tag{11.1}$$

such that f is scaled by a power product of the unit measure scaling factors.

An equation describing a physical model does not need to be complete for the model to be valid. In fact, the commonly used form of the link equation (2.14) or (2.17) for the power of a transmission line, is not a complete equation, since it contains

terms $\sin\delta_{ij}$ and $\cos\delta_{ij}$. Based on the logic provided above, the nodal voltage angles δ_i and δ_j should be dimensionless. However, they have dimension 'plane angle'. The link equation can be turned into a complete equation by using δ_{ij}/δ_0 instead of δ_{ij}, with δ_0 a reference angle.

11.2 Types of scaling

Based on dimensional analysis, we consider two ways to scale variables and equations: per unit scaling and matrix scaling.

11.2.1 Per unit system

The per unit (p.u.) system is commonly used in electricity networks, and extended in [17] to a heat network. We introduce a more general extension of the p.u. system to heat and gas networks. In the p.u. system, a quantity x is scaled by a base value:

$$x_{\text{p.u.}} = \frac{x_a}{x_b} \tag{11.2}$$

Here, x_a is the unscaled or actual quantity, usually in S.I. units, x_b is a chosen base value with the same dimension as x_a, and $x_{\text{p.u.}}$ is the scaled quantity. The scaled quantity is dimensionless but is given p.u. as unit. Hence, the scaled quantity is also called the per unit quantity or value.

There are two main differences between the p.u. system and changing the unit measures. The first is that the base value has a dimension, unlike the scaling factor of the unit measure. Second, only the unit measure scaling factors of the primary dimensions are chosen, whereas in the per unit system, the base value for derived quantities might be chosen. The first point has no consequence for the arguments outlined in Section 11.1 which result in (11.1). However, the second point can lead to some difficulties.

Since derived quantities are combinations of other quantities, and applying the same logic that results in a complete equation, only a limited set of base values can be specified. The base values for the other quantities then follow from dimensional analysis. The set of base values that can be specified is not unique, neither are the resulting base values of the other quantities. However, it is possible to find a set of base values such that the equation remains a complete equation. For such a set of base values, the argumentation resulting in (11.1) is still valid. We can now investigate the effect of the p.u. system on the LF equations.

Suppose we have a (complete) equation of the form $F(\boldsymbol{x}_a, \boldsymbol{p}_a)$, with $\boldsymbol{x}_a \in \mathbb{R}^{N_x}$ all the variables, and $\boldsymbol{p}_a \in \mathbb{R}^{N_p}$ all other quantities, dimensionless or not, appearing in the algebraic form of F. We take a set of base values $b_1, \ldots, b_{N_b}$, with $N_b \leq N_x + N_p$, and scale each $x_a \in \boldsymbol{x}_a$ and $p_a \in \boldsymbol{p}_a$ according to (11.2), with x_b and p_b power products of the base values $b_1, \cdots, b_{N_b}$. If the base values are chosen such that the equation F remains a complete equation after scaling, the equation is scaled according to:

$$F(\boldsymbol{x}_a, \boldsymbol{p}_a) = \left[b_1^{\alpha_1} \cdots b_{N_b}^{\alpha_{N_b}}\right] F(\boldsymbol{x}_{\text{p.u.}}, \boldsymbol{p}_{\text{p.u.}})$$

Usually, only the variables are explicitly denoted as arguments for the function, such that $F(\boldsymbol{x}_a, \boldsymbol{p}_a)$ is written as $F(\boldsymbol{x}_a)$ and $F(\boldsymbol{x}_{\text{p.u.}}, \boldsymbol{p}_{\text{p.u.}})$ as $F(\boldsymbol{x}_{\text{p.u.}})$. For the scaled

equation we then find

$$F(\boldsymbol{x}_a) = [b_1^{\alpha_1} \cdots b_{N_b}^{\alpha_{N_b}}] F(\boldsymbol{x}_{\text{p.u.}}, \boldsymbol{p}_{\text{p.u.}}) := F_b F(\boldsymbol{x}_{\text{p.u.}}) \tag{11.3}$$

where $F_b := [b_1^{\alpha_1} \cdots b_{N_b}^{\alpha_{N_b}}]$ is called the base value of the function F.

Equation (11.3) means that, for a suitable set of base values, the same expression of the LF equations can be used for both the unscaled and p.u. quantities, and all independent variables and all LF equations can be scaled to similar orders of magnitude.

For an electricity network, the base values of the voltage amplitude and the (complex) power are chosen. The base values of the other variables and of the parameters of the LF equations (e.g. admittance) are determined by the requirement that the LF equations remain complete equations, using dimensional analysis (e.g. [3]).

The p.u. system is then easily extended to the gas and heat SCN, and to a MES. We choose the base values for pressure and flow in the gas network, and for pressure, mass flow, temperature, and power in the heat network. The base values of the other variables and parameters are determined based on dimensional analysis. For the couplings in a MES, we choose the base values of the power of every carrier involved in the coupling, and again determine the base values of the other quantities according to dimensional analysis. See Appendix D.1 for details on the base values.

The advantage of scaling derived quantities instead of scaling primary dimensions becomes clear when considering transformers in an electrical network, or compressors in a gas network. These components change the voltage or pressure level, and their link equation (e.g. (3.5) for a compressor) has the general form $F(x_1, x_2, r) = x_1 - rx_2 = 0$, with x_1 and x_2 the voltages or pressures, and r some ratio. Since x_1 and x_2 have the same dimension, r must be dimensionless. Hence, changing the unit measures will scale the values of x_1 and x_2 with the same factor, and will leave r unscaled. In practice, x_1 and x_2 might be orders of magnitude apart when using the same unit measure. In the p.u. system, it is possible to use a different base value for x_1 and x_2, such that both $x_1 \sim 1\,\text{p.u.}$ and $x_2 \sim 1\,\text{p.u.}$. Note that the scaled x_1 and x_2 now have different unit measures, despite both of their units being denoted by p.u.. Due to the requirement for addition of dimensional quantities, r needs to scaled with $r_b = (x_1)_b \,/\, (x_2)_b$.

11.2.2 Matrix scaling

Another option is to scale the independent variables and the equations only, using transformation matrices (see Section 5.2). Taking non-singular matrices T_x, $T_F \in \mathbb{R}^{N \times N}$, the scaled variables $\hat{\boldsymbol{x}}$ and scaled equations $\hat{\boldsymbol{F}}$ are given by:

$$\hat{\boldsymbol{x}} = T_x \boldsymbol{x} \tag{11.4a}$$

$$\hat{\boldsymbol{F}}(\hat{\boldsymbol{x}}) = T_F \boldsymbol{F}\left(T_x^{-1} \hat{\boldsymbol{x}}\right) = T_F \boldsymbol{F}(\boldsymbol{x}) \tag{11.4b}$$

Unlike the p.u. scaling, scaling with matrices also requires base values to scale the equations, instead of only base values for the variables. On the other hand, p.u. scaling requires base values for all parameters in every equation. Furthermore, matrix scaling is generally easier to implement than p.u. scaling.

11.2.3 Equivalence of per unit and matrix scaling

If we take T_x as a diagonal matrix with $(T_x)_{nn} = (x_b)_n$, where $(x_b)_n$ is the base value of $x_n \in \boldsymbol{x}$ used in p.u. scaling, it follows from (11.3) that T_F is a diagonal matrix with $(T_F)_{nn} = (F_b)_n$, where $(F_b)_n$ is the base value of $F_n \in \boldsymbol{F}$ found in p.u. scaling, see Appendix D.2 for details. Therefore, in infinite precision, the p.u. scaling and matrix scaling will result in the same scaled system of equations $\hat{\boldsymbol{F}}$ and the same scaled variables $\hat{\boldsymbol{x}}$. Hence, the p.u. system and matrix scaling are said to be equivalent.

Matrix scaling does not affect the NR iterations, see Section 5.2. Since p.u. scaling and matrix scaling are equivalent, p.u. does not affect the NR iterations either.

11.3 Finite precision

The analyses in Section 5.2 and Section 11.2.3 only hold in infinite precision. In finite precision, p.u. and matrix scaling might not be equivalent, such that an NR step might be affected.

In the p.u. system, the scaled variables and parameters are substituted into (4.11) to obtain the scaled system of equations, denoted by $\boldsymbol{F}_{\text{p.u.}}$. With matrix scaling, the unscaled variables and parameters are used in (4.11). Then, the scaled system of equations $\hat{\boldsymbol{F}}$ is given by (11.4b). Due to round-off errors, generally $\boldsymbol{F}_{\text{p.u.}} \neq \hat{\boldsymbol{F}}$, even though $\boldsymbol{F}_{\text{p.u.}}$ and $\hat{\boldsymbol{F}}$ will be close. Similarly, $J_{\text{p.u.}} \neq \hat{J}$, such that for the NR update we have $\hat{\boldsymbol{s}}^k \neq \boldsymbol{s}^k_{\text{p.u.}} \neq T_x \boldsymbol{s}^k$.

11.4 Scaling in steady-state load flow problems

We model two small MESs to investigate the effect of finite precision on NR for the two different scaling options. The first MES is similar to the one in Section 7.1, but some of the network elements are modeled differently. The second is the same MES as used in Chapter 6.

11.4.1 Networks and models

The first MES we consider is similar to the one used in Section 7.1, but we only consider the MCN coupled with a GB and a CHP, giving the network in Figure 7.1a.

For the gas network and the electrical network we use the same models as in Section 7.1, but we use different models in the hydraulic part of the heat network, and for the coupling units. The parameter values used in the equations are summarized in Tables C.32–C.34 in Appendix C.4.

In the heat network, all links represent pipes. For the hydraulic model, we use the steady-state flow equation (2.20), with the pipe constant (2.22), pressure drop (2.21), and Pole's friction factor (2.5). For the thermal pipe model, we use (2.28).

Node 0^c represents a GB and node 1^c a CHP, which we model using (2.33) and

(2.36) respectively, such that the nodal coupling equations (3.26) are

$$F_{0^c}^{c,E} = \Delta\varphi_{0^c0^h} - \eta_{\mathrm{GB}}\mathrm{GHV}q_{2^g0^c} \tag{11.5a}$$

$$F_{1^c}^{c,E} = \mathrm{GHV}q_{2^g1^c} - \frac{P_{1^c1^e}}{\eta_{\mathrm{CHP}}^{ge}} - \frac{\Delta\varphi_{1^c0^h}}{\eta_{\mathrm{CHP}}^{gh}} \tag{11.5b}$$

To form the system of LF equations, we use node set 1 from Table 7.1 for the BCs, and we use the full formulation (4.1) in the gas part, and the standard formulation (4.9) in the heat part, with hydraulic link equations (3.4b). The values of the BCs are given in Tables C.37–C.41.

The second MES is the same as the one used in Chapter 6, but we only consider network 1 and network 2, shown in Figure 6.1a and Figure 6.1b respectively.

In total, we consider three MCNs.

11.4.2 Solving the load flow problem

The systems of nonlinear equations (4.11) for the three networks are solved using the per unit system and using matrix scaling. For the former, the resulting scaled systems $\boldsymbol{F}_{\mathrm{p.u.}}$ are solved using unscaled NR, see Algorithm 5.1, whereas for the latter scaled NR is applied, see Algorithm 5.2.

For comparison, we also solve the unscaled system for the first MES using NR. To compare the unscaled error (5.4) at each NR iteration with the error of NR for the scaled systems, we calculate the scaled error of the unscaled NR iteration by $\tilde{e}^k = \|T_F\boldsymbol{F}(\boldsymbol{x}^k)\|_2$. Note that $\tilde{e}^k$ is different from the error $\hat{e}^k$ of scaled NR (5.6), since scaled NR uses the scaled update $\hat{\boldsymbol{s}}^k$ instead of $\boldsymbol{s}^k$.

For both algorithms, we set the tolerance to $\tau = 10^{-6}$. As base values for the first MES, we take the values given in Table C.36, and for the second MES we take the values given in Table C.17.

Table 11.1: Errors of NR using scaling, for the first MES, with $\tilde{e}^k = \|T_F\boldsymbol{F}^k\|_2$, $\hat{e}^k = \|\hat{\boldsymbol{F}}^k\|_2$, and $e_{\mathrm{p.u.}}^k = \|\boldsymbol{F}_{\mathrm{p.u.}}^k\|_2$.

k	$\tilde{e}^k$	$\hat{e}^k$	$e_{\mathrm{p.u.}}^k$	$\lvert\tilde{e}^k - \hat{e}^k\rvert/\lvert\tilde{e}^k\rvert$	$\lvert\tilde{e}^k - e_{\mathrm{p.u.}}^k\rvert/\lvert\tilde{e}^k\rvert$
0	$1.0310 \cdot 10^{6}$	$1.0310 \cdot 10^{6}$	$1.0310 \cdot 10^{6}$	0	0
1	$1.3081 \cdot 10^{3}$	$1.3081 \cdot 10^{3}$	$1.3081 \cdot 10^{3}$	$2.6421 \cdot 10^{-14}$	$1.0951 \cdot 10^{-14}$
2	$5.7417 \cdot 10^{-1}$	$5.7417 \cdot 10^{-1}$	$5.7417 \cdot 10^{-1}$	$1.5071 \cdot 10^{-12}$	$9.6527 \cdot 10^{-13}$
3	$7.0379 \cdot 10^{-4}$	$7.0379 \cdot 10^{-4}$	$7.0379 \cdot 10^{-4}$	$6.5244 \cdot 10^{-10}$	$7.7472 \cdot 10^{-10}$
4	$3.2883 \cdot 10^{-9}$	$3.2890 \cdot 10^{-9}$	$3.2886 \cdot 10^{-9}$	$1.8566 \cdot 10^{-4}$	$7.4581 \cdot 10^{-5}$
5	$6.6172 \cdot 10^{-11}$	-	-	-	-

Table 11.1 and Table 11.2 give the errors of NR for the first and second MES, respectively. We can see that the NR errors for per unit scaling and matrix scaling are unequal, but close, to each other and, for the first MES, to the error of unscaled NR. Hence, scaling affects NR in finite precision.

In these examples, this effect does not result in a significant difference between the solutions to the LF problem. This shows that scaling by matrix multiplication is

indeed equivalent to scaling using the per unit system, when the same base values are used, and the parameters in the LF equations are scaled accordingly for the per unit system.

Table 11.2: Errors of NR using scaling, for the second MES, with $\hat{e}^k = \|\hat{\boldsymbol{F}}^k\|_2$ and $e^k_{\text{p.u.}} = \|\boldsymbol{F}^k_{\text{p.u.}}\|_2$.

	Network 1			Network 2		
k	$\hat{e}^k$	$e^k_{\text{p.u.}}$	$\lvert\hat{e}^k - e^k_{\text{p.u.}}\rvert/\lvert\hat{e}^k\rvert$	$\hat{e}^k$	$e^k_{\text{p.u.}}$	$\lvert\hat{e}^k - e^k_{\text{p.u.}}\rvert/\lvert\hat{e}^k\rvert$
0	$2.1756 \cdot 10^{3}$	$2.1756 \cdot 10^{3}$	$2.0903 \cdot 10^{-16}$	$3.1521 \cdot 10^{3}$	$3.1521 \cdot 10^{3}$	$4.3280 \cdot 10^{-16}$
1	$9.2049 \cdot 10^{2}$	$9.2049 \cdot 10^{2}$	$4.9403 \cdot 10^{-16}$	$6.8240 \cdot 10^{2}$	$6.8240 \cdot 10^{2}$	$3.3320 \cdot 10^{-16}$
2	$1.6054 \cdot 10^{2}$	$1.6054 \cdot 10^{2}$	$5.3111 \cdot 10^{-16}$	$5.3596 \cdot 10^{1}$	$5.3596 \cdot 10^{1}$	$3.1818 \cdot 10^{-15}$
3	$2.4988 \cdot 10^{-1}$	$2.4988 \cdot 10^{-1}$	$1.5817 \cdot 10^{-13}$	$5.4506 \cdot 10^{-1}$	$5.4506 \cdot 10^{-1}$	$5.6319 \cdot 10^{-13}$
4	$5.9439 \cdot 10^{-4}$	$5.9439 \cdot 10^{-4}$	$3.0217 \cdot 10^{-10}$	$5.0576 \cdot 10^{-5}$	$5.0576 \cdot 10^{-5}$	$6.8517 \cdot 10^{-9}$
5	$5.9071 \cdot 10^{-7}$	$5.9071 \cdot 10^{-7}$	$2.0139 \cdot 10^{-7}$	$1.6610 \cdot 10^{-8}$	$1.6610 \cdot 10^{-8}$	$7.4091 \cdot 10^{-6}$

11.5 Scaling in optimal flow problems

Scaling affects the iterates of an optimizer, unlike the iterates of NR, and is often required for an optimization method to converge [27]. For instance, scaling changes the steepest-descent direction. In finite precision, p.u. scaling and matrix scaling are not equivalent due to round-off errors. Therefore, the type of scaling can influence the iterates and convergence of the optimization algorithm.

To investigate the effect of scaling on optimization, we consider the same MES as in Section 10.5.3 (see also Appendix C.5 for details). We only consider the base case network, consisting of 3 nodes per SCN. We compare matrix scaling with per unit scaling for the 24 formulations and solution methods of the OF problem, using SLSQP and IPOPT as optimizers.

We set the tolerance for the OF problem, for the extended LF problem τ_h, and τ_u to 10^{-6}. The maximum number of iterations for the optimizers is 50, and the maximum number of iterations for NR to solve the extended LF problem (10.2) within formulation II is 20. For both matrix scaling and p.u. scaling, we take the base values as used in Section 10.5.3, which are also given in Table C.46.

Table 11.3 gives the results for the base network using p.u. scaling, where a dash ('-') indicates the optimizer did not find a solution for that particular case.

We compare Table 11.3 with Table 10.6 to look at the effect of scaling. There are minor differences between matrix scaling and p.u. scaling. With matrix scaling (Table 10.6), SLSQP with formulation II.B finds a solution for the OF problem without bounds on q_k, $m_{i,l}$, and $|S_k|^2$, nodal formulation in gas, and terminal link formulation in heat (case 9), while no solution is found with per unit scaling (Table 11.3) in that case. On the other hand, with p.u. scaling, IPOPT with II.B finds a solution for the OF problem with bounds on q_k, $m_{i,l}$, and $|S_k|^2$, full formulation in gas, and standard formulation in heat (case 18), while no solution is found with matrix scaling in that case. Furthermore, there is some difference in the number of iterations when a solution is found with both types of scaling. Compare, for instance, SLSQP with I for the OF problem without bounds on q_k, $m_{i,l}$, and $|S_k|^2$, full formulation in gas, and

Table 11.3: Optimizer information of the OF problem for the base network, using p.u. scaling.

					# iters		# f	
case	**bounds on q_k, $\lvert S_k\rvert^2$, $m_{i,l}$**	**form. gas**	**form. heat**	**OF form.**	**SLSQP**	**IPOPT**	**SLSQP**	**IPOPT**
1	no	full	term. link	I	12	41	22	59
2				II.A	15	-	46	-
3				II.B	15	-	46	-
4			standard	I	16	13	32	14
5				II.A	6	-	16	-
6				II.B	6	-	16	-
7		nodal	term. link	I	13	16	23	18
8				II.A	-	-	-	-
9				II.B	-	-	-	-
10			standard	I	16	19	31	20
11				II.A	7	10	7	11
12				II.B	7	10	7	11
13	yes	full	term. link	I	12	27	13	33
14				II.A	7	21	7	29
15				II.B	7	21	7	29
16			standard	I	16	36	32	42
17				II.A	7	20	7	28
18				II.B	7	20	7	28
19		nodal	term. link	I	13	29	23	35
20				II.A	7	21	7	29
21				II.B	7	21	7	29
22			standard	I	14	33	17	91
23				II.A	7	18	7	26
24				II.B	7	18	7	26

terminal link flow formulation in heat (case 1), or SLSQP with I for the OF problem with bounds on q_k, $m_{i,l}$, and $|S_k|^2$, nodal formulation in gas, and terminal link flow formulation in heat (case 19).

Finally, the solutions found with matrix scaling are slightly different from the ones found with p.u. scaling. This is most noticeable for the OF problem of the base network with bounds on q_k, $m_{i,l}$, and $|S_k|^2$, nodal formulation in gas, and terminal link flow formulation in heat, using SLSQP and formulation I (case 19). With matrix scaling, SLSQP requires 11 iterations and 12 function evaluations, whereas with p.u. scaling SLSQP requires 13 iterations and 23 function evaluations. Figure 11.1 shows the error of the scaled LF equations $\|\hat{\boldsymbol{F}}\|_2$ or $\|\boldsymbol{F}_{\text{p.u.}}\|_2$ at each iteration of the optimizer for this case. We can see that the iterates with matrix scaling and p.u. scaling are not the same, even though the same base values are used. We have seen similar results for the other cases of the base network, and for the networks with larger size. In many of cases where matrix scaling and p.u. scaling resulted in the same of number of iterations of the optimizers, the iterates themselves where still different.

We have seen similar results for MES 1, used in Section 10.5.2, and for the extended network of this MES. Therefore, matrix scaling and p.u. scaling are not equivalent if solving the OF problem.

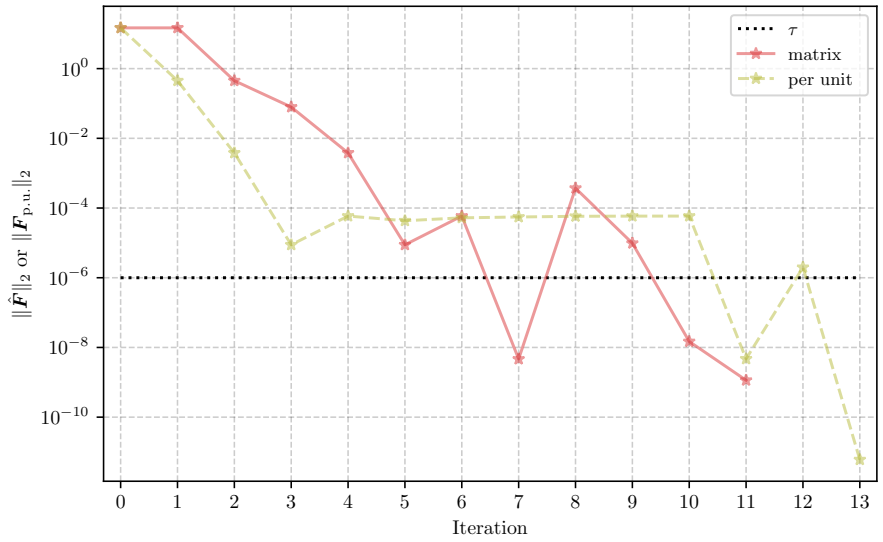

Figure 11.1: Error of scaled LF equations $\|\hat{\boldsymbol{F}}\|_2$ or $\|\boldsymbol{F}_{\text{p.u.}}\|_2$ at every iteration of the optimizer, using matrix scaling and p.u. scaling, for case 19.

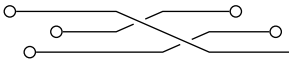

CHAPTER 12

Conclusions and recommendations

Important tools for the design and operation of energy systems are steady-state simulation and optimization. Steady-state simulation, solving the load flow (LF) problem, is concerned with determining the flow of energy carriers through the system and the values of other quantities, such as voltages and pressures, throughout the system for given demands. In operational optimization, solving the optimal flow (OF) problem, the distribution of generation over the various sources, or the set points of controllable elements, are determined such that some objective is optimized and such that the system is operated within physical limits. LF and OF problems for single-carriers (SCs) systems have been widely studied, but have only been proposed recently for multi-carrier energy systems (MESs). In this chapter, we give conclusions on and some recommendations for steady-state simulation and optimization of general MESs.

12.1 Conclusions

In this thesis, we developed a graph-based model framework for steady-state LF analysis of general MESs, consisting of gas, electricity, and heat. The framework is based on connecting the single-carrier networks (SCNs) to heterogeneous coupling nodes, using homogeneous dummy links, to form one connected multi-carrier network (MCN). Load flow equations are associated with each network element, including the coupling nodes. A coupling node allows for bidirectional flow, and can represent a variety of couplings, such as a single converter component or an energy hub. This network representation makes it possible to describe integrated energy systems in a very effective way.

To formulate the LF problem of a MES, the models of all network elements of the connected MCN are combined with boundary conditions (BCs) to form one integrated system of nonlinear equations. If the coupling energies are known, the SCNs would effectively be decoupled. If they are unknown, additional BCs in the single-carrier part of the network are required, leading to new node types. The node types and location of the coupling nodes in the network must be carefully chosen. Certain combinations of node types, or graph topologies, can result in systems of equations that are not (uniquely) solvable.

We showed that our proposed model framework can be used to formulate and

solve the steady-state LF for general MESs. Moreover, our framework can be used with different components and models, both in the SCNs and for the coupling units. Therefore, our framework includes and extends the currently available LF models for MESs.

As an alternative to solving the integrated system of equations of a connected MCN, we also formulated a decoupled approach for the same problem. In the decoupled approach, a connected MCN is split into its SC parts and its coupling part, such that a general MES is represented as a disconnected MCN. The interaction between the SC networks and the coupling network is modeled using interface conditions (IFCs), and the LF problem for each subnetwork, including the coupling network, is formulated. Combining the IFCs with these LF subproblems gives a system of (non)linear equations that models the LF problem for the integrated MES.

We showed that the decoupled approach can be used to solve the LF problem of integrated MESs. However, using the decoupled approach to perform LF analysis is slower than solving the LF problem of the connected MCN. On the other hand, the decoupled approach allows the use of dedicated solvers for the LF problem of the SC subnetworks, and the decoupled approach does not require sharing of detailed model and network data amongst the various subsystems.

We provided an analysis of the effect of the LF equations on the solvability of the OF problem for general MESs, and we provided a optimization framework for general single- and multi-carrier energy systems. The formulation of the LF equations, both the individual equations and the system of equations, influences the solvability and convergence of the OF problem. The formulation of the system of LF equations determines which variables are state variables and which are derived variables. This subsequently determines the nonlinearity of the (in)equality constraints and objective function. Moreover, the formulation of the system of LF equations is related to the choice of BCs for the LF problem, which determines the choice of control variables in the OF problem. The best formulation of the LF equations, and the best choice for the control variables, depends on the specific problem and network.

The LF equations can be included in the OF problem as equality constraints or as subsystem, and both result in a solvable OF problem. The latter reduces the size of the optimization space compared with the former, but increases the nonlinearity of the objective function and constraints. When the LF equations are included as subsystem, the LF equations are solved separately for multiple iterations of the optimizer. This allows the use of a dedicated separate solver for the LF problem. Furthermore, it ensures the LF equations are satisfied at each iteration of the optimizer. However, it might increase CPU time.

Scaling is often required for solution methods to solve the LF problem, and especially for optimization methods to solve the OF problem. We considered two types of scaling to scale the equations and variables: per unit (p.u.) scaling and matrix scaling. In this thesis, we introduced a p.u. scaling for the LF equations of MESs, by extending the p.u. scaling of an electricity network to gas and heat. We showed that base values can be chosen such that p.u. scaling is equivalent to matrix scaling for the LF problem, in infinite precision. The Newton-Raphson method (NR) is used to solve the (scaled) system of nonlinear LF equations. In finite precision, both scaling methods show the same convergence behavior for NR in the considered examples, despite numerical (round-off) errors.

Scaling does affect the iterates of an optimizer. In finite precision, p.u. scaling and matrix scaling show different iterates for some examples, due to round-off errors. These examples show that the type of scaling can influence the iterates and convergence of the optimization algorithm. Therefore, p.u. scaling and matrix scaling are not equivalent when solving the OF problem.

Summarizing, we developed a graph-based model framework for steady-state LF analysis of general MESs, consisting of gas, electricity, and heat, which includes and extends the currently available LF models for MESs. As an alternative to this framework, a decoupled approach can be used to solve the LF problem of an integrated MES. Furthermore, we provided a framework for operational optimization of single- or multi-carrier energy systems, which includes the detailed LF equations. The formulation of the system of LF equations, based on the coupling components, network topology, models for the individual network elements, and choice of BCs, influences the solvability of the LF and OF problems and influences the convergence of the solution methods.

12.2 Recommendations

In this thesis, we focused on steady-state LF analysis and operational optimization of MESs consisting of gas, electricity, and heat. This section provides possible topics for future research.

We have applied our steady-state LF framework to small MESs, where each coupling node represented coupling components which physically did not allow bidirectional flow. Several other example networks and extensions or adaptations to this framework can be considered. A first option for such an example network could be one with coupling components that do allow bidirectional flow, as the coupling node concept, in combination with the dummy links, allows for such components. Moreover, the coupling node could be used to represent a complete heterogeneous network as single node, which could lead to a hierarchical approach. Furthermore, the framework itself is generic, and could be extended to include other energy carriers, such as cooling. Finally, a steady-state approach might not be accurate enough for short-term operational purposes, especially for heating systems. Moreover, storage, which is essential in exploiting the full potential of MES, can only be modeled accurately if time is taken into account. Therefore, transient models might be considered for any of the SC systems and for the MES.

Our systematic approach to the graph representation of MESs, and corresponding formulation of the system of LF equations, provides insight into which coupling nodes and node types lead to a system that is uniquely solvable. However, this is still an open problem, and further research is required to determine definitive guidelines on which combinations of node types, or graph topologies, result in a well-posed LF problem, both for the integrated and the decoupled approach.

We have looked at the convergence of solution methods for steady-state LF problems and for OF problems, using several small MESs. Larger networks should be considered to see how these methods scale with the size of the network, and if the qualitative results also hold for larger networks. Furthermore, the decoupled approach is slow, even for small networks. Further research is required to accelerate the fixed-point method (FP) and NR used in the decoupled approach.

Finally, in the OF problems, we only considered the system of LF equations based on a connected MCN. Another option is to extend the decoupled approach for LF problems to OF problem, for instance by including the system of LF equations based on a disconnected MCN in the OF problem.

Bibliography

[1] Thorsten Koch, Benjamin Hiller, Marc E. Pfetsch, and Lars Schewe. *Evaluating Gas Network Capacities*. Society for Industrial and Applied Mathematics, Philadelphia, PA, USA, 2015. doi: 10.1137/1.9781611973693. URL `https://epubs.siam.org/doi/abs/10.1137/1.9781611973693`.

[2] Andrzej J. Osiadacz. *Simulation and analysis of gas networks*. Spon, London, 1987. ISBN 0419124802.

[3] Pieter Schavemaker and Lou van der Sluis. *Electrical power system essentials*. Wiley, Chichester, West Sussex, 2008. ISBN 9780470510278.

[4] Svend Frederiksen and Sven Werner. *District Heating and Cooling*. Studentlitteratur AB, Lund, first edition, 2013. ISBN 9789144085302.

[5] Pierluigi Mancarella. MES (multi-energy systems): An overview of concepts and evaluation models. *Energy*, 65:1–17, July 2014. doi: 10.1016/j.energy.2013.10.041.

[6] Martin Geidl and Göran Andersson. Optimal Power Flow of Multiple Energy Carriers. *IEEE Transactions on Power Systems*, 22(1):145–155, 2007. ISSN 0885-8950. doi: 10.1109/TPWRS.2006.888988.

[7] Amin Shabanpour-Haghighi and Ali Reza Seifi. Simultaneous integrated optimal energy flow of electricity, gas, and heat. *Energy Conversion and Management*, 101:579–591, 2015. ISSN 0196-8904. doi: 10.1016/j.enconman.2015.06.002.

[8] Xuezhi Liu, Nick Jenkins, Jianzhong Wu, and Audrius Bagdanavicius. Combined analysis of electricity and heat networks. *Applied Energy*, 162:1238–1250, 2016. ISSN 18766102. doi: 10.1016/j.egypro.2014.11.928.

[9] Emmanouil Loukarakis and Pierluigi Mancarella. A sequential programming method for multi-energy districts optimal power flow. *2017 IEEE Manchester PowerTech, Powertech 2017*, pages 1–6, 2017. doi: 10.1109/PTC.2017.7980850.

[10] Jean Duquette, Andrew Rowe, and Peter Wild. Thermal performance of a steady state physical pipe model for simulating district heating grids with variable flow. *Applied Energy*, 178:383–393, 2016.

[11] Amin Shabanpour-Haghighi and Ali Reza Seifi. An integrated steady-state operation assessment of electrical, natural gas, and district heating networks. *IEEE Transactions on Power Systems*, 31(5):3636–3647, 2016. ISSN 08858950. doi: 10.1109/TPWRS.2015.2486819.

[12] Cheol Park and Stanley T. Liu. Performance of a commercial hot water boiler. Technical Report 6226, U.S. Department of Commerce, National Institute of Standards and Technology (NIST), 1998.

[13] Tuula Savola and Ilkka Keppo. Off-design simulation and mathematical modeling of small-scale chp plants at part load. *Applied Thermal Engineering*, 25:1219–1232, 2005.

[14] Maunu Kuosa, Kaisa Kontu, Tapio Mäkilä, Markku Lampinen, and Risto Lahdelma. Static study of traditional and ring networks and the use of mass flow control in district heating applications. *Applied Thermal Engineering*, 54 (2):450–459, 2013. ISSN 13594311. doi: 10.1016/j.applthermaleng.2013.02.018.

[15] Jacek Wasilewski. Integrated modeling of microgrid for steady-state analysis using modified concept of multi-carrier energy hub. *International Journal of Electrical Power and Energy Systems*, 73:891–898, 2015. ISSN 01420615. doi: 10.1016/j.ijepes.2015.06.022.

[16] Sebastian Long, Alessandra Parisio, and Ognjen Marjanovic. A conversion model for nodes in multi-energy systems. *2017 IEEE Manchester PowerTech, Powertech 2017*, 2017. doi: 10.1109/PTC.2017.7981052.

[17] Getnet Tadesse Ayele, Pierrick Haurant, Björn Laumert, and Bruno Lacarrière. An extended energy hub approach for load flow analysis of highly coupled district energy networks: Illustration with electricity and heating. *Applied Energy*, 212: 850–867, December 2018. ISSN 03062619. doi: 10.1016/j.apenergy.2017.12.090.

[18] Seungwon An, Qing Li, and T.W. Gedra. Natural gas and electricity optimal power flow. *IEEE PES Transmission and Distribution Conference and Exposition*, pages 138–143, 2003. ISSN 1098-6596. doi: 10.1109/TDC.2003.1335171.

[19] Albero Martinez-Mares and Claudio R. Fuerte-Esquivel. A Unified Gas and Power Flow Analysis in Natural Gas and Electricity Coupled Networks. *IEEE Transactions on Power Systems*, 27(4):2156–2166, 2012. ISSN 0885-8950. doi: 10.1109/TPWRS.2012.2191984.

[20] Zhaoguang Pan, Qinglai Guo, and Hongbin Sun. Interactions of district electricity and heating systems considering time-scale characteristics based on quasi-steady multi-energy flow. *Applied Energy*, 167:230–243, 2016. ISSN 03062619. doi: 10.1016/j.apenergy.2015.10.095.

[21] Muditha Abeysekera and Jianzhong Wu. Method for Simultaneous Power Flow Analysis in Coupled Multi-vector Energy Networks. *Energy Procedia*, 75:1165–1171, 2015. ISSN 18766102. doi: 10.1016/j.egypro.2015.07.551.

[22] Xuezhi Liu and Pierluigi Mancarella. Modelling, assessment and Sankey diagrams of integrated electricity-heat-gas networks in multi-vector district energy systems. *Applied Energy*, 167:336–352, 2016. ISSN 03062619. doi: 10.1016/j.apenergy.2015.08.089.

[23] L. Huijzer. Redesign of the Solution Algorithms in Wanda, 2018.

[24] Brian Stott. Review of Load-Flow Calculation Methods. *Proceedings of the IEEE*, 62(7):916–929, 1974. ISSN 15582256. doi: 10.1109/PROC.1974.9544.

[25] Baljinnyam Sereeter, Cornelis Vuik, and Cees Witteveen. On a comparison of Newton-Raphson solvers for power flow problems. *Journal of Computational and Applied Mathematics*, 360:157–169, November 2019. doi: 10.1016/j.cam.2019.04.007.

[26] C. T. C. Arsene, A. Bargiela, and D. Al-Dabass. Modelling and Simulation of Water Systems Based on Loop Equations. *J. of SIMULATION*, 5(1):1–2, 1989. ISSN 1473-8031.

[27] John E. Jr. Dennis and Robert B. Schnabel. *Numerical Methods for Unconstrained Optimization and Nonlinear Equations*. Society for Industrial and Applied Mathematics, Philadelphia, PA, USA, 1996. ISBN 0-89871-364-1.

[28] E. Gill, Philip, Walter Murray, and H. Wright, Margaret. *Practical Optimization*. Acadamic Press, London, 1981. ISBN 0-12-283952-8.

[29] Jorge Nodecal and Stephen J. Wright. *Numerical Optimization*. Springer, New York, second edition, 2006. ISBN 978-0387-30303-1.

[30] M. B. Giles and N. A. Pierce. An Introduction to the Adjoint Approach to Design. *Flow, Turbulence and Combustion*, 65:393–415, 2000.

[31] Linda Petzold, Shengtai Li, Yang Cao, and Radu Serban. Sensitivity analysis of differential-algebraic equations and partial differential equations. *Computers & Chemical Engineering*, 30(10):1553 – 1559, 2006. ISSN 0098-1354. doi: 10.1016/j.compchemeng.2006.05.015. Papers form Chemical Process Control VII.

[32] P. N. Biskas, N. G. Kanelakis, A. Papamatthaiou, and I. Alexandridis. Coupled optimization of electricity and natural gas systems using augmented Lagrangian and an alternating minimization method. *International Journal of Electrical Power & Energy Systems*, 80:202–218, 2016. ISSN 01420615. doi: 10.1016/j.ijepes.2016.01.045.

[33] Zhengmao Li and Yan Xu. Optimal coordinated energy dispatch of a multi-energy microgrid in grid-connected and islanded modes. *Applied Energy*, 210:974–986, 2018.

[34] Eduardo Alejandro Martínez Ceseña and Pierluigi Mancarella. Energy Systems Integration in Smart Districts: Robust Optimization of Multi-Energy Flows in Integrated Electricity, Heat and Gas Networks. *IEEE Transactions on Smart Grid*, 10(1):1122–1131, January 2019.

[35] Pauli Virtanen, Ralf Gommers, Travis E. Oliphant, Matt Haberland, Tyler Reddy, David Cournapeau, Evgeni Burovski, Pearu Peterson, Warren Weckesser, Jonathan Bright, Stéfan J. van der Walt, Matthew Brett, Joshua Wilson, K. Jarrod Millman, Nikolay Mayorov, Andrew R. J. Nelson, Eric Jones, Robert Kern, Eric Larson, C J Carey, İlhan Polat, Yu Feng, Eric W. Moore, Jake VanderPlas, Denis Laxalde, Josef Perktold, Robert Cimrman, Ian Henriksen, E. A. Quintero, Charles R. Harris, Anne M. Archibald, Antônio H. Ribeiro, Fabian Pedregosa, Paul van Mulbregt, and SciPy 1.0 Contributors. SciPy 1.0: Fundamental Algorithms for Scientific Computing in Python. *Nature Methods*, 17:261–272, 2020. doi: 10.1038/s41592-019-0686-2.

[36] Andreas Wächter and Lorenz T. Biegler. On the implementation of an interior-point filter line-search algorithm for large-scale nonlinear programming. *Math. Program.*, 106:25–57, 2006. doi: 0.1007/s10107-004-0559-y.

[37] Richard H. Byrd, Mary E. Hribar, and Jorge Nocedal. An interior point algorithm for large-scale nonlinear programming. *SIAM J. Optim.*, 9(4):877–900, 1999.

[38] Dieter Kraft. A software package for sequential quadratic programming. Technical Report DFVLR-FB 88-28, DLR German Aerospace Center – Institute for Flight Mechanics, Köln, Germany, 1998.

[39] J. C. Gibbings. *Dimensional Analysis*. Springer, London, 2011.

[40] Gjerrit Meinsma. Dimensional and scaling analysis. *SIAM Review*, 61(1):159–184, 2019. doi: 10.1137/16M1107127.

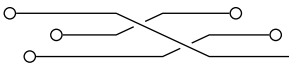

APPENDIX A

The effect of transforming the system of equations and variables on the Newton-Raphson method

Scaling or permuting the system of equations $\boldsymbol{F}$ or the variables $\boldsymbol{x}$ is called a transformation. In infinite precision, the Newton-Raphson method (NR) is not affected by a transformation of $\boldsymbol{F}$ or of $\boldsymbol{x}$. We repeat the proof by Dennis and Schnabel [27, pp. 155–159] when only $\boldsymbol{x}$ is transformed, and show it also holds when $\boldsymbol{F}$ is transformed.

To solve the system $\boldsymbol{F}(\boldsymbol{x}) = \boldsymbol{0}$, the iteration scheme of NR in multiple dimensions, without transformations, is given by:

$$J\left(\boldsymbol{x}^k\right)\boldsymbol{s}^k = -\boldsymbol{F}\left(\boldsymbol{x}^k\right) \tag{A.1a}$$

$$\boldsymbol{x}^{k+1} = \boldsymbol{x}^k + \boldsymbol{s}^k \tag{A.1b}$$

with $\boldsymbol{x} \in \mathbb{R}^N$ the variables and $\boldsymbol{F}(\boldsymbol{x}) \in \mathbb{R}^N$ the system of nonlinear equations. Let T_x, $T_F \in \mathbb{R}^{N\times N}$ be nonsingular matrices, called transformation matrices. We define the transformed variables as $\hat{\boldsymbol{x}} := T_x\boldsymbol{x}$ and the transformed equations as $\hat{\boldsymbol{F}} := T_F\boldsymbol{F}(\boldsymbol{x})$. The iteration scheme (A.1) is adjusted to

$$\hat{J}\left(\boldsymbol{x}^k\right)\hat{\boldsymbol{s}}^k = -\hat{\boldsymbol{F}}\left(\boldsymbol{x}^k\right) \tag{A.2a}$$

$$\hat{\boldsymbol{x}}^{k+1} = \hat{\boldsymbol{x}}^k + \hat{\boldsymbol{s}}^k \tag{A.2b}$$

with the Jacobian matrix defined as

$$\hat{J}(\boldsymbol{x}) := \frac{\boldsymbol{\partial}\hat{\boldsymbol{F}}}{\boldsymbol{\partial}\hat{\boldsymbol{x}}} \tag{A.3}$$

Since $\boldsymbol{F}(\boldsymbol{x}) = \boldsymbol{F}\left(T_x^{-1}\hat{\boldsymbol{x}}\right)$, we find that

$$\begin{aligned}\frac{\partial F_n}{\partial \hat{x}_m} &= \frac{\partial F_n}{\partial x_1}\frac{\partial x_1}{\partial \hat{x}_m} + \cdots + \frac{\partial F_n}{\partial x_N}\frac{\partial x_N}{\partial \hat{x}_m} \\ &= \frac{\partial F_n}{\partial x_1}\left(T_x^{-1}\right)_{1m} + \cdots + \frac{\partial F_n}{\partial x_N}\left(T_x^{-1}\right)_{Nm}\end{aligned}$$

This holds for all $F_n \in \boldsymbol{F}$ and $\hat{x}_m \in \hat{\boldsymbol{x}}$, such that:

$$\begin{aligned}
\frac{\partial \boldsymbol{F}}{\partial \hat{\boldsymbol{x}}} &= \begin{pmatrix} \frac{\partial F_1}{\partial \hat{x}_1} & \cdots & \frac{\partial F_1}{\partial \hat{x}_N} \\ \vdots & \ddots & \vdots \\ \frac{\partial F_N}{\partial \hat{x}_1} & \cdots & \frac{\partial F_N}{\partial \hat{x}_N} \end{pmatrix} \\
&= \begin{pmatrix} \frac{\partial F_1}{\partial x_1}\left(T_x^{-1}\right)_{11} + \cdots + \frac{\partial F_1}{\partial x_N}\left(T_x^{-1}\right)_{N1} & \cdots & \frac{\partial F_1}{\partial x_1}\left(T_x^{-1}\right)_{1N} + \cdots + \frac{\partial F_1}{\partial x_N}\left(T_x^{-1}\right)_{NN} \\ \vdots & \ddots & \vdots \\ \frac{\partial F_N}{\partial x_1}\left(T_x^{-1}\right)_{11} + \cdots + \frac{\partial F_N}{\partial x_N}\left(T_x^{-1}\right)_{N1} & \cdots & \frac{\partial F_N}{\partial x_1}\left(T_x^{-1}\right)_{1N} + \cdots + \frac{\partial F_N}{\partial x_N}\left(T_x^{-1}\right)_{NN} \end{pmatrix} \\
&= \begin{pmatrix} \frac{\partial F_1}{\partial x_1} & \cdots & \frac{\partial F_1}{\partial x_N} \\ \vdots & \ddots & \vdots \\ \frac{\partial F_N}{\partial x_1} & \cdots & \frac{\partial F_N}{\partial x_N} \end{pmatrix} \begin{pmatrix} \left(T_x^{-1}\right)_{11} & \cdots & \left(T_x^{-1}\right)_{1N} \\ \vdots & \ddots & \vdots \\ \left(T_x^{-1}\right)_{N1} & \cdots & \left(T_x^{-1}\right)_{NN} \end{pmatrix} \\
&= \frac{\partial \boldsymbol{F}}{\partial \boldsymbol{x}} T_x^{-1}
\end{aligned} \tag{A.4}$$

Using (A.4), the transformed Jacobian (A.3) is given by:

$$\begin{aligned}
\hat{J}(\boldsymbol{x}) := \frac{\partial \hat{\boldsymbol{F}}}{\partial \hat{\boldsymbol{x}}} &= T_F \frac{\partial \boldsymbol{F}}{\partial \hat{\boldsymbol{x}}} \\
&= T_F \frac{\partial \boldsymbol{F}}{\partial \boldsymbol{x}} T_x^{-1} \\
&= T_F J(\boldsymbol{x}) T_x^{-1}
\end{aligned} \tag{A.5}$$

with $\hat{\boldsymbol{s}}^k$ the update of NR at iteration k, for the transformed system of equations. If we substitute (A.5) in (A.2a), and using (A.1a), we find:

$$\begin{aligned}
\hat{J}(\boldsymbol{x}^k)\hat{\boldsymbol{s}}^k &= -\hat{\boldsymbol{F}}(\boldsymbol{x}^k) \\
\hat{\boldsymbol{s}}^k &= -\hat{J}(\boldsymbol{x}^k)^{-1}\hat{\boldsymbol{F}}(\boldsymbol{x}^k) = -\left[T_F J(\boldsymbol{x}^k) T_x^{-1}\right]^{-1} T_F \boldsymbol{F}(\boldsymbol{x}^k) \\
&= -T_x J(\boldsymbol{x}^k)^{-1} T_F^{-1} T_F \boldsymbol{F}(\boldsymbol{x}^k) = -T_x J(\boldsymbol{x}^k)^{-1} \boldsymbol{F}(\boldsymbol{x}^k) \\
&= T_x \boldsymbol{s}^k
\end{aligned}$$

Using this transformed NR update $\hat{\boldsymbol{s}}^k$ in (A.2b) gives a transformed new iterate $\hat{\boldsymbol{x}}^{k+1}$ for NR. Transforming back, we get

$$\begin{aligned}
\boldsymbol{x}^{k+1} &= T_x^{-1}\hat{\boldsymbol{x}}^{k+1} = T_x^{-1}(\hat{\boldsymbol{x}}^k + \hat{\boldsymbol{s}}^k) \\
&= T_x^{-1}\hat{\boldsymbol{x}}^k + T_x^{-1}\hat{\boldsymbol{s}}^k \\
&= \boldsymbol{x}^k + \boldsymbol{s}^k
\end{aligned}$$

for the original new iterate. This is equal to the new iterate computed by NR (A.1b). Assuming $\boldsymbol{x}^k = T_x^{-1}\hat{\boldsymbol{x}}^k$ for some iteration k, this means that NR is unaffected by the transformation of the system of equations $\boldsymbol{F}$ or of the variables $\boldsymbol{x}$, in infinite precision. Hence, if the same initial iterate $\boldsymbol{x}^0$ is used for both the original and the transformed system, NR will give the same iterates.

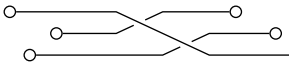

APPENDIX B

Jacobian matrices

NR uses the Jacobian matrices of the LF equations to solve the steady-state LF problem for energy systems. This chapter gives details on the computation of the various Jacobian matrices.

B.1 Jacobians for single-carrier parts of multi-carrier networks

This section gives the Jacobian matrices for the SC gas, electricity, and heat networks, and discusses possible problems with certain initial guesses.

B.1.1 Gas

For the gas part, using the full formulation (4.1), the Jacobian is given by

$$J^{gg} = \begin{pmatrix} A^{g\prime} & 0 \\ \frac{\partial \boldsymbol{F}^L}{\partial \boldsymbol{q}} & \frac{\partial \boldsymbol{F}^L}{\partial \boldsymbol{p}} \end{pmatrix} \tag{B.1}$$

The submatrix $\frac{\partial \boldsymbol{F}^L}{\partial \boldsymbol{q}}$ is a diagonal matrix with entries $\frac{\partial \boldsymbol{F}_k}{\partial q_k}$ for each link k with link equation (3.3). This derivative is zero for a link representing a compressor. The submatrix $\frac{\partial \boldsymbol{F}^L}{\partial \boldsymbol{p}}$ can be calculated as

$$\frac{\partial \boldsymbol{F}^L}{\partial \boldsymbol{p}} = \frac{\partial \boldsymbol{F}^L}{\partial \boldsymbol{\Delta p}} \frac{\partial \boldsymbol{\Delta p}}{\partial \boldsymbol{p}} \tag{B.2}$$

with $\frac{\partial \boldsymbol{F}^L}{\partial \boldsymbol{\Delta p}}$ a diagonal matrix with entries $\frac{\partial \boldsymbol{F}_k}{\partial \Delta p_k}$ for each link k with link equation (3.3).

For the gas part, using the nodal formulation (4.3), the Jacobian is given by

$$J^{gg} = A^{g\prime} \frac{\partial \boldsymbol{q}}{\partial \boldsymbol{p}} = A^{g\prime} \frac{\partial \boldsymbol{q}}{\partial \boldsymbol{\Delta p}} \frac{\partial \boldsymbol{\Delta p}}{\partial \boldsymbol{p}} \tag{B.3}$$

with $\frac{\partial \boldsymbol{q}}{\partial \boldsymbol{\Delta p}}$ a diagonal matrix with entries $\frac{\partial q_k}{\partial \Delta p_k}$ for each link k, where $q_k(\Delta p_k)$ is obtained from the link equation (3.3), see for instance (B.5).

If link k represents a pipe, we can use (3.4a) or (3.4b) as the link equation. The partial derivatives of (3.4a), required for the Jacobian, are given by

$$\frac{\partial F_k^{q(\Delta p)}}{\partial q_k} = 1 + \frac{1}{2} C_k^g \text{sign}\left(\Delta p_k\right) \left|\Delta p_k\right|^{\frac{1}{2}} \mathrm{f}_k^{-\frac{3}{2}} \frac{\mathrm{d}\mathrm{f}_k}{\mathrm{d}q_k} \tag{B.4a}$$

$$\frac{\partial F_k^{q(\Delta p)}}{\partial \Delta p_k} = -\frac{1}{2} C_k^g \mathrm{f}_k^{-\frac{1}{2}} \left|\Delta p_k\right|^{-\frac{1}{2}} \tag{B.4b}$$

Note that $\frac{\partial F_k^{q(\Delta p)}}{\partial q_k} = 1$ if f_k is independent of q_k. In the nodal formulation, (3.4a) is rewritten to obtain an expression for the link flow q_k:

$$q_k = C_k^g \text{sign}\left(\Delta p_k\right) \mathrm{f}_k^{-\frac{1}{2}} \left|\Delta p_k\right|^{\frac{1}{2}} \tag{B.5}$$

which is an implicit equation if f_k is a function of q_k, such that

$$\frac{\partial q(\Delta p)_k}{\partial \Delta p_k} = \frac{1}{2} C_k^g \mathrm{f}_k^{-\frac{1}{2}} \left|\Delta p_k\right|^{-\frac{1}{2}} \tag{B.6}$$

If $p_i = p_j$ for any link k from node i to node j, the pressure drop $\Delta p_k = 0$ for that link. This means that $q_k = 0$ if (B.5) is used, and that (B.4b) and (B.6) are undefined.

Therefore, taking a flat initial guess for $\boldsymbol{p}$ results in undefined Jacobian matrices (B.1) and (B.3), for the full formulation with (3.4a) for the link equations and for the nodal formulation, respectively.

The partial derivatives of (3.4b), required for the Jacobian, are given by

$$\frac{\partial F_k^{\Delta p(q)}}{\partial q_k} = -2(C_k^g)^{-2} |q_k| (\mathrm{f}_k + \frac{1}{2} q_k \frac{\mathrm{d}\mathrm{f}_k}{\mathrm{d}q_k}) \tag{B.7a}$$

$$\frac{\partial F_k^{\Delta p(q)}}{\partial \Delta p_k} = 1 \tag{B.7b}$$

If $q_k = 0$, we find from (B.7a) that $\frac{\partial F_k^{\Delta p(q)}}{\partial q_k} = 0$. Therefore, taking $\boldsymbol{q} = \boldsymbol{0}$ as initial guess gives $\frac{\boldsymbol{\partial F}^L}{\boldsymbol{\partial q}} = 0$, such that the Jacobian matrix (B.1) is a block diagonal matrix, if (3.4b) is used for the link equations.

B.1.2 Electricity

For the electrical part, using the complex power formulation in polar coordinates, the Jacobian is given by

$$J^{ee} = \begin{pmatrix} \frac{\boldsymbol{\partial F}^P}{\boldsymbol{\partial \delta}} & \frac{\boldsymbol{\partial F}^P}{\boldsymbol{\partial |V|}} \\ \frac{\boldsymbol{\partial F}^Q}{\boldsymbol{\partial \delta}} & \frac{\boldsymbol{\partial F}^Q}{\boldsymbol{\partial |V|}} \end{pmatrix}$$

Here, $\frac{\boldsymbol{\partial F}^P}{\boldsymbol{\partial \delta}}$ and $\frac{\boldsymbol{\partial F}^Q}{\boldsymbol{\partial \delta}}$ are the real and imaginary part of $\frac{\boldsymbol{\partial F}^S}{\boldsymbol{\partial \delta}}$ respectively. Similarly, $\frac{\boldsymbol{\partial F}^P}{\boldsymbol{\partial |V|}}$ and $\frac{\boldsymbol{\partial F}^Q}{\boldsymbol{\partial |V|}}$ are the real and imaginary part of $\frac{\boldsymbol{\partial F}^S}{\boldsymbol{\partial |V|}}$ respectively.

Using (4.6) for F_i^P and F_i^Q, we have

$$\frac{\partial F_i^S}{\partial \delta_j} = \left[\mathrm{i} \cdot \mathrm{Diag}\left(\boldsymbol{V}\right)\left(\mathrm{Diag}\left(Y\boldsymbol{V}\right)^* - Y^*\mathrm{Diag}\left(\boldsymbol{V}\right)^*\right)\right]_{ij}$$
$$\frac{\partial F_i^S}{\partial |V_j|} = \left[\mathrm{Diag}\left(\boldsymbol{V}\right)\left(\mathrm{Diag}\left(Y\boldsymbol{V}\right)^* + Y^*\mathrm{Diag}\left(\boldsymbol{V}\right)^*\right)\mathrm{Diag}\left(|\boldsymbol{V}|\right)^{-1}\right]_{ij}$$

with $\mathrm{Diag}\left(\boldsymbol{x}\right)$ a diagonal matrix with $\boldsymbol{x}$ on the diagonal, and $\boldsymbol{V}$ the vector of nodal voltage phasors V.

B.1.3 Heat

For the heat part, using the terminal link formulation (4.7), the Jacobian is given by

$$J^{hh} = \begin{pmatrix} A^{h\prime} & \frac{\partial \boldsymbol{F}^m}{\partial \boldsymbol{m}^{TL}} & 0 & 0 & 0 & 0 & 0 \\ \frac{\partial \boldsymbol{F}^L}{\partial \boldsymbol{m}^L} & 0 & \frac{\partial \boldsymbol{F}^L}{\partial \boldsymbol{p}} & 0 & 0 & 0 & 0 \\ \frac{\partial \boldsymbol{F}^{T^s}}{\partial \boldsymbol{m}^L} & \frac{\partial \boldsymbol{F}^{T^s}}{\partial \boldsymbol{m}^{TL}} & 0 & \frac{\partial \boldsymbol{F}^{T^s}}{\partial \boldsymbol{T}^s} & 0 & \frac{\partial \boldsymbol{F}^{T^s}}{\partial \boldsymbol{T}^{TL,s}} & 0 \\ \frac{\partial \boldsymbol{F}^{T^r}}{\partial \boldsymbol{m}^L} & \frac{\partial \boldsymbol{F}^{T^r}}{\partial \boldsymbol{m}^{TL}} & 0 & 0 & \frac{\partial \boldsymbol{F}^{T^r}}{\partial \boldsymbol{T}^r} & 0 & \frac{\partial \boldsymbol{F}^{T^r}}{\partial \boldsymbol{T}^{TL,r}} \\ 0 & \frac{\partial \boldsymbol{F}^{\varphi}}{\partial \boldsymbol{m}^{TL}} & 0 & \frac{\partial \boldsymbol{F}^{\varphi}}{\partial \boldsymbol{T}^s} & \frac{\partial \boldsymbol{F}^{\varphi}}{\partial \boldsymbol{T}^r} & \frac{\partial \boldsymbol{F}^{\varphi}}{\partial \boldsymbol{T}^{TL,s}} & \frac{\partial \boldsymbol{F}^{\varphi}}{\partial \boldsymbol{T}^{TL,r}} \\ 0 & 0 & 0 & \frac{\partial \boldsymbol{F}^{\Delta T}}{\partial \boldsymbol{T}^s} & \frac{\partial \boldsymbol{F}^{\Delta T}}{\partial \boldsymbol{T}^r} & \frac{\partial \boldsymbol{F}^{\Delta T}}{\partial \boldsymbol{T}^{TL,s}} & \frac{\partial \boldsymbol{F}^{\Delta T}}{\partial \boldsymbol{T}^{TL,r}} \end{pmatrix} \tag{B.8}$$

Here, the submatrices $\frac{\partial \boldsymbol{F}^{\varphi}}{\partial \boldsymbol{m}^{TL}}$, $\frac{\partial \boldsymbol{F}^{\varphi}}{\partial \boldsymbol{T}^{TL,s}}$, $\frac{\partial \boldsymbol{F}^{\varphi}}{\partial \boldsymbol{T}^{TL,r}}$, $\frac{\partial \boldsymbol{F}^{\Delta T}}{\partial \boldsymbol{T}^{TL,s}}$, and $\frac{\partial \boldsymbol{F}^{\Delta T}}{\partial \boldsymbol{T}^{TL,r}}$ are diagonal matrices. As for the gas part with the full formulation, the submatrix $\frac{\partial \boldsymbol{F}^L}{\partial \boldsymbol{m}^L}$ is a diagonal matrix with entries $\frac{\partial F_k}{\partial m_k}$ for each link k with hydraulic link equation (3.15), and the submatrix $\frac{\partial \boldsymbol{F}^L}{\partial \boldsymbol{p}}$ is given by (B.2), with $\frac{\partial \boldsymbol{F}^L}{\partial \boldsymbol{\Delta p}}$ a diagonal matrix with entries $\frac{\partial F_k}{\partial \Delta p_k}$ for each link k with hydraulic link equation (3.15).

For the heat part, using the standard formulation (4.9), the Jacobian is given by

$$J^{hh} = \begin{pmatrix} A^{h\prime} & 0 & \frac{\partial \boldsymbol{F}^m}{\partial \boldsymbol{T}^s} & \frac{\partial \boldsymbol{F}^m}{\partial \boldsymbol{T}^r} \\ \frac{\partial \boldsymbol{F}^L}{\partial \boldsymbol{m}^L} & \frac{\partial \boldsymbol{F}^L}{\partial \boldsymbol{p}} & 0 & 0 \\ \frac{\partial \boldsymbol{F}^{T^s}}{\partial \boldsymbol{m}^L} & 0 & \frac{\partial \boldsymbol{F}^{T^s}}{\partial \boldsymbol{T}^s} & \frac{\partial \boldsymbol{F}^{T^s}}{\partial \boldsymbol{T}^r} \\ \frac{\partial \boldsymbol{F}^{T^r}}{\partial \boldsymbol{m}^L} & 0 & \frac{\partial \boldsymbol{F}^{T^r}}{\partial \boldsymbol{T}^s} & \frac{\partial \boldsymbol{F}^{T^r}}{\partial \boldsymbol{T}^r} \end{pmatrix} \tag{B.9}$$

The submatrices $\frac{\partial \boldsymbol{F}^L}{\partial \boldsymbol{m}^L}$, $\frac{\partial \boldsymbol{F}^L}{\partial \boldsymbol{p}}$, $\frac{\partial \boldsymbol{F}^{T^s}}{\partial \boldsymbol{m}^L}$, and $\frac{\partial \boldsymbol{F}^{T^r}}{\partial \boldsymbol{m}^L}$ are the same as in the terminal link formulation.

For the submatrices $\frac{\partial \boldsymbol{F}^L}{\partial \boldsymbol{m}^L}$ and $\frac{\partial \boldsymbol{F}^L}{\partial \boldsymbol{p}}$, the same analysis holds as for the gas network in Appendix B.1.1. That is, a flat initial guess for $\boldsymbol{p}$ results in an undefined Jacobian matrix.

The temperatures T_{ij}^s or T_{ji}^s and T_{ij}^r or T_{ji}^s in the mixing rules (3.20) are obtained from the thermal link equation (3.21). If (2.28) is used as the thermal pipe model, these temperatures are a function of the mass flow m. Specifically, the temperature drop factor (2.29) is part of the mixing rules, after substituting (2.28) for the appropriate temperatures. This temperature drop factor, and its derivative to m, is

undefined if $m = 0$. Therefore, a zero flow initial guess $\boldsymbol{m} = \boldsymbol{0}$ results in undefined Jacobian matrices (B.8) and (B.9).

In the full formulation, (3.23) is used in $\boldsymbol{F}^{\varphi}$, which has zero first partial derivatives if $m_{i,l} = 0$ or if $\Delta T_{i,l} = 0$. If both $m_{i,l} = 0$ and $\Delta T_{i,l} = 0$, all partial derivatives of $\boldsymbol{F}^{\varphi}$ are zero, such that the Jacobian (B.8) is singular.

In the standard formulation, (3.23) is rewritten to obtain an expression for the terminal link flow $m_{i,l}$:

$$m_{i,l} = \frac{\Delta\varphi_{i,l}}{C_p \Delta T_{i,l}} \tag{B.10}$$

which is then substituted into $\boldsymbol{F}^{m}$, $\boldsymbol{F}^{T^s}$, and $\boldsymbol{F}^{T^r}$. If the supply and return temperatures in (3.13a) are equal, we have $\Delta T_{i,l} = 0$, such that (B.10) is undefined. Therefore, the Jacobian for the standard formulation can be undefined if the initial guesses $\boldsymbol{T}^s$ and $\boldsymbol{T}^r$ are chosen incorrectly. Furthermore, the Jacobian can be ill-conditioned if $T^s \approx T^r$.

Finally, the Jacobian can become singular if the mass flows are such that a node has only inflow or outflow, as discussed in Section 5.3.3. Therefore, the initial guesses to $\boldsymbol{m}^L$ and $\boldsymbol{m}^{TL}$ should be chosen such that every node has both inflow and outflow.

B.2 Jacobian for a decoupled multi-carrier network

This section gives the Jacobian matrix for the LF problem of a decoupled MCN, given by the system $\boldsymbol{y} = \boldsymbol{g}(\boldsymbol{y})$, see (8.8). It consists of IFCs (8.6) and LF subproblems (8.7) for each carrier $\alpha \in \{g, e, h, c\}$. To determine the Jacobian of $\boldsymbol{g}$, the partial derivatives of the IFCs and LF subproblems need to computed, for each carrier.

The IFCs (8.6) are given by linear systems (8.5), such that the (partial) derivatives are

$$\frac{\boldsymbol{\partial u}^{\alpha}}{\boldsymbol{\partial v}^{\beta}} = A^{\beta\alpha} \tag{B.11}$$

for $\alpha, \beta \in \{g, e, h, c\}$ and $\alpha \neq \beta$.

For decoupled LF, only part of the extended state variables and BCs of each subnetwork are of interest, which are denoted as $\boldsymbol{v} \subseteq \boldsymbol{x}$ and $\boldsymbol{u} \subseteq \boldsymbol{b}$. Given $\boldsymbol{u}$, the extended LF problem (8.1) is solved for each subnetwork to obtain $\boldsymbol{v}$, which is written as (8.7), or

$$\boldsymbol{v}^{\alpha} = \boldsymbol{g}^{\alpha}(\boldsymbol{u}^{\alpha}) \tag{B.12}$$

We can obtain the $\boldsymbol{v}$ from the extended state variables $\boldsymbol{x}$ as $\boldsymbol{v} := P\boldsymbol{x}$, with P a $\mathbb{R}^{N_v} \times \mathbb{R}^{N_x}$ matrix, with $N_v \leq N_x$, that selects the appropriate variables from $\boldsymbol{x}$. The function $\boldsymbol{g}$ depends on $\boldsymbol{u}$ only, and its derivative is then given by

$$\frac{\mathbf{d}\boldsymbol{g}^{\alpha}}{\mathbf{d}\boldsymbol{u}^{\alpha}} = \frac{\mathbf{d}\boldsymbol{v}^{\alpha}}{\mathbf{d}\boldsymbol{u}^{\alpha}} = P\frac{\mathbf{d}\boldsymbol{x}^{\alpha}}{\mathbf{d}\boldsymbol{u}^{\alpha}} \tag{B.13}$$

Deriving the extended LF subproblem (8.1), using the same approach as in Section 9.4, gives

$$\frac{\boldsymbol{\partial h}^{\alpha}}{\boldsymbol{\partial x}^{\alpha}}\frac{\mathbf{d}\boldsymbol{x}^{\alpha}}{\mathbf{d}\boldsymbol{u}^{\alpha}} = -\frac{\boldsymbol{\partial h}^{\alpha}}{\boldsymbol{\partial u}^{\alpha}}$$

For each $\alpha \in \{g, e, h, c\}$, the derivative of (B.12) is then determined by solving this equation for $\frac{\mathbf{d}\boldsymbol{x}^{\alpha}}{\mathbf{d}\boldsymbol{u}^{\alpha}}$, and substituting the result in (B.13).

The Jacobian of $\boldsymbol{g}$ is obtained by collecting the derivatives (B.11) and (B.13). If the system $\boldsymbol{y} = \boldsymbol{g}(\boldsymbol{y})$ is ordered as (8.9), the Jacobian of $\boldsymbol{g}$ is given by

$$J = \begin{pmatrix} \frac{\partial \boldsymbol{g}_1}{\partial \boldsymbol{y}_1} & \vdots & \frac{\partial \boldsymbol{g}_1}{\partial \boldsymbol{y}_2} \\ \cdots & \cdots & \cdots \\ \frac{\mathrm{d}\boldsymbol{g}_2}{\mathrm{d}\boldsymbol{y}_1} & \vdots & 0 \end{pmatrix} = \left(\begin{array}{ccccccc:c} 0 & \frac{\mathrm{d}\boldsymbol{v}^g}{\mathrm{d}\boldsymbol{u}^g} & 0 & 0 & 0 & 0 & 0 & 0 \\ 0 & 0 & 0 & 0 & 0 & 0 & A^{cg} & 0 \\ 0 & 0 & 0 & \frac{\mathrm{d}\boldsymbol{v}^e}{\mathrm{d}\boldsymbol{u}^e} & 0 & 0 & 0 & 0 \\ 0 & 0 & 0 & 0 & 0 & 0 & A^{ce} & 0 \\ 0 & 0 & 0 & 0 & 0 & \frac{\mathrm{d}\boldsymbol{v}^h}{\mathrm{d}\boldsymbol{u}^h} & 0 & 0 \\ 0 & 0 & 0 & 0 & 0 & 0 & A^{ch} & 0 \\ 0 & 0 & 0 & 0 & 0 & 0 & 0 & \frac{\mathrm{d}\boldsymbol{v}^c}{\mathrm{d}\boldsymbol{u}^c} \\ \hdashline A^{gc} & 0 & A^{ec} & 0 & A^{hc} & 0 & 0 & 0 \end{array}\right)$$

If the system is ordered as (8.10), the Jacobian is given by

$$J = \begin{pmatrix} 0 & \vdots & 0 & \vdots & 0 & \vdots & \frac{\mathrm{d}\boldsymbol{g}_1}{\mathrm{d}\boldsymbol{y}_4} \\ \cdots & \cdots & \cdots & \cdots & \cdots & \cdots & \cdots \\ \frac{\mathrm{d}\boldsymbol{g}_2}{\mathrm{d}\boldsymbol{y}_1} & \vdots & 0 & \vdots & 0 & \vdots & 0 \\ 0 & \vdots & \frac{\mathrm{d}\boldsymbol{g}_3}{\mathrm{d}\boldsymbol{y}_2} & \vdots & 0 & \vdots & 0 \\ \cdots & \cdots & \cdots & \cdots & \cdots & \cdots & \cdots \\ 0 & \vdots & 0 & \vdots & \frac{\mathrm{d}\boldsymbol{g}_4}{\mathrm{d}\boldsymbol{y}_3} & \vdots & 0 \end{pmatrix} = \left(\begin{array}{ccc:c:c:ccc} 0 & 0 & 0 & 0 & 0 & \frac{\mathrm{d}\boldsymbol{v}^g}{\mathrm{d}\boldsymbol{u}^g} & 0 & 0 \\ 0 & 0 & 0 & 0 & 0 & 0 & \frac{\mathrm{d}\boldsymbol{v}^e}{\mathrm{d}\boldsymbol{u}^e} & 0 \\ 0 & 0 & 0 & 0 & 0 & 0 & 0 & \frac{\mathrm{d}\boldsymbol{v}^h}{\mathrm{d}\boldsymbol{u}^h} \\ \hdashline A^{gc} & A^{ec} & A^{hc} & 0 & 0 & 0 & 0 & 0 \\ \hdashline 0 & 0 & 0 & \frac{\mathrm{d}\boldsymbol{v}^c}{\mathrm{d}\boldsymbol{u}^c} & 0 & 0 & 0 & 0 \\ \hdashline 0 & 0 & 0 & 0 & A^{cg} & 0 & 0 & 0 \\ 0 & 0 & 0 & 0 & A^{ce} & 0 & 0 & 0 \\ 0 & 0 & 0 & 0 & A^{ch} & 0 & 0 & 0 \end{array}\right)$$

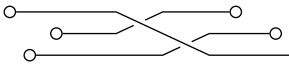

APPENDIX C

Network topologies and data

Several MESs, represented by various MCNs, are used throughout this thesis. In this appendix, we provide details on network topologies and models, and on the values of parameters, BCs, and other quantities, for these networks.

C.1 Gas-electricity multi-carrier energy system

This small gas-electricity MES is used in Section 8.5.1, and consist of a two-node gas network and a two-node electrical network, connected to each other with two coupling nodes. Figure C.1 shows the connected and the decoupled network representation of this MES.

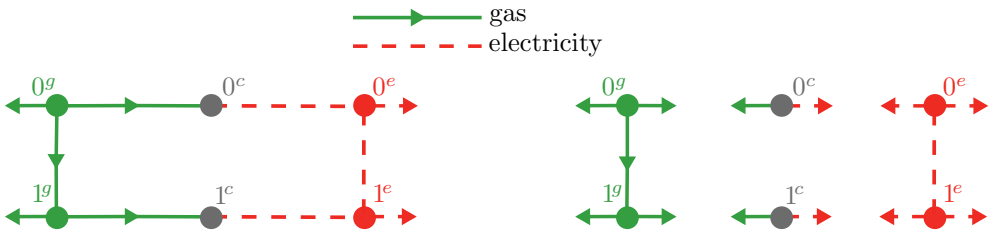

(a) Connected MCN. **(b)** Decoupled MCN.

Figure C.1: Connected and decoupled network representation of a gas-electricity MES. Arrows on links and terminal links show defined direction of flow.

In the gas network, node 0^g is a source and node 1^g is a sink. The link from 0^g to 1^g represents a pipe, which is modeled using the steady-state flow equation (2.1), with the pipe constant (2.2) and pressure drop (2.3) for low-pressure systems, and with Pole's friction factor (2.5). In the electrical network, both nodes are sinks. The link from 0^e to 1^e represents a transmission line, which is modeled as a short line with (2.17) and (2.18) for the active and reactive powers. Both coupling nodes represent a gas-fired generator (GG), for which we use the linear model (2.31). Table C.1 gives the link parameters and the parameters for the coupling models, and Table C.2 gives the parameters of the gas.

Table C.1: Link parameters and parameters of the coupling models for the networks in Figure C.1, per carrier.

Carrier	Link parameters		Unit	Parameters
gas	L	D	GG at 0^c	η_0
	500 m	0.15 m		0.6
electricity	b	g	GG at 1^c	η_1
	−0.3 S	0.03 S		0.7

Table C.2: Parameters of the gas carrier for the networks in Figure C.1.

Carrier	Parameters			
gas	T_n	T	R_{air}	p_n
	288 K	288 K	287.001 J/(kg K)	$1 \cdot 10^5$ Pa
	Z	S	GHV	
	1	0.589	60 134 305 J/kg	

To form the system of LF equations (4.11) or (8.8), we use the full formulation (4.1) in the gas network. We use (3.4b) for the link equation $F_{01}(q_{01}, p_0, p_1)$ of the gas pipe, and the active and reactive powers P_{01}, P_{10}, Q_{01}, and Q_{10} of the electrical transmission line are function of $\delta_0, \delta_1, |V_0|, |V_1|$, given by (2.17) and (2.18). Table 8.1 gives the node type sets we use as BCs, for the connected and the disconnected MCN.

The extended LF problems of the subnetworks of the decoupled MCN, which are solved in the decoupled approach to obtain the subproblems (8.7) of (8.8), are

$$\boldsymbol{F}^g(\boldsymbol{x}^{F,g}) = \begin{pmatrix} -q_1 + q_{01} - q_{1,1} \\ F_{01}\left(q_{01}, p_0, p_1\right) \end{pmatrix} = \boldsymbol{0}, \quad \boldsymbol{x}^{F,g} = \begin{pmatrix} q_{01} \\ p_1 \end{pmatrix}$$
$$\boldsymbol{G}^g(\boldsymbol{x}^{G,g}, \boldsymbol{x}^{F,g}) = \begin{pmatrix} -q_0 - q_{01} - q_{0,1} \end{pmatrix} = \boldsymbol{0}, \quad \boldsymbol{x}^{G,g} = \begin{pmatrix} q_{0,1} \end{pmatrix}$$

for the gas subnetwork,

$$\boldsymbol{F}^e(\boldsymbol{x}^{F,e}) = \begin{pmatrix} P_0 + P_{0,1} + P_{01} \end{pmatrix} = \boldsymbol{0}, \quad \boldsymbol{x}^{F,e} = \begin{pmatrix} \delta_0 \end{pmatrix}$$
$$\boldsymbol{G}^e(\boldsymbol{x}^{G,e}, \boldsymbol{x}^{F,e}) = \begin{pmatrix} P_1 + P_{1,1} + P_{10} \\ Q_0 + Q_{0,1} + Q_{01} \\ Q_1 + Q_{1,1} + Q_{10} \end{pmatrix} = \boldsymbol{0}, \quad \boldsymbol{x}^{G,e} = \begin{pmatrix} P_{1,1} \\ Q_{0,1} \\ Q_{1,1} \end{pmatrix}$$

for the electrical subnetwork, and

$$\boldsymbol{F}^c(\boldsymbol{x}^{F,c}) = \begin{pmatrix} P_{0^c} - \eta_{0^c}\text{GHV}(-q_{0^c}) \\ P_{1^c} - \eta_{1^c}\text{GHV}(-q_{1^c}) \end{pmatrix} = \boldsymbol{0}, \quad \boldsymbol{x}^{F,c} = \begin{pmatrix} -q_{1^c} \\ P_{0^c} \end{pmatrix}$$

for the coupling network. Based on (8.2) and (8.3), the IFCs for the disconnected MCN in Figure 8.2b are

$$q_{0,1} = -q_{0^c}, \quad P_{0,1} = -P_{0^c}, \quad Q_{0,1} = -Q_{0^c}$$
$$q_{1,1} = -q_{1^c}, \quad P_{1,1} = -P_{1^c}, \quad Q_{1,1} = -Q_{1^c}$$

With the node set given in Table 8.1, the variables for the LF problem of the disconnected MCN are given in (8.16):

$$\begin{aligned}
&\boldsymbol{v}^g = \begin{pmatrix} q_{0,1} \end{pmatrix}, \quad \boldsymbol{v}^e = \begin{pmatrix} P_{1,1} & Q_{0,1} & Q_{1,1} \end{pmatrix}^T, \quad \boldsymbol{v}^c = \begin{pmatrix} -q_{1^c} & P_{0^c} \end{pmatrix}^T, \\
&\boldsymbol{u}^g = \begin{pmatrix} q_{1,1} \end{pmatrix}, \quad \boldsymbol{u}^e = \begin{pmatrix} P_{0,1} \end{pmatrix}, \qquad\qquad\qquad \boldsymbol{u}^c = \begin{pmatrix} q_{0^c} & P_{1^c} & Q_{0^c} & Q_{1^c} \end{pmatrix}^T
\end{aligned}$$

With these variables, the IFCs (8.6) for the disconnected MCN are then

$$\begin{aligned}
\boldsymbol{u}^g &= \begin{pmatrix} 1 & 0 \end{pmatrix} \boldsymbol{v}^c \\
\boldsymbol{u}^e &= \begin{pmatrix} 0 & -1 \end{pmatrix} \boldsymbol{v}^c \\
\boldsymbol{u}^c &= -I \begin{pmatrix} \boldsymbol{v}^g \\ \boldsymbol{v}^e \end{pmatrix}
\end{aligned}$$

with I the 4×4 identity matrix. The LF problem (8.8) for the disconnected MCN is obtained by combining the LF subproblems and the IFCs.

Using the same ordering of equations and variables as is done in (4.11), the LF problem for the connected MCN is given by

$$\boldsymbol{F}(\boldsymbol{x}) = \begin{pmatrix} \boldsymbol{F}^g \\ \cdots \\ \boldsymbol{F}^e \\ \cdots \\ \boldsymbol{F}^c \end{pmatrix} = \begin{pmatrix} -q_0 - q_{01} - q_{0^g0^c} \\ -q_1 + q_{01} - q_{1^g1^c} \\ F_{01}(q_{01}, p_0, p_1) \\ \cdots\cdots\cdots\cdots\cdots\cdots \\ P_0 + P_{0^e0^c} + P_{01} \\ P_1 + P_{1^e1^c} + P_{10} \\ Q_0 + Q_{0^e0^c} + Q_{01} \\ Q_1 + Q_{1^e1^c} + Q_{10} \\ \cdots\cdots\cdots\cdots\cdots\cdots \\ P_{0^c0^e} - \eta_{0^c} \mathrm{GHV} q_{0^g0^c} \\ P_{1^c1^e} - \eta_{1^c} \mathrm{GHV} q_{1^g1^c} \end{pmatrix} = \boldsymbol{0}, \quad \boldsymbol{x} = \begin{pmatrix} \boldsymbol{x}^g \\ \cdots \\ \boldsymbol{x}^e \\ \cdots \\ \boldsymbol{x}^c \end{pmatrix} = \begin{pmatrix} q_{01} \\ p_1 \\ \cdots\cdots \\ \delta_0 \\ \cdots\cdots \\ q_{0^g0^c} \\ q_{1^g1^c} \\ P_{0^c0^e} \\ P_{1^c1^e} \\ Q_{0^c0^e} \\ Q_{1^c1^e} \end{pmatrix} \tag{C.1}$$

We can reorder the equations and variables in this LF problem of the connected MCN to match the structure of the LF problem of the disconnected MCN, as described in Section 8.4. The LF problem (C.1) is then permuted to

$$\boldsymbol{F}(\boldsymbol{x}) = \begin{pmatrix} -q_1 + q_{01} - q_{1^g1^c} \\ F_{01}\left(q_{01}, p_0, p_1\right) \\ -q_0 - q_{01} - q_{0^g0^c} \\ \cdots\cdots\cdots\cdots\cdots\cdots \\ P_0 + P_{0^e0^c} + P_{01} \\ P_1 + P_{1^e1^c} + P_{10} \\ Q_0 + Q_{0^e0^c} + Q_{01} \\ Q_1 + Q_{1^e1^c} + Q_{10} \\ \cdots\cdots\cdots\cdots\cdots\cdots \\ P_{0^c0^e} - \eta_{0^c} \mathrm{GHV} q_{0^g0^c} \\ P_{1^c1^e} - \eta_{1^c} \mathrm{GHV} q_{1^g1^c} \end{pmatrix} = \boldsymbol{0}, \quad \boldsymbol{x} = \begin{pmatrix} q_{01} \\ p_1 \\ q_{0^g0^c} \\ \cdots\cdots \\ \delta_0 \\ P_{1^c1^e} \\ Q_{0^c0^e} \\ Q_{1^c1^e} \\ \cdots\cdots \\ q_{1^g1^c} \\ P_{0^c0^e} \end{pmatrix} \tag{C.2}$$

Table C.3 gives the base values used to scale the LF problem, both for the connected and the disconnected MCN, with E^g given by (2.30).

Tables C.4–C.6 give the solution to the LF problem for this example MES, obtained by solving (C.1) using matrix scaling. The values that are used as BCs for the LF problem of the connected MCN are shown in bold.

Table C.3: Base values used to scale the LF problem of the networks in Figure C.1.

Carrier	Base values		
gas	p_b^g	q_b	E_b^g
	50 mbar	0.1 kg/s	1 MW
elec.	$\lvert V\rvert_b$	δ_b	$\lvert S\rvert_b$
	$10/\sqrt{3}$ kV	1 rad	1 MW

Table C.4: Results for the gas part of the network in Figure C.1a, using matrix scaling. BCs are denoted in **bold**.

Node	p [mbar]	q^{inj} [kg/s]	Link	q [kg/s]
0	**50.000**	**-0.121**	0–1	0.093
1	32.981	**0.010**		

Table C.5: Results for the electrical part of the network in Figure C.1a, using matrix scaling. BCs are denoted in **bold**.

Node	$\lvert V\rvert$ [kV]	δ [rad]	S^{inj} [MW]	Link	S_{ij}^{loss} [MW]
0	**5.376**	-0.101	**2.0 +1.0**i	0–1	0.014 +0.143i
1	**5.774**	**0**	**2.5 +1.5**i		

Table C.6: Results for the coupling part of the network in Figure C.1a, using matrix scaling. BCs are denoted in **bold**.

Unit	q [kg/s]	P [MW]	Q [Mvar]
GG at 0	0.028	1.000	0.500
GG at 1	0.083	3.514	2.143

C.2 Electricity-heat multi-carrier energy system

This small electricity-heat MES is used in Section 8.5.2, and consists of a two-node electrical network and a two-node heat network, connected to each other with two coupling nodes. Figure C.2 shows the connected and the decoupled network representation.

In the electrical part of the connected network, both nodes are sinks. The link from 0^e to 1^e represents a transmission line, which is modeled as a short line. We use (2.17) and (2.18) for the active and reactive powers in (4.4). In the heat part of the connected network, both nodes are sinks. The link from 0^h to 1^h represents a pipe. For the hydraulic model, we use the steady-state flow equation (2.20), with pipe constant (2.22) and pressure drop (2.21), and with Pole's friction factor (2.5). For the thermal pipe model, we use (2.28). Both coupling nodes represent an energy hub (EH), for which we use the linear model (2.38). Table C.7 gives the link parameters and the parameters for the coupling models, and Table C.8 gives the parameters of

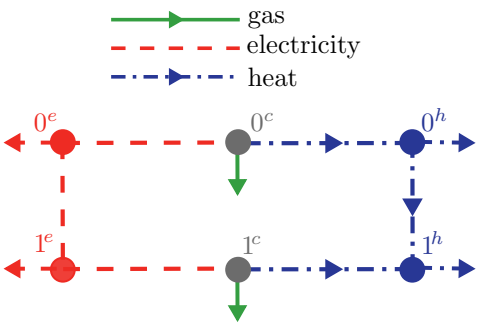

(a) Connected multi-carrier network.

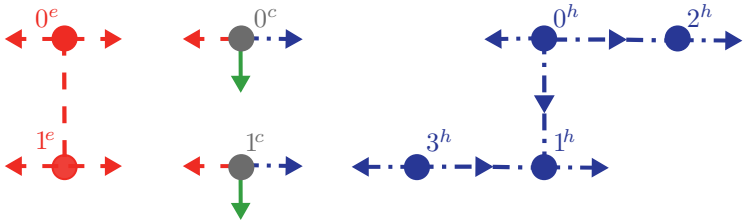

(b) Decoupled multi-carrier network.

Figure C.2: Connected and decoupled network representation of an electricity-heat MES. Arrows on links and terminal links show defined direction of flow.

the gas and water.

Table C.7: Link parameters and parameters of the coupling models for the networks in Figure C.2, per carrier.

Carrier	**Link parameters**			**Unit**	**Parameters**	
electricity	b	g		EH at 0^c	c_0^{ge}	c_0^{gh}
	$-0.3\,\mathrm{S}$	$0.03\,\mathrm{S}$			0.249	0.751
heat	L	D	λ	EH at 1^c	c_1^{ge}	c_1^{gh}
	$500\,\mathrm{m}$	$0.15\,\mathrm{m}$	$0.2\,\mathrm{W/(m\,K)}$		0.510	0.218

IFCs conditions are required to form the system of LF equations (8.8) for the decoupled MCN. Based on (8.3) and (8.4), the IFCs for the disconnected MCN in Figure C.2b are

$$\begin{aligned} P_{0,1} &= -P_{0^c}, & m_0 &= m_{0^c}, & T^s_{0,0} &= T^s_{0^c}, \\ P_{1,1} &= -P_{1^c}, & m_3 &= m_{1^c}, & T^s_{3,0} &= T^s_{1^c}, \\ Q_{0,1} &= -Q_{0^c}, & \Delta\varphi_0 &= \Delta\varphi_{0^c}, & T^r_{0,0} &= T^r_{0^c}, \\ Q_{1,1} &= -Q_{1^c}, & \Delta\varphi_3 &= \Delta\varphi_{1^c}, & T^r_{3,0} &= T^r_{1^c} \end{aligned}$$

To form the systems of LF equations for the heat (part of the) network, we use the terminal link formulation (4.7), with (3.16) for the hydraulic link equations.

Table C.8: Parameters of the gas and heat carriers for the networks in Figure C.2.

Carrier	**Parameters**			
gas	T_n	T	R_{air}	p_n
	288 K	288 K	287.001 J/(kg K)	$1 \cdot 10^5$ Pa
	Z	S	GHV	
	1	0.589	60 134 305 J/kg	
heat	ρ	T^a	C_p	
	960 kg/m^3	0 °C	$4.182 \cdot 10^3$ J/(kg K)	

Table C.9 gives the base values used to scale the LF problem, both for the connected and the disconnected MCN, with E^g given by (2.30).

Table C.9: Base values used to scale the LF problem of the networks in Figure C.2.

Carrier	**Base values**			
gas	q_b	E_b^g		
	0.1 kg/s	1 MW		
elec.	$\lvert V\rvert_b$	δ_b	$\lvert S\rvert_b$	
	$10/\sqrt{3}$ kV	1 rad	1 MW	
heat	p_b^h	m_b	T_b	φ_b
	100 m$\approx$9.418 bar	1 kg/s	100 °C	1 MW

Tables C.10–C.13 give the solution to the LF problem for this example MES, obtained by solving the system of LF equations for the connected MCN using matrix scaling. The values that are used as BCs for the LF problem of the connected MCN are shown in bold.

Table C.10: Results for the electrical network in Figure C.2a, using matrix scaling. BCs are denoted in **bold**.

Node	$\lvert V\rvert$ [kV]	δ [rad]	S^{inj} [MW]	**Link**	S_{ij}^{loss} [MW]
0	**5.376**	-0.101	**2.0 +1.0**i	0–1	0.014 +0.143i
1	**5.774**	**0**	**2.5 +1.5**i		

Table C.11: Results for the hydraulic part of the heat network in Figure C.2a, using matrix scaling. BCs are denoted in **bold**.

Node	p [bar]	m^{inj} [kg/s]	**Link**	m [kg/s]
0	**9.418**	9.518	0–1	4.830
1	9.384	12.075		

Table C.12: Results for the thermal part of the heat network in Figure C.2a, using matrix scaling. BCs are denoted in **bold**.

Node	T^s [°C]	T^r [°C]	$\Delta\varphi^{\text{inj}}$ [MW]	**Link**	$\Delta\varphi^{\text{loss}}$ [MW]
0	100.000	49.753	**2.0**	0–1	0.015
1	99.506	50.000	**2.5**		

Table C.13: Results for the coupling part of the network in Figure C.2a, using matrix scaling. BCs are denoted in **bold**.

Unit	q [kg/s]	P [MW]	Q [Mvar]	m [kg/s]	$\Delta\varphi$ [MW]	T^s [°C]
EH at 0	-0.067	1.000	0.500	14.348	3.015	**100.000**
EH at 1	-0.115	3.514	2.143	7.245	1.500	**99.506**

C.3 Multi-carrier energy system used for validation

This small MES is used in Chapter 6, Section 8.5.3, Section 10.5.2, and Section 11.4. It is based on a case study introduced in [11], which is later adapted in [17] using an extended EH approach. We consider three different ways of coupling the single-carrier networks of this MES; two similar to the couplings used in [11] and one similar to [17].

Figure C.3 shows the networks for the three ways of coupling. In network 1, we use a GG at node 0^c, a gas boiler (GB) at node 1^c, and a combined heat and power plant (CHP) at node 2^c for the coupling. In network 2, we use two EHs. In network 3, we use a GG at node 0^c, a GB at node 1^c and at node 3^c, and a CHP at node 2^c for the coupling. For all three networks, the same models are used in the SC part, based on the models used in [11].

In the gas network, the links from 0^g to 1^g, from 0^g to 2^g, and from 3^g to 2^g, represent pipes, and the link from 1^g to 2^g represents a compressor. The pipes are modeled using the steady-state flow equation (2.1), with the pipe constant (2.2) and pressure drop (2.3) for high-pressure networks. For the friction factor, we use the implicit Colebrook-White equation (2.6).

In the electrical network, all links represent transmission lines, which we model as short lines by (2.17) and (2.18).

In the heat network, all links represent pipes. For the hydraulic model, we use the steady-state flow equation (2.20), with the pipe constant (2.22), pressure drop (2.21), and friction factor (2.6). For the thermal pipe model, we use (2.28).

Table C.14 gives the link parameters used in all three networks, and Table C.15 gives the parameters of the gas and the water.

In network 1, node 0^c represents a GG, node 1^c a GB, and node 2^c a CHP. We use linear models (2.33) and (2.36), for the GB and the CHP, and the nonlinear model (2.32) for the GG.

In network 2, both nodes represent an EH, modeled by (2.38), with $\boldsymbol{E}_{\text{out}} = \begin{pmatrix} P_{\text{out}} & \Delta\varphi_{\text{out}} \end{pmatrix}^T$, and $\boldsymbol{E}_{\text{in}} = \begin{pmatrix} E^g_{\text{in}} \end{pmatrix}$. Figure C.4 shows a representation of the EHs, illustrating the relation to the coupling units in network 1. The coupling matrices

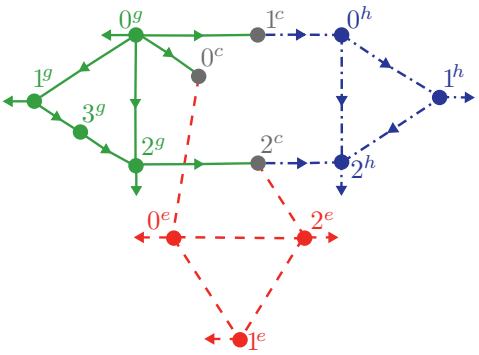

(a) Network 1: GG, GB, and CHP.

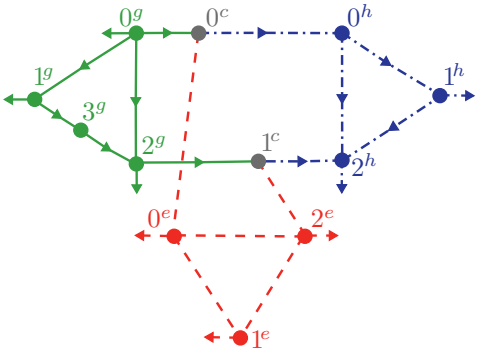

(b) Network 2: EHs.

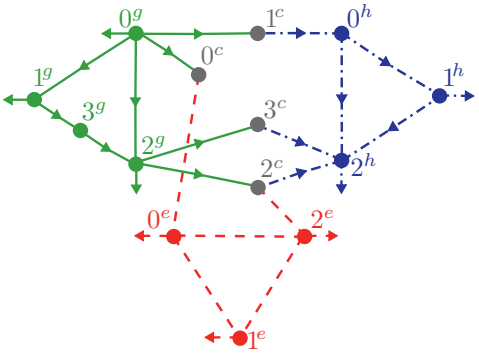

(c) Network 3: GG, two GBs, and CHP.

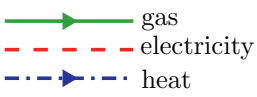

Figure C.3: MES network topologies. Network 1 (a) and 3 (c) are based on [11], network 2 (b) is based on [17]. Arrows on links and terminal links show defined direction of flow.

Table C.14: Link parameters for the networks in Figure C.3, per carrier.

Carrier	**Link parameters**			
gas	L	D	ϵ	r
	$30 \cdot 10^3$ m	0.15 m	$0.05 \cdot 10^{-3}$ m	1.3
electricity	b	g		
	-5.941 S	0.5941 S		
heat	L	D	ϵ	λ
	$30 \cdot 10^3$ m	0.15 m	$1.25 \cdot 10^{-3}$ m	0.2 W/(m K)

are chosen such that the EHs model the same conversion of energy as the coupling components in network 1, such that $c^{ge} = \nu_0 \eta_{\text{GG}}$ and $c^{gh} = (1-\nu_0)\eta_{\text{GB}}$ for the EH at node 0^c, and $c^{ge} = \nu_1 \eta_{\text{CHP}}$ and $c^{gh} = (1-\nu_1)\eta_{\text{CHP}}$ for the EH at node 0^c, with ν_0 and ν_1 dispatch factors. To ensure consistency with network 1, we take $\eta_{\text{GG}} = \widetilde{P}_{0^c0^e}/(\text{GHV}\widetilde{q}_{0^g0^c})$, $\nu_0 = \widetilde{q}_{0^g0^c}/(\widetilde{q}_{0^g0^c}+\widetilde{q}_{0^g1^c})$, and $\nu_1 = \widetilde{P}_{2^c2^e}/(\widetilde{P}_{2^c2^e}+\Delta\widetilde{\varphi}_{2^c2^h})$, with

Table C.15: Parameters of the gas and heat carrier for the networks in Figure C.3.

Carrier	Parameters			
gas	T_n	T	R_{air}	p_n
	273.15 K	281.15 K	287.001 J/(kg K)	$1.013\,25 \cdot 10^5$ Pa
	Z	S	μ	GHV
	0.8	0.6106	$0.288 \cdot 10^{-6}$ m^2/s	$5.4297 \cdot 10^7$ J/kg
heat	ρ	T^a	μ	C_p
	960 kg/m^3	10 °C	$0.294 \cdot 10^{-6}$ m^2/s	$4.182 \cdot 10^3$ J/(kg K)

Table C.16: Parameters of the coupling models for the networks in Figure C.3.

Unit	Parameters				
GG	η_{GG}	a	b	c	d
	0.45	$2.931 \cdot 10^{-9}$	1.1724	$4.3965 \cdot 10^7$	$4.3965 \cdot 10^6$
	e	$P^{\min}$			
	$5 \cdot 10^{-7}$	0 W			
GB	η_{GB}	$r_1 E_{ss}$	r_2		
	0.88	−37 780.1 W	0.797 347		
CHP	η_{CHP}	a	b	d	r_1
	0.88	0.463	−45 320	$4.49 \cdot 10^6$	0.0736
	r_2	L_1	L_2	$\Delta\varphi^{\min}$	$\Delta\varphi^{\max}$
	0.0845	0.8	0.6	10^7 W	$14 \cdot 10^6/0.48$ W
EHs	ν_0	ν_1			
	0.77	0.27			

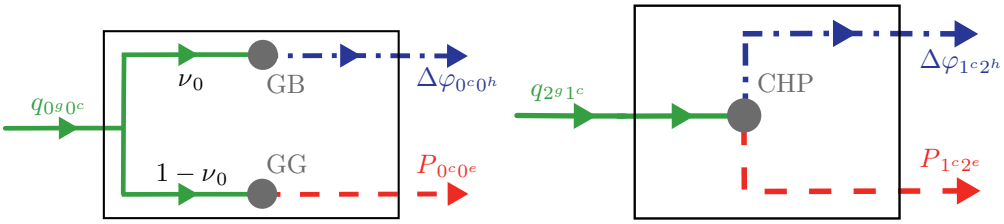

(a) EH at 0^c. **(b)** EH at 1^c.

Figure C.4: Representation of the EHs in network 2, related to network 1. Arrows show actual direction of flow.

$\widetilde{q}$, $\widetilde{P}$, and $\Delta\widetilde{\varphi}$ the coupling flows of network 1.

In network 3, node 0^c represents a GG, node 1^c and 3^c a GB, and node 2^c a CHP. We use the models (2.34) and (2.37) for the GBs and CHP, as proposed in [11]. The parameter values in these model are chosen to match the solution given in [11]. For

the GG, we use the same model as in network 1.

Table C.16 gives the parameters for the coupling models, for all three networks.

For the decoupled approach used in Section 8.5.3, the IFCs for the disconnected MCN, based on (8.2)–(8.4), are

$$\begin{aligned} q_{0,1} &= -q_{0^c}, & P_{0,1} &= -P_{0^c}, & m_0 &= m_{0^c}, & T^s_{0,0} &= T^s_{0^c}, \\ q_{2,1} &= -q_{1^c}, & P_{2,1} &= -P_{1^c}, & m_3 &= m_{1^c}, & T^s_{3,0} &= T^s_{1^c}, \\ & & Q_{0,1} &= -Q_{0^c}, & \Delta\varphi_0 &= \Delta\varphi_{0^c}, & T^r_{0,0} &= T^r_{0^c}, \\ & & Q_{2,1} &= -Q_{1^c}, & \Delta\varphi_3 &= \Delta\varphi_{1^c}, & T^r_{3,0} &= T^r_{1^c} \end{aligned}$$

Table C.17 gives the base values used to scale the LF problem in Chapter 6 and in Section 11.4, Table C.18 gives the base values used to scale the LF problem in Section 8.5.3, and Table C.19 gives the base values used to scale the OF problem in Section 10.5.2, with E^g given by (2.30).

Table C.17: Base values used in Chapter 6 and in Section 11.4 to scale the LF problem of the networks in Figure C.3.

Carrier	**Base values**			
gas	p^g_b	q_b	E^g_b	
	10^5 Pa	1 kg/s	$10 \cdot 10^6$ W	
elec.	$\lvert V\rvert_b$	δ_b	$\lvert S\rvert_b$	
	$10/\sqrt{3} \cdot 10^3$ V	1 rad	$10 \cdot 10^6$ W	
heat	p^h_b	m_b	T_b	φ_b
	10^5 Pa	1 kg/s	130 °C	$10 \cdot 10^6$ W

Table C.18: Base values used in Section 8.5.3 to scale the LF problem of the networks in Figure C.3.

Carrier	**Base values**			
gas	p^g_b	q_b	E^g_b	
	$50 \cdot 10^5$ Pa	2.1922 kg/s	$1 \cdot 10^6$ W	
elec.	$\lvert V\rvert_b$	δ_b	$\lvert S\rvert_b$	
	$10/\sqrt{3} \cdot 10^3$ V	1 rad	$1 \cdot 10^6$ W	
heat	p^h_b	m_b	T_b	φ_b
	10^5 Pa	10 kg/s	100 °C	$1 \cdot 10^6$ W

As initial guess $\boldsymbol{x}^0$ to the solution vector used in NR, with the full formulation (4.1) in the gas network and the terminal link formulation (4.7) in the heat network, we take the values given in Tables C.20–C.22.

The LF calculations are done in S.I. units, such that $\boldsymbol{x}^0$ should also be given in S.I. units (except T^s and T^r, which are in °C). Specifically, the nodal pressures for the heat nodes are used in the calculations, rather than nodal heads.

Table C.19: Base values used in Section 10.5.2 to scale the OF problem of the networks in Figure C.3.

Carrier	**Base values**			
gas	p_b^g	q_b	E_b^g	
	$30 \cdot 10^5$ Pa	2.1922 kg/s	$100 \cdot 10^6$ W	
elec.	$\lvert V\rvert_b$	δ_b	$\lvert S\rvert_b$	
	$10/\sqrt{3} \cdot 10^3$ V	1 rad	$100 \cdot 10^6$ W	
heat	p_b^h	m_b	T_b	φ_b
	$94.176 \cdot 10^5$ Pa	50 kg/s	130 °C	$100 \cdot 10^6$ W

Table C.20: Initial values of $\boldsymbol{x}^0$ used for NR, for network 1.

Node	**Initial values**	**Link**	**Initial values**
0^g	-	0^g–1^g	$q = 4.384$ kg/s
1^g	$p^g = 40 \cdot 10^5$ Pa	0^g–2^g	$q = 4.384$ kg/s
2^g	-	3^g–2^g	$q = 4.384$ kg/s
3^g	$p^g = 40 \cdot 10^5$ Pa	1^g–3^g	$q = 4.384$ kg/s
0^e	-		
1^e	$\lvert V\rvert = 10^4/\sqrt{3}$ V, $\delta = 0$ rad		
2^e	$\delta = 0$ rad		
0^h	$T^s = 100$ °C, $T^r = 50$ °C	0^h–1^h	$m = 60$ kg/s
1^h	$T^s = 120$ °C, $T^r = 50$ °C, $h = 10$ m, $m = 20$ kg/s	0^h–2^h	$m = 30$ kg/s
2^h	$T^s = 120$ °C, $T^r = 50$ °C, $m = 20$ kg/s	1^h–2^h	$m = 60$ kg/s
	Coupling part		
Link	**Initial values**	**Link**	**Initial values**
0^c–0^e	$P = 50 \cdot 10^6$ W, $Q = 0$ W	0^g–0^c	$q = 2.192$ kg/s
1^c–0^h	$m = 10$ kg/s, $\Delta\varphi = 30 \cdot 10^6$ W	0^g–1^c	$q = 0.6577$ kg/s
2^c–2^e	$P = 10 \cdot 10^6$ W, $Q = 0$ W	2^g–2^c	$q = 0.6577$ kg/s
2^c–2^h	$m = 10$ kg/s, $\Delta\varphi = 25 \cdot 10^6$ W		

Tables C.23–C.31 give the solution to the LF problem for networks 1, 2, and 3. For comparison, the values of the solution as given in [11] and [17] are also included in the tables, if available. Results in the gas network are not reported in [17], and results for the pressure in the heat network are not given in [11].

Table C.21: Initial values of $\boldsymbol{x}^0$ used for NR, for network 2.

Node	Initial values	Link	Initial values
0^g	-	0^g–1^g	$q = 4.384\,\mathrm{kg/s}$
1^g	$p^g = 45 \cdot 10^5\,\mathrm{Pa}$	0^g–2^g	$q = 4.384\,\mathrm{kg/s}$
2^g	$p^g = 47 \cdot 10^5\,\mathrm{Pa}$	3^g–2^g	$q = 4.384\,\mathrm{kg/s}$
3^g	$p^g = 45 \cdot 10^5\,\mathrm{Pa}$	1^g–3^g	$q = 4.384\,\mathrm{kg/s}$
0^e	-		
1^e	$\lvert V\rvert = 10^4/\sqrt{3}$ V, $\delta = 0\,\mathrm{rad}$		
2^e	$\delta = 0\,\mathrm{rad}$		
0^h	$T^s = 100\,°\mathrm{C}$, $T^r = 50\,°\mathrm{C}$	0^h–1^h	$m = 65\,\mathrm{kg/s}$
1^h	$T^s = 120\,°\mathrm{C}$, $T^r = 50\,°\mathrm{C}$, $h = 254\,\mathrm{m}$, $m = 20\,\mathrm{kg/s}$	0^h–2^h	$m = 30\,\mathrm{kg/s}$
2^h	$T^s = 120\,°\mathrm{C}$, $T^r = 50\,°\mathrm{C}$, $h = 4300\,\mathrm{m}$, $m = 20\,\mathrm{kg/s}$	1^h–2^h	$m = -60\,\mathrm{kg/s}$
	Coupling part		
Link	**Initial values**	**Link**	**Initial values**
0^c–0^e	$P = 50 \cdot 10^6\,\mathrm{W}$, $Q = 0\,\mathrm{W}$	0^g–0^c	$q = 2.192\,\mathrm{kg/s}$
0^c–0^h	$m = 10\,\mathrm{kg/s}$, $\Delta\varphi = 30 \cdot 10^6\,\mathrm{W}$	2^g–1^c	$q = 0.6577\,\mathrm{kg/s}$
1^c–2^e	$P = 10 \cdot 10^6\,\mathrm{W}$, $Q = 0\,\mathrm{W}$		
1^c–2^h	$m = 10\,\mathrm{kg/s}$, $\Delta\varphi = 25 \cdot 10^6\,\mathrm{W}$		

Table C.22: Initial values of $\boldsymbol{x}^0$ used for NR, for network 3.

Node	Initial values	Link	Initial values
0^g	-	0^g–1^g	$q = 4.384\,\mathrm{kg/s}$
1^g	$p^g = 25 \cdot 10^5\,\mathrm{Pa}$	0^g–2^g	$q = 4.384\,\mathrm{kg/s}$
2^g	$p^g = 30 \cdot 10^5\,\mathrm{Pa}$	3^g–2^g	$q = 4.384\,\mathrm{kg/s}$
3^g	$p^g = 40 \cdot 10^5\,\mathrm{Pa}$	1^g–3^g	$q = 4.384\,\mathrm{kg/s}$
0^e	-		
1^e	$\lvert V\rvert = 10/\sqrt{3} \cdot 10^3$ V, $\delta = 0\,\mathrm{rad}$		
2^e	$\delta = 0\,\mathrm{rad}$		
0^h	$T^s = 120\,°\mathrm{C}$, $T^r = 50\,°\mathrm{C}$	0^h–1^h	$m = 60\,\mathrm{kg/s}$
1^h	$T^s = 120\,°\mathrm{C}$, $T^r = 50\,°\mathrm{C}$, $h = 10\,\mathrm{m}$, $m = 20\,\mathrm{kg/s}$	0^h–2^h	$m = 30\,\mathrm{kg/s}$
2^h	$T^s = 120\,°\mathrm{C}$, $T^r = 50\,°\mathrm{C}$, $h = 4000\,\mathrm{m}$, $m = 20\,\mathrm{kg/s}$	1^h–2^h	$m = 60\,\mathrm{kg/s}$
	Coupling part		
Link	**Initial values**	**Link**	**Initial values**
0^c–0^e	$P = 50 \cdot 10^6\,\mathrm{W}$, $Q = 0\,\mathrm{W}$	0^g–0^c	$q = 2.192\,\mathrm{kg/s}$
1^c–0^h	$m = 10\,\mathrm{kg/s}$, $\Delta\varphi = 30 \cdot 10^6\,\mathrm{W}$	0^g–1^c	$q = 0.6577\,\mathrm{kg/s}$
2^c–2^e	$P = 10 \cdot 10^6\,\mathrm{W}$, $Q = 0\,\mathrm{W}$	2^g–2^c	$q = 0.6577\,\mathrm{kg/s}$
2^c–2^h	$m = 10\,\mathrm{kg/s}$	2^g–3^c	$q = 0.6577\,\mathrm{kg/s}$
3^c–2^h	$m = 10\,\mathrm{kg/s}$		

Table C.23: Results for the gas network, for network 1 (a), 2 (d), and 3 (b), and from [11] (c).

	p [bar]				q^{inj} $[10^3\,\text{m}^3/\text{h}]$					q $[10^3\,\text{m}^3/\text{h}]$			
Node	(a)	(b)	(c)	(d)	(a)	(b)	(c)	(d)	**Link**	(a)	(b)	(c)	(d)
0	50.000	50.000	50.000	50.000	-46.715	-47.108	-47.108	-46.715	0-1	18.233	18.233	29.831	18.233
1	29.102	29.102	40.816	29.102	10.865	10.865	10.000	10.865	0-2	16.408	16.408	4.810	16.408
2	34.077	34.077	49.783	34.077	20.000	20.000	20.000	20.000	3-2	7.368	7.368	18.966	7.368
3	37.833	37.833	53.061	37.833	-	-	-	-	1-3	7.368	7.368	18.966	7.368

Table C.24: Results for the electrical network, for network 1 (a), 3 (b), and from [11] (c).

	$\lvert V\rvert$ [p.u.]			δ [°]			S^{inj} [MW]		
Node	(a)	(b)	(c)	(a)	(b)	(c)	(a)	(b)	(c)
0	1.060	1.060	1.060	0.000	0.000	0.000	0.145 +0i	0.145 +0i	0.145 +0i
1	0.980	0.980	0.980	-6.989	-7.022	-7.022	30.000 +15i	30.000 +15i	30.000 +15i
2	1.000	1.000	1.000	-6.048	-6.115	-6.116	30.136 +15i	30.136 +15i	30.136 +15i
	S_{ij} [MW]			S_{ji} [MW]			S_{ij}^{loss} [MW]		
Link	(a)	(b)	(c)	(a)	(b)	(c)	(a)	(b)	(c)
0-1	26.862 +15.801i	26.980 +15.811i	26.981 +15.811i	-26.429 -11.479i	-26.545 -11.459i	-26.545 -11.459i	0.432 +4.322i	0.435 +4.352i	0.435 +4.352i
0-2	23.492 +11.551i	23.740 +11.552i	23.741 +11.552i	-23.187 -8.501i	-23.430 -8.451i	-23.430 -8.450i	0.305 +3.050i	0.310 +3.102i	0.310 +3.102i
1-2	-3.571 -3.521i	-3.455 -3.541i	-3.455 -3.541i	3.584 +3.652i	3.467 +3.669i	3.467 +3.669i	0.013 +0.131i	0.013 +0.127i	0.013 +0.127i
Total							0.750 +7.502i	0.758 +7.581i	0.758 +7.581i

Table C.25: Results for the electrical network, for network 2 (d) and from [17] (e).

	$\lvert V\rvert$ [p.u.]		δ [°]		S^{inj} [MW]	
Node	(d)	(e)	(d)	(e)	(d)	(e)
0	1.060	1.060	0.000	0.000	0.145 +0i	0.145 +0i
1	0.980	0.980	-6.989	-7.022	30.000 +15i	30.000 +15i
2	1.000	1.000	-6.048	-6.116	30.136 +15i	30.136 +15i
	S_{ij} [MW]		S_{ji} [MW]		S_{ij}^{loss} [MW]	
Link	(d)	(e)	(d)		(d)	(e)
0-1	26.861 +15.801i	26.981 +15.811i	-26.429 -11.479i		0.432 +4.322i	0.435 +4.352i
0-2	23.492 +11.551i	23.740 +11.552i	-23.187 -8.501i		0.305 +3.049i	0.310 +3.102i
1-2	-3.571 -3.521i	-3.455 -3.541i	3.584 +3.652i		0.013 +0.131i	0.013 +0.127i
Total					0.750 +7.502i	0.758 +7.581i

Table C.26: Results for the hydraulic part of the heat network, for network 1 (a), 2 (d), 3 (b), from [11] (c), and from [17] (e).

	h [m]				m^{inj} [kg/s]				m [kg/s]				
Node	(a)	(b)	(d)	(e)	(a)	(b)	(d)	**Link**	(a)	(b)	(c)	(d)	(e)
0	5517.000	5517.000	5517.000	5517.000	-	-	-	0-1	64.687	64.699	64.694	64.687	65.962
1	225.103	223.052	225.066	10.666	121.223	121.228	121.223	0-2	31.408	31.448	31.453	31.409	29.893
2	4268.109	4264.918	4268.046	4383.800	65.026	65.030	65.026	1-2	-56.537	-56.529	-56.533	-56.537	-58.778

Table C.27: Results for the thermal part of the heat network, for network 1 (a), 3 (b), and from [11] (c).

	T^s [°C]			T^r [°C]			$\Delta\varphi^{\text{inj}}$ [MW]				$\Delta\varphi^{\text{loss}}$ [MW]		
Node	(a)	(b)	(c)	(a)	(b)	(c)	(a)	(b)	(c)	**Link**	(a)	(b)	(c)
0	120.000	120.000	120.000	48.680	48.681	48.681	-	-	-	0-1	0.890	0.890	0.890
1	119.040	119.037	119.037	50.000	50.000	50.000	35.000	35.000	35.000	0-2	0.877	0.877	0.877
2	123.546	123.541	123.541	49.534	49.534	49.534	20.000	20.000	20.000	1-2	0.910	0.910	0.910
										Total	2.677	2.677	2.677

Table C.28: Results for the thermal part of the heat network, for network 2 (d) and from [17] (e).

	T^s [°C]		T^r [°C]		$\Delta\varphi^{\text{inj}}$ [MW]			$\Delta\varphi^{\text{loss}}$ [MW]	
Node	(d)	(e)	(d)	(e)	(d)	(e)	**Link**	(d)	(e)
0	120.000	120.000	48.680	48.536	-	-	0-1	0.890	0.890
1	119.039	117.090	50.000	50.000	35.000	35.000	0-2	0.877	0.873
2	123.546	123.541	49.534	49.035	20.000	20.000	1-2	0.910	0.884
							Total	2.677	2.647

Table C.29: Results for the coupling part of the network, for network 1 (a) and from [11] (c).

	q [10^3 m^3/h]		P [MW]		Q [Mvar]		m [kg/s]	$\Delta\varphi$ [MW]		T^s [°C]
Unit	(a)	(c)	(a)	(c)	(a)	(c)	(a)	(a)	(c)	(a)
GG	9.338	9.450	50.499	50.866	27.352	27.363	-	-	-	-
GB	2.736	3.018	-	-	-	-	96.095	28.661	28.677	120.000
CHP	3.776	3.776	10.533	10.173	10.151	10.218	90.154	29.016	29.000	126.493

Table C.30: Results for the coupling part of the network, for network 2 (d) and from [17] (e).

	q [10^3 m^3/h]	P [MW]		Q [Mvar]		m [kg/s]	$\Delta\varphi$ [MW]		T^s [°C]
Unit	(d)	(d)	(e)	(d)	(e)	(d)	(d)	(e)	(d)
EH 0	12.074	50.498	50.866	27.352	27.363	96.096	28.662	28.647	120.000
EH 1	3.776	10.533	10.173	10.151	10.218	90.153	29.015	29.000	126.493

Table C.31: Results for the coupling part of the network, for network 3 (b) and from [11] (c).

	q [10^3 m^3/h]		P [MW]		Q [Mvar]		m [kg/s]	$\Delta\varphi$ [MW]		T^s [°C]
Unit	(b)	(c)	(b)	(c)	(b)	(c)	(b)	(b)	(c)	(b)
GG	9.450	9.450	50.866	50.866	27.363	27.363	-	-	-	-
GB 1[c]	3.018	3.018	-	-	-	-	96.148	28.677	28.677	120
CHP	3.358	3.358	10.173	10.173	10.218	10.218	74.292	25.000	25.000	130
GB 3[c]	0.417	0.417	-	-	-	-	15.818	4.000	4.000	110

C.4 Multi-carrier energy system used for solvability and scaling

This small MES is used in Section 7.1 and Section 11.4. Each SC network consists of three nodes all connected to each other. This MES is created to investigate the effect of coupling on the solvability and well-posed of the LF problem, which is why we consider different types of coupling. We couple nodes 2^g, 1^e, and 0^h of these networks in two different ways, giving two different MCNs, as shown in Figure C.5. The first network, shown in Figure C.5a, uses a GB and a CHP which creates a loop between the SC nodes 2^g and 0^h, while the second network, shown in Figure C.5b, uses an EH and avoids such a loop.

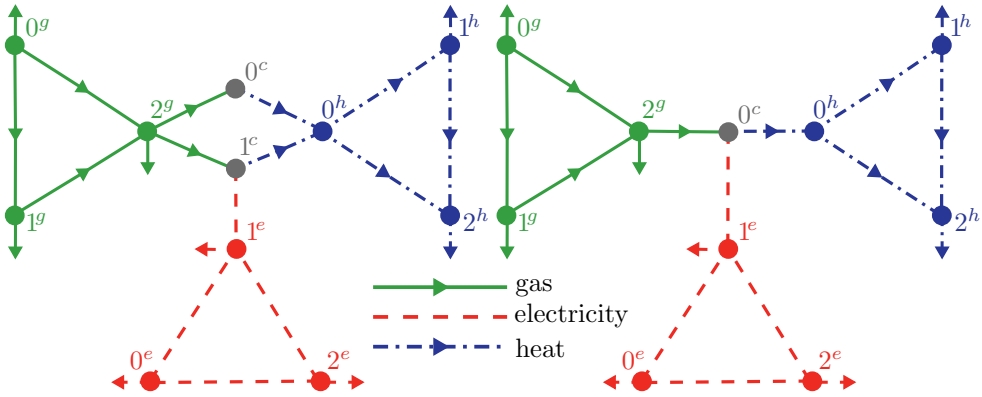

(a) Coupled with a GB (0^c) and a CHP (1^c). **(b)** Coupled with an EH.

Figure C.5: Network topologies of one MES. Arrows on links and terminal links show defined direction of flow.

Node 1 and node 2 are sinks in each SC network. The gas network and power grid have an external source, connected at node 0^g and 0^e respectively. The heat network has no external source; all heat is provided by the gas network. For both networks, the same models are used in the SC part.

Table C.32: Link parameters in networks in Figure C.5, per carrier.

	Link parameters					
Carrier	**Section 7.1**			**Section 11.4**		
gas	L	D		L	D	
	500 m	0.08 m		500 m	0.15 m	
electricity	b	g		b	g	
	−0.3 S	0.03 S		−0.3 S	0.03 S	
heat	L	D	λ	L	D	λ
	500 m	0.15 m	0.2 W/(m K)	500 m	0.15 m	0.2 W/(m K)

Table C.33: Parameters of the gas and heat carrier for the networks in Figure C.5.

Carrier	Parameters			
gas	T_n	T	R_{air}	p_n
	288 K	288 K	287.001 J/(kg K)	10^5 Pa
	Z	S	GHV	
	1	0.589	$6.013\,43 \cdot 10^7$ J/kg	
heat	ρ	T^a	C_p	
	960 kg/m^3	0 °C	$4.182 \cdot 10^3$ J/(kg K)	

In the gas network, all links represent pipes, which are modeled using the steady-state flow equation (2.1), with the pipe constant (2.2) and pressure drop (2.3) for low-pressure networks, and with Pole's friction factor (2.5). In the electrical network, all links represent transmission lines, which we model as short lines by (2.17) and (2.18). In the heat network, all links represent pipes. For the thermal pipe model, we use (2.28). Different models are used in Section 7.1 and Section 11.4 for the hydraulic part of the heat network, and for the coupling units.

Table C.34: Parameters of the coupling models for the networks in Figure C.5.

	Parameters			
Unit	**Section 7.1**		**Section 11.4**	
GB	η_{GB}		η_{GB}	
	0.8		0.81	
CHP	η_{CHP}		η^{ge}_{CHP}	η^{gh}_{CHP}
	0.9		0.65	0.81
EH	ν	μ	-	-
	0.358 26	0.668 37		

Table C.32 gives the link parameters used in each example, Table C.33 gives the carrier parameters used in both examples, and Table C.34 gives the parameters of the coupling models.

C.4.1 Example for solvability and well-posedness

This is the example as used in Section 7.1. For the hydraulic model of the pipes in the heat network, we use the steady-state flow equation for resistors (2.23), with constant $C^h = 1/\rho g$.

In the first network, see Figure C.5a, node 0^c represents a GB and node 1^c a CHP, which we model using (2.33) and (2.35).

In the second network, see Figure C.5b, the GB and CHP are represented by one EH, as shown in Figure C.6. The coupling matrix is chosen such that the EH models the same conversion of energy as the GB and CHP. Using (2.38), with $\boldsymbol{E}_{\text{out}} = \begin{pmatrix} P_{\text{out}} & \Delta\varphi_{\text{out}} \end{pmatrix}^T$, and $\boldsymbol{E}_{\text{in}} = \begin{pmatrix} E^g_{\text{in}} \end{pmatrix}$, we have $c^{ge} = \mu(1-\nu)\eta_{\text{CHP}}$ and $c^{gh} = \nu\eta_{\text{GB}} +$

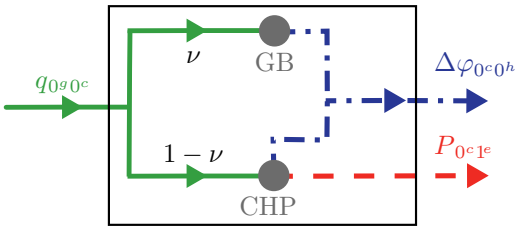

Figure C.6: Model representation of the EH in Figure C.5b.

$(1-\mu)(1-\nu)\eta_{\text{CHP}}$, with ν the factor of gas dispatched to the GB, and μ the factor of gas converted to active power by the CHP.

Table C.35 gives the base values used to scale the LF problem, with E^g given by (2.30).

Table C.35: Base values used in Section 7.1 to scale the LF problem of the networks in Figure C.5.

Carrier	Base values			
gas	p_b^g	q_b	E_b^g	
	0.016 629 Pa	0.016 629 kg/s	10^6 W	
elec.	$\lvert V\rvert_b$	δ_b	$\lvert S\rvert_b$	
	1 p.u.	1 rad	1 p.u.	
heat	p_b^h	m_b	T_b	φ_b
	53 848.32 Pa	2.3912 kg/s	100 °C	10^6 W

C.4.2 Example for scaling

In this example, used in Section 11.4, only the first network shown in Figure C.5a is used.

Table C.36: Base values used in Section 11.4 to scale the LF problem of the network in Figure C.5a.

Carrier	Base values			
gas	p_b^g	q_b	E_b^g	
	1 Pa	0.05 kg/s	10^6 W	
elec.	$\lvert V\rvert_b$	δ_b	$\lvert S\rvert_b$	
	$10/\sqrt{3}\cdot 10^3$ V	1 rad	10^6 W	
heat	p_b^h	m_b	T_b	φ_b
	1 Pa	2.3912 kg/s	100 °C	10^6 W

For the hydraulic model of the pipes in the heat network, we use the steady-state

flow equation (2.20), with the pipe constant (2.22), pressure drop (2.21), and Pole's friction factor (2.5).

In the network in Figure C.5a, node 0^c represents a GB and node 1^c a CHP, which we model using (2.33) and (2.36).

Table C.36 gives the base values used to scale the LF problem, with E^g given by (2.30).

Table C.37: Results for the gas network in Figure C.5a, using matrix scaling. BCs are denoted in **bold**.

Node	p [mbar]	q^{inj} [kg/s]	**Link**	q [kg/s]
0	**50.000**	-0.240	0–1	0.118
1	22.734	**0.090**	0–2	0.122
2	21.172	**0.045**	1–2	0.028

Table C.38: Results for the electrical network in Figure C.5a, using matrix scaling. BCs are denoted in **bold**.

Node	$\lvert V\rvert$ [kV]	δ [rad]	S^{inj} [MW]	**Link**	S_{ij}^{loss} [MW]
0	**5.774**	-0.105	-1.000 -0.151i	0–1	0.000 +0.004i
1	**5.658**	**-0**	**1** +1.000i	0–2	0.029 +0.294i
2	4.951	-0.208	**2** **+2**i	1–2	0.025 +0.247i
				Total	0.054 +0.545i

Table C.39: Results for the hydraulic part of the heat network in Figure C.5a, using matrix scaling. BCs are denoted in **bold**.

Node	p [bar]	m^{inj} [kg/s]	**Link**	m [kg/s]
0	**9.418**	-	0–1	5.993
1	9.366	4.821	0–2	6.106
2	9.364	7.278	1–2	1.172

Table C.40: Results for the thermal part of the heat network in Figure C.5a, using matrix scaling. BCs are denoted in **bold**.

Node	T^s [°C]	T^r [°C]	$\Delta\varphi^{\text{inj}}$ [MW]	**Link**	$\Delta\varphi^{\text{loss}}$ [MW]
0	**100**	49.705	-	0–1	0.015
1	99.602	49.803	**1.000**	0–2	0.015
2	99.284	50.000	**1.500**	1–2	0.015
				Total	0.045

Table C.41: Results for the coupling part of the network in Figure C.5a, using matrix scaling. BCs are denoted in **bold**.

Unit	q [kg/s]	P [MW]	Q [Mvar]	m [kg/s]	$\Delta\varphi$ [MW]	T^s [°C]
GB	0.031	-	-	6.049	-1.525	**110**
CHP	0.074	2.054	1.958	6.049	-1.019	**90**

Tables C.37–C.41 give the solution to the LF problem for this example, using matrix scaling. The values that are used as BCs for the LF problem are shown in bold.

C.5 Multi-carrier energy system of adjustable size

This MES is used in Section 7.2, Section 10.5.3, and Section 11.5, and allows for MCNs of various sizes. Moreover, different couplings are used to couple the SCNs, resulting in various MESs.

The MES consists of a base network, coupling 3-node SC gas, electricity, and heat networks, which can be extended by replacing the sink at node 3 of each SC network by a tree-like structure.

C.5.1 Base network

For each 3-node SCN, node 1 is a source, and node 3 is a sink. For the electrical network and the heat network, node 2 is an additional source. We consider coupling components that convert gas to electricity, heat, or both, to connect the SC networks. One electrical and one heat source are replaced with a coupling, such that the SCNs are coupled at node 1 or at node 2. The networks are coupled by a single node representing a CHP or an EH, or by two nodes representing a GB and a GG. Figure C.7 shows the possible topologies for the base case MES. For all four types of coupling, and for both the base case and the extended case, the same models are used in the SC part.

In the gas network, all links represent pipes, which are modeled using the steady-state flow equation (2.1), with the pipe constant (2.2) and pressure drop (2.3) for high-pressure networks, and with Weymouth's friction factor (2.4).

In the electrical network, all links represent transmission lines, which we model as medium-length lines by (2.14) and (2.15). For each link k, we use $b_k = -x_k/|z_k|^2$ and $g_k = r_k/|z_k|^2$, where r_k and x_k are given by

$$r_k = \frac{4\rho L_k}{\pi D_k^2}$$
$$x_k = 10 r_k$$

with $\rho = 1.6 \cdot 10^{-8}\,\Omega\,\mathrm{m}$. If the link represents a medium-length transmission line, we additionally use $b_k^{\mathrm{sh}} = 2\pi f c L_k \cdot 10^{-12}$, with $c = 100\,\mathrm{nF/km}$ and $f = 50\,\mathrm{Hz}$, and where the factor 10^{-12} is needed to convert c to S.I. units.

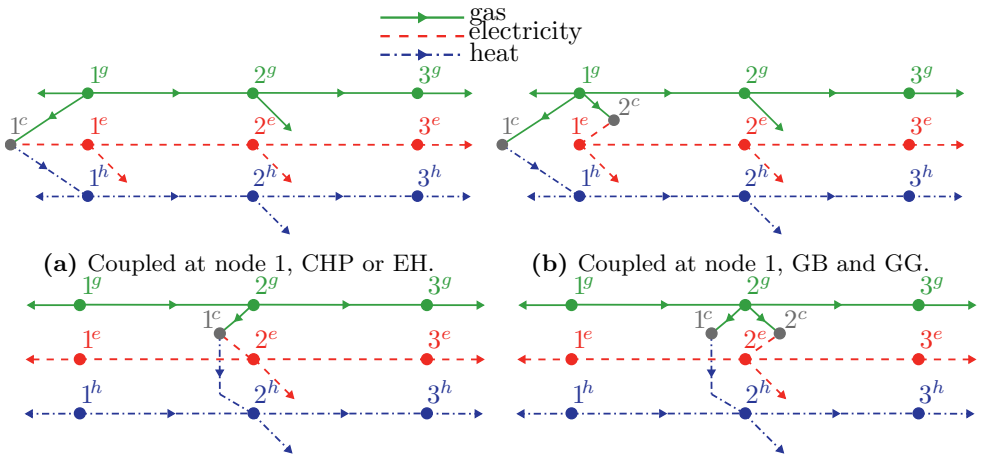

(a) Coupled at node 1, CHP or EH. **(b)** Coupled at node 1, GB and GG.

(c) Coupled at node 2, CHP or EH. **(d)** Coupled at node 2, GB and GG.

Figure C.7: MES network topologies, using various couplings. Arrows on links and terminal links show defined direction of flow.

In the heat network, all links represent pipes. For the hydraulic model, we use the steady-state flow equation (2.20), with pipe constant (2.22) and pressure drop (2.21), and with Pole's friction factor (2.5). For the thermal pipe model, we use (2.28).

Table C.42: Link parameters in networks in Figure C.7, per carrier.

	Link parameters							
Carrier	**Section 7.2**				**Section 10.5.3 and Section 11.5**			
gas	L_{12}	L_{23}	D	E	L_{12}	L_{23}	D	E
	4 km	5 km	10 cm	0.98	4 km	5 km	10 cm	0.98
electricity	L_{12}	L_{23}	D		L_{12}	L_{23}	D	
	4 km	5 km	10 cm		4 km	5 km	1 cm	
heat	L_{12}	L_{23}	D	λ	L_{12}	L_{23}	D	λ
	4 km	5 km	30 cm	0.002 W/(m K)	4 km	5 km	15 cm	0.2 W/(m K)

Table C.43: Parameters of the gas and heat carrier for the networks in Figure C.7.

Carrier	**Parameters**			
gas	T_n	T	R_{air}	p_n
	288 K	288 K	287.002 J/(kg K)	10^5 Pa
	Z	S	GHV	
	1	0.589	$6.013\,43 \cdot 10^7$ J/kg	
heat	ρ	T^a	C_p	
	960 kg/m^3	10 °C	$4.182 \cdot 10^3$ J/(kg K)	

Table C.44: Parameters of the coupling models for the networks in Figure C.7.

Unit	Parameters						
GG	η_{GG}	a	b	c	d	e	$P^{\min}$
	0.7	$2.931 \cdot 10^{-9}$	1.1724	2931	293.1	$5 \cdot 10^{-7}$	0 W
GB	η_{GB}						
	0.8						
CHP	η^{ge}_{CHP}	η^{gh}_{CHP}					
	0.7	0.8					
EH	c^{ge}	c^{gh}					
	0.35	0.4					

For the coupling components, we use linear models (2.33) and (2.36) for the GB and CHP, we use linear model (2.31) or nonlinear model (2.32) for the GG, and we use (2.38) for the EH, with $\boldsymbol{E}_{\mathrm{out}} = \begin{pmatrix} P_{\mathrm{out}} & \Delta\varphi_{\mathrm{out}} \end{pmatrix}^T$, $\boldsymbol{E}_{\mathrm{in}} = \begin{pmatrix} E^g_{\mathrm{in}} \end{pmatrix}$, $c^{ge} = 1/2\eta_{\mathrm{GG}}$, and $c^{gh} = 1/2\eta_{\mathrm{GB}}$.

Table C.45: Base values used in Section 7.2 to scale the LF problem of the networks in Figure C.7.

Carrier	Base values			
gas	p^g_b	q_b	E^g_b	
	10^5 Pa	1 kg/s	10^6 W	
elec.	$\lvert V\rvert_b$	δ_b	$\lvert S\rvert_b$	
	$50 \cdot 10^3$ V	1 rad	10^6 W	
heat	p^h_b	m_b	T_b	φ_b
	10^5 Pa	1 kg/s	100 °C	10^6 W

Table C.46: Base values used in Section 10.5.3 and Section 11.5 to scale the OF problem of the networks in Figure C.7, and of the extended network.

Carrier	Base values			
gas	p^g_b	q_b	E^g_b	
	$10 \cdot 10^5$ Pa	1 kg/s	10^6 W	
elec.	$\lvert V\rvert_b$	δ_b	$\lvert S\rvert_b$	
	$50 \cdot 10^3$ V	1 rad	10^6 W	
heat	p^h_b	m_b	T_b	φ_b
	$10 \cdot 10^5$ Pa	1 kg/s	100 °C	10^6 W

Table C.42 gives the link parameters used in each example, Table C.43 gives the carrier parameters, and Table C.44 gives the parameters of the coupling models.

Table C.47: Results of LF for the gas part of the network in Figure 7.4a, as used in Section 10.5.3 and Section 11.5, using matrix scaling. BCs are denoted in **bold**.

Node	p [bar]	q^{inj} [kg/s]	**Link**	q [kg/s]
1	**50.000**	-1.03	1–2	1.00
2	48.045	**0.00**	2–3	1.00
3	45.483	**1.00**		

Table C.48: Results for the electrical part of the network in Figure 7.4a, as used in Section 10.5.3 and Section 11.5, using matrix scaling. BCs are denoted in **bold**.

Node	$\lvert V\rvert$ [kV]	δ [rad]	S^{inj} [MW]	**Link**	S_{ij}^{loss} [MW]
1	**50.000**	**0**	-0.5 +0.0i	1–2	0.000 -0.310i
2	**49.985**	-0.004	**-0.4** -1.0i	2–3	0.002 -0.374i
3	49.686	-0.009	**1.5 +1.5**i		
				Total	0.002 -0.684i

Table C.49: Results for the hydraulic part of the heat part of the network in Figure 7.4a, as used in Section 10.5.3 and Section 11.5, using matrix scaling. BCs are denoted in **bold**.

Node	p [bar]	m^{inj} [kg/s]	**Link**	m [kg/s]
1	**9.000**	-	1–2	3.213
2	8.881	-6.787	2–3	10.000
3	7.435	10.000		

Table C.50: Results for the thermal part of the heat part of the network in Figure 7.4a, as used in Section 10.5.3 and Section 11.5, using matrix scaling. BCs are denoted in **bold**.

Node	T^s [°C]	T^r [°C]	$\Delta\varphi^{\text{inj}}$ [MW]	**Link**	$\Delta\varphi^{\text{loss}}$ [MW]
1	**100**	46.797	-	1–2	0.100
2	87.704	49.055	**-1.0**	2–3	0.116
3	85.868	50.000	**1.5**		
				Total	0.217

Table C.51: Results for the coupling part of the network in Figure 7.4a, as used in Section 10.5.3 and Section 11.5, using matrix scaling. BCs are denoted in **bold**.

Unit	q [kg/s]	P [MW]	Q [Mvar]	m [kg/s]	$\Delta\varphi$ [MW]	T^s [°C]
EH at 1	0.030	0.625	-0.176	3.213	0.715	100.000

Table C.45 gives the base values used to scale the LF problem in Section 7.2, and Table C.46 gives the base values used to scale the OF problem in Section 10.5.3, with E^g given by (2.30).

Tables C.47–C.51 give the solution to the LF problem for the base network coupled at node 1 with an EH in Figure C.7a, using matrix scaling. The values that are used as BCs for the LF problem are shown in bold. This solution is used as the reference solution in Section 10.5.3.

C.5.2 Extended network

The base case can be extended by replacing the sink at node 3 of each SC network by a tree-like structure which we call 'streets'. There are s streets, S_1 – S_s, which are all connected to node 3 of the base SC network through a junction node. Each street consists of n loads, L_1 – L_n, connected to the main street links by junctions, m of which, J_1 – J_m, are connected to two loads. Figure C.8 shows the topology of such an extended SC network, which consists of $3+s(2n-m+1)$ nodes and $2+s(2n-m+1)$ links. The extended MES is created by coupling the SCNs in the same way as for the base network.

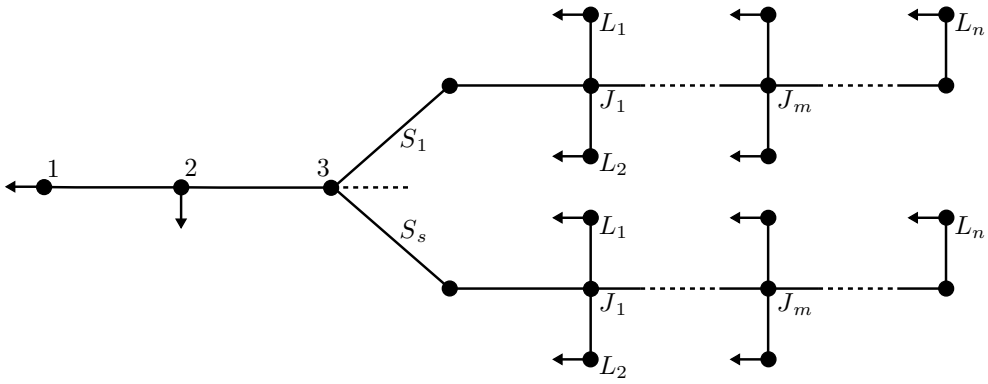

Figure C.8: Extension of SC networks, with s streets consisting of n loads. Arrows on links and terminal links show defined direction of flow.

The total injected flow of node 3 of each base SC network is distributed evenly over all the added load nodes, such that for a load node L_i we have $q_{L_i} = q^{\text{inj}}/(ns)$, $P_{L_i} = P^{\text{inj}}/(ns)$, $Q_{L_i} = Q^{\text{inj}}/(ns)$, and $\Delta\varphi_{L_i} = \Delta\varphi^{\text{inj}}/(ns)$, with q^{inj}, P^{inj}, Q^{inj}, and $\Delta\varphi^{\text{inj}}$ the total injected flows.

The pipes and transmission lines in the streets and from the junctions to the loads are dimensioned based on the (expected) fraction of total load going through that pipe or line, and based on some length L_S and diameter D_S. Algorithm C.1 gives the dimensions of the links between junctions in each street. The dimensions of a link k from a junction to a load are given by $L_k = L_S/n$ and $D_k = D_S/\sqrt{n}$.

We use the same carrier and coupling parameters for the extended case as in the base case, given in Table C.43 and Table C.44, but we use the link parameters for the extended case as given in Table C.52 and set $L_S = L_{23}$ and $D_S = D$ in Algorithm C.1.

Algorithm C.1 Dimensions of link k between two junctions in the extended network.

Set L_S and D_S.
Set number of junction per street $N_J := n - m$.
for $k = 1, \ldots, N_J$ **do**:
  if $k \leq m$ **then**
    Set $l := (n - 2k)/n$
  else
    Set $l := (n - 2m - (k - m))/n$
  end if
end for
Set $L_k := lL_S$
Set $D_k := \sqrt{l} D_S$

Table C.52: Link parameters for the extended network shown in Figure C.8, per carrier.

Carrier	**Link parameters**			
gas	L_{12}	L_{23}	D	E
	4 km	5 km	10 cm	0.98
electricity	L_{12}	L_{23}	D	
	4 km	5 km	1 cm	
heat	L_{12}	L_{23}	D	λ
	4 km	5 km	30 cm	0.002 W/(m K)

We take the same base values as for the base cases, except for p^g for which we take $p_b^g = 50 \cdot 10^5$ Pa, see Table C.53.

We use a flat initial guess for NR, except for $\boldsymbol{p}^g$, $\boldsymbol{p}^h$, and $\boldsymbol{T}^s$, for which we create a linear profile, where the nodes furthest from the source have the lowest value. We define a lower and an upper fraction of the reference values, and create a linear profile between these values for the nodes in each street S. For the three nodes in the base part of the extended network, we take a linear profile between the reference value and the upper fraction of the reference value.

Table C.53: Base values used in Section 7.2 to scale the LF problem of the extended case.

Carrier	**Base values**			
gas	p_b^g	q_b	E_b^g	
	$50 \cdot 10^5$ Pa	1 kg/s	10^6 W	
elec.	$\lvert V \rvert_b$	δ_b	$\lvert S \rvert_b$	
	$50 \cdot 10^3$ V	1 rad	10^6 W	
heat	p_b^h	m_b	T_b	φ_b
	10^5 Pa	1 kg/s	100 °C	10^6 W

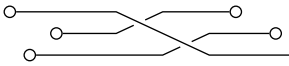

APPENDIX D

Base values for scaling

The LF equations can be scaled using p.u. scaling or using matrix scaling. In this appendix, we provide details on how to choose base values for both types of scaling.

D.1 Variables and parameters

In the per unit system, the base values of some of the primary or derived quantities are chosen. The appropriate base values of the other model quantities are derived based on the requirement that the LF equations remain complete equations, using dimensional analysis after substituting $x_a = x_b x_{\text{p.u.}}$ for all quantities in the equation, see Section 11.2.1. With matrix scaling, only the variables of the LF problem are scaled and not the model parameters.

D.1.1 Electricity

For an electricity network, the base values $|V|_b$ and δ_b of the voltage amplitude and angle and the base value $|S|_b$ of the complex power are generally chosen. The base values of the other variables and of the parameters of the LF equations are then (e.g. [3]):

$$|I|_b = \frac{|S|_b}{\sqrt{3}|V|_b}$$
$$y_b = \frac{|S|_b}{|V|_b^2}$$

This base value $|I|_b$ for the current amplitude holds for a three-phase system. The base value y_b holds for, amongst others, short-line and π-line models.

D.1.2 Heat

In [17], the p.u. system is extended to the heat network, but we adopt a slightly altered extension. The main difference is that we scale the temperature itself, instead of scaling the shifted temperature $T' := T - T^a$. Furthermore, we specify the base values p_b^h, m_b, T_b, and φ_b of the LF variables.

For pipes, we can assume $p_i \sim p_j$, such that we can use the same base value for both pressures. The pressure drop Δp over a pipe, given by (2.21), is then also scaled with the same base value. We substitute $x_a = x_b x_{\text{p.u.}}$, with $x \in \{p^h, m, C^h, \text{f}\}$, in the steady-state flow equation (2.20) of a pipe. Based on dimensional analysis and the requirement that the flow equation remains a complete equation, and dropping the superscript h for notational simplicity, we find that

$$\frac{C_b\sqrt{p_b}}{m_b\sqrt{\text{f}_b}} = 1$$

If we do not scale the friction factor f, and keep it in S.I. units instead, the base value of the pipe constant is given by

$$C_b = \frac{m_b}{\sqrt{p_b}}$$

Similarly, for the thermal model (2.28) of a pipe, we find that

$$\frac{\lambda_b L_b}{(C_p)_b m_b} = 1 \tag{D.1}$$

For the heat power equation (2.25) of a heat exchanger, represented by a terminal link, we find

$$(C_p)_b = \frac{\varphi_b}{m_b T_b} \tag{D.2}$$

If we keep the length L (and the diameter D) of a pipe in S.I. units, and if we substitute (D.2) in (D.1), we find

$$\lambda_b = (C_p)_b m_b$$

D.1.3 Gas

We use the same approach, based on the requirement that the LF equations remain complete equations and using dimensional analysis, to extend the p.u. system to gas networks. We specify the base values p_b^g of the pressure and q_b of the gas flow.

For pipes, we can assume $p_i \sim p_j$, such that we use the same base value for both pressures. In the gas network, the pressure drop equation and pipe constant, and subsequently the steady-state flow equation, are different for low-pressure and for high-pressure systems. For the steady-state flow equation (2.1) of a pipe, with the pipe constant given by (2.2) and the pressure drop given by (2.3), we find

$$\begin{aligned} \frac{C_b\sqrt{p_b}}{q_b\sqrt{\text{f}_b}} &= 1, \quad \text{for low-pressure systems} \\ \frac{C_b p_b}{q_b\sqrt{\text{f}_b}} &= 1, \quad \text{for high-pressure systems} \end{aligned} \tag{D.3}$$

If we do not scale the friction factor f and keep it in S.I. units instead, like we did for the heat network, the base value for the pipe constant is given by

$$C_b = \begin{cases} \dfrac{q_b}{\sqrt{p_b}}, & \text{for low-pressure systems} \\ \dfrac{q_b}{p_b}, & \text{for high-pressure systems} \end{cases}$$

For a compressor, the pressures p_i and p_j generally have a different base value. If a compressor is modeled by (2.7), we find

$$r_b = \frac{(p_j)_b}{(p_i)_b}$$

D.1.4 Coupling

For conversion units, such as those given in Section 2.4, we can assume $E^g \sim P \sim Q \sim \Delta\varphi$, with E^g given by (2.30). For consistency throughout the MES, we could use the same base values for these coupling energy flows. We specify the base values E^g_b, P_b, and φ_b. Again, requiring the model equations in Section 2.4 to remain complete, and using dimensional analysis, the base values of the parameters in the models of a conversion unit can be determined.

For gas, we choose to specify the base value q_b of the gas flow. Since we also specify E^g_b, it follows from (2.30) that

$$\mathrm{GHV}_b = \frac{E^g_b}{q_b}$$

D.2 Functions

In the p.u. system, all variables and parameters in the LF equations are scaled, such that the LF equations will be scaled as well. With matrix scaling, the variables in the LF equations are scaled, but not the parameters, such that the LF equations need to be scaled separately. If the base values of the variables are the same as in the p.u. system, the base values for the LF equations can be determined from (11.3), such that the equations are scaled in the same way as they are scaled in the p.u. system.

To derive the appropriate base values for the equations, we substitute $x_a = x_b x_{\mathrm{p.u.}}$ for all quantities in the equation, with the base values as given in Section D.1. Rewriting the resulting expression to the form in (11.3) gives the required base values.

As an example, we derive the base values for the steady-state flow equation of a gas pipe. We consider two formulations of the link equation for a link representing a pipe, $F^{q(\Delta p)}$ and $F^{\Delta p(q)}$, given by (3.4a) and (3.4b) respectively, with the pipe constant given by (2.2) and the pressure drop given by (2.3). For link equation (3.4b) in a high-pressure system, assuming $(p_i)_b = (p_j)_b := p_b$ and using (D.3), we find

$$\begin{aligned}
F^{\Delta p(q)}\left(q_a, (p_i)_a, (p_j)_a\right) &= (p_i)_a^2 - (p_j)_a^2 - (C^g_a)^{-2}\mathrm{f}_a|q_a|q_a \\
&= p_b^2(p_i)^2_{\mathrm{p.u.}} - p_b^2(p_j)^2_{\mathrm{p.u.}} - \frac{\mathrm{f}_b|q_b|q_b}{(C^g_b)^2}(C^g_{\mathrm{p.u.}})^{-2}\mathrm{f}_{\mathrm{p.u.}}|q_{\mathrm{p.u.}}|q_{\mathrm{p.u.}} \\
&= p_b^2\left[(p_i)^2_{\mathrm{p.u.}} - (p_j)^2_{\mathrm{p.u.}} - (C^g_{\mathrm{p.u.}})^{-2}\mathrm{f}_{\mathrm{p.u.}}|q_{\mathrm{p.u.}}|q_{\mathrm{p.u.}}\right] \\
&= p_b^2 F^{\Delta p(q)}\left(q_{\mathrm{p.u.}}, (p_i)_{\mathrm{p.u.}}, (p_j)_{\mathrm{p.u.}}\right)
\end{aligned}$$

Comparing this expression with (11.3), we find $F_b^{\Delta p(q)} = p_b^2$ for a high-pressure system. Using the same approach, we find $F_b^{\Delta p(q)} = p_b$ for low-pressure systems, and $F_b^{q(\Delta p)} = q_b$ for high-pressure and low-pressure systems.

Curriculum Vitæ

Anne Markensteijn was born in Bodegraven, the Netherlands, on September 30, 1992. After finishing secondary education (gymnasium) at De Goudse Waarden in Gouda in 2010, she studied Applied Physics and Applied Mathematics at the Delft University of Technology. As a Bachelor student, she was a member of several committees of the study association Christiaan Huygens, and of the study association V.v.T.P. She obtained her Bachelor's degree in Applied Physics and her Bachelor's degree in Applied Mathematics in 2014. As part of the master specialization Computational Science and Engineering, she completed an internship at Atlas Copco in Antwerp, Belgium, where she worked on signal analysis of a vibration signal, measured at the caging of an air compressor, to predict the motor rotational speed. Her master thesis research was conducted at Shell Global Solutions International B.V. in Rijswijk, the Netherlands, under supervision of Johan Romate and Cor van Kruijsdijk. She worked on the loss of strict hyperbolicity in three-phase flow models for reservoir simulation. After obtaining her Master's degree in Applied Mathematics in 2016, she started her PhD project in the Numerical Analysis group within the Delft Institute of Applied Mathematics of the Delft University of Technology, under supervision of Johan Romate and Kees Vuik. She worked on formulating and solving steady-state load flow problems and optimization problems for multi-carrier energy systems. In addition to her research, she was president of the SIAM student chapter in the first year of her PhD, she lectured calculus, and she supervised the thesis project of a bachelor student. After finishing her PhD in 2021, she took up a position as scientific software developer at VORtech.

Journal papers

Baljinnyam Sereeter, Anne S. Markensteijn, Maria E. Kootte, Cornelis Vuik, and Cornelis Witteveen. A novel linearized power flow approach for transmission and distribution networks. *Journal of Computational and Applied Mathematics*, April 2021 [In Press. Available online]. doi: 10.1016/j.cam.2021.113572

Anne S. Markensteijn, Johan E. Romate, and Cornelis Vuik. Optimal flow for general multi-carrier energy systems, including load flow equations. *Results in Control and Optimization*, January 2021 [Under review]

Anne S. Markensteijn, Johan E. Romate, and Cornelis Vuik. A graph-based model framework for steady-state load flow problems of general multi-carrier energy systems. *Applied Energy*, 280:115286, December 2020. ISSN 0306-2619. doi: 10.1016/j.apenergy.2020.115286

Peer-reviewed conference papers

Anne S. Markensteijn, Johan E. Romate, and Cornelis Vuik. Scaling of the steady-state load flow equations for multi-carrier energy systems. In *Numerical Mathematics and Advanced Applications ENUMATH 2019*, volume 139 of *Lecture Notes in Computational Science and Engineering*. Springer, May 2021. ISBN 978-3-030-55874-1

Anne S. Markensteijn and Cornelis Vuik. Convergence of Newton's Method for Steady-State Load Flow Problems in Multi-Carrier Energy Systems. In *IEEE PES Innovative Smart Grid Technologies (ISGT Europe 2020)*, 2020

Anne S. Markensteijn, Johan E. Romate, and Cornelis Vuik. On the Solvability of Steady-State Load Flow Problems for Multi-Carrier Energy Systems. In *IEEE Milan PowerTech 2019*, 2019

Technical reports

Anne S. Markensteijn, Johan E. Romate, and Cornelis Vuik. Optimal flow for general multi-carrier energy systems, including load flow equations. Technical

Report 20-06, Delft University of Technology, Delft Institute of Applied Mathematics, December 2020

Anne S. Markensteijn, Johan E. Romate, and Cornelis Vuik. A graph-based framework for steady-state load flow analysis of multi-carrier energy networks. Technical Report 19-01, Delft University of Technology, Delft Institute of Applied Mathematics, 2019

Anne S. Markensteijn and Cornelis Vuik. A Literature Study on Modeling Integrated Energy System Networks. Technical Report 17-08, Delft University of Technology, Delft Institute of Applied Mathematics, 2017. URL `http://http://ta.twi.tudelft.nl/nw/users/vuik/papers/Mar18V.pdf`

Conferences

IEEE PES Innovative Smart Grid Technologies (ISGT), 26-28 October 2020, Presentation, Convergence of Newton's Method for Steady-State Load Flow Problems in Multi-Carrier Energy Systems

PowerWeb Alliander, 4 December 2019, Poster, Load Flow Model for Multi-Carrier Energy Systems

EnuMath, 30 September – 4 October 2019, Presentation, Steady-state load flow for multi-carrier energy systems

IEEE PowerTech, 23–27 June 2019, Presentation, On the solvability of Steady-State Load Flow Problems for Multi-Carrier Energy Systems

Symposium Modellering van geïntegreerde energienetwerken, 1 May 2019, Presentation, Load flow simulations for multi-carrier energy systems

SIAM CSE, 24 February – 1 March 2019, Presentation, A Load Flow Model for Multi-Carrier Energy Systems

Energy Open, 30 November 2018, Presentation, A load flow model for multi-carrier energy systems

PowerWeb 2018, Poster, Modeling Multi-Carrier Energy Systems

National eScience Symposium, 12 October 2017, Presentation, Modeling Integrated Energy Systems

Woudschoten, 4–6 October 2017, Poster, Modeling integrated energy systems; heat, electricity, and gas

SIAM anual meeting, July 2017, Poster, Modeling a district heating network, gas network and power grid as an integrated system

Acknowledgements

First of all, I would like to thank Kees Vuik and Johan Romate for giving me the opportunity to do this project, and for their supervision over the past four years, and before that during my master thesis. Dear Kees, thank you for cultivating an open and friendly academic environment at the numerical analysis department. Dear Johan, thank you for giving me the freedom to make this research my own, and thank you for taking the time during our meetings. I appreciated our discussions, both research and non-research related. I truly enjoyed working with you.

Second, I would like to thank Petra, Remco, and Ni, for their perspective and valuable discussions. And of course thanks to Martijn at Alliander and Paul at AMS, and to everyone else involved with the Regional Energy Self-Sufficiency project.

In addition, I would like to thank the other members of the committee for reading my thesis and accepting the invitation for my defense.

Further, I would like to thank my colleagues at the numerical analysis department. Thanks for the nice and fun times, and for the support, during and outside of research. Thank you for letting me be a part of the Krylov Tigers, despite my abominable soccer skills. Marieke and Baljaa, thanks for being my energy buddies in a mathematical world, it was a pleasure collaborating with you.

Bart, Pien, Merel, Marieke, Roel, Marijn, Jeffrey, Casper, and Merel, thank you for reading (part of) my thesis and providing valuable feedback.

Ik zou graag mijn vrienden binnen en buiten Delft bedanken voor alle hulp en voor de nodige afleiding in de vorm van spelletjes, sport en goede gesprekken. Merel, Jeffrey, bedankt voor jullie steun en geduld.

Oma Meta, hartelijk dank voor alle sokken die me warm hebben gehouden tijdens het thuiswerken. Lies, Tim en Bart, bedankt dat jullie altijd voor me klaar staan. Pap, mam, bedankt voor jullie onvoorwaardelijke steun en vertrouwen, het betekent veel voor me. Ik weet dat dit proefschrift niet hetzelfde is als het vervangen van een fietsband, maar ik hoop dat jullie toch trots op me zijn.

Anne Markensteijn
Delft, May 2021